Measurement and Visualisation of Slurry Flow Using Electrical Resistance Tomography

By

Yousef Faraj

BEng, MSc, AFHEA

Submitted in accordance with the requirements for the degree of
Doctor of Philosophy

The University of Leeds
Institute of Particle Science and Engineering
School of Process, Environmental and Materials Engineering

March, 2013

The candidate confirms that the work submitted is his own, except where work which has formed part of jointly authored publications has been included. The contribution of the candidate and the other authors to this work has been explicitly indicated below. The candidate confirms that appropriate credit has been given within the thesis where reference has been made to the work of others.

Chapter 4 and Chapter 5 of the thesis contain some materials from the five jointly-authored publications given below;

1. Faraj, Y. and Wang, M. (2011). Slurry flow regime and velocity profile visualisation in horizontal pipeline using Electrical Resistance Tomography (ERT). *PSFVIP-8, the 8th Pacific Symposium Flow* Visualisation *and Image Processing*, Moscow, Russia.
2. Faraj, Y. and Wang, M. (2011). Slurry flow measurement in pipeline via Electrical Resistance Tomography (ERT). *BAAF, Beihang Autumn Academic Forum*. Beijing, China.
3. Faraj, Y. and Wang, M. (2012). ERT investigation on horizontal and counter-gravity slurry flow in pipelines. *Journal of Procedia Engineering*. **42**, pp. 588-606
4. Faraj, Y., Wang, M. (2013). ERT based volumetric flow rate measurement in vertical upward flow. *ChemEngDayUk, Proceedings of Chemical Engineering Day Uk*, Imperial College London, London, UK.
5. Faraj, Y. and Wang, M. and Jia, J. (2013). Application of the ERT for slurry flow regime characterisation. *WCIPT7, 7th World Congress on Industrial Process Tomography*, Krakow, Poland. (Accepted in Journal of Procedia Engineering)

All the experimental work presented in the above five publications was carried out by the candidate (Yousef Faraj) under the supervision of Prof. M. Wang (co-author, supervisor). The candidate is also the lead author of these publications, however, advise was also given by Prof. M. Wang during the experimental work for all the above publications, and some contribution by Dr. J. Jia (co-author) during manuscript preparation of publication number 5.

The development of internal structure of a slurry pipeline can accurately represent modern Western Societies. The reduction of transport velocity, gives rise to three layers within the pipeline, while unpredictable instabilities within the society creates a pronounced social stratification, which are classified as upper class, middle class and lower class...the less difference is between the velocities of each layer in the pipeline, the safer and more economical transport is achieved...

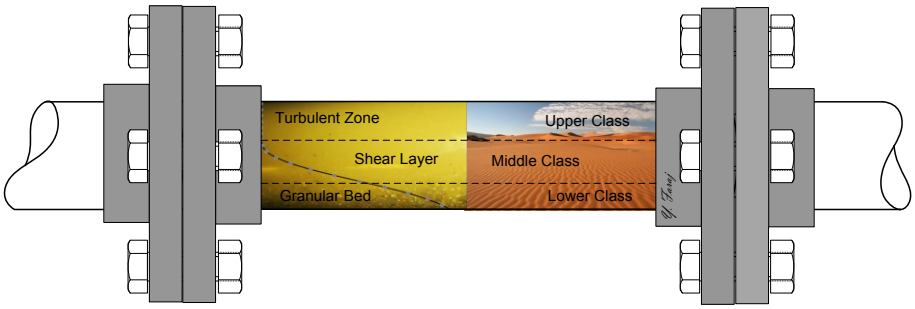

The concept of slurry transport has been employed long time ago...it is undoubtedly considered as a dirty and murky mixture... No matter how murky it can be, it is always seen as a clear water in the eyes of the ERT, through which the systematic movement of each particle can be visualised.

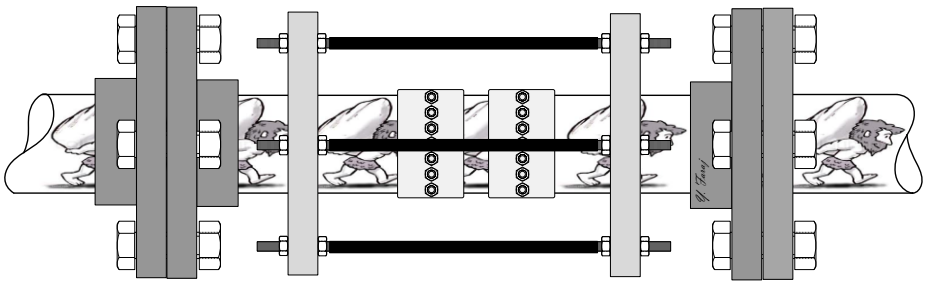

This thesis is dedicated to

my dear father, my beloved wife and my wonderful children

Acknowledgements

Finally, the long episode of my PhD study has successfully reached the end. My journey towards the PhD degree could not have had a better end. Now, it is time to cordially appreciate the heart whelming support and encouragement provided by many individuals, who made this journey more thrilling, and consequential.

First and foremost, I would like to express my greatest appreciation to my supervisor Prof. M. Wang, who has been the source of inspiration that made me complete this project successfully. Prof. Wang, thank you for all the monumental support you have provided to enable me reach the target. Your simplicity and attitude of long life learning has always been a catalyst for my motivation and encouragement to learn and explore different aspects of science and technology. Words are inadequate in offering my thanks to Miss. Judith Squires for her kind support, encouragement and inspiration in every trial that came on my way during my PhD study. I wish to express my deep sense of gratitude to Dr. Basit Munir, who has had a research project with interest in slurry flows, for sharing his timely guidance and discussions we have had to solve technical problems. I would also like to convey my thanks to all the members of OLIL group for their assistance at all times. As with any experimental PhD, a number of research technicians have rendered their support and I wish to offer my thanks to all of them, especially Mr. Robert Harris, Mr. John Cran & Mr. Peter Dawson for their valuable time and help in building the flow system, Mr. R. Guest and Mr. Steve Caddick for the loan of those bits and pieces whenever required. My thanks and appreciations also go to many PhD students and post-doctoral fellows in IPSE, who have abundantly shared their knowledge, their ideas and numerous tips, all of which culminated in the completion of this project. I take immense pleasure in thanking Mr. Geoff Oxtaby and his co-worker Tom from O.G. Fabrication for conducting an excellent work in manufacturing and building all the steel work required for the flow rig.

Finally, heartiest thanks to my wife; her support has been instrumental throughout my PhD timeline, as without her love, understanding, endless patience and encouragement this thesis could not have been completed. I wish to express the sense of love to my wonderful children, Alain, Arman & Anushik, whom in their own ways inspired me and subconsciously contributed a tremendous amount of support in this degree.

Abstract

Slurry transport has been a progressive technology for transporting a huge amount of solid materials across the world in both, long distance and short commodity pipelines. The occurrence of separation and slippage of the constituent phases within the pipeline make these flows unpredictable and time dependent. Therefore, it is paramount for the operator of slurry pipelines to monitor and measure the flow continuously, particularly from the local point of view. Undoubtedly, the measurement of local parameters governing the flow, requires an instrument that provides high temporal resolution. Besides, since each phase has different behaviour and flow characteristics within the pipe, it is enormously difficult to measure the flow parameters of each phase using only one conventional flow meter. Thus, a second auxiliary sensor is required to develop a compact and multiphase flow meter.

This project proposes a new automated online slurry measurement, visualisation and characterization technique, in which a high performance dual-plane Electrical Resistance Tomography (ERT) system is employed with a capability of acquiring data at a rate of 1000 dual-frames per second. It also proposes an ERT based technique, which combines the ERT and an Electromagnetic Flow meter (EMF), to measure volumetric flow rate of each phase, and thus the total slurry volumetric flow rate. The ERT is further combined with the cross-correlation technique to estimate and image the axial solid's velocity distribution, through which the transient phenomena of horizontal flow regimes can be visualised. The ERT is used for estimation of several parameters of stratified flow. The development of a novel automated technique for recognition of horizontal slurry flow regimes is also described. A series of experiments were carried out on horizontal and upward vertical sand-water flow through a pilot scale flow system with 50 mm ID pipeline. Two sands, medium and coarse, were employed in two throughput concentrations (2% and 10%) within the range of transport velocities 1.2-5.0 m/s. The solids volumetric concentration and velocity, along with slurry volumetric flow rate are compared with the corresponding results obtained from a sampling vessel.

Table of Contents

List of Tables

List of Figures

Main Notations used

Symbol	Description	Unit
A	Cross sectional area of pipe	[m^2]
A_B	Area of the lower layer in the two layer model	[m^2]
A_U	Area of the upper layer in the two layer model	[m^2]
C_D	Drag coefficient of the solid particles	[-]
C_v	Volumetric solids concentration	[-]
C_{vb}	Volume fraction of solids in the bed	[-]
C_x	In-situ solids concentration	[-]
D	Pipe diameter	[m]
d_{50}	Median particle diameter size of the slurry	[m]
d_{85}	Particle diameter so that 85% of particles are under that diameter size	[m]
D_i	Pipe inner diameter	[m]
d_p	Particle diameter	[m]
dp/dx	Pressure gradient or pressure drop	Pa/m
f_c	The friction factor due to the Coulombic friction (or coefficient of kinematic friction between the particles and the pipe)	[-]
F_L	Durand's factor.	[-]
F'_L	Modified Durand's factor.	[-]
z	Height of the inclined pipe from ground in inclined two-layer Model.	[m]
ΔD	Difference in Durand factor based on pipe inclination angle.	[-]
F_N	Normal inter-granular force against pipe wall.	$\left[\frac{kg.m}{s^2}\right]$
f_n	Fanning friction factor	[-]
k	Discharge coefficient of the differential pressure meter.	[-]
F_w	Submerged weight of the particles in the lower layer	$\left[\frac{kg.m}{s^2}\right]$
h	Differential pressure	[m]
g	Acceleration due to gravity (9.81 m/s^2)	[m/s^2]

i_m	Hydraulic gradient of the mixture (slurry), expressed in terms of meter of water per meter of pipe	$\left[\frac{\mathrm{m_{water}}}{\mathrm{m_{pipe}}}\right]$
K_p	Constant of the system	$\left[\frac{\mathrm{m_{water}}}{\mathrm{m_{pipe}}}\right]$
m	A constant which is a function of the solid's concentration in equation (2.11)	[-]
m	The coordinate of the pixel in cross correlation	[-]
n	The coordinate of the pixel in cross correlation	[-]
N	Number of electrodes mounted on tomography sensor	[-]
R	The error function, which gives transition time τ in cross correlation	[-]
Re	Reynolds number	[-]
R_w	Cross sectional area of the bed divided by the bed width	[m]
S	Ratio of density of solid particles to density of liquid	[-]
P	Pressure loss	$\left[\frac{kg.m}{s^2}\right]$
S_x	The signal on the plane x, one of the twine planes in ERT sensor	[-]
S_y	The signal on the plane y, one of the twine planes in ERT sensor	[-]
T	The total time over which the measurement is taken in cross correlation	[s]
U	The axial velocity	[m/s]
V	Slurry mean transport velocity	[m/s]
V_D	Deposition velocity	[m/s]
V_1	Velocity at which the pipe blocks	[m/s]
V_2	Transitional velocity from moving bed flow to stationary bed flow	[m/s]
V_3	Transitional velocity from asymmetric flow to moving bed flow	[m/s]
V_4	Transitional velocity from symmetric flow to asymmetric flow	[m/s]
V_c	Critical velocity and is taken to be identical to V_3 and V_D	[m/s]
V_t	Particle terminal settling velocity	[m/s]

V_X	The value of the pixel (n,m) on plane X	[-]
V_Y	The value of the pixel (n,m) on plane Y	[-]
W	Terminal settling velocity of the particles in three-layer model	[m/s]
WP_B	Perimeter of the lower layer of the pipe in the two layer model	[m]
WP_U	Perimeter of the upper layer of the pipe in the two layer model	[m]
WP_i	Perimeter at the interface between the two layers in two-layer model	[m]
x	A constant which is a function of solid's concentration in equation (2.11)	[-]
y	The vertical coordinate, perpendicular to the pipe axis	[m]
$\Delta P/L$	Pressure gradient	[pa/m]
ΣF	The total force per unit forces exerted normal to the pipe in the two layer	$\left[\frac{kg.m}{s^2}\right]$

Greek Letters

Symbol	Description	Unit
α_c	Volume fraction of the dispersed phase (solids volume fraction).	[-]
γ	Pipe inclination angle from horizontal	[deg]
ε	Roughness of the pipe	[-]
θ	Half of the angle subtended at the pipe centre due to the upper surface of the bed	[deg]
Φ_r	Angle of repose of the solid particles	[deg]
λ_s	Coefficient of static friction of the solid particles against the pipe wall	[-]
μ_l	Liquid viscosity	$\left[\frac{kg}{m.s}\right]$

ρ_L	Density of carrier liquid	[kg/m^3]
ρ_l	Density of carrier liquid	[kg/m^3]
ρ_m	Mixture (slurry) density	[kg/m^3]
ρ_s	Density of solids in a mixture	[kg/m^3]
ρ_B	Effective density of the lower layer in two-layer model	[kg/m^3]
ρ_U	Effective density of the upper layer in two-layer model	[kg/m^3]
σ_1	Conductivity of the first phase (water)	[mS/cm]
σ_2	Conductivity of the second phase (i.e. dispersed particles)	[mS/cm]
σ_m	Local slurry mixture conductivity distribution	[mS/cm]
τ_i	The interfacial shear stress	[kg/m.s^2]
τ_U	Shear stress of the upper layer in the two layer model	[kg/m.s^2]
τ_B	Shear stress of the lower layer in the two layer model	[kg/m.s^2]

Other notations have been used are defined as they occur in the text.

List of Abbreviations

AARE	Average Absolute Relative Error
ABS	Acrylonitrile-Butadien-Styrene
ACF	Auto Correlation Functions
AIMFLOW	Advanced Imaging and Measurement for Flow, Multiphase Flow and Complex Flow in the Industrial Plant
ANN	Artificial Neural Network
BZP	Bright Zinc Plated
CHS	Circular Hollow Section
CPVC	Chlorinated Poly(Vinyle Chloride)
DAS	Data Acquisition System
Dfps	Dual-Frames Per Second
DWV	Drain-Waste-Vent
ECT	Electrical Capacitance Tomography
ECTFE	Ethylene-Chlorotrifluoroethylene
EIT	Electrical Impedance Tomography
EMF	Electromagnetic Flow meter
EMR	Electron Magnetic Resonance
EMT	Electromagnetic Tomography
ERT	Electrical Resistance Tomography
ET	Electrical Tomography
FFT	Fast Fourier Transform
FICA	Fast Impedance Camera System
HET	Heterogeneous Flow Regime
ID	Pipe Internal Diameter
LBP	Linear Back Projection
LDA	Laser Doppler Anemometry

LDV	Laser Doppler Velocimetry
MB	Moving Bed Flow Regime
MRI	Magnetic Resonance Imaging
MSS	Mean Square Spectrum
NMR	Nuclear Magnetic Resonance
OD	Pipe Outer Diameter
OLIL	Online Instrumentation Laboratory(University of Leeds/UK)
P	Pseudo-homogeneous Flow Regime
PDF	Probability Density Functions
PE	Polyethylene
PEPT	Positron Emission Particle Tracking
PET	Positron Emission Tomography
PFA	Perfluoro(Alkoxyalkane) Copolymer
PFC	Parallel Flange Channels
PIV	Particle Image Velocimetry
PP	Polypropylene
PSD	Particle Size Distribution
PSDF	Power Spectral Density Functions
PTFE	Polytetrafluoroethylene
PVC	Poly Vinyl Chloride
PVDC	Poly(Vinylidene Chlride)
PVDF	Poly(Vinylidene Fluoride)
RF	Radio Frequency
SB	Stationary Bed
SBP	Sensitivity Back Projection
SCG	Sensitivity Conjugate Gradient
SHS	Square Hollow Section
SNR	Signal-to-Noise Ratio
STDEV	Standard Deviation

SVM	Support Vector Machine
TEP	Perfluoro (Ethylene-Proplylene) Copolymer
UB	Universal Beam
UC	Universal Column
UDVP	Ultrasonic Doppler Velocity Profiler
uPVC	Unplastisized Poly Vinyl Chloride

Definitions of slurry flow characteristics

The basic characteristics of slurry flow in pipelines used throughout the thesis are defined in the following list.

Flow characteristic	Definition
Transport velocity	The bulk (or mean) slurry velocity.
Slurry velocity	The bulk (or mean) slurry velocity.
EMF velocity	Carrier liquid (or conducting phase) velocity. This velocity is used to represent the mean slurry velocity, where both phases move in a similar velocity or with negligible slip between the two phases, especially in vertical slurry flow.
ERT velocity	The axial velocity of solid particles within the pipeline, which is measured by the ERT in conjunction with Cross-Correlation method.
Slip velocity	The difference between the velocities of the two flowing phases caused by gravitational effects.
Discharge velocity	The bulk (or mean) slurry velocity at the slurry discharge point into the mixing tank (the other end of the flow loop). It is measured using the flow diversion technique into the measuring tank
Solids velocity	The velocity of solid particles (sand) in the carrier liquid flowing through the pipeline.
Local solids velocity	The axial velocity of solid particles measured at a particular location within the pipe cross-section, measured by the ERT in conjunction with Cross-Correlation method
In-situ velocity	The average local axial solids velocity within the pipe cross-section measured by the ERT in conjunction with Cross-Correlation method.
Predicted velocity	The actual phase velocity within the pipeline.

Local concentration	The solid volume fraction within the mixture measured at a particular location within the pipe cross-section, measured by the ERT.
Insitu concentration	The average local solids volume fraction within the pipe cross-section measured by the ERT. It is also called spatial concentration.
(Throughput concentration)	The pre-known solids volume fraction within the mixing tank, which is introduced to the flow loop.
(Delivered concentration)	The solids volume fraction in the slurry at the other end of the pipeline (discharge point).
(Discharge concentration)	Similar to delivered solids concentration.
Grannular bed	The settled solid particles at the bottom of the pipe, either moving or stationary, or both.
Moving bed	The settled moving deposit (or solid particles) moving along the bottom of the pipe.
Stationary bed	A non-moving deposit (or solid particles), which are in permanent contact with each other and the pipe wall.
Loss poured bed	The deposit at the bottom of the pipe. The solid particles within this type of bed are not well packed (i.e. void exists within the bed).

Chapter 1
Introduction

1.1 Hydraulic transport of solids in pipes

The presence of solid particles in a carrier liquid form a mixture, which is referred to as slurry. Slurry flows cover a wide spectrum of applications and are the focus of considerable interest in engineering research. The concept of slurry transport has been employed long time ago and it is widely utilised in many industries such as minerals, chemical, coal, pharmaceutical, water, dredging and other industries. It is worth mentioning that in some specific applications, such as dredging, hydraulic transport is the only means of transportation of solids through pipelines. In mid-nineteenth century slurry transport was first used by mining industry, an example of which is the transport of slurry used to reclaim gold from placers in California (Abulnaga, 2002). Pneumatic conveying is also another means of transporting solid particles, in which gas (commonly air) is used instead of liquid. However, as it is associated with some disadvantages such as high specific power consumption, potential for particle breakage and degradation, high wear rate on components and used for relatively short distance, some drawbacks are seen to this technology (Dhodapkar *et al*., 2006). On the other hand, a great interest and attention has been given to hydraulic transport due to its advantages namely environmentally friendly, low operation and maintenance costs, relative simplicity in its infrastructure etc. It has been a progressive technology for transporting a vast amount of different solid materials through various sizes of pipelines with different orientations, such as sands, iron concentrates, copper concentrates, phosphate matrix, tailings, limestone and sewage, in different densities, shapes, sizes up to 150 mm (6"), such as those pumped from fields of phosphate matrix (Abulnaga, 2002). These are the examples of long distance commodity pipelines. However, it has also been transported through short in plant pipelines, such as that of nuclear, chemical, pharmaceutical and food industry. The most commonly used carrier fluid is water, which is referred to as “hydraulic transportation”.

Since these mixtures are encountered in a wide range of industries, their classification is very important for describing their physical appearance and flow behaviour. There are two broad classifications for hydraulic transportation, which are referred to as settling (or heterogeneous) and non-

settling (or homogeneous) slurries. These classifications based on two considerations, physical properties and flow behaviour (or rheological behaviour). In other words, whether the solid particles in the slurry can settle under the influence of gravity or are suspended within the carrier fluid. In settling slurries the solid particles tend to separate from the carrier liquid and segregate at the bottom of the pipe, either horizontal or inclined, under the influence of gravity. This suggests that the settling slurries can be stratified either fully or partially (Matousek, 2005). In contrast, non-settling or homogeneous slurries composed of particles of colloidal dimensions, which are characterised by primary particle diameters of typically less than 2 μm. They are also highly concentrated and maintained in suspension by molecular movement within the liquid, which is referred to as Brownian motion (Peker *et al.*, 2008). Their non-settling behaviour is probably due to hindering settling, as do occur in most paints and emulsions (Brown and Heywood, 1991). It is worth mentioning that non-settling slurries are beyond the scope of this thesis, therefore, no further reference will be made to non-settling slurries.

The behaviour of slurry flow through pipelines has been systematically investigated since 1950s (Matousek, 1996). The focus was mainly based on experimental investigations dealing with prediction of pressure drops and demarcation of flow regimes with different velocities, using various particles and pipe sizes, and then using the collected data to construct empirical models. Then 1970s and 1980s marked the emergence of another approach, by which the researchers were more focusing on the fundamental principles or the rheological based continuum approach. This approach was strictly applied to ultra fine non-colloidal particle slurries, such as the basics of the macroscopic two-layer model by Wilson (1970) and microscopic slurry flow by Shook and Roco (1991). Whereas the contemporary approach entail the rapid development of measuring techniques and substantial computational effort, which is still available approach to describe the complex behaviour and nature of settling slurry flow through pipelines (Matousek, 2005; Lahiri, 2009). Despite the excellent research work and progress in the field our understanding of the fundamental and complex nature of settling slurry flow is still not enough to satisfy the engineering requirements. Since the slurry engineer requires a viable and reliable methodology that suits all the conditions met in industry. Therefore, the investigation of all the relevant variables is crucial.

A wide range of experimental results have been reported in the literature including different operating conditions, material type and shape and different flow orientations. In horizontal and inclined flow as the gravity acts at right angle to the flow, the separation of phases occurs and gives rise to several flow regimes, pseudo-homogeneous, heterogeneous, moving bed and stationary bed. Whereas in vertical flow, especially upward flow, the gravity acts counter to the dynamic forces, as a result the slippage of the phases occurs (Parvareh *et al.*, 2010). The occurrence of separation and slippage of the constituent phases in settling solid-liquid flow in pipelines makes the flow unpredictable and time dependent. Therefore it is paramount for the operator of these pipelines to monitor and measure the flow continuously, particularly from the local point of view (i.e. the knowledge of internal structure of flow is necessary) so as to ensure safe transport and maintaining acceptable control limits. In order to understand the internal structure of such flows, solids volume fraction distribution and solids velocity distribution are of great importance. Therefore, this study focuses mainly on qualitative and quantitative measurement of these two parameters.

As noticed in the literature, there are many challenges that have to be highlighted to boost our knowledge and tackle the limitations in understanding and measuring settling slurry flows. In the past, several intrusive methods, such as traditional probes, have been used to measure solids volumetric concentration and velocity. The disadvantages of using these probes have been reported, particularly for solid-liquid flow, Brown and Heywood (1991). It is highly unlikely that these devices can survive the harsh condition inside the pipelines due to abrasive nature of slurry. In many cases solids may accumulate around them and cause pipe blockage. Also it is well known that intrusive devices introduce an undesirable physical disturbance and alter the internal structure of the flow (Heindel *et al.*, 2008). In order to overcome this limitation, researchers across the world developed a variety of non-intrusive measurement techniques to highlight the internal characteristics of two or multiphase flows, such as optical, ultrasound, nuclear, conductance and electrostatic transducers. Nonetheless, each of the above techniques suffers from serious limitations, especially for the complex solid-liquid flows. For example, since slurries are opaque and flow through opaque enclosures, then using optical techniques can be quite difficult if not impossible. Although nuclear techniques provide an accurate measurement, they are very expensive and suffer from low temporal resolution and environmental issues (Thorn *et al.*, 1997). Amongst all of the above techniques Electrical Resistance Tomography (ERT), as one of the

family of non-intrusive sensors, has attracted the interest of many researchers. This is due to the fact that the ERT offers many advantages, such as non-intrusive, relatively low cost, no environmental restrictions, providing quantitative and qualitative on-line measurement, fast etc. Within the last two decades the ERT has seen a significant development and has been applied to many industrial process involving two/multiphase systems. Particularly the application of the ERT to solid-liquid flow has been reported by many investigators (Razzak *et al.*, 2009; Giguère *et al.*, 2008; Lucas *et al.*, 1999; Wood and Jones, 2003; Wang *et al.*, 2003; Pachowko *et al.*, 2004). All of the above studies have been carried out on vertical and/or horizontal flows used the conventional ERT system, which acquires up to 200 images per second (Dyakowski *et al.*, 2000). To the authors' knowledge no attempt has been made to measure solids volume fraction and solids axial velocity using the combination of high performance ERT system in conjunction with cross-correlation technique. It is evident that measurement of the two parameters, especially velocity, in fast evolving processes requires high frame rates (fast) of milliseconds. Therefore, this study uses a high performance dual-plane electrical resistance tomography system, which is called Fast Impedance Camera System (FICA) and is capable of acquiring data at a rate of 1000 dual-frames per second (dfps). As horizontal and vertical sections jointly make most of the pipelines, it is important to study both orientations simultaneously with similar conditions, so as to reveal the effect of one on another. However, at higher velocities (pseudo-homogeneous) there may be higher degree of similarities in the internal structure of the flow in the two orientations, but the differences could well be noticed for the transport velocities below the deposition velocity, where the homogeneity of vertical flow is still preserved, whereas a strata is formed in the horizontal pipe invert.

Although it can be argued that most of pipelines in industry are horizontal and vertical, inclined settling slurry flows are still play an important role, despite that they have not been the subject of extensive studies. Unlike horizontal and vertical flows, very limited work has been conducted in this flow orientation. In fact since 1950s a very limited number of published body work covers the characterisation and measurement of solid liquid flows in inclined pipelines. Therefore, this project attempts to design and build a pilot scale slurry flow loop, in the aim that it can be used as a tool for further understanding and characterisation of inclined slurry flow and identifying flow effects on its measurement scheme. The whole design strategies and methodologies are described in Chapter 6, where the reader will be taken

through the whole journey from the preliminary design to the erection stage and testing. However, no experimental work on inclined flow will be mentioned throughout the present work. The reader is referred to several previous works conducted on inclined pipeline: Worster and Denny (1955), Brook (1962), Kao and Hwang (1979), Wilson *et al.* (1992), Shook *et al.* (1974), Wilson and Tse (1984), Matousek (1997), Doron and Barnea (1997), Lucas *et al.* (1999).

1.2 Motivation of present work

1. In order to understand the complex nature of slurry flow and optimising the slurry flow systems a reliable method (or technique) is required to continuously monitor and capture the internal images of the pipeline through localised flow measurement, so that a safe transport is ensured and acceptable control limits are maintained. It is quite apparent that an automated and on-line internal measurement of pipe flow offers great advantages, such as providing fast on-line measurements, reducing labour resources and the requirement for additional sampling equipment. However, the selection of which technique to use is strongly dependent on several important issues, such as cost, simplicity in design, safety, reliability, robustness, speed and non-intrusive. Due to the fact that the ERT offers all the above advantages, then it is proposed to be the meter of choice. Although the some previous works have made use of the ERT, all of them used the conventional ERT system, which acquires 200 images per second (Dyakowski *et al.*, 2000). Therefore, this thesis employs a high performance Electrical Resistance Tomography system (ERT) to explore its capability in localised measurements and visualisation of horizontal and vertical slurry flow (i.e. solids concentration distribution and solids axial velocity distribution within the carrier fluid), with capability of acquiring data at a rate of 1000 dual frames per second.
2. In terms of industrial application the volumetric flow rate of the phases in two/multiphase flows is very important flow parameter to the pipeline operator. However, due to the complexity of multiphase/two phase flow, particularly solid-liquid flow, it is enormously difficult to accurately measure the flow parameters of each phase individually using only one conventional flow meter. Thus, a secondary sensor is required to determine the volumetric flow rate of each phase and so the total mixture volumetric flow rate. A survey of the literature and commercially available flow meters raised the alarm that currently there is almost no

multiphase/two phase flow meter practically available to majority of industrial applications for measurement of volumetric flow rate of constituent phases and total mixture (Li *et al.*, 2005; Thorn *et al.*, 1997). Therefore, this research proposes an ERT based technique, which combines the Electrical Resistance Tomography (ERT) and the Electromagnetic Flow meter (EMF), to measure the volumetric flow rate of each phase (continuous and dispersed) and producing the total slurry volumetric flow rate.

3. Since settling slurries contain much coarser particles (up to few millimetres), such as sand, coal-water, gravel, then these particles tend to accumulate at the bottom of the pipe and produce several flow regimes. As highlighted in the literature, these flow regimes affect one of the most important parameter in settling slurry flow, which is pressure drop, particularly in stratified flow. This may in itself cause partially or fully pipe blockage, which reduces the efficiency. They also influence pipe erosion and some other performance characteristics (Doron and Barnea, 1995). Thus, the recognition of these flow regimes is very important. Furthermore, the identification and evaluation of the information regarding these flow regimes are usually performed by visual inspection through graphic illustration, which sometimes difficult to interpret or identify, either due to the system being opaque or with high velocity. Therefore, this work explores the validity and applicability of the ERT as an automated online flow regime recognition technique through statistical analysis of its signal.
4. Although it can be argued that in most of plants handling slurry flow, the pipelines are either horizontal or vertical, inclined flows is still encountered and essential in dredging ladder, pump-box feed systems and many long overland pipelines, which have to go through dunes and hills. A survey through the literature concluded that there is a lack of information regarding the behaviour of inclined slurry flow, as very limited work has been carried out in this type of pipeline orientation. It was also found that to avoid the blockage of the line once the flow is shut down, a commonly used design restriction of 10-16% (5.7°-9°) is often considered due to lack of knowledge of the critical slope of the inclined pipe. As Kao and Hwang (1979) criticised using the rule of thumb for the design of critical slope. Their criticism was based on the fact that lack of properly designed critical slope in an inclined pipe adds to construction costs and capital expenses. Moreover, our present knowledge of the fundamentals, behaviour of inclined slurry flow and the flow effects on its measurement is still in its stage of infancy. This implies that almost no correlation has been

developed for inclined flow. Due to this reason, most of the designers do not take the pipe inclination into account, but rather the whole transport line as horizontal. Therefore, This work has attempted to design and build a pilot scale inclinable multiphase flow loop, meeting all the design requirements for slurry flow, so as to be used to gain insight of complex inclined slurry flow and the potential effects on flow measurements. However, This study attempts only the design and installation of the entire flow loop and associated instrumentations and equipments, while conducting experiments and performing measurements on inclined slurry flow is beyond the scope of this research, due to the limited timeline of this study. In other words, this thesis is limited to the measurement and visualisation of horizontal and counter-gravity slurry flow.

5. A review in literature reveals that little work has been carried out within the boundary of stationary bed flow regime in horizontal flows, this is undoubtedly due to the fact that the risk of blockage is dominant in this region. As a result of this, an investigation into the boundary of stationary bed and pipeline blockage is conducted. Firstly, to gain further knowledge regarding the minimum velocity within the frame of this flow regime, secondly, to explore the functionality of the dual-plane ERT sensor electrodes, while they are covered by a settled thick granular bed at the bottom of the pipe.
6. Narrow Particle Size Distribution (PSD) has been used in most of the investigations carried out in slurry flow, while the Particle Size Distribution in industry is very broad. Therefore, this research deals with flow characterisation and measurement of two broadly graded sands, medium sand (d15 = 170 μm, d50 = 242 μm, d85 = 430 μm) and coarse sand (d15 = 270 μm, d50 = 480 μm, d85 = 2240 μm).

1.3 Scope of present work

The present work makes an extensive use of the Electrical Resistance Tomography system and supporting instrumentation (EMF) for measurement and characterisation of horizontal and vertical settling slurry flow. The local flow characteristics of the above two flow orientations is determined. Non-uniform shape and size and used as solid particles and tap water as a carrier liquid. Only two sands are attempted, medium and coarse with PSD (d15 = 170 μm, d50 = 242 μm, d85 = 430 μm) and (d15 = 270 μm, d50 = 480 μm, d85 = 2240 μm) respectively. The validation of each parameter, obtained from the ERT and the EMF or the combination of both, is carried

out using a flow diversion technique, the results of which is presented within the body of this thesis. Visualisation and recognition of each flow regime encountered in settling slurry flow is attempted based on ERT localised measurements. No work will be carried out on inclined flow, except the design, erection and testing of an inclinable slurry flow loop.

1.4 Research objectives

The overall objective of this project is to explore the validity and applicability of a new settling slurry flow measurement and visualisation technique, in which the Electrical Resistance Tomography used as the main flow meter and the EMF as a supporting auxiliary sensor. The ERT flow visualisation scheme is also planned to characterise and reveal the mechanisms occurring in horizontal and vertical solid-liquid flow. In order to achieve the main aim of this study, the following specific objectives have to be fulfilled:

1. Localised measurement and visualisation of horizontal slurry flow.
2. Characterisation of stratified slurry flow, including the blockage phenomena.
3. Localised measurement and visualisation of vertical slurry flow.
4. Characterisation of counter-gravity solid-liquid flow.
5. Slurry flow regime visualisation and characterisation in horizontal slurry flow.
6. Estimation of phase volumetric flow rate through combination of the ERT and the EMF.
7. Explore the validity of the results obtained from the measurement scheme.
8. Develop an automated (on-line) horizontal flow regime recognition technique.
9. Evaluation of the proposed measurement and recognition technique.
10. Design and erection of an inclinable settling slurry flow system.

1.5 Thesis layout

Chapter 2 presents the literature concerning the settling slurry flow in various flow orientations, horizontal, vertical and inclined. This chapter describes some of the previous work carried out on each orientation, particularly in horizontal flow, with mentioning the common flow regimes and governing physical mechanisms.

Chapter 3 critically reviews the current commercially available techniques for measurement and visualisation of slurry flow and highlights the limitations associated with each mentioned technique. The current status of the Electrical Resistance Tomography is also discussed along with its applications in various engineering field.

Chapter 4 describes the experimental methodology and the strategy used to carry out each experiment. The test facility and the equipments used are also highlighted in this chapter along with the instrumentations used for measurement of the desired parameters. The calibration procedure of the instrumentations are detailed and the results are illustrated quantitatively.

Chapter 5 contains a bulk of experimental findings and observations concerning the measurement of horizontal and upward vertical slurry flow. The measurement results cover various integral flow characteristics (slurry velocity, pressure, special concentration, solids axial velocity, delivered solids concentration and slurry volumetric flow rate) and local flow characteristics (local solids concentration, solids concentration profile, mean solids axial velocity, solids axial velocity distribution, liquid volumetric flow rate, and solids volumetric flow rate). An analysis of horizontal stratified flow is also reported in this chapter. An evaluation of each estimated parameter is summarised.

Chapter 6 discusses the design and erection of a multiphase inclinable flow system with focusing on main design requirement for settling slurry flow. Various design procedures are described and the selection criteria for the associated instrumentations are enclosed. The design of the inclinable table and the most suitable lifting method is also detailed in this chapter.

Chapter 7 Develops a novel technique for recognition of common flow regimes encountered in horizontal flow using statistical analysis of the ERT signal. The evaluation of the proposed recognition scheme is presented with summarising the overall success rate in recognising each flow regime.

Chapter 8 Draws the conclusions of each finding and observation with a summary of the contribution from the present work. This chapter ends with highlighting the future directions and recommendation for further studies in slurry measurement, visualisation and characterisation.

Chapter 2
Hydraulic transport of solid particles in pipeline

In this chapter the literature and previous work on slurry flow is critically reviewed, with considering different pipe configuration, horizontal, vertical and inclined. The common four flow regimes are described, along with the techniques used to recognise these regimes, by the previous investigators. The boundary between the flow regimes are also detailed with the physical mechanisms governing settling slurry flow.

2.1 Introduction

Settling slurry flow in pipeline is encountered in many industries such as energy, chemical, pharmaceutical, petroleum, wastewater processing and mining industry. It is worth mentioning that in some specific applications, such as dredging, hydraulic transport is the only mean of transportation of solids through pipelines. These mixtures are transported through different pipeline orientations, mainly horizontal and vertical. Settling slurry flow is a very complex and has attracted considerable attention of many investigators across the world. A wide range of experimental results have been reported in literature including different operating conditions, material type, shape and different flow orientations (Newitt *et al.*, 1955; Newitt *et al.*, 1961; Wasp *et al.*, 1970; Roco and Shook, 1984; Bartosik, 1996; Gillies and Shook, 2000; Hong *et al.*, 2002; Barigoua *et al.*, 2003; Pachowko *et al.*, 2004; Pohlman *et al.*, 2006; Divoux and Geminard, 2007; Pougatch and Sacudean, 2008; Matousek, 2009; Munir, 2011).

In horizontal flow as the gravity acts at right angle to the flow, the separation of phases occurs and gives rise to several flow regimes, pseudo-homogeneous, heterogeneous, moving bed and stationary bed. Similar flow regimes are encountered in inclined flow with occurrence of backflow (Doron *et al.*, 1997; Matousek, 2002; Yamaguchi *et al.*, 2011). Each flow regime is described in the following sections and has been the subject of many studies in literature such as (Wilson and Pugh, 1988; Gillies *et al.*, 1991; Doron and Barnea, 1993; Brown, 1991). Whereas in vertical flow, especially upward flow, the gravity acts counter to the dynamic forces, as a result the slippage of the phases occurs (Shook and Bartosik,1994; Parvareh *et al.*, 2010). The occurrence of separation and slippage of the constituent phases in settling

solid-liquid flow in pipeline configuration makes the flow unpredictable and time dependent. Therefore it is paramount for the operator of these pipelines to monitor and measure the flow continuously, particularly from the local point of view, i.e. the knowledge of internal structure of flow is necessary, so as to ensure safe transport and maintaining acceptable control limits.

This chapter highlights the previous work of others carried out within the past years and critically review the knowledge gained from them. The phenomenon of slurry flow in different pipe configurations (horizontal, vertical and inclined) will be described, with particular attention to horizontal and vertical flow. Since the distinction of flow regimes is very important for flow measurement, design, maintaining control limits and economical transport, then it will be covered along with transitional velocities. Also, in order to understand the behaviour of settling slurry flow and evaluate the accuracy and reliability of an instrument, especially those are used for measurement of local flow parameters, this chapter covers the stratification phenomenon, particle deposition velocity, pressure drop and physical mechanisms governing settling slurry flow. One of the most important parameters of slurry flow is the recognition of flow regimes, especially for the purpose of metering (i.e. for flow regime dependent flow meters), therefore, the last sections highlight the importance of flow regime recognition in general and critically review the techniques proposed by previous researchers in the field.

2.2 Slurry flow in pipelines

Slurry is a mixture of solid particles in a carrier liquid. The carrier liquid may be water, Newtonian or non-Newtonian liquid. However, the carrier liquid used in the vast majority of slurry flows is water. The hydraulic transport of solid particles in pipes is widely used in many industrial applications, such as chemical and mining industry. The aim of transporting these solids is either for transporting of bulk solids or physical/chemical processes between the carrier liquid and solids (Xia *et al.*, 2004; Wilson *et al.*, 2006). As previously mentioned, slurries are classified into two categories, settling and non-settling, however, this research deals only with settling slurries and no reference will be made to non-settling slurries.

The large number and range of variables in slurry flow in pipelines influences the behaviour of slurry flow and makes it very complex. These variables are pipeline configuration (horizontal, vertical and inclined), solid particle size, solids shape, solids density, liquids density, liquids viscosity, mean slurry

velocity, pipe diameter and flow direction (ascending or descending flow). It is worth mentioning that the occurrence of such a large number of variables can affect slurry metering and optimisation of slurry flow meters become very difficult and variable dependent. For example, as the ERT is flow regime dependent (Pachowko, 2004), then occurrence of these flow regimes in horizontal slurry flow creates a challenge in measurement of dispersed flow.

It is apparent that most of industrial applications employ horizontal pipe configuration for transportation of solid materials. However, vertical pipe configuration is also paramount for many industries such as mining, (Munir, 2011). Although it can be argued that most of pipe configurations are horizontal and vertical, which are connected through elbows and fittings, inclined flow can also play an important role for certain long distance overland pipeline, thickener feed systems, pump box feed systems etc. (Abulnaga, 2002). Therefore, this chapter gives a description over the behaviour of slurry flow in each pie configuration. In horizontal and inclined pipes, gravity tends to stratify the mixture and split it into two distinct layers, the solid particles at the bottom of the pipe and the carrier liquid at the top. On the other hand, in vertical pipes, the flow conditions are straight forward, without deposition of solid particles on the pipe invert. Since horizontal flow makes the majority of the pipelines and the gravity in this flow orientation plays an important role for creation of several flow regimes, therefore, a large portion of the chapter is devoted to horizontal flow rather than the other two flow orientations.

2.3 Horizontal flow

Flow of settling slurry in horizontal pipeline is complex and has been the subject of a vast number of studies from the early work of Blatch (1906), Howard (1939), Durand (1952), Durand and Condolios (1953), Newitt *et al.* (1955) and many others. The vast majority of literature devoted to pressure drop, mixture velocity and critical velocity, friction characteristics, visualisation and behaviour of solid particles within the carrier liquid, determination of the internal structure of slurry flow via solids concentration and solids velocity. The complexity of this type of flow is due to the influence of gravity, which gives rise to different flow regimes from pseudo-homogenous at high velocity to stationary bed and blockage at low slurry velocity. The emergence of these flow regimes, which are sometimes called flow patterns in literature, affects the pressure drop and influences pipe wear

and other performance characteristics. This suggests that settling slurry flow suffers from flow discontinuity, due to the occurrence of these flow regimes, thus affects the flow meters, which are flow regimes dependent. Therefore, a description of each individual flow regime is presented in the following sections, along with the effects of each flow regime on each flow parameter.

2.3.1 Slurry flow regimes

Flow regimes are normally described in terms of the distribution of solids within the cross-section of the pipeline. In other words, they can be used to describe the motion of the particles in horizontal or near horizontal slurry flow, often based on visual observation and have been the subject of numerous experimental studies, (Durand and Condolios, 1952; Matousek, 2009; Doron *et al.*, 1997; Matousek, 2002; Parvareh *et al*., 2010; Brown, 1991; Giguère *et al.*, 2008).

Since the settling slurry flow is very complex and the determination of a certain flow regime relies mostly on visual inspection, the literature has shown different names and definitions to certain regime. Durand (1952) conducted the initial study on horizontal slurry flow regimes, in which he classified the slurry flow in horizontal pipes into “non-deposit flow regime” and a “regime with deposits” based on the specific gravity of the particles used in the investigation. In (1963) the same classification was used by Condolios and Chapus. However, this classification was refined, based on the relationship between the particle size, concentration and deposition velocity, by Newitt *et al.* (1955), Ellis and Round (1963), Thomas (1964), Shen *et al.* (1970) and Wicks (1971). It is important to note that the term “saltation”, referred to as a “moving bed”, was incorporated into the classifications of flow regimes by Bain and Bonnington (1970). One of the most common classification was done by Vocaldo and Charles (1972) and Parzonka *et al.* (1981), who classified the slurry flow regimes into four main categories, “homogeneous flow”, “heterogeneous flow”, heterogeneous and sliding bed flow” and “ saltation and stationary bed flow” (Doron and Barnea, 1996). While some investigators have refined the classification into further categories, such as Lazarus and Neilson (1978), who classified slurry flow patterns into “homogeneous flow”, “pseudo-homogeneous flow”, “heterogeneous flow”, “fully moving bed” and “stationary bed”. Then Ercolani *et al.* (1979) attempted to show the form and outline of “pseudo-homogeneous flow”, “heterogeneous flow”, “limit deposit condition”, “moving-stationary bed”, “moving dunes” and “stationary bed”. Some other works have been reported in the literature regarding slurry flow regimes in

horizontal pipe, such as Govier and Aziz (1972), who categorised slurry flow regimes based on the particle size, as shown in Table 2.1.

Table 2.1 Flow regime classification by Govier and Aziz based on particle size.

Particle name	Particle size	Predicted flow pattern
Ultra fine	d_p<10μm	Fully suspended, (gravitational force negligible).
Fine	10μm <d_p<100μm	Usually fully suspended, (subject to concentration and gravitational force).
Medium size	100μm <d_p<1000μm	Move with a deposit at the bottom with a concentration gradient.
Coarse	1000μm <d_p<10000μm	Rarely fully suspended and a deposit is formed at the bottom of the pipe.
Ultra coarse	d_p>10mm	Particles transported as a moving bed at the bottom of the pipe.

However, based on the refined classification of settling slurry flow regimes, there are four main flow regimes in a slurry flow through a horizontal and inclined pipe, based on solids volume fraction and particle size, as shown in Figures 2.1 and 2.2 respectively:

1. Pseudo-homogeneous or homogeneous with all solids in suspension.
2. Heterogeneous with all solids in suspension.
3. Moving bed and saltation (with or without suspension).
4. Stationary bed.

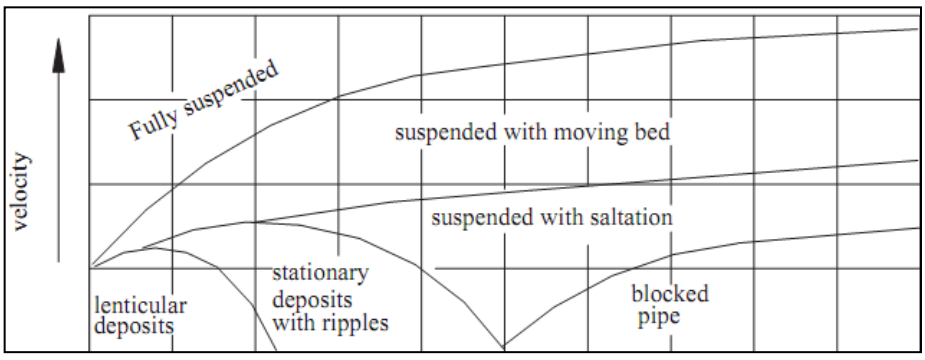

Figure 2.1 Flow regimes in a horizontal pipe in terms of velocity versus concentration (Newitt *et al.*, 1955)

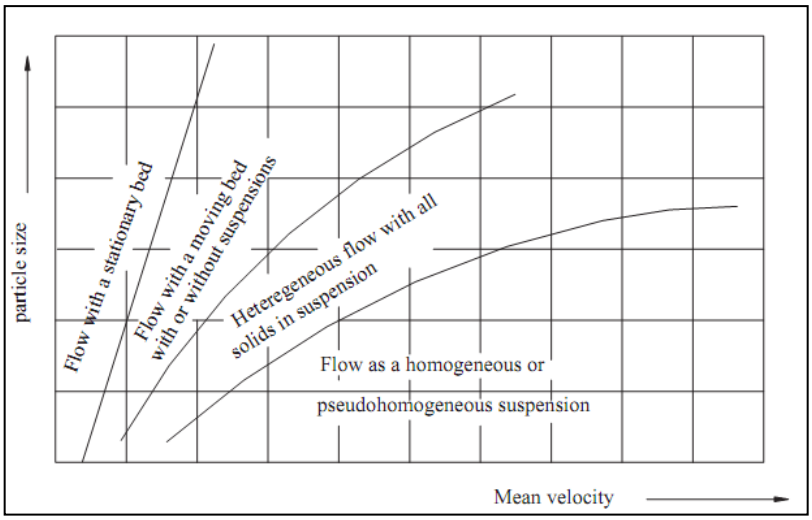

Figure 2.2: Flow regimes in a horizontal pipe in terms of particle size versus mean velocity (Shen *et al.*, 1970)

The characterisation of the above four main flow regimes is crucial for design, optimisation and the control of processes involving slurry flow. Therefore, each regime will be explained individually in this chapter. Every flow regime is summarised by a schematic diagram of particle distribution within the vertical plane of the horizontal pipe, typical solids concentration profile and typical solids axial velocity profile. The author has summarised each flow regime, based on existing literature, as a schematic representation of solids flow within the pipeline.

2.3.1.1 Homogeneous flow regime

This type of flow is considered as fully suspended flow regime, usually at high velocities well above that used commercially for such slurry (say 3.5 m/s or above) (Brown and Heywood, 1991; Pashowko, 2004). The investigators, such as Thomas (1964), Doron and Barnea (1993), Govier and Aziz (1972), have used different terms for this type of flow pattern, Pseudo-homogeneous, homogeneous or symmetric flow regime. However, there is a slight difference between homogeneous and pseudo-homogeneous flow regime. When the solid particles are distributed evenly across the pipe cross section, the flow is homogeneous. Whereas when the solid particles approach even distribution, the flow is referred to as pseudo-homogeneous or quasi-homogeneous. It is important to note that the true homogeneous flow rarely occur in settling slurries. However, the true homogeneous flow can easily occur in non-settling slurries, where the solid

particles are equally distributed between the top and the bottom half of the pipe. Ideally, in homogeneous (or pseudo-homogeneous) flow regime, solids concentration gradient and solids velocity gradient across the pipe cross-section is absent. As the flow is single phased and generally observed as a vertical line. Therefore, Newitt *et al.* (1955) used the equivalent fluid model for this type of flow. The schematic presentation of this type of flow regime, along with typical solids volumetric concentration profile and solids axial velocity profile is summarised as shown in Figure 2.3. This type of flow is typical of the fine particles, which are all suspended in the carrier fluid and the slurry property approaches that of a single fluid.

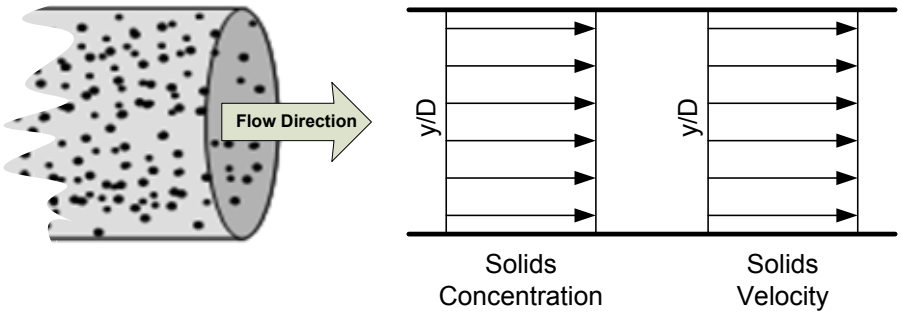

Figure 2.3 Schematic presentation of fully suspended flow regime and solids concentration and velocity profile

2.3.1.2 Heterogeneous flow regime

This regime is the most complex flow regime, as the solid particles are not evenly mixed in the horizontal plane and a gradient of solid concentration and solids axial velocity exists in the vertical plane, as summarised in Figure 2.4. Some particles are suspended and supported by fluid turbulence at the top half of the pipe, particularly the finer ones, and the coarser once either suspended at the bottom half of the pipe, which is referred to as intermediate flow regimes, or may be present in the form of a bed. This phenomenon is due to occurrence of minimum hydraulic gradient, as the superficial velocity of the settling velocity is reduced (Brown and Heywood, 1991). Wasp *et al.* (1977) found through experiments that in heterogeneous flow the solids have lower concentration and larger particle size compared to homogeneous flow. Also, Shook and Roco (1991) noted in heterogeneous flow that the deposition velocity depends on the particle size, particle density, solids concentration and the pipe diameter. Heterogeneous flows require a minimum carrier velocity, which casually referred to as the critical velocity. Heterogeneous flows are encountered in many industries such as mining and dredging applications (Wilson *et al.*, 2006).

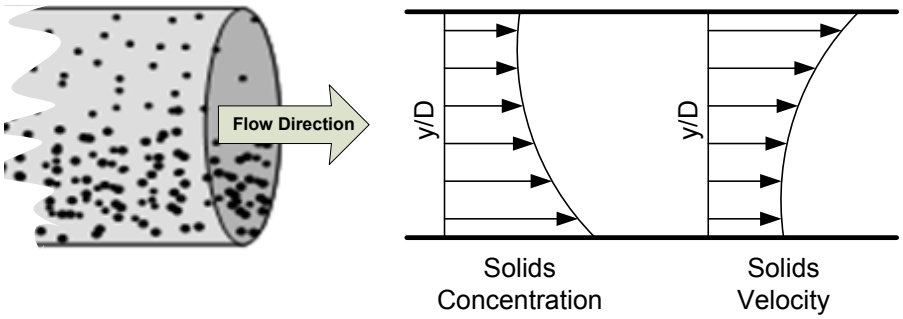

Figure 2.4 Schematic presentation of heterogeneous flow regime and solids concentration and velocity profile

2.3.1.3 Moving bed flow regime

In this type of flow regime, when the flow rate is low and a large number of coarse particles exist, the larger particles tend to accumulate at the bottom of the pipe and form a packed layer, which is referred to as bed. The bed moves along the bottom of the pipe like desert sand dunes, which is described by Sinclair (1962) as motion of the bed. The accumulated packed layer also called longitudinal waves by Thomas (1964). Many terms and definitions for this type of flow regime have been seen in literature, e.g. saltation flow (i.e. the fluid above the bed tends to move the finer solid particles by entrainment) by Turian and Yuan (1977) and two layer flow/moving bed by Lazarus and Nilson (1978). According to Ercolani *et al.* (1979) the upper layers of the bed move faster than the lower layers in a horizontal pipe. This is due to the difference in sizes and settling velocities of the solid particles forming the bed. The concentration of this layer corresponds to maximum, while the upper part of the pipe still contains a heterogeneous mixture, as summarised in Figure 2.5.

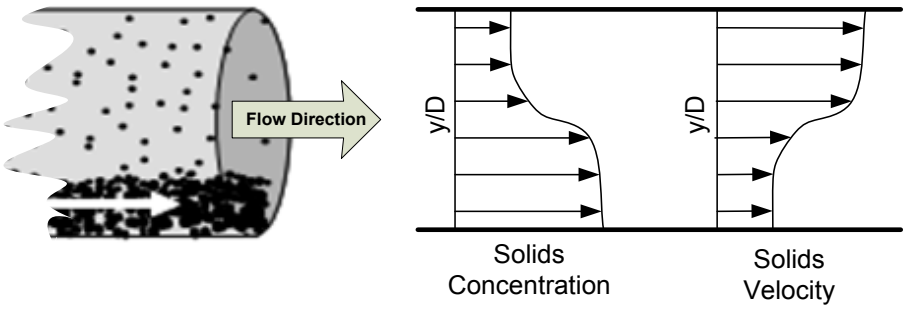

Figure 2.5 Schematic presentation of moving bed flow regime and solids concentration and velocity profile

2.3.1.4 Stationary bed flow regime

As the mean slurry velocity is decreased, which unable to move all immersed particles, particularly the coarser ones, which have highest settling velocity, settle and build up the bed, whilst the lowest settling velocity particles are suspended asymmetrically. As the mean velocity drops even further, the required suspension force reduces and the bed thickens, as a result the lower layer of particles that is in contact with the pipe becomes stationary, as summarised in Figure 2.6. However, the fluid above the bed tends to move the finer solid particles by entrainment. This phenomenon is known as saltation, where dune-like forms on the upper part of the bed could be observed. In other words, the finer solid particles occupying the upper part of the bed tend to roll and tumble. Flow with saltation and asymmetric suspension occur just above the speed of blockage. Therefore, further reduction in the flow rate, increases the pressure drop quite high that is impossible to maintain the flow and as a consequence the pipe blocks up (Wilson *et al.*, 2006, Matousek, 2005). According to Cartens (1969) and Govier and Aziz (1972) an asymmetric suspension above the bed could be maintained by decreasing the pipe diameter, which increases the mean velocity of the slurry.

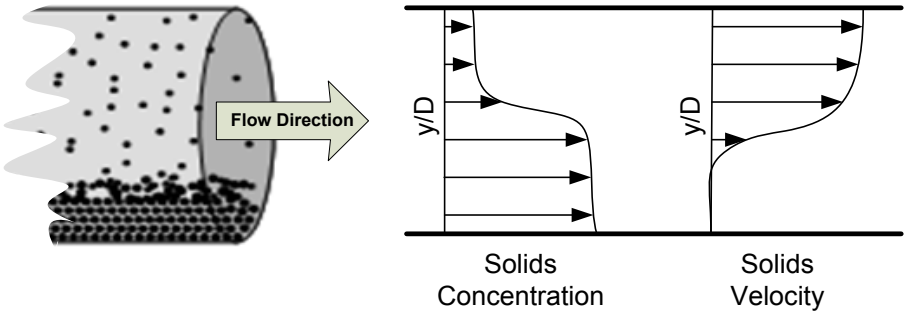

Figure 2.6 Schematic presentation of stationary bed flow regime and solids concentration and velocity profile

2.3.2 Transition velocities

The transition velocities are the boundaries that split the four distinctive flow regimes described above. This is based on photographic evidences observed in the literature, at any solid's concentration and mixture velocity (Abulnaga, 2002; Pachowko, 2004). The transition and boundaries between horizontal (or inclined) flow regimes are generally presented via a plot of the pressure gradient versus mean velocity of the slurry. Figure 2.7 showing the typical plot of the pressure gradient versus mean mixture velocity, where the

main four flow regimes can be presented. Normally, the definition of transition velocities depends on the definition of the flow regime. Therefore, the terminology for the transition velocities is quite confusing. According to Abulnaga (2002) and Pachowko (2004) the transition velocities can be defined as explained below:

1. **V_1**: The velocity at or above which the bed at the lower half of the pipe is stationary. However, at the upper half of the pipe, some solid particles may move either by saltation or suspension. It is important to mention that little work has been carried out within the boundary of this flow regime, and that is due to the fact that the risk of blockage is dominant in this region.
2. **V_2**: The velocity at or above which the solid particles are transported by suspension at the upper half of the pipe and the coarser particles forming a moving bed.
3. **V_3**: The velocity at or above which all solid particles are transported in asymmetric suspended form.
4. **V_4**: The velocity at or above which all solid particles are fully suspended and transported as a symmetric suspension.

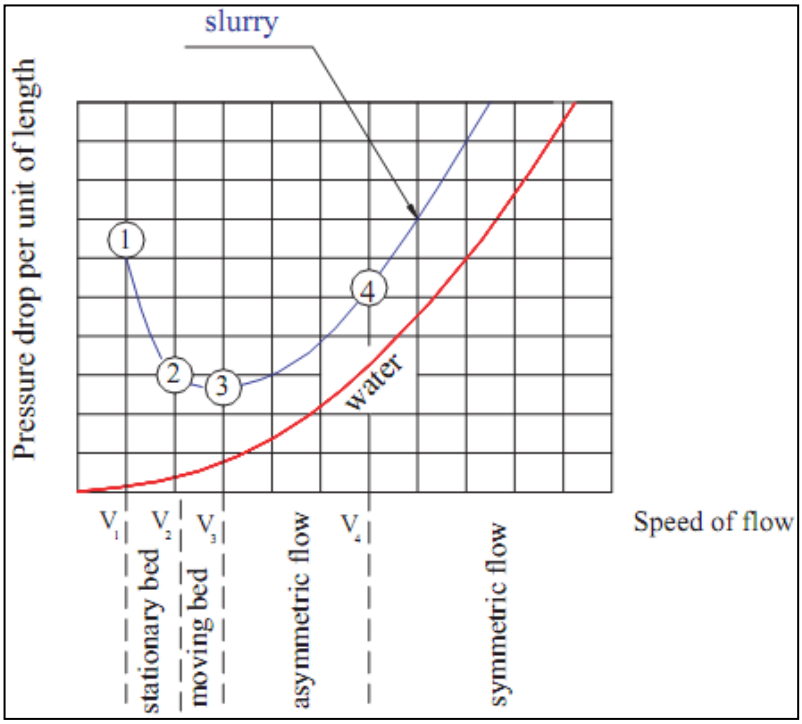

Figure 2.7 Showing transitional velocities on a typical plot of the pressure gradient versus mean mixture velocity (Abulnaga, 2002)

It is important to note that there are many and different definitions in the literature for V_3, as a result this creates a great confusion. Zandi and Govatos (1967); Vocadlo and Charles (1972); Ercolani *et al.*(1979); Oroskar and Turian (1980); Davies (1987) and Turian *et al.* (1987) used the term "Critical Velocity", which was defined by them as the velocity below which deposited particles exist. Whilst Bain and Bonnington (1970); Stevens and Charles (1972); Kazanskij (1979), Graf *et al.* (1970), Doron and Barnea (1996) used this transition velocity as "Critical Deposit Velocity", which was defined as the transition velocity between deposit and non-deposit flow regime. "Deposition Velocity" was used by Shook and Roco (1991) and they defined it as the limit velocity at which the stationary bed is formed. In addition, "Deposit Velocity" was used by Parzonka *et al.* (1981) and Wood (1979), who used the same definition as that of Shook and Roco (1991). In some other cases the term "Limit Deposit Velocity" was employed by Wilson *et al.* (1972).

However, despite the fact that different terminologies used for this transition velocity, the prevention of this minimum velocity is necessary to avoid partial pipe blockage, which affects the efficiency of pipeline operation and enhances pipe wear.

2.3.3 Available models to determine transition velocities

The transitional velocities could be calculated via the correlations found in the literature Govier and Aziz (1972); Shook and Roco (1991); Abulnaga (2002) and Wilson *et al.* (2006). It was also found that the limit deposit velocity has been the most investigated, as it plays an important role in the design of slurry pipeline.

The transitional velocity V_1 is mostly interesting in research and it is obviously not used in the operation of slurry line, as it is associated with pipe blockage.

While the transitional velocity V_2 can be used to determine the height of the bed and derivation of the stratification ratio. Normally, pressure measurements of the pressure gradient are used to determine the transition velocity V_2 calculated from the pressure measurements of the pressure gradient. Wilson (1970) developed a model for the early motion of solid particles at the velocity V_2. He assumed that a hydrostatic pressure is influenced by the solid particles on the pipe wall, and then he proposed the following equation:

$$\frac{1}{\rho_L}\left(\frac{\Delta P}{L}\right)\left[\frac{\theta - \sin\cos\theta}{4} + \frac{R_w}{D_i}\left(\sin\theta - \frac{\theta\lambda_s}{\tan\phi_r}\right)\right] = \frac{\lambda_s\,(s-1)C_{vb}\,(\sin\theta - \cos\theta)g}{2} \tag{2.1}$$

The transitional velocity V_3, or sometimes called deposition velocity (V_D) or critical velocity (V_c), is extremely important, as the pressure gradient is at the minimum. In other words, it is the minimum slurry velocity that is required to prevent the formation of the bed on the pipe invert and pipe blockage. The knowledge and study of this transitional velocity is very important for the design and operation of the slurry pipeline. Therefore, a detailed review of the literature regarding the works has been conducted on this transitional velocity will be carried out.

According to Vocaldo and Charles (1972) the operating velocity in settling slurry transport in horizontal pipes should be 1.3 times greater than the critical velocity. Wilson (1942) claims that this transitional or critical velocity occurs at minimum pressure gradient, as shown in equation 2.2, which is the first equation of critical velocity and gathers some important parameters of the system, such as pipe diameter, solids concentration and particle density. Then Wilson (1945) brought another idea that the critical velocity occurs just before the pipe blocks, which is not necessarily true.

$$V_c = \frac{\left(K_p S C_v g D V_t\right)^{1/3}}{1 + C_v(S-1)} \tag{2.2}$$

Durand (1952) and Durand and Condolios (1953) conducted a massive investigation on the critical velocity and derived a correlation for uniformly sized sand and gravel, which is shown in equation 2.3.

$$V_D = V_3 = F_L\left\{2gD_i\left[\frac{(\rho_s - \rho_L)}{\rho_L}\right]\right\}^{1/2} \tag{2.3}$$

However, there is a limitation to Durand's correlation, and that is due to Durand's velocity factor FL, which can be determined by a graph, Durand's velocity factor versus particle size, for single or narrow graded particles. Since most slurry contain a mixture of different size particles, Durand's velocity factor has been refined and modified by a number of authors, such

as Wasp *et al.* (1977), who represented the critical velocity in terms of modified factor F'L including a ratio between the particle diameter and the pipeline diameter , as shown in equation 2.4.

$$V_D = V_3 = F_L' \left[2gD_i \frac{\rho_s - \rho_L}{\rho_L}\right]^{1/2} \left[\frac{d_p}{D_i}\right]^{1/6} \quad (2.4)$$

Moreover, Spells (1955) conducted a study, where he used fine particulate slurry in horizontal pipe and developed a correlation to determine the critical velocity, which he called minimum velocity, in terms of particle size, solid and liquid density, slurry density and pipe diameter, as shown in equation 2.5. He also defined the critical velocity as the minimum velocity required to prevent the deposition of the particles at the bottom of the pipe.

$$V_C^{1.225} = 0.0251 g d_{85} \left[\frac{D\rho_m}{\mu_l}\right]^{0.775} (S - 1) \quad (2.5)$$

Spells equation 2.5 created a great confusion regarding the particle size, which was presented as d85, as a result it was believed that the correlation is only applicable to a narrow range of slurry Reynolds number, but d85 could represent colloidal range or coarse particles. Despite the fact that Smith (1955) recommended that in pressure and critical velocity correlations the particle size should be represented by weighted mean diameter.

Newitt *et al.* (1955) developed a correlation for the transitional velocity V_3 between heterogeneous flow regime and moving bed (saltation), or critical velocity, in terms of terminal velocity of particles, as shown in equation 2.6.

$$V_3 = 17V_t \quad (2.6)$$

It can be noticed that Newitt's equation is very simple, although it was used as the basis for developing many models, such as that of Cairns *et al.* (1960), as shown in equation 2.7, which is applicable to particle size between 242 μm and 380 μm at low solids concentration, specific gravity up to 2.6 and pipe diameter not more than 50 mm.

$$\frac{V_C^2}{gd_{50}} = 9.8\left[\frac{C_V D V_C \rho_l}{\mu_l}\right]^{0.3}(S-1)^{0.6} \tag{2.7}$$

The transition velocity V4, which demarcates the boundary between the two flow regimes Heterogeneous (asymmetric) and pseudo-homogeneous (symmetric), has also been investigated by some investigators, such as Newitt *et al.* (1955), Spells (1955), Govier and Aziz (1972). Newitt *et al.* (1955) developed a correlation, in which the transitional velocity V_4 is determined in terms of terminal velocity, as shown in equation 2.8.

$$V_4 = (1800 D_i V_t)^{1/3} \tag{2.8}$$

Whilst Govier and Aziz (1972) improved Newitt's correlation by applying Newton's law and rewrote the equation in terms of drag coefficient (C_D), which is 0.44 according to Newton's law, as shown in equation 2.9.

$$V_4 = 38.7 D_i^{\frac{1}{3}} \frac{4gd_p}{3C_D}(S-1)^{\frac{1}{6}} \tag{2.9}$$

Goniewr and Aziz (1972) also derived equation 2.10 by analysing the work of Spells (1955), which was done on solid particles with a diameter between 80 μm and 800 μm (mesh 180<dp<20).

$$V_4 = 134 C_D^{0.816} D_i^{0.633} V_t^{1.63} \tag{2.10}$$

It is important to take the notice that the above correlations for the transitional velocities, between heterogeneous and pseudo-homogenous flow patterns, ignore the influence of solid's concentration, but rather provide order of magnitude of V_4.

The transitional velocities have not only been investigated in a horizontal pipes, but also in pipe bends, such as the one of Giguère *et al.* (2009), who studied the influence of pipe bend between the downward and horizontal flows on the transitional velocities between slurry flow regimes and introduced fantastic results. Their measurements indicated that flow is homogeneous directly after the bend outlet and that the transition velocities

decreased after the bend outlet. This indicates that the slurry velocity decreases after the bend, which in itself decreases the transition velocity and the distance where these transition occur. They also concluded that the solid's concentration can influence these transitions, whilst there is little effect of high concentration on the transitions on downward bend.

2.3.4 Pressure drop in slurry pipeline

Pressure drop, or sometimes known as pressure gradient or hydraulic gradient, is the most important parameter for slurry transport in mineral and many industries handling solid-liquid flows. Since the pressure drop influences the power consumption and the whole economics of the slurry transport, therefore the slurry pipeline design is based on optimisation of pressure drop (Lahiri, 2009).

The first real equation, for calculating the pressure drop was first generated by Howard (1939), who used his data in combination with that of Blatch (1906) and Hazen and Hardy (1906). Equation 2.11 shows Howard's equation, which he used for calculating the head loss:

$$i_m = mV^x \tag{2.11}$$

However, his equation was not taken as a universal equation that could apply to other systems. Wilson (1942) came and divided the pressure drop into two components, pressure drop due to fluid along and pressure drop due existence of the solid particles.

In addition, numerous investigators, such as Wilson (1942); Durand and Condolios (1952); Shook and Daniel (1969); Turian and Yuan (1977); Wasp *et al.* (1977); Gillies *et al.* (1999); Kaushal and Tomita (2002) and Lahiri (2009), have attempted and proposed many empirical, semi-theoretical and theoretical correlations related to the pressure drop along with some other flow parameters, such as solid's density, liquid's density, particle size, solid's concentration, solid's velocity, pipe diameter and slurry viscosity. However, these correlations are associated with some rate of error, as shown in Table 2.2 in terms of Average Absolute Relative Error (AARE). Nevertheless, a considerable reduction in the prediction error can be noticed.

Table 2.2 Performance of difference correlations for pressure drop (Lahiri, 2009)

Authors	AARE (%)
Wilson (1942)	49.51
Durand and Condolios (1953)	36.53
Newitt *et al.* (1955)	93.43
Zandi and Govatos (1967)	50.02
Shook and Daniel (1969)	34.50
Turian and Yuan (1977)	39.97
Wasp *et al.* (1977)	26.68
Gillies *et al.* (1999)	22.31
Kaushal *et al.* (2002)	22.01
Lahiri (2009)	12.70

Pressure drop is different from one orientation to another, for example pressure drop in horizontal flow is slightly different to that in vertical flow or inclined flow. In horizontal flow the total pressure drop is composed mainly of frictional energy dissipation, whereas in vertical flow is due to static head contribution. In a straight horizontal pipeline, without any pipe fittings or joints, which is the source of energy dissipation, the pressure drop along the tested pipeline length is equal to the pressure drop due to friction. In other words, the total pressure drop in the mixture flow is due to both frictional head losses, carrying liquid and presence of solid particles (Matousek, 2002). It is worth to mention that the presence of solid particles, especially the coarser ones with greater density, increases the overall pressure drop. On the other hand, if the same horizontal pipe section is inclined, the total pressure drop changes significantly. The change in the total pressure reflects considerably in both inclined flow directions, ascending and descending. Relative to horizontal flow in the same section, the total pressure drop increases in the ascending flow and decreases in the descending flow. This change in the total pressure is due to hydrostatic pressure drop as a result of a change of a geodetic position of one end of the pipe section relative to the other end, Matousek (2002).

2.3.5 Physical mechanisms governing settling slurry flow

When solid particles in a carrier liquid is transported within a pipe, they are acted upon by several forces, which are resulted from particle-particle interaction, particle-liquid interaction and particle-pipe wall interaction. The forces, which are resulted from particle-particle interaction, are transmitted as an inter-particle stress. However, when a granular bed is formed (i.e. the particles are in continuous contact), the Coulombic stress is created on the particles, while Bagnold stress is created on the surface of the granular bed as a result of sheared granular bed and the particles move in a sporadic fashion. On the other hand, the forces, which are resulted from particle-liquid interaction are buoyancy force, drag force and lift force, and if the carrier liquid is turbulent, then the turbulent diffusive force is generated (Bagnold, 1954; Wilson, 2006).

A settling slurry flow, in a horizontal or inclined pipe, normally tends to stratify. In other words, at the velocity used during the practical operations, the particle distribution across a pipe cross section is non-uniform. Under these circumstances the flow can be fully or partially stratified. If all solid particles form the granular bed (stationary or sliding), then the flow is fully stratified, and if a portion of the solid particles form the granular bed (where particles are virtually in permanent contact with each other) and the remaining particles are suspended within carrier fluid, then the flow is partially stratified.

The previous description of particle motion was explained by Bagnold (1956), who developed a concept that the solid particles are supported by two major physical mechanisms: fluid suspension and inter-granular contact. For the first mechanism, Wilson *et al.* (2002) observed that the particles are suspended in the carrier fluid is due to turbulent diffusion.

Obviously, settling slurries composed of fine and coarse particles. The friction behaviour of suspended coarse particles differs from that of fine particles. The suspended coarse particles interact with each other and the pipe wall. It is important to mention that the contact is not permanent, but rather sporadic, which is due to turbulent dispersive action and collision dispersive action. In other words, the solid particles are dispersed to all directions by turbulent eddies and also the particles are collided with the other particles of different velocities and impelled in the direction of the wall (Matousek, 2005; Wilson, 2006). According to Brown and Heywood (1991) the fluid suspension mechanism can come to play, when the velocity of

turbulent eddies is greater than the settling velocity and by further increasing the mean velocity the more solid particles is suspended by the fluid force.

In the case of fully stratified flow, it can be noted that the settling velocity of the solid particles is greater than the velocity of the turbulent eddies, therefore the particles fall and are supported by granular contact rather than fluid suspension. These particles are designated as contact load, in either cases stationary or moving bed (Wilson, 2006). The motion of the particles within the contact load can be analysed by applying the force balance, which was first used by Wilson (1970) and Wilson *et al.* (1972), then it was latter used to determine the limit deposition velocity for fully stratified flow.

2.3.6 Flow regime recognition

Since the settling slurry flow is a very complex flow and the coarser solid particles tend to settle and form a bed at the pipe invert, various flow regimes (or patterns) may occur, which depends on several parameters, such as solid's concentration, particle size, particle and liquid density, mixture velocity and pipe diameter. It is worth pointing out that the common four flow regimes, described in the previous sections, are mainly dependent on mean slurry velocity. Therefore, the recognition of these flow regimes, which would exist in the pipe, for any given set of operational condition, is very important for design and operation of pipeline conveying settling slurries. Also, since there are different pressure drop correlations for different flow regimes, it is significantly important to apply an appropriate pressure drop correlation for the given flow regime (Lahiri, 2009). Moreover, the recognition of these flow regimes is similarly essential for optimisation and correction of flow meters, which are flow regime dependent (such as ERT).

Over the years, since 1953, researchers have attempted to establish various methods to characterise and recognise the flow regimes encountered in the pipeline. Pressure drop measurement has been one of the most common methods that have been adopted to recognise flow regimes. Some of these researchers are Newitt *et al.* (1955), Doron and Barnea (1993, 1996), Doron *et al.* (1997), Gillies *et al.* (1999), Kaushal and Tomita (2002), Matousek (2002), Kaushal *et al.* (2005).

Another method has been used by some researchers, based on signal analysis, such as Albino *et al.* (2007). They have depended on different output signals, such as passive acoustic signals, to identify the occurring flow regimes.

A glance of the literature reveals that several correlations or techniques have been reported regarding the recognition of settling slurry flow regimes. However, it can be noticed that each of them more or less associated with some degree of limitations and cannot predict the prevailing flow regime over a wide of range of conditions, such as solids concentration, particle size, slurry velocity, pipe diameter and configuration etc. Therefore a novel technique is proposed in this study (Chapter 7), through which the prevailing flow regime is identified regardless the condition, in which the flow operates, such as physical properties, pipe diameter etc.

Usually the flow regimes are recognised by either subjective operator judgements, which is done by visual inspections, although in some cases an analysis of the spectral content is performed, where the desired information cannot be extracted visually (Abulnaga, 2002), or by objective indication by representing the boundaries between the flow regimes via flow regime maps. Early investigators, such as Newitt *et al.* (1955) and Durand and Condolios (1953) have carried out extensive studies to investigate the detailed features of the flow. Their results are often displayed in the form of flow regime maps. These flow regime maps represent the boundaries between various flow regimes under different conditions, though these boundaries are not distinctive lines, but rather poorly defined transition zones. The transition from one flow regime normally occurs, as the flow regime becomes unstable and causes transition (Brown and Heywood, 1991). However, there are limitations and problems with these flow regime maps that they are often dimensional and cannot be applied on a different operational condition. Despite the fact that some investigators have tried to generalise these flow regime maps, so they can be applied to different fluids and pipes of different sizes, but they could not achieve total generalisation, as most flow regime maps represent several transitions.

Turian and Yuan (1977) also have represented some flow regime maps in terms of mixture velocity and delivered concentration. Doron and Barnea (1993, 1995 and 1996) carried out an analysis as an extension of Doron *et al.* (1987) for the two layer model, where they employed three layer model (stationary bed, moving bed and heterogeneous mixture) for the drawing of flow regime maps, which is in term of slurry velocity versus solids velocity, as shown in Figure 2.8. It can be seen on the map that the two regimes, heterogeneous and pseudo-homogeneous, have not been distinguished, but rather explained only in one term “Fully suspension”. Their flow regime maps

used to represent the flow patterns and the effect of the operational variables on the transitional lines.

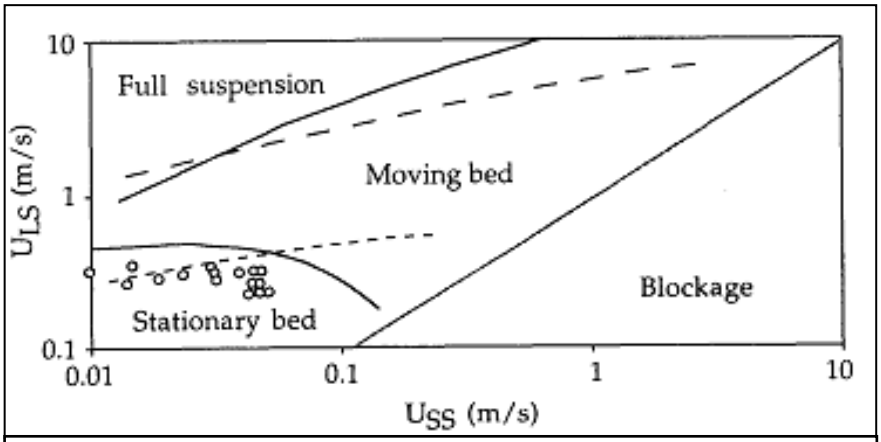

Figure 2.8 Superficial velocities flow pattern map (Taken from Doron and Barnea, 1996)

Albino *et al.* (2007) used an acoustic probe to determine the flow regimes in horizontal pneumatic transport of fine powders. The method was based on extracting the information, regarding the flow behaviour, by identification of specific frequencies. In other words, the strategy was based on determining the flow regimes using acoustic signals.

More recently, Giguère *et al.* (2008a) adopted a strategy to analyse slurry flow of regimes in pipes. The strategy is the direct interpretation of ERT measurement to identify homogeneous and heterogeneous flow without using image reconstruction. They used ERT to visualise slurry flows in horizontal and vertical pipe (up to 20% v/v and velocities up to 2.2 m/s). The solid concentration was estimated using direct resistance measurement. The slurry (mixture) used in the experiment consisted of tap water and non-conductive glass beads (of 100 μm in diameter and density of 2500 Kg/m3). Further experiments were carried out by Giguère *et al.* (2009), who used ERT and investigated the effect of pipe bend on the transitional velocities.

Besides, Lahiri (2009) has successfully applied Artificial neural Network (ANN), using Support Vector Machine (SVM) modelling to identify different flow regimes in a horizontal pipe, based on a data bank of 800 measurements in the literature. Lahiri's method has shown a great success and advantages, as there is no need to calculate some parameters, such as the drag co-efficient (C_D) and some empirical co-efficient, settling velocity and Froud number. The method is based on evaluating the flow regime using some basic flow data, such as pipe diameter, solid's concentration and fluid velocity. Then after evaluation the correct flow regime, an appropriate correlation can be used to determine the pressure drop. His method can deliver only 1.5% error, unlike Turian and Yuan (1977) correlation, where the delivered accuracy is 25% error.

2.4 Vertical slurry flow

As previously mentioned, in vertical slurry flow, no granular bed is formed and no dunes can be observed and it is rather straight forward flow. The solid particles are fully suspended with no component of the submerged particle acting on the pipe wall and tend to have a symmetrical distribution across the pipe cross-section, (Matousek, 2001; Clift & Clift, 1981, Munir, 2011, Wilson *et at*., 1979, Wilson, 2004). The force of the submerged particle is acting downward and resists the flow of particles. As a result the slip velocity occur between the solid particles and the carrier liquid. Normally, the difference between the mixture velocity and the velocity of the solid particles is smaller than hindered settling velocity of the solid particles. If the particles are less than 150 μm, then the whole mixture behaves as a liquid and The Equivalent Liquid Model can used for friction loss analysis (i.e. the flow can be considered as pseudo-homogeneous). However, if the particles are between (200 μm-2 mm), then these particles cannot directly exhibit the liquid like friction, as the particles are large enough and cannot be trapped within the laminar sub-layer. As a result, the particles migrate away from the pipe wall towards the centre of the pipe (Barigoua, 2003; Wilson, 2006).

Shook and Bartosik (1994) carried out an investigation on vertical slurry flow and claimed that the behaviour of solid particles to be due to Bagnold dispersive stress, which acts against the pipe wall. In the meantime, they concluded that, in vertical upward flow, the solids effect due to Bagnold stress for flowing medium sand can be negligible. On the other hand, for flowing coarse particle sand, the Bagnold stress on the pipe wall can be

generated as a result of mutual collision between the particles and the pipe wall, where the carrier liquid acts on the particles and repels them from the pipe wall due to liquid lift force. Also, Worster and Denny (1955) has investigated the aspect of pressure loss in vertical slurry flow and concluded that the solid particles does not affect the pressure loss due to hydraulic friction.

An earlier analysis of vertical slurry flow was carried out by Hagler (1956), who proposed a device (U-tube), which has been studied by several researchers such as Brook (1962), Clift and Clift (1981). The schematic drawing of the device is shown in Figure 2.9. It is worth mentioning that the analysis carried out by Clift and Clift assumed to be more complete than the others. The device is very simple and used for slurry flow rate measurement. It consists of two vertical tubes, ascending and a descending, with four elbows and a pair of pressure taps on each vertical line. The mean slurry velocities of both branches (upward and downward) are equal, thus the wall shear stress are also the same. Based on the analysis carried out by Clift and Clift (1981), the In-situ solids concentration is approaching the delivered solids concentration (i.e. their values are close, but not identical). However, they concluded that as the difference between both values is subtle and can be considered as negligible. Therefore, the delivered solids volume concentration can represent the in-situ solids volume concentration within a vertical pipe.

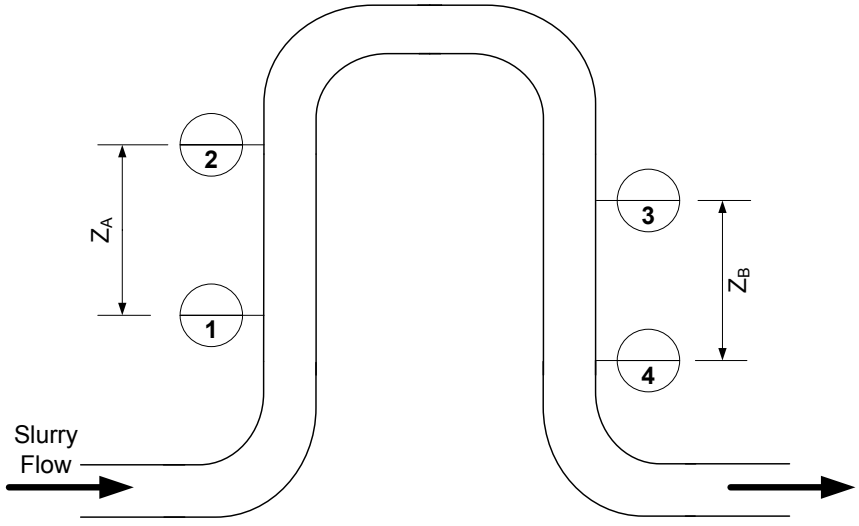

Figure 2.9 Inverted U-tube device for slurry flow rate measurement

2.5 Inclined slurry flow

The prediction of the flow characteristics is practically important in inclined pipes. Sometimes pipe inclination is unavoidable, especially for a long distance overland pipeline, due to naturally occurrence of dunes and hills. However, for any inclined pipeline design, the restriction in the inclination angle should be followed, which is minimisation of the inclination angle, particularly in inclined upward flow. This is due to the fact that both, pressure drop and deposition velocity are significantly affected by the angle of inclination (Doron and Barnea, 1997). As Wilson *et al.* (2006) indicate that, compared to horizontal flow, upward inclined flow tends to require higher velocities so as to avoid deposition velocities. In coarse particle flows this phenomena appears to be of greatest significant.

Despite the importance of inclined flow in pipelines, it can be noticed from literature that very little analysis have been attempted. One of the reasons is due to difficulty in building experimental facilities, since in a flow loop, where an inclined section is included, long pipes are required to investigate the fully developed flow (Doron and Barnea, 1997). Lucas et al., (1999), investigated the flow of plastic bead particles in an inclinable flow loop with 2.5 m test section. Although they achieved a good estimation of solids volume fraction and solids axial velocity, the scale of their facility could not represent an industrial scenario. Since an inclined pipeline section in industry consists of a large and long section, through which a murky slurry with particles of different sizes and shapes are flowing.

An experimental work was conducted by Matousek (1996), who showed a strong influence of pipe inclination on slurry flow stratification. He used a 150 mm diameter pipe with an inclination between -35° and +35° and four slurries, a medium sand, two coarse sands and a fine gravel. He employed a collimated beam of γ-rays to measure concentration profiles. He observed that the concentration profiles were blunter (less stratified) for rising inclinations and more stratified for descending inclinations, as shown in Figure 2.10. Through this, Matousek (1996) developed a two layer model for inclined pipes. The concept of two layer bipolar flow is depicted in Figure 2.11, and for further detailed analysis the reader is directed to (Matousek, 1996).

The fundamental equations for the two layers by Matousek are:

For the upper layer:

$$\frac{d(P-\rho_U gz)}{dx}=\frac{\tau_U WP_U+\tau_{UB}WP_{UB}}{A_U} \tag{2.12}$$

For the lower layer:

$$\frac{d(P-\rho_B gz)}{dx}=\frac{\tau_B WP_B-\tau_i WP_i+f_c\sum F_N\cos\gamma+F_W\sin\gamma}{A_B} \tag{2.13}$$

Fw is the submerged weight of the sediments in the lower layer.

The force balance for the whole pipe is then:

$$\frac{d(P-\rho_U gz)}{dx}=\frac{\tau_B WP_B+\tau_U WP_U+f_c\sum F_N\cos\gamma+F_W\sin\gamma}{A} \tag{2.14}$$

Matousek indicated that his approach was different to that of Shook and Roco (1991), who did not include the pipe axis component of the submerged weight (due to buoyancy) $F_W\,sin\,\gamma$. He also claimed that at pipe inclinations close to the angle of internal friction of the transport solids, the behaviour of solid particles was different for upward and downward inclination, where the solids have the same concentration and velocity. It was noted that the difference was significant with coarser particles than the finer ones and the deformation of the lower layer was due to the submerged weight of the solids at the bottom of the pipe.

Although the two layer model is very simple and can be applied to any set of operational conditions and its results are quite satisfactory, it is associated with some limitations, which lacks the ability to predict accurately the existence of stationary bed at low flow velocities.

In this case applying two-layer model for pressure drop can lead to unsatisfactory prediction due to reduced reliability of the model. As a result, Doron and Barnea (1993) in an attempt to solve this problem, introduced three-layer model, the concept of which is illustrated in Figure 2.12.

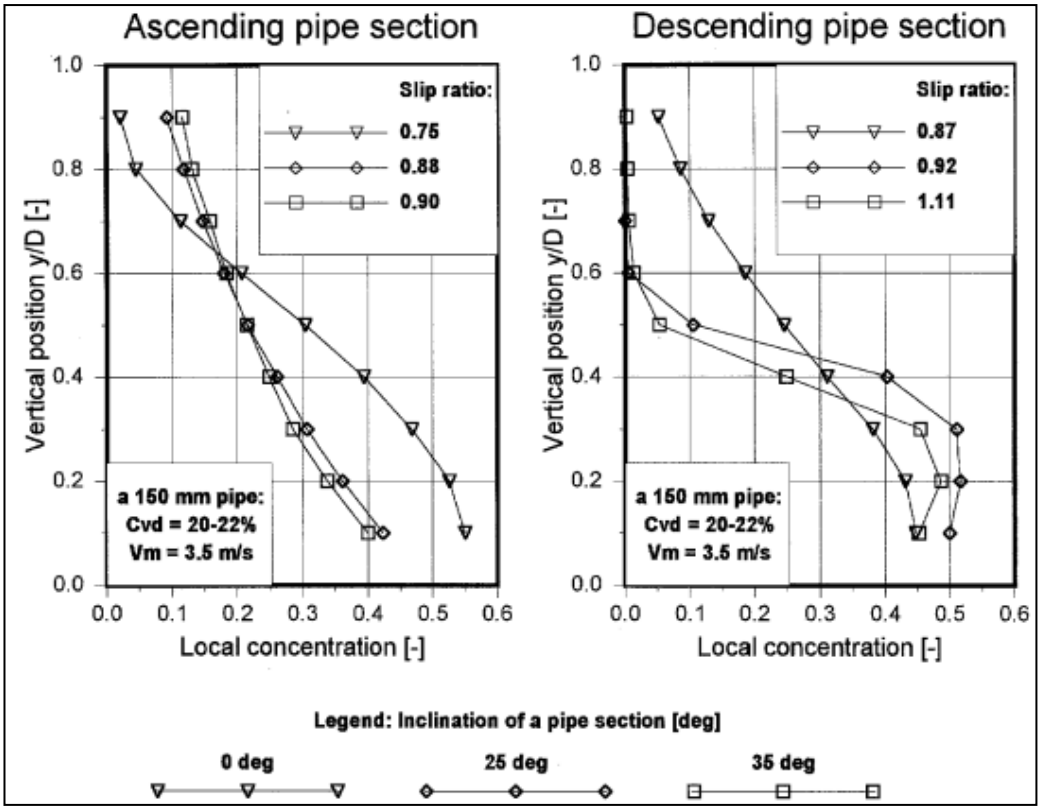

Figure 2.10 Concentration profile of ascending and descending inclined sand water flow at 3.5 m/s, (Matousek, 1996)

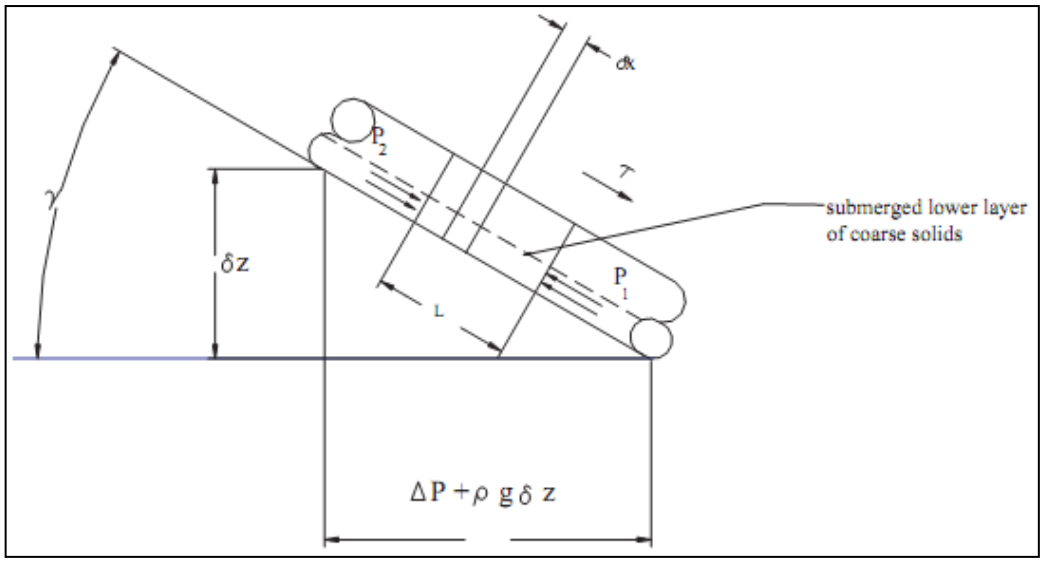

Figure 2.11 Concept of the two layer bipolar flow of slurry at an angle of inclination, (Abulnaga, 2002)

There are three flow regions in three-layer flow: a heterogeneous mixture at the top of moving bed, a moving bed above a stationary bed and a stationary bed over the pipe wall. However, as this thesis will not detail whole analysis

of three-layer model, therefore, for further detail of the model, the reader is referred to Doron and Barnea (1993).

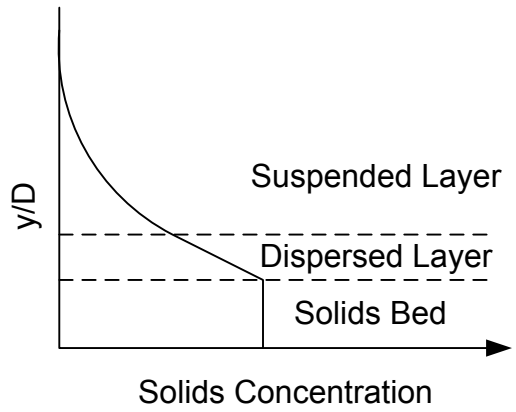

Figure 2.12 Assumed concentration profile in three layer model

Since both models assumes no slip velocity, , the author believes that both models are associated with serious limitations. As the solid particles tend to deposit at the bottom of the pipe and form a strata, then this suggests the existence of slip velocity between the two phases.

2.6 Deposition velocity in horizontal and inclined flow

As previously mentioned, the critical transition velocity (V_3) (or deposition velocity) in either horizontal or inclined flow defines the lowered of the range of desirable operating velocities. The great significance of coarse-particle flow in upward inclined pipeline is that, compared to horizontal configuration, it requires higher throughput velocities, so as to avoid deposition (Wilson, 2006).

Through an extensive literature survey, it was found that the approach of Wilson and Tse (1984) is a useful tool to estimate the deposition velocity in an inclined pipe. The concept of this method is based on estimating the deposition velocity for horizontal flow first, then extending the analysis to inclined pipes, based on the difference in Durand factor between the two configurations (horizontal and inclined). The deposition velocity for horizontal flow can be estimated from equation 2.4. Then if the analysis is extended for inclined flow, it is appropriate to present the deposition velocity or Durand factor F_L (or ΔD) and neglecting the ratio between the particle diameter and the pipeline diameter, as it is a very small value:

$$F_L = \frac{V_3}{\left[2gD_i \frac{\rho_s - \rho_L}{\rho_L}\right]^{1/2}} \tag{2.15}$$

From the above equation, it can be noticed that the Durand factor is proportionally related to the deposition velocity. In other words, The Durand factor increases with increase of deposition velocity. Comparing to horizontal flow, every increase in inclination angle would produce an increase in deposition velocity as well as Durand factor. Wilson & Tse (1984) establish a method to give adequate prediction of the change of deposition velocity for different angles of inclination. Figure 2.13 can be used for estimation of the difference in Durand factor (which is ΔD on the graph), plotted against the angle of inclination θ.

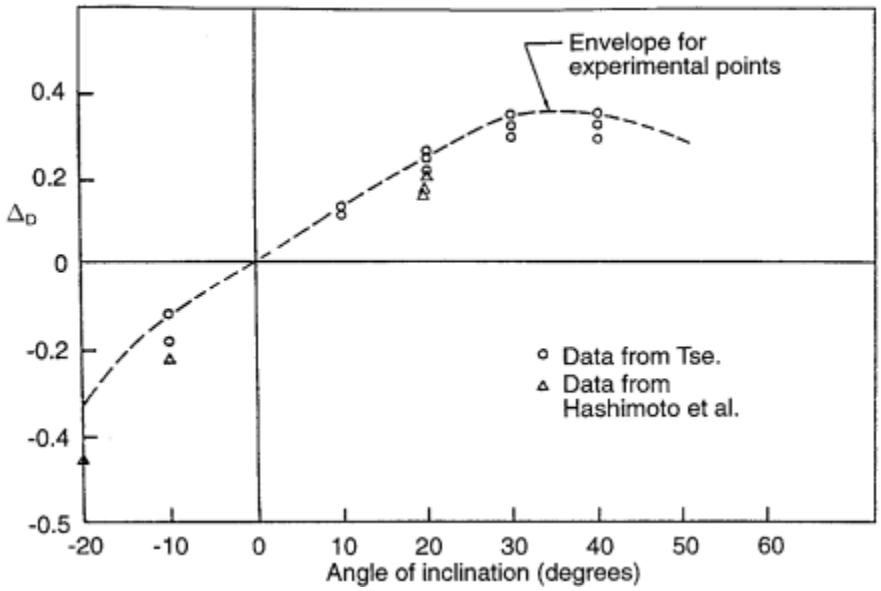

Figure 2.13 Effect of inclination angle on Durand deposition parameter, after Wilson & Tse (1984)

The deposition velocity is first estimated for horizontal flow, and then the difference in Durand factor ΔD can be obtained for the required angle θ. The difference in deposition velocity between the two configurations can be calculated using the following equation:

$$\Delta V_D = \Delta V_3 = \Delta D \left[2gD_i \frac{\rho_s - \rho_L}{\rho_L}\right]^{1/2} \tag{2.16}$$

By adding the above quantity to the value found for the horizontal case, the deposition velocity for the inclined case can be determined.

2.7 Conclusions

This chapter critically reviewed the literature concerning the settling slurry flow in different flow orientations, horizontal, vertical and inclined. The previous work regarding the flow regimes that occur as a result of particle settling tendency and the recognition of each of them, pressure drop in slurry pipelines, the physical mechanisms governing the flow and deposition velocity have been extensively reviewed. It is concluded that, despite a significant technical progress in the field, our knowledge concerning the behaviour of solids and liquids is still limited. It is also concluded that all the models and techniques that have been reported in the literature have their own limitations, due to complexity and poor understanding of solid-liquid flow. This clearly a major effect on the aspect of slurry flow metering. Therefore, a good understanding of the underlying phenomena is crucial for development and optimisation of slurry flow meters, which play an important role in controlling the whole flow system.

Chapter 3
Review of slurry flow measurement and visualisation techniques

This chapter presents a review of flow measurement and visualisation techniques widely employed for slurry applications. It will broadly highlight the techniques that are commercially available, while the main emphasis is placed upon the Electrical Resistance Tomography technique.

3.1 Introduction

The measurement and visualisation of slurry flow in pipeline is a challenging task due to complex nature of the flow, abrasive and viscous nature of the material. There are some experimental techniques that have been developed for measuring slurry flow, some of which are commercially available and the others still at the stage of development and purely used for research in laboratory tests (Brown and Heywood, 1991; Pachowko, 2004; Mohinder and Nayyar, 2000). However, this work presents only the solutions that are commercially available for measurement of slurry flow.

The choice of a correct instrument or method depends on a number of factors, such as properties of the solid particles (size, shape and abrasiveness), typical fluid characteristics (pressure, temperature, density, viscosity and conductivity. Also depending on the application, in which the metering is performed, further parameters have to be considered, such as accuracy, repeatability, calibration, pipe geometry, ease of maintenance and the effect of up and down stream pipeline on the meter.

This chapter is split into three main sections. Since phase volume fraction and phase velocity inform about the internal structure of the flow, therefore, the first section is devoted to a review of available techniques used for measurement of phase fraction and phase velocity. Also the detailed discussion will be confined to only the meters that are used in this study, such as Electromagnetic Flow meter (EMF), Coriolis mass flow meter and Ultrasonic Doppler Velocity Profiler (UDVP). It is important to note that no reference regarding Coriolis is given in this chapter. A discussion over Coriolis mass flow meter can be found in Chapter 6. The second section highlights the widely used techniques for visualisation and imaging of flow. The last major section covers the Electrical Resistance Tomography system

from working principle and sensing strategy to the limitations, along with previous work carried out by the others.

3.2 A review of phase fraction and phase velocity measurement

The mechanism of solid liquid transport in slurry pipelines is dependent on several flow parameters, of which the most important are phase fraction and phase velocity. These two parameters also determine the prevailing flow regime within the pipeline. Therefore, it is vital that the operator continuously monitor these two parameters, so as to prevent a potential line blockage at an earlier stage. In other words, these two parameters are the governing parameters, which can determine the internal structure of flow, and if the internal structure of the flow is known to the operator, then control limits can easily be maintained.

A number of commercially available techniques for measurement of these two parameters are employed and mounted on slurry pipelines of many industries such as chemical, food, mining, dredging etc. This section reviews seven measurement techniques, which are commonly used for solid-liquid flow. Besides, they are used in single and multiphase flow measurements.

3.2.1 Differential pressure technique

Calculation of fluid flow rate, based on pressure loss across a pipe restriction, may be the most common flow measurement technique in industrial applications. The pressure drop across a section can be generated by a wide variety of geometrical restrictions, which have been characterised over the years.

The theory of differential pressure devices is based on Bernoulli relationship. Restrictions in cross sections increase in fluid acceleration, and the energy of this acceleration is obtained from the fluid's static pressure. As a result the pressure drop occurs in the section. Once the pressure differential, created by the device, is known, then the velocity of the flow can be obtained by the following equation:

$$V = k\left(\frac{h}{\rho_L}\right)^{0.5} \tag{3.1}$$

It is worth pointing out that only two types of pressure differential devices can be applied for slurry flow, which are venturi, flow tube and segmental wedge. Nevertheless, the most commonly used for slurry tend to be venturi,

due to the fact that most of pressure drop can be recovered in venturi flow meters. As venturi is the most common pressure differential device for slurry measurement, then no further detail will be given to the other types of differential pressure elements.

The venturi meter consists of an approach section, which has the same internal diameter as the system pipeline, and a conical nozzle section followed by a short parallel throat and a conical diverging section, which rejoin the venturi system to the system pipeline. The rejoin will be gradually by returning the internal diameter up to that of the line system, as shown in Figure 3.1.

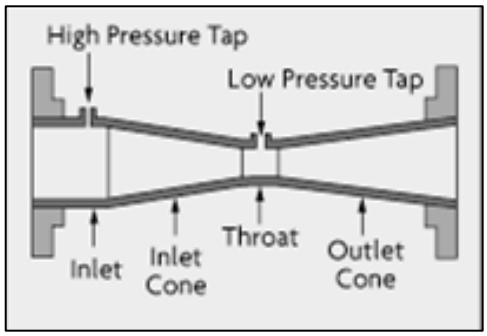

Figure 3.1 Showing components of a short-form of a venturi tube (taken from www.omega.co.uk)

Although the initial cost of venturi meters are high, the total cost of ownership can still be satisfactory, due to savings in installation, operating and maintenance costs. Venturi has been used 100 years ago, and it design and improvement still continues. There are many companies out there producing a high accuracy venturi for a variety of applications, including slurry, such as WYATT ENGINEERING (wyattflow.com), who produces venturi tubes with accuracy flow measurement of ±0.50 for standard meters (without calibration).

Experimental and theoretical studies have been carried out by many researchers to assess the ability of venturi meter on various flow measurements. For example, Shook and Masliyah (1974) and Shook (1982) carried out experiments on stratified slurry flow using venturi meters. They concluded that venturi meters can be reliably used, without any calibration for measurement of non-stratified coarse particle slurry flows. They also concluded that for the other flow regimes, the effect of pipeline conditions must be well investigated. However, using venturi for stratified or partially stratified slurry flow could be a potential for pipeline blockage.

3.2.2 Probes

Probe techniques are methods of making local measurements such as phase volume fraction and phase velocity. Since the local concentration of particles is reflected by the local resistively of the slurry, then conductivity probes can be used to measure the local concentration and solids axial velocity in slurries, as in the case of Nasr-El-Din *et al.* (1987), who used a four-ring conductivity probe. Usually the resistively of the fluid is measured by two pairs of electrodes contained along the body of the probe.

This technique has been used on a wide range of slurries and shown a potentially useful tool to measure volume fraction and velocity (MacTaggart *et al.*1993; Lucas *et al.*, 1999 and Liu *et al.* 2007). However, the local conductivity probes are considered as an intrusive and invasive technique, therefore, it is not really favoured by many researchers.

3.2.3 Electromagnetic Flow Meter (EMF)

Electromagnetic flow meters have been used for several decades and based on the principle of Faraday's conduction (Wang *et al*., 2007). The industrial interest in this type of flow meter grew in the 1950s, (Baker, 2000). Nowadays, it is exclusively applied in industry to a variety of flows, particularly multiphase flow, in which there is a high contrast between the conductivity of the two phases (continuous and dispersed). The continuous phase is often the high conducting material, such as water, whereas the dispersed phase is often the low conducting material, or may even be totally insulators, such as sand in slurry flow, oil, gas etc. (Brown and Heywood, 1991 and Baker, 2000). Electromagnetic flow meter is the most widely used meter for slurry measurement, due to the advantage that it offers, which is explained in the next sections.

Figure 3.2 showing the arrangement of an electromagnetic flow meter. The electromagnets, two electrodes and electronic circuitry are mounted on a flow tube. The electromagnets are positioned on the outside of the flow element. However, the two electrodes are mounted opposite each other in the wall of the flow tube and are in direct with the fluid. The fluid flows into the circular cross-sectional and a uniform magnetic field is generated across the pipe by the pair of electromagnetic. A voltage is induced into the fluid in a direction at right angles to the magnetic field. The voltage signal picked-up by the two electrodes, is conditioned and converted to a flow rate (or velocity) (Baker, 2000 and Brown and Heywood, 1991).

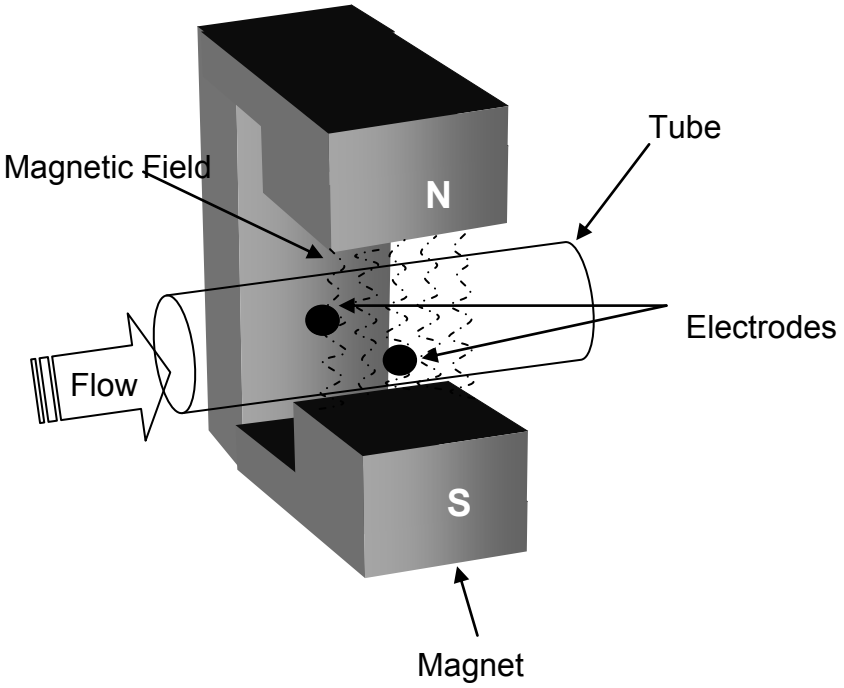

Figure 3.2 Showing the arrangement of the electromagnets and pick-up electrodes (Modified from Baker, 2000)

It is clear that the tube must be made from a non-magnetic material, so that the magnetic field can penetrate the tube. Electromagnetic flow meters could also be applied to a media with low conductivity. This can be done by using in direct capacitive coupling to extend the operating range of EMF.

The theory of Electromagnetic flow meter belongs to the subject of Magneto-hydrodynamics, which is the combination of the classical disciplines of fluid dynamics and electromagnetism (Wang *et al.* 2007).

As the fluid flowing through the tube, mentioned in Figure 3.2, perpendicular to the magnetic field, with a velocity V, then a voltage is generated between its ends with a value of BlV. Where B is the magnetic flux density and l is its length. The voltage distribution inside the pipe can be given by a Poisson type equation, of the following form, which is given by Shercliff (1962) and Bevir (1970):

$$\nabla^2 U = div(V * B) \tag{3.2}$$

However, Shercliff (1962) derived another equation, based on the above equation, for determining the voltage between the two electrodes, as shown below:

$$\nabla U = BDV_m \tag{3.3}$$

Where, B is the magnetic flux density (in tesla), D is the diameter of the tube inside the EMF (in m) and $\mathrm{V_m}$ The fluid mean velocity in the tube (in m/s).

Shercliff's equation is the basic equation for electromagnetic flow meter and its validity is based on the two assumptions, the magnetic field is uniform and the velocity profile is asymmetric. These two criteria will certainly impose limitations in the theory. Shercliff (1962) then suggested a mean of predicting the effected distorted profiles by using, as he called, a weight function.

A weight function describes the combination of the velocity, in different parts of the flow meter cross-section, to the total output signal (voltage). This weight function shows that the flow near the electrodes have more influence on the signal than at any point with increasing distance from the electrodes.

Furthermore, Bevir (1970) extended the weight function concept to three-dimensional (or weight vector), as shown by the following equation:

$$\Delta U = \iiint VW \, d\tau \tag{3.4}$$

Where, V is velocity at every point, τ is the flow meter volume, and the integral is taken over τ, W is weight vector and can be given by:

$$\mathrm{W} = \mathrm{Bj} \tag{3.5}$$

Where, j is hypothetical current velocity, which is known as the virtual current. In order to improve the theoretical performance, another approach has been used, in which large electrodes are used to have an integral effect on the signal (Baker, 2000).

According to some manufacturers the preferred installation of electromagnetic flow meter is in vertical upward flow. Matousek (2005) also claims that electromagnetic flow meters should be installed in the vertical line of a slurry system. This is to ensure that the entrained air bubbles are carried up with flow and solid particles are not settled on the electrodes. Also, a vertical line, which is a common installation position in slurry flow

systems, it will be necessary to allow for any slip that may occur between the carrier liquid and solid particles.

According to manufacturers valves should not be installed close upstream of EMF, even if fully open, (www.icenta.co.uk and www.abb.co.uk). They are likely to have an effect of ±0.5% even if the distance is 15D upstream, (i.e. the distance equivalent to 15 times the internal pipe diameter). However, due to design differences between electromagnetic flow meters, it is not possible to follow absolute guidelines that would be equally valid for all designs.

Also, non-uniformity in conductivity in the flow meter can cause changes in the EMF signal, due to the changes in the size of the shorting currents. For certain conditions of turbulent flow, field shape and conductivity profile a signal change of 3% may be expected. However, as Baker (2000) claims, the value of uncertainty in the EMF reading may be given as a percentage or a velocity. Manufacturers give uncertainty between ±0.3% -±1.5% rate for flow range 2%-2.5% and 100%-50% respectively.

Application of EMF, for multiphase flows, where a marked difference in velocity of the dispersed and continuous phase occur (such as slurry), has been the centre of the debate as to what velocity is really measured. Despite that, it is generally accepted that, for example in slurry flow, the EMF measures the velocity of the mixture rather than that of the carrier liquid.

Cha *et al.* (2002) stated that “The electromagnetic flow meter has been used successfully and accurately to measure the mean liquid velocity in various industries...”. Also, it is obvious that electromagnetic flow meter detects the potential difference, through the pair of electrodes, when a conducting liquid is passing through the magnetic field. Therefore, this fact can be used in favour of the argument that EMF measures the velocity of conducting continuous phase rather than the dispersed phase or the mixture, such as water in slurry flow.

Bernier and Brennen (1983) carried out an investigation regarding the use of electromagnetic flow meter in measuring a multiphase flow. They concluded that the EMF could well be used to measure the velocity of a multiphase flow, in a condition that the continuous phase has a minimum conductivity. However, Wyatt (1986) investigated the conclusion of Bernier and Brennen (1983) and argued that this is only the case when the dispersed phase consists of uniformly and randomly distributed particles.

Furthermore, Wang *et al.* (2007) investigated the relationship between the induced voltage and the velocity distribution profile of the continuous phase, in a two-phase flow to which electromagnetic field was applied. In their study they modelled an AC current electromagnetic flow meter to investigate the characteristics of an EMF in multiphase flow. They achieved the most important findings that induced potential differences measured using an array of boundary electrodes, could conceivably be used to infer the axial velocity distribution of the flow.

Despite development and widely use of EMF on flow, like all flow meters, it has advantages and limitations, which are shown in Table 3.1.

Table 3.1 Advantages and limitations of EMF

Advantages	Limitations
• Widely used. • The flow measurement is independent of fluid rheology, density, temperature and pressure. • Compact design (no moving parts). • Its flow tubes available in standard inner diameter from 3-3000 mm. • Accuracy is much better that 1% of the range of the instruments for flow rates in excess of 10% of the range.	• Restriction to conducting liquids. • The preferred vertical orientation may not always be ideal, as even in clear fluids, swirling flows experienced downstream from bends are responsible for systematic error. • The conducting fluid must have a minimum conductivity of 2 μS/mm. However special EMF with capacitive signal pick-up are available that can be used with conductivities as low as 0.005 μS/mm. • For application on settling slurries, such as sand, the insulating deposits tend to coat the exposed electrodes. • Entrained air bubbles adversely influence measurements, if the flow tube is installed horizontally, and such that the electrodes are positioned at the top and the bottom of the tube.

3.2.4 Cross-Correlation

Since 1960s the theory of cross correlation has been applied to measure the physical parameters of a system, especially velocity. Some investigators used the technique in the field of flow measurement, such as Dyakowiski and Williams (1996); Lucas *et al.* (1999); Wu *et al.* (2005).

For calculation of axial velocities, using the method of cross-correlation, the sensors must be fitted with dual electrode plane sensors. The general concept of cross correlation is measuring the time between to signals generated by turbulence of the fluid or suspended particles flowing along the pipe through two sensors. In other words, if a fluid flows through two sensors with a distance L between them and the downstream sensor detects the signal after a certain period τ at the downstream sensor. An example of dual plane ERT sensor is shown in Figure 3.3. Then the velocity V can be calculated from the following equation (Deng *et al.*, 2001):

$$V = \frac{L}{\tau} \tag{3.6}$$

Based on using dual-plane ERT sensor, according to Lucas *et al.* (1999), for a 50 mm distance between the two plane electrodes and minimum velocity of 4.5 m/s, a sampling rate of 450 frame/s is required from each plane.

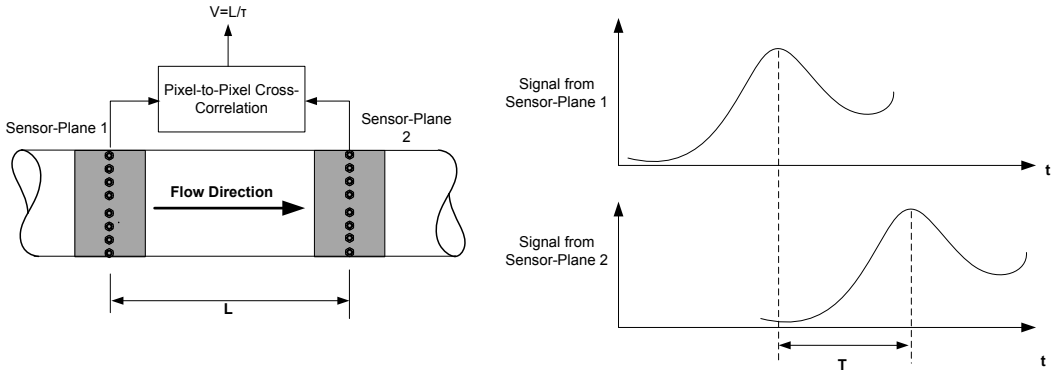

Figure 3.3 The principle of velocity measurement by cross correlation of ERT signals

It must be mentioned that the distance between the dual planes (sensors) must be suitably selected so as to realise the cross correlation. In order to select the distance between the two planes two important factors must be considered simultaneously; the dynamic behaviour of the system (mixture

velocity) and the resolution of measurement of the transit time. In other words, the smaller the distance the better similarity of the signals can be obtained. However, the relatively slow speed of data acquisition and image reconstruction requires longer distance. According to Deng *et al.* (2001) the distance between the two planes could be 50, 75, 85 or 100mm. However, they recommend that having L (the distance) adjustable, so as to coordinate it with different cases and various flow velocities.

The signals can be correlated in different methods; point to point correlation and best correlation pixels. Point to point correlation has been reviewed by Dai *et al.* (2004), who suggests that the cross correlation measurement is based on measuring the data obtained from two planes placed axially along the flow stream. The basic concept of this method is to find similarities between the two signals measured at each plane, as shown in Figure 3.4, in which X denotes plane 1 and Y denotes plane 2.

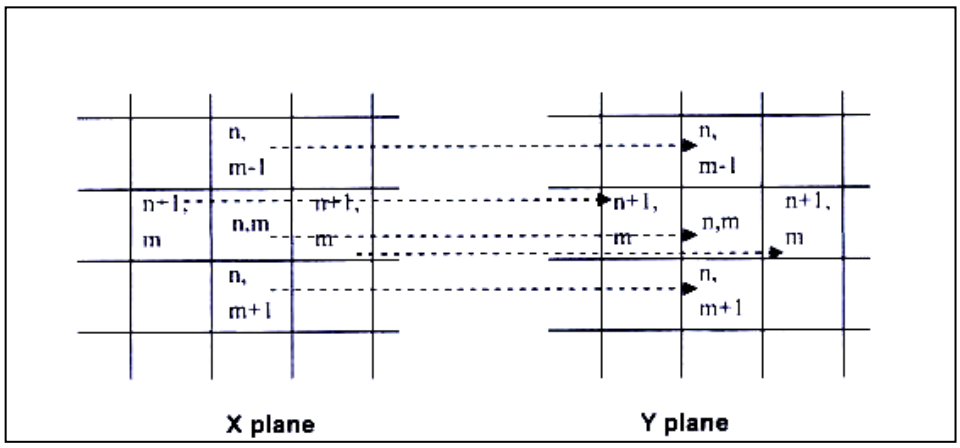

Figure 3.4 Principle of point-by-point cross correlation method (Dai *et al.*, 2004)

The basic function in which the time delay is calculated in terms of error function ($R_{minimum}$), gives the time delay as:

$$R_{sx,sy}(\tau) = \lim_{T\to\infty} \int_0^T S_x(t) S_y(t+\tau) dt \qquad (3.7)$$

While the point to point correlation is based on the assumption that the flow trajectories are parallel to each other and perpendicular to the two planes. As the nature of the flow is quite complex, then the basic of the assumption can be a limitation in itself.

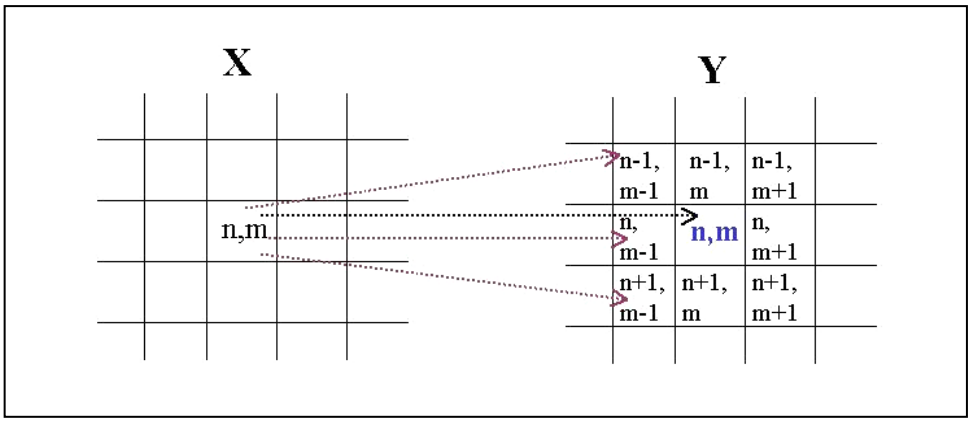

Figure 3.5 The cross correlation between X(n,m) and the vicinity of pixel Y(n,m), (Dai *et al.*, 2004)

While in best correlation pixels method the direction of the flow is no longer assumed, instead it states that the signal from one pixel on plane 1 could be better correlated with one of the signal at the vicinity of the axially corresponding pixel, as shown in Figure 3.5.

Dai *et al.*, (2004) successfully used this method for calculating axial, angular and radial velocity profile in air-water swirling flow. He also proposed the following correlation for best correlation method:

$$R_{X[n,m]Y[n-i,m-j]}[p] = \sum_{K-0}^{T-1} V_{X[n,m]Y[n-i,m-j]}[k+p], (i,j) \in B \qquad (3.8)$$

3.3 Flow visualisation and imaging techniques

In order to better understand the hydrodynamic characteristics of slurry flow and for the pipeline operator to control the processes handling solid-liquid flow, visualisation and quantitative information regarding the flow is extremely important. Many visualisation and imaging techniques have been reported throughout the literature, such as optical methods, ultrasonic methods, Magnetic Resonance Imaging (MRI), tomography techniques etc., (Li, 2007). Each of these techniques has its own advantages and limitations. The choice of a particular technique is usually restricted by many factors such as physical properties of each phase, continuous and dispersed, the required spatial and temporal resolution, total and ownership cost, physical dimension and weight, robustness and flexibility of operation and potential

hazards to the personnel (Gamma-ray is an example of potential health hazard), (Munir, 2011).

This section reviews the widely used and commercially available techniques for measurement and visualisation of constituent phases within two-phase flow, particularly slurry flow. Since slurries are opaque and contained in opaque enclosures , then optical visualisation of the flow is quite difficult, (Heindel, 2008). Thus, optical techniques. such as laser Doppler Velocimetry (LDV), Laser Doppler Anemometry (LDA) and Particle Image Velocimetry (PIV) (Van Dinther *et al.*, 2012), is excluded in this work. In the meantime, it must be noted that the above three optical methods offer a great benefit for measurement of micro-channels, non-slurry and diluted slurry applications. However, their major drawback in settling slurry applications is that they are less sensitive when coarse particles are used, besides their measurements are affected by wall effects, (Van Dinther *et al.*, 2012). The section will mainly split into two categorised techniques, tomography techniques and others. The tomography techniques will cover Electrical Resistance Tomography (ERT), Electrical Capacitance Tomography (ECT), Electromagnetic Tomography (EMT), Ultrasound Tomography and Nucleonic Tomography techniques. Whereas, other techniques will be confined only to Magnetic resonance Imaging and Ultrasonic techniques.

3.3.1 Ultrasonic technique

Application of ultrasonic flow meters has become really attractive in the past 50 years or so, after a significant development in the piezoelectric transducers (Baker, 2000). This is due to the fact that ultrasonic techniques can be used for fast and on-line characterisation of particularly dense and opaque slurries and suspensions. Ultrasonic techniques offer potential of measurement of changes in acoustic velocity, attenuation and frequency of the propagating waves.

Through a journey into the literature, it was found that most of studies have used attenuation methods. Nevertheless, studies of the variations in acoustic velocity is also common, such as that of Shukla and Prakash (2006), who used variations in acoustic velocity to determine changes in particle size and concentration in two- and three-phase slurry and gas-liquid-solid respectively.

One of the advantages of ultrasonic techniques is that it can offer a non-intrusive measurement of the flow. Therefore, it has been attracted to many

researchers and industries such as food, oil and many others handling slurry flows.

The main concept of ultrasonic flow meter is based on the fact that they use acoustic energy (or acoustic waves) at frequencies above the limits of human ability. These waves travel, in form of sound, with the speed of sound relative to the medium and consist of pressure perturbation in gases and liquids. However, in solid particles, the connecting wave can also move as a shear, that is due to the elasticity of the solid shear.

There are three types of ultrasonic flow meters, which are listed below (Brown and Heywood, 1991; Baker, 2000).

- Transit Time (or time of flight).
- Doppler.
- Cross-correlation.

However, most of units that are available commercially based on one of two principles, either frequency shift (Doppler) or time of flight (transit time).

The transit time flow meter is the most accurate type of acoustic flow meter family, which is from a fraction of a percent to about 5% uncertainty. This type of flow meter utilises the difference in transit time in an upstream and downstream direction. In other words, the acoustic signal increased when the direction of propagation is in the direction of flow, and decrease if it is in the opposite direction. The difference between the two signals can be used to calculate the velocity of the flow.

The Doppler flow meter is very different device. It requires particles in the flow to reflect back the acoustic signal as shown in Figure 3.6, unlike transit time, which transmits signal through the flow. The Doppler is widely used and its measurement uncertainty is unlikely to be better than about ±2%. On the other hand, installation affects significantly its performance.

The cross-correlation flow meter requires a distributed liquid or a multiphase flow to operate properly. It is more expensive than the other two types of ultrasonic flow meters.

Since this study uses the Ultrasound Velocity Profiler (UDVP) type, then the focus will only be on Doppler, and the discussion in the following sections will be confined to the Doppler technique.

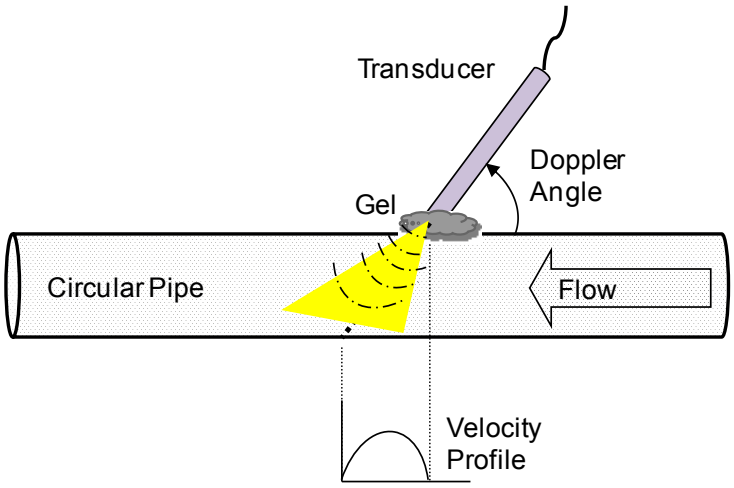

Figure 3.6 Showing working principle of UDVP

The Ultrasound Doppler Velocity Profiler uses a single transducer to transmit and another to receive the reflected signal. An ultrasonic wave is emitted into the flow media at a set frequency. As the pulse approach and hit the particle present in the flowing fluid, it reflected back towards the receiving transducer. Then the time delay and frequency shift received by the transducer can be used to calculate the local velocity of the particle (or in-situ particle velocity).

According to Met-Flow (Met-Flow.com), who designed various models of transducers with emitting frequencies 0.5-1-2-4-8 MHz, lower frequencies allow for longer distance range and higher velocity measurement, due to their propagation ability. However, transducers with higher frequencies are used for low velocity measurement (or small flow dimensions), where high special resolution is required, due to the feature of short wave length. Clearly, if a stationary object reflects the outgoing signal, then there will not be any difference in frequency between the outgoing and the reflected signals. Thus the two signals retain their wave length and frequency.

The frequency used by manufacturers varies greatly and is commonly within the range of 16KHz-10MHz. Besides, the transducers are manufactured in different sizes and emitting frequencies, so that each transducer suits an intended application. For example, Signal-Processing (signal-processing.com) manufactures transducers with different frequency, diameter, case dimensions and temperature range, as illustrated in Figure 3.7.

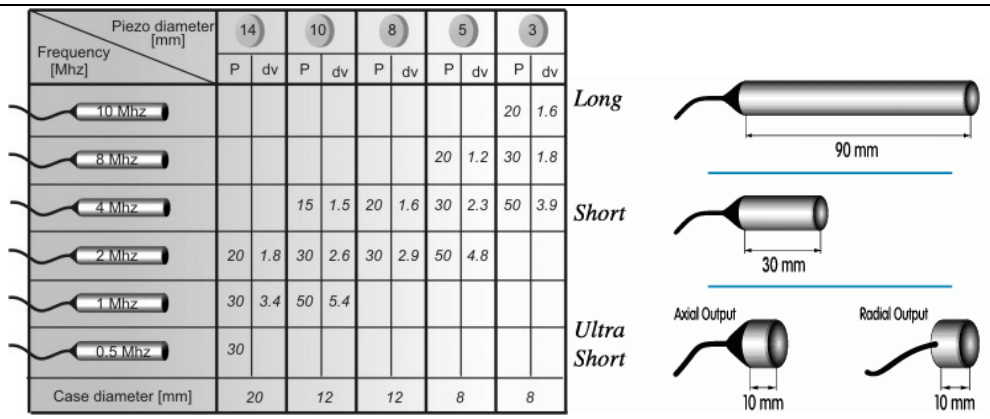

P= Maximum pressure (bar), dv= Half diverging angle (degree)

Figure 3.7 Standard transducers supplied by Signal-Processing and case dimensions

The Doppler theory is illustrates in Figure 3.8. The transducer A transmits acoustic signal into the flow, where a moving particle present with a velocity v. The acoustic signal approaches the particle with a velocity c, then reflected and picked-up by the transducer B. However, the sound speed still remains c after reflection, as the sound speed is not affected by frequency, but the period between two reflected waves is not $\lambda t/c$. Instead it will be $\lambda t/(c\text{-}v)$ seconds for each peak, as the wave hits the particle at a velocity $(c\text{-}v)$. Successive peaks will make contact with particle at different particle position; therefore, for the peaks to reach the starting point of the first peak, they will need to travel $\lambda t+V/(c\text{-}v)$. Thus the period required for this additional travel is $\lambda t+V/c(c\text{-}v)$ seconds. If the time between peaks is τ, then the value of τ is given by the following equation:

$$\tau = \frac{\lambda_t}{c}\frac{1+v/c}{1-v/c} \tag{3.9}$$

Using the binomial theorem to expand the above equation, the frequency of reflected waves can be determined by the following equation, providing v^2/c^2 is ignored:

$$f_r = \frac{c}{\lambda_t}\left(1-\frac{2v}{c}\right) \tag{3.10}$$

Also the frequency shift can be given as:

$$\Delta f = f_t - f_r \tag{3.11}$$

Then,

$$\Delta f = 2f_t \frac{v}{c} \tag{3.12}$$

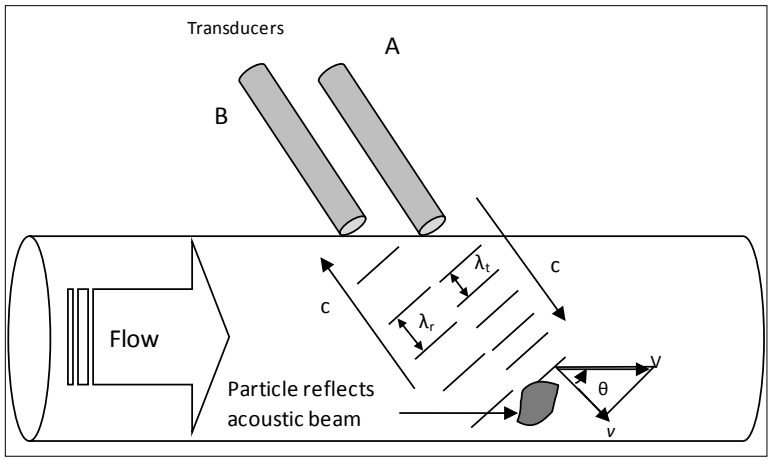

Figure 3.8 Showing the Doppler Effect (Modified from Baker, 2000)

The main application of acoustic Doppler velocity estimation is in biomedical and oceanographic measurements. However, the application of acoustic Doppler was found to suit abroad range of flows, particularly slurry and suspension flow. According to Baker (2000) the Doppler flow meters are oversold as an all purpose flow meter. According to manufacturers of Doppler flow meter, the device can be used for measuring flows of mining slurries, coal slurries, sewage, sludge, raw water, sea water, pulp, acids, cement slurry, emulsion paint, fruit juice and contaminated oil, (Met-Flow, Signal processing).

Jaafar *et al.*, (2009) used Ultrasound Pulse Doppler Velocimetry to investigate the velocity in turbulent pipe flow. Their measurements successfully demonstrated the ability of the instrument to measure unsteady turbulent velocities and to investigate experimentally the statistical properties of homogeneous and isotropic turbulence. They claim that the UDVP does not require any calibration; hence it is a potentially useful tool for measuring velocities in laboratory experiments or industry. Wang *et al.* (2004) carried out an investigation on the effect of temperature gradient on the velocity profile measured by UDVP. They concluded that non-isothermal conditions have two important consequences; first it changes the flow behaviour, second it increases the UDVP measurement error. Then it can be concluded that this phenomenon is due to the fact that the speed of sound is independent on temperature.

Some other researchers have used UDVP, not only in slurry transport, but also in slurry mixing, such as Syrajänen *et al.* (2009), who used UDVP to measure three-dimensional velocity profile in a sand-water stirred tank. The conclusion of their investigation showed that the measurement of particle velocities was in a good agreement with the predicted values. However, they observed deviation of the results near the tank wall, with increasing solids concentration. Moreover, Vuarnoz *et al.*, (2002) have also used UDVP for characterisation of ice-slurry flow and concluded that the UDVP can be used as a potential tool to characterise the slurry flow.

Manufacturers suggest that installation should allow 6D upstream and 4D downstream. Also, according to Baker (2000), the emitting and receiving transducers should be next to each other for large pipes, whereas on opposite sides for small pipes. The transducers can be used with a wide variety of pipe materials, such as carbon steel, stainless steel, PVC and copper. However, some pipe materials may not allow the signal to pass through, such as concrete, fibre glass, iron and plastic pipes with liners (www.coleparmer.co.uk). The transducers can be permanently bonded to the pipe using epoxy adhesive. However, this may not suit laboratory studies; therefore, temporary acoustic coupling can be applied using grease or water based gel. Brown and Heywood (1991) recommend strongly securing the transducers with straps.

As any other flow meter, the UDVP has also its own advantages and disadvantages, which are highlighted in Table 3.2.

Table 3.2 Advantages and limitations of ultrasound Doppler

Advantages	Limitations
• Non-intrusive. • Portable and useful for troubleshooting. • No calibration required.	• Less effective for clean fluids, such as that of power stations. • The speed of sound dependent on temperature. • Sometimes the transducer giving wrong readings, due to the presence of air bubbles at the top of the pipe. • The depth of penetration of the signal dependent on the pipe materials, the coupling medium and the nature of the slurry.

3.3.2 Magnetic Resonance Imaging

Magnetic Resonance Imaging (MRI) is the most advanced and sophisticated tool that generate almost real-time 3-D images of the material under investigation. It allows the determination of phase volume fraction, physical behaviour and properties, which are related to the state of the physical system, (Van Dinther *et al.*, 2012). The concept of MRI is that the object subjected to a strong magnetic field and its hydrogen nuclei (or single proton), which is spinning randomly is lined up in the direction of the magnetic field. They are then hit by a burst of a Radio Frequency (RF) and they flip round. Once they return to their original orientation they emit the radio signal in the form of echo (Windt, 2007). This phenomenon is known as Nuclear Magnetic Resonance (NMR). The Electron Magnetic Resonance (EMR) is closely related to (NMR) and sense the free or unpaired electrons, (Raguin *et al.*, 2007). The spatial resolution of an MRI image can be 400 μm and a temporal resolution of 1 m/s (Muller *et al.*, 2008 and Kalaga *et al.*, 2009).

Despite the developments in the field, the MRI limitations have not been overcome yet. Since MRI technique has limitations in maximum size of the object, say in centimetres, as the object should be smaller than the magnetic field. Also MRI cannot be applied for objects with any material, as the object should contain either hydrogen or carbon atom. Therefore, this implies that MRI is a relatively specialised technique and cannot be used for today's industry (Fukushima, 1999; Hoult *et al.*, 1986).

3.3.3 Tomography techniques

The basic idea of tomography is to install a number of sensors at the periphery of the pipe or vessel to be imaged. Then these images reveal valuable information regarding the nature and distribution of the components within the flow.

According to Williams and Beck (1995) there are many types of tomography sensors such as ERT, ECT, PET, ultrasound tomography, nuclear etc. Each of them has its own advantages and disadvantages. The choice is based on the material under investigation, however some other considerations must be made to safety issues, expenses and simplicity and applicability before choosing the suitable type. For example, electrical tomography techniques have been rated as the most attractive techniques, due to its safety issues, unlike Gamma-ray and their moderate spatial resolution of the produced image, unlike X-ray, electric field cannot be confined to a receiver.

Therefore, this study employs Electrical Tomography (ET) to visualise and measure the parameters of slurry flow and the special attention will be paid to electrical topography, particularly ERT. In the meantime some general facts over the other types of electrical tomography (ECT, EIT, and EMT) will be addressed briefly.

3.3.3.1 Electrical Resistance Tomography (ERT)

Electrical Resistance Tomography (ERT) has attracted a great interest from researchers and engineers due to its safe application, relatively low price (Windth, 2007; Cheney *et al.*, 1999), design simplicity, despite that the continuous phase must be conductive. Its application increases progressively, not only in industrial processes but also in environmental areas, such as monitoring of the hydraulic response of the rock mass in Yucca Mountain, where thermo-mechanical and thermo-hydrological of this horizon was studied (Deng *et al.*, 2001).

The working principle of ERT system is to image mixtures, in pipes or vessels, where the continuous phase is conductive and the dispersed phase is insulating or less conductive, such as water and sand, as it is used in this study.

Normally the ERT sensors composed of 16 equally spaced electrodes at the periphery of the pipe or the vessel (mounted flush with inside surface of the pipe), in a way that can be in direct contact with the fluid. The operating principle is based on applying an alternating current and measuring the potential differences across the cross section of the pipe or the vessel. There are different strategies of measuring the voltage differences, as discussed previously, however, the current study employs the adjacent electrode strategy, which is injection of an electric current through a pair of electrodes and measuring the voltage difference between the remaining of electrode pairs and the procedure continues until the full rotation is complete. The standard measurement protocol for measuring the conductivity if $N(N-3)/2$ measurements, which is 104 measurements for 16 electrodes, as shown in Figure 3.9, (Williams and Beck, 1995; Wang *et al.*, 2002; Pashowko, 2004; Giguère *et al.*, 2008b, 2009; Reinecke *et al.*, 1998).

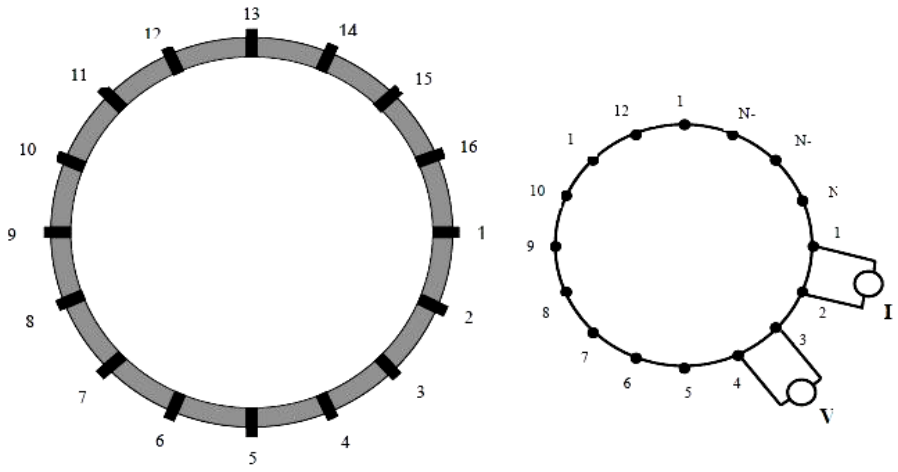

(a) (b)

Figure 3.9 Showing (a) The ERT sensor ring (b) The normal adjacent strategy (Taken from the ITS, 2005)

3.3.3.2 Electrical Capacitance Tomography

Electrical Capacitance Tomography (ECT) is used for imaging processes containing dielectric materials. The principle is to measure the changes in capacitance, which is caused by the change in dielectric material distribution. The main aim of ECT is to image permittivity distributions in very low or ideally non conducting materials (Marashdeh *et al.*, 2008). The capacitance is measured via a series or electrode sensors (typically 8 or 12), which are placed on the periphery of the pipe or the vessel, as shown in Figure 3.10. The electrodes are mounted to insulating pipe and an outer earthed conducting shield (Yang, 2010). The standard measurement protocol for measuring the capacitance between all combinations of single source and detector gives $N\ (N\text{-}1)/2$ measurements (Plaskowski *et al.*, 1996). ECT dual plane sensors also have been constructed and the images are analysed by comparison in order to infer dynamic information. The permittivity distribution is taken from the cross sectional image, which is reconstructed from the capacitance measurement mathematically using a type of algorithm.

ECT is considered as a soft-field technique, due to non-linear relationship between the measurements and the permittivity distribution, therefore, the reconstruction of images is complicated and difficult. However, ECT can offer some advantages, such as non-intrusive, fast, lack of radiation, relatively low cost, withstanding high temperature and pressure (Ismail *et al.*, 2005).

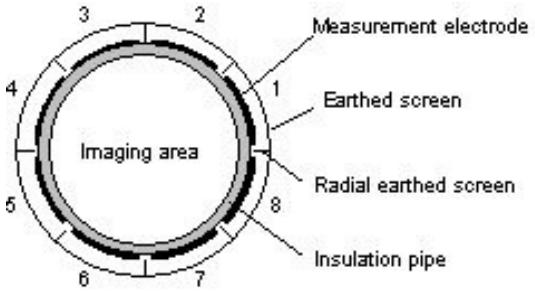

Figure 3.10 Showing 8-electrode ECT sensor, (www.ect-instruments.com)

3.3.3.3 Electromagnetic Tomography (EMT)

An EMT sensor comprises of a set of excitation coils, which creates a magnetic field within a cross section of a pipe or a vessel, and then the set of detection coil measure the changes in permeability and conductivity of the interest field, as shown in Figure 3.11. According to (Ismail *et al.*, 2005) the higher the excitation frequency is produced the higher the sensitivity can be obtained. The EMT sensors have a number of advantages, such as no contact required with the sensing field or material and flexibility in design.

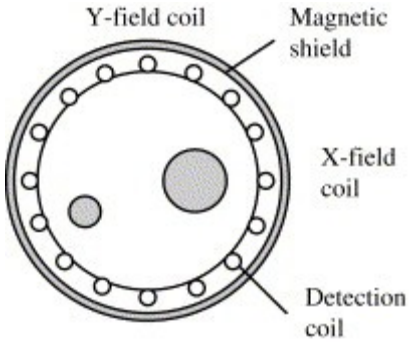

Figure 3.11 Showing EMT sensor, (Ismail *et al.*, 2005)

3.3.3.4 Ultrasound Tomography

Ultrasonic sensors are widely used in medical imaging and have successfully been applied in flow measurement. The sensors are made of transmitting and receiving sensors. They are non-intrusive and axially spaced along the flow stream (Abdul Rahim *et al.*, 2006). This type of sensors can be used for particle velocity measurements. The principle of ultrasound tomography is that the ultrasonic beam is scattered and the signal is interacted with the object in the flow, then the reflected signal is picked-up by the receiving sensor.

Fazalul Rahiman *et al.* (2008) designed and modelled ultrasonic tomography for a mixture of two component high acoustic impedance. The information they obtained in their study could be used for further development of the image reconstruction of ultrasound tomography. (Abdul Rahim *et al.*, 2007) carried out another investigation, where they used ultrasound tomography for imaging liquid and gas flow. They concluded that the ultrasound system could be used for flow pattern identification and measurement of the cross-sectional void fraction. They also revealed that low operating transducers is sufficient to do the measurement, as long as the acoustic energy is passed through the vessel.

3.3.3.5 Nucleonic Tomography

Nucleonic tomography techniques use both, X-ray and Gamma-ray, which have very short wavelength, thus, they penetrate into an object without any attenuation. This character, obviously makes them a potential hazard in using them for flow measurement, (Munir, 2011). These techniques are described below.

3.3.3.5.1 X-ray and Gamma-ray Tomography

These techniques appears to be the oldest technique for imaging. The principle of X-ray is similar to that of Gamma-ray. However, there is only one difference between them, which is the source of radiation. When X-ray or gamma-ray passes through a medium, most of the radiation is absorbed by the media and the rest is attenuated, which is received at the other end (Kalaga *et al.*, 2009). This technique is usually used for steady state images of the object. The density of the medium and the distance between the source and the detector has a direct effect on the attenuated radiation.

Boden *et al.* (2008) used X-ray tomography to obtain a 3-D gas hold up distribution in stirred tank with high accuracy. They concluded that the high accuracy in time-average phase fraction distribution is achieved by proper and practical corrections measures for the problem of beam hardening and radiation scattering. Schmit *et al.* (2004) applied X-ray tomography on a packed column to measure the flow distribution. They observed the ring like artefacts in the images, which indicate that the method is well suited to monitor the flow.

Schubert *et al.* (2008) investigated a high resolution Gamma-ray for trickle bed reactor using glass beads and porous catalyst beads. They successfully concluded that Gamma-ray could be used for study of hydrodynamics of this nature. Many others have used Gamma-ray in view of applicability of the

technique for industry, such as Wang and Yin (2001), Yin *et al.* (2002), Roy *et al.* (2005), and Jin *et al.* (2005). Most interestingly Tortora *et al.* (2008) used a multimodality tomography method, where they used Electrical Impedance Tomography (EIT) in conjunction with Gamma-ray for circulating fluidised bed, and they confirmed a good accuracy of using the two technique.

3.3.3.5.2 Positron Emission Tomography (PET)

PET is a radioactive tracer that enables visualisation of real processes taking place within the opaque boundaries. The principle of PET is based on detecting the pairs of back-to-back gamma-rays produced when a positron annihilates (or emitted in radioactive decay) with an electron. It is widely used in medicine, however, in chemical engineering applications a extensive use has been made of the alternative technique of Positron Emission Particle Tracking (PEPT). In PEPT a single tracer particle is radioactively labelled and can be accurately tracked at high speed (Seville *et al.*, 2009). PEPT has the capability of tracking tracer particles down to approximately 60 μm is size.

PEPT has successfully been used for monitoring and measuring particle velocities in gas fluidised beds, mixers and other chemical applications (Stein *et al.*, 1997). Portillo *et al.* (2010) examined the movement of particles within a continuous powder mixer, in which PEPT was employed. They claimed that the particles along the vessel could be measured non-invasively and the measurements were promising.

3.4 Electrical Resistance Tomography system detail

3.4.1 Introduction

Tomography is an imaging technique that is used to visualise the contents of a closed system or body, such as a pipe or a vessel without physically looking inside. Tomography originally is a Greek word, which is composed of two words, “tomos” meaning “to slice” and “graph” meaning “image” (Williams and Beck, 1995). In the late 1970s the technique was very popular in medical fields, where tomography resistivity measurement was used by biomedical engineers and considered as an alternative to the successful X-ray scanner, due to its low cost and portability.

Since late 1980s tomography techniques have gone through a major development and are used to provide a novel means of non-intrusively

visualising the internal behaviour of industrial processes, such as gas-liquid, gas-oil-water in oil pipelines, gas-solid flows in pneumatic conveyers, solid-liquid in slurry transfer system and mixing or separation processes in vessels. Thus it is often called “industrial processes Tomography” or “Process Tomography” (Williams and Beck, 1995). In process tomography the signals are sent across the system through the electrodes that are placed at the periphery of the pipe or the vessel, then depending on the signals received, images of the cross sectional plane are constructed. Thus the use of tomography can provide an image of the whole flow and can be considered as a new type of multiphase flow meter. It is important to mention that the current multiphase flow meters are non-linear, which are caused by their flow regime dependency, while tomography can compensate their non-linearity, therefore it is also a viable tool that can be used to determine the flow regime (Ismail *et al.*, 2005).

Many types of tomography systems can be found in the literature, such as Electrical, ultrasonic or acoustic, radiation, Nuclear Magnetic Resonance (NMR), microwave and optical, which are mainly based on different sensing methods. However, this project employs Electrical Tomography (ET) due to its advantages over the other tomography techniques for being cheap lack of radiation and fast response. Based on the principle of electrical sensitivity, electrical tomography is further classified into Electrical Impedance Tomography (EIT), Electrical Capacitance Tomography (ECT), Electrical Resistance Tomography and Electromagnetic Tomography (EMT) (Williams and Beck, 1995). Amongst all the above electrical tomography forms, ERT has been found to be the most attractive method, which is used in this project to visualise the mechanisms of slurry flow systems and measure its parameters. This attractiveness has come from its advantages, such as simplicity, high speed capability and sufficiently robust to cope with the most industrial environment, safe and cheap in comparison to nuclear techniques, which makes them suitable for research as well as industry. It is therefore widely used in different chemical engineering processes, such mixing process (Wang and Yin, 2001); cyclonic separation (Williams *et al.*, 1999) and the mixing processes (Holden *et al.*, 1999). However, the drawback of ERT lays in its low spatial resolution, which has been reported to be between 5 and 10% pipe diameter (Dyakowski *et al.*, 2000).

Since ERT is still within development period, there are some challenges, which need to be reported.

- Increase of sensor spatial resolution.
- Development of more accurate image reconstruction, as inaccurate image will interpret inaccurate flow parameters, such as volume flow rate.
- Increase the efficiency of data processing.
- Improve the design of the sensors mechanically and the electronic hardware in order to increase the safety and reliability either in the laboratory as well as the industry.

The structure of a typical ERT system composed of a hardware part, which includes the sensor with electrode rings, the data acquisition system and the image reconstruction system, which is the host computer, from which the image are generated (Parvareh *et al.*, 2010). Figure 3.12 showing the components of a tomography system.

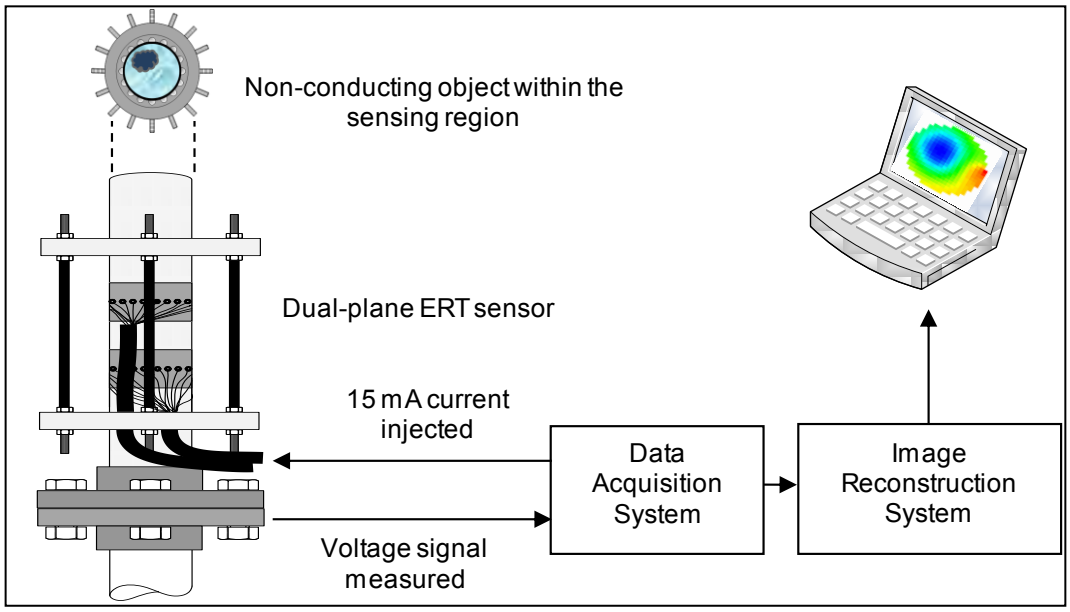

Figure 3.12 Showing the components of the ERT system

3.4.2 Concept and working principle

ERT can be used as a non-intrusive technique to measure and visualise a multiphase flow, in which the continuous phase is an electrically conductive fluid. The technique generates a 2D or 3D image (tomogram), by using electrical resistance measurements and image reconstruction. A tomogram shows the distribution of the conductivity within the flow system, and this is determined by several colours. The basic idea of these colours is to interpret the conductivity within the flow or a mixing system. In tomograms, usually,

the blue colours show the non-conductive component in a particular region of the pipe or the vessel. In this study the liquid phase is tap water, which is conductive and the solid phase is sand, which is non conductive. Hence the blue colours determine the distribution of the less or non conductive phase (sand) and the red colours determine the distribution of the phase with higher conductivity (tap water). The value of the in-situ phase fraction at a given location in the pipe or the vessel corresponds to the local mixture conductivity by using the relationship derived by Maxwell, (Maxwell, 1881). However, it is important to address that the ERT lacks the ability to measure the flow rate of the continuous phase (Water), which causes a difficulty of obtaining an absolute value. Therefore, this study proposes a new in-situ measurement method, in which the Electrical Resistance Tomography (ERT) is combined with the Electromagnetic Flow Meter (EMF) to measure the flow rates of individual phases (Water and sand), described in Chapter 5.

The ERT sensors use one or more planes (electrode rings), which is positioned at the periphery of a vessel, tank or a pipe. ERT employs a sensing technique, which has an excellent time resolution due to fast electrical measurements (Giguère *et al.*, 2008b)

The working principle of ERT consists of injecting a low electrical current, typical 15 mA, between adjacent pairs of neighbouring boundary of electrodes and measuring the potential difference between the remaining electrodes. This procedure is repeated for the other electrode pairs until the full rotation of the electrical field is completed, which form a set of measurements. Then each data sheet generated, will be interpreted by an image reconstruction algorithm in order to compute the cross sectional image corresponding the electrical conductivity field within the pipe or the vessel, in other words corresponding to the pipe or vessel cross sectional area, which is called the concentration tomogram. This cross sectional image provides valuable information on the process, which later can be used for visualisation, monitoring, intelligent control or mathematical model verification (Ismail *et al.*, 2005).

3.4.3 Voltage measurement strategy

Namely there are four strategies, which can be assigned to the Data Acquisition System (DAS), whereby the voltage is measured, (Mann and Wang, 1997; Hosseini *et al.*, 2010):

- Adjacent strategy.
- Opposite strategy.

- Diagonal or cross strategy.
- Conducting boundary strategy

This study will employs adjacent strategy, as it requires less hardware and presents fast image reconstruction. Therefore, it will be the only strategy that is discussed in detail here, and for the rest of strategies the reader will be referred to the references given above.

In the adjacent strategy, an electrical current is applied through two adjacent electrodes and the potential different is measured for the remaining adjacent pairs of electrodes, then the injection and measurement procedure is continued until the full independent combination is completed, as shown in Figure 3.13. The standard measurement protocol for adjacent strategy gives $N(N-3)/2$ measurements, where N is the number of electrodes. For example, for a plane with 16 electrodes provides 104 individual voltage measurements (Tapp *et al.*, 2003). These measurements are communicated to the image reconstruction computer by the Data Acquisition System (DAS), and then the data are processed via a suitable image reconstruction algorithm.

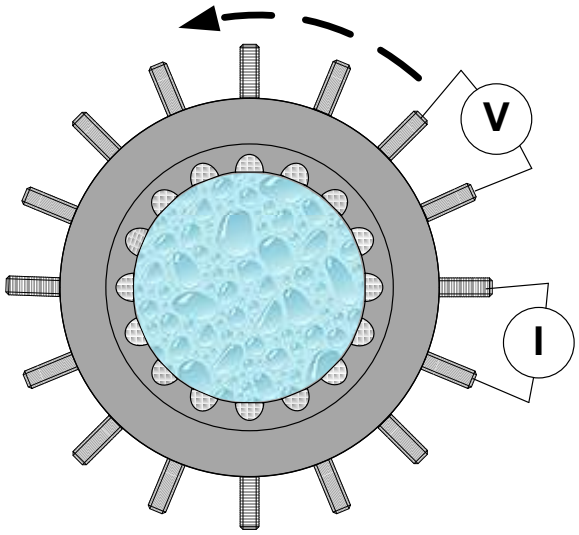

Figure 3.13 Adjacent electrode pair strategy for 16 electrode ERT sensor

3.4.4 Fast Impedance Camera system (FICA)

The high performance ERT system (or a high performance electrical impedance tomography system), is in house built (Online Instrumentation Laboratory/University of Leeds/UK). With regard to the main ERT system (Data Acquisition Hardware), the software and hardware of which have been enhanced and consolidated by OLIL group (Online Instrumentation

Laboratory/University of Leeds). Figure 3.14 showing the actual photograph of FICA system. It is worth pointing out that one of the advantages of this system is the efficiency of the hardware and simplicity of the operation of the control software. The principle of the hardware operating system and the operation of the control software is described in detail in Schlagerg *et al.* (2008).This development of the conventional EIT system could be considered as a response to the requirement of many industrial processes such as two/multiphase flow, where a higher (faster) frame rates is required to measure and monitor the flow behavior. The Data Acquisition System (DAS) is based on the phase sensitive demodulation and both the amplitude and the phase of the measurement can be obtained. Once the system is connected it allows the Data Acquisition System to operate in two modes, continuous (on-line) and block mode.

Figure 3.14 Actual photograph of FICA system

In continuous mode, a single frame of data for one or two planes is acquired, captured, transferred and displayed in the selected format. This mode can capture data at a frame rate up to 50 dual-frames per second (dfps), which is equivalent to 20 ms; whereas block mode can capture data up to 8000 frames at a rate up to 1000 dfps. At the end of acquisition of each data block, it is then transferred and read by the PC, where it is processed and can be visualised or saved on an external hard drive for later analysis. The image reconstruction system can produce images for both amplitude and phase of the domain, by using one of the versions of Linear Back Projection (LBP) algorithm, which is called Sensitivity Back Projection (SBP) algorithm. The reconstruction algorithm (SBP) can provide further option of displaying images for real and imaginary part.

3.4.5 ERT Sensor design

The aim of ERT is to acquire the conductivity distribution in the domain of concern. This is done by, as previously mentioned, injecting an electrical

current and measuring the voltage difference through the electrodes placed on the boundary of the area of concern. Amongst the three components of ERT system, the design of sensor (electrodes) is the most important part, since the better design of electrodes the more efficient they can be to sense the conductivity of the area of interest (Seagar *et al.*, 1987). The electrode material is normally fabricated from platinum, gold, silver, brass, stainless steel or alloys, such as silver platinum. However, there are several factors that can be considered prior to design the electrodes, such as the position of the electrodes, the size of the electrodes and number of the electrodes (Mann and Wang, 1997). As these factors are important for reconstruction algorithm, measuring the conductivity field distribution, collecting the data and reconstructing the image. Usually the electrodes are placed around the boundary of the pipe or the vessel in order to make electrical contact with the content of the pipe or vessel in a non-intrusive fashion or slightly intrusive, as they are introduced to the field of interest through the wall of the pipe or the vessel, which makes them invasive. The other ends of the electrodes are connected to the Data Acquisition System (DAS) through co-axial cables so as to avoid or reduce the electromagnetic noise or interference (Williams and Beck, 1995). A dual plane ERT sensor was designed to be used in this study, a geometry and dimensions of which is shown in Chapter 6.

3.4.6 Image reconstruction analysis

The aim of image reconstruction in Electrical tomography is to compute a tomogram, which is representing the electrical conductivity of the material flowing through the pipe or the vessel (Giguère *et al.*, 2008b).

Generally there are two types of algorithms that are used to process the data for image reconstruction; non iterative algorithm as Linear Back Projection (LBP) and iterative algorithm as Sensitivity Conjugate Gradient (SCG) (Wang, 2002). The selection of the most suitable depends on accuracy, speed and expense. Over the years many image reconstructions have been proposed for electrical tomography, however, the most widely used algorithm is still Linear Back Projection that is due to its advantages over the iterative algorithms, which is computationally more time consuming and too slow for real-time image reconstruction. Therefore, this study employs the non-iterative algorithm (LBP). This algorithm is simple and fast, but it offers qualitative images only. If the image needs to be enhanced, an iterative image reconstruction algorithm can be employed (Ismail *et al.*, 2005)

In order to obtain the conductivity distribution a grid of small equal squares is applied on the area of interest. Each individual tomogram consists of a 20x20 pixel array, which gives 400 spatial elements. The circular image is constructed using 316 pixels from 400 pixels squares grid. Some of these pixels lay outside the pipe or the vessel circumference, but the image is constructed from the pixels inside of the pipe or the vessel, as the sensors are placed on the boundary of the body (Hosseini *et al.*, 2010).

Electrical Tomography is considered as a soft-field technique, since the image is based on measurements at the boundary of the sensor. The sensitivity changes across the sensing zone and also the sensitivity of a particular position within that zone depends on the spatial variation of the physical parameter been imaged within the whole sensing zone. Therefore, due to this linear behaviour the reconstructing of the image can be difficult. Despite some development in image reconstruction, some concerns have been raised, particularly ERT, regarding the performance, validation and limitations of quantitative image reconstruction technique. Most of the efforts made to improve the image reconstruction algorithm were made in Electrical Capacitance Tomography (ECT). However, the image reconstruction techniques used for ECT can be transposed to ERT, as there is a simple mathematical analogy between them (Giguère *et al.*, 2008b).

Most image analysis is based on the images produced by Linear Back Projection (LBP). There are a number of approaches to analyse the images, one of which is the generation of summary statistics (mean, maximum etc.), which is the simplest. Statistics can be calculated either for the whole image or for the smaller regions, such as concentric zones or course square tiles, and this is done by dividing the image into zones. This method can be used to define the heterogeneity parameters, as studied have been conducted on flow regimes in bubble columns. Some other approaches are based on comparison, such as comparing successive images (frames), multiple planes. Cross correlation analysis can be used to obtain information on particle velocities, mixing and diffusion. Here pixel correlations are computed within frames, between successive frames or planes (Tapp *et al.*, 2003)

3.4.7 Application of the ERT

The Electrical Resistance Tomography not only offers the opportunity to visualise the two or multiphase flows, but also capable of measuring some flow parameters, such as solid's concentration and velocity (Parvareh *et al.*, 2010). In other words, the ERT can be sued to obtain qualitative and quantitative data, representing the real life of what is really occurring inside

the process under investigation, and that is with the aid of one frame or tomogram generated via image reconstruction system.

As solid and liquid used in this study, then the right choice must be made as to which technique has to be used to visualise and measure the process. The preferred method in the field of slurry transport is ERT, as it is safe robust and more suitable to interpret the whole process fast and continuously unlike Gamma-ray densitometry, which is only capable to measure the local density value in one chord (vertical y-axis) in one plane and not giving the full understanding of settling behaviour in slurry pipelines (Brown and Heywood, 1991; Pugh, 1995; Matousek, 1997).

From a review of the literature in the last fifteen-twenty years, despite appearing some new applications, it was found that the large scale application has been in mixing process, particularly solid-liquid applications, and two/multiphase flow. Tomography was used by McKee *et al.* (1995), who studied the optimal agitation speed and its influence on the concentration profile. It was also used by Williams (1995) for measuring a mixing index. One year later Williams *et al.* (1996) used tomography again to study the effect of impeller size, impeller type and particle distribution on the mixing index. Wang *et al.* (1999) used ERT as a suitable technique for identifying non-uniform density regions within foam, which suggests that ERT can well be a viable method for process control in a foaming system. Wang *et al.* (2000) studied gas liquid in a stirred vessel, where they used ERT to investigate the effect liquid viscosity on the mixing behaviour. Kim *et al.* (2006) investigated the mixing process and dispersion velocity of two miscible liquids in a vessel with a rotating agitator. They used four-plane ERT to calculate the mixing time from the temporal trend of cross sectional conductivity distribution and concluded that data analysis method with ERT to measure and analyse the mixing. In another study by Cho *et al.* (1999) EIT used to visualise the bubble distribution in two phase flow, where they decreased the image reconstruction time using an adaptive mesh grouping method. Kim *et al.* (2001) designed an EIT system and employed to visualise two phase flow system. When they obtained the image from the image reconstruction, they found that the image quality was not very good. However, they suggested that EIT could be used to visualise two phase flow system. Giguère *et al.* (2008b) used ERT to visualise slurry flows in horizontal and vertical pipe. They analysed slurry flow regimes using a strategy based on the direct interpretation of ERT measurements.

Although ERT technique is a promising technique to visualise slurry flow, there are limitations in terms of quantitative ERT images, which makes them difficult to exploit the quantitative images, furthermore the validation of these quantitative images are necessary. Giguère *et al.* (2008a) has described the development of quantitative ERT image reconstruction software, in which the validation of the results for the case of static solid particle bed, at the bottom of the pipe sensor, has been carried out. He has also successfully shown good agreement between a calibration curves, using ERT relating the size of particle bed with experimental values using LBP.

3.4.8 Conductivity conversion to solids concentration

When the ERT is used to measure a mixture, for example slurry, it obviously measures the conductivity distribution, or map the conductivity of phases, and if the concentration of the dispersed phase (such as solid) is required, then there must be a method or correlation to convert the measured conductivity distribution to concentration of the dispersed phase or particles. Within the last three centuries a number of correlations have been proposed for conversion of conductivity to concentration of the non-conductive dispersed phase. The most important of all are those of Maxwell (1881); Brggeman (1935); Mridith and Tobias (1962); Prager (1963) and Weissberg (1963).

Maxwell (1881) derived an equation for diluted mixture, as shown in equation 3.13, in which relates conductivity distribution and particle concentration distribution, which is expressed in terms of solids (or dispersed phase) volume fraction, α_c, (Maxwell, 1881; Lucas *et al.*, 1999; Pashowko, 2004).

$$\alpha_c = \frac{2\sigma_1 + \sigma_2 - 2\sigma_m - \left(\frac{\sigma_m \sigma_2}{\sigma_1}\right)}{\sigma_m - \left(\frac{\sigma_2}{\sigma_1}\right)\sigma_m + 2(\sigma_1 - \sigma_2)} \tag{3.13}$$

If it is assumed that the dispersed particles are non-conductive, as sand is used in this study, then the conductivity of sand is considered to be zero and the above equation can be simplified to:

$$\alpha_c = \frac{2\sigma_1 - 2\sigma_m}{\sigma_m + 2\sigma_1} \tag{3.14}$$

The above equation can well be used to calculate the particle volume fraction, but only in case of isothermal condition, where the temperature of the mixture remain constant or inevitably with slight change. Since any change in temperature can affect its conductivity values.

Maxwell believed that his equation can only apply on diluted mixtures. However, Turner (1976) confirmed that Maxwell's equation can also be used for high solids concentration, even with maximum packing concentration of the slurry.

Bruggeman (1935) studied a mixture of non-conducting spherical particles in a conducting media, and generated the following equation:

$$\sigma_m = \sigma_1(1-\alpha_c)^{1.5} \tag{3.15}$$

Meredith and Tobias (1962) also generated an equation relating the conductivity and local solid's concentration:

$$\sigma_m = \sigma_1\left[\frac{8(2-\alpha_c)(1-\alpha_c)}{(4+\alpha_c)(4-\alpha_c)}\right] \tag{3.16}$$

Another correlation proposed by Prager (1963), who derived a generalised diffusion model for the suspension of irregular shaped particles, based on random geometry:

$$\sigma_m = \sigma_1\left[\frac{(3-\alpha_c)(1-\alpha_c)}{3}\right] \tag{3.17}$$

Weissberg (1963) carried out further work and proposed another correlation, in which he considered that the spherical particles were randomly distributed in an idealised bed:

$$\sigma_m = \sigma_1\left[\frac{2(1-\alpha_c)}{2-\ln(1-\alpha_c)}\right] \tag{3.18}$$

Now, as there are five correlations, by which the concentration of the dispersed phase could be determined, then a question may raise here as to which of the above correlations perform better. The answer could be given by Holdich and Sinclair (1992), who found that the prediction of the conductivity in all the above five correlations is similar, only if the solid or the dispersed particles volume fraction is less that 30% (Pachowko, 2004). Therefore this suggests that the prediction of all the above correlations differ only when the solid bed is formed, since the solid bed is formed when the solid's volume fraction is more than 40%. Despite that, this study is still employs Maxwell's correlation, as it is well preferred by many researchers and used in ERT system to convert the conductivity distribution to solid's concentration.

3.4.9 Limitation of the ERT

The previous sections have clearly highlighted the advantages of ERT over the other measurement techniques. However, there is still scope for improving some aspects of ERT, such as spatial resolution, conductivity resolution and ability of distinguishing single particles. These limitations are discussed below.

3.4.9.1 Spatial resolution

According to Seagar *et al.* (1987) this helps in identifying a minimum particle size. Wang *et al.* (1999) found out that by varying the particle to vessel or pipe diameter ratio and keeping the mixture conductivity constant and measurement error less than 1%, a typical spatial resolution of 5% pipe diameter can be achieved. As previously discussed, this study uses 50 mm pipe diameter, and according to Wang *et al.* (1999) the ERT sensor can identify sand particle size of 2.5 mm or greater.

3.4.9.2 Conductivity resolution

This parameter determines the minimum conductivity deviation in individual pixels, which enable the image reconstruction algorithm to pick up the change and demonstrate it in the images. Wang *et al.* (1999) carried out an investigation regarding this aspect and found out that at least a deviation of 10% of conductivity is required for the object to be imaged, for fixed particle to vessel diameter ratio and measurement error is less than 1%. This study uses water and sand as the components of the slurry. The typical conductivity of tap water is between 0.3 and 0.45 mS/cm, and the conductivity of sand far less than this value, which makes more than 10%.

Therefore, the ERT could easily pick up the sand particles in the produced images.

3.4.9.3 Ability of distinguishing single particle

This parameter determines the minimum distance between each single particle so that the ERT would be able to distinguish each of them. Through an investigation by Wang *et al.* (1999), the minimum value for this parameter was found to be 20% of the vessel or pipe diameter, if the measurement error is less than 1%. Since this study uses a 50 mm pipe diameter, then a minimum distance of 10 mm is required between each sand particle, so that they can clearly be seen in the tomograms, otherwise they will be seen as a single particle. This suggests the impossibility of ERT to distinguish every single particle in the slurry flow used in this study, unless a very low concentration and very coarse sand are used in homogeneous flow regime. However, this may not have an importance when the contact load of bed is formed.

3.5 Conclusions

This chapter has reviewed the current techniques available for measurement of solid-liquid flow. It was found that the abrasiveness, opacity and complex nature of solid-liquid flow are considerable challenges to its measurement. It was also concluded that amongst all commercially available techniques, whether conventional or novel sensors, no technique measures face fraction and face velocity without limitations. Functionality and applicability of current flow meters over a wide range of conditions still remain unsolved. The settling tendency of solid particles, which results in arising several flow regimes within the pipelines, is still considered as a remarkable challenge to slurry flow measurement. Particularly for measurement of stratified flow, as the strata creates a coat over the sensors and affecting their functionality. A light was also shed on the current status of electrical resistance tomography technique, and it was gathered that the ERT, compared to the rest of novel sensors, has a remarkable package of advantages, namely relatively low-cost, having high temporal resolution, non-intrusive, providing qualitative data as well as visual information about the flow, safe, robust and reliable. However, despite a progressive work, it still suffers from low spatial resolution, which requires to be overcome.

Chapter 4
Horizontal and vertical flow experimental set up and calibration procedure

This chapter describes the laboratory experiments and the operating procedure conducted on 50 mm horizontal and vertical pipeline. The calibration procedure carried out on various instrumentations is also presented along with the results of each calibration.

4.1 Introduction

In order to fulfil the objectives mentioned in Chapter 1, it is essential to establish an effective and comprehensive methodology along with a flow loop system that allows an easy measurement, visualisation and validation of slurry flow parameters. The most important parameters that this study is concerned are slurry velocity, solids velocity and its profile, in-situ and delivered solids concentration. The flow loop used in the experiments and its associated instrumentation are also discussed in the following sections.

The experiments were focused on the observations of both, the integral flow characteristics and the local flow characteristics of settling slurry pipeline. Since the measurement of the local flow characteristics is crucial for the identification of the mechanisms governing the process of slurry flow, then the ERT technique was employed to interrogate the internal structure of slurry flow in the pipeline under various slurry flow conditions. Besides, the ERT system was used to generate some of the integral flow characteristics, such as mean solids concentration and mean solids velocity across horizontal and vertical test section of the pipeline. Due to the dynamic and rapid change of the internal structure of slurry flow, it was believed that a fast measuring technique is required to provide continuous information about the development of slurry flow inside pipelines. Therefore, the Fast Impedance Camera system was used in these experiments with capability of acquiring 1000 dual frames per second.

The first approach is experimental measurement and visualisation of horizontal and vertical flow. The experimental measurement and visualisation involve intense utilisation of the ERT and the Electromagnetic Flow meter (EMF). The ERT is used to determine solids concentration and

solids velocity distribution across the pipe cross section. EMF will be used to measure mean slurry velocity. As settling slurry flow suffers from flow discontinuity (or phase change), which adversely affects the measurement scheme due to occurrence of various flow regimes in horizontal flow. Therefore, a technique is proposed for recognition of the prevailing flow regime, which is discussed in Chapter 7.

The following sections present the installation and measuring technique together with the measured data for characteristics of the dispersed phase (sand). The experimental data for slurry flow through the two orientations are presented and discussed with an analysis of the measurement results in Chapter 5.

4.2 Aims of the experimental work

The main aim of the experimental work was to evaluate the suitability and applicability of the ERT (Fast Impedance Camera System-FICA) for visualisation and measurement of settling slurry flow. This evaluation was carried out by observing the behaviour of slurry flow in horizontal and vertical pipeline and measuring the flow characteristics appropriate to the detection and analysis of mechanisms governing the process of slurry flow measurement. The measured characteristics had to be appropriate for the verification of the components measured via the ERT system. In order to achieve this, two types of flow parameters were measured:

a. The integral flow characteristics, which refers to the mean values of a quantity in a pipeline cross-section (i.e. slurry velocity, pressure, spatial solids concentration, solids axial velocity and delivered solids concentration).
b. The local flow characteristics in horizontal and vertical pipeline, which refers to the In-situ flow parameters (i.e. local concentration at different positions in the vertical plane of the pipe cross-section and local solids axial velocity at different positions in the vertical plane of the pipe cross-section).

The fulfilment of the main objective required the execution of several specific tasks, which are listed below:

1. Validation of slurry flow rate via flow diversion technique using measuring tank.
2. Online visualisation of slurry flow through image reconstruction of pipe cross-section.

3. Verification of 3-D solids velocity profile across the pipe cross-section in horizontal flow.
4. Validation of solids volumetric distribution against the real flow photographs captured at the very same flow conditions of the ERT measurement.
5. Investigation of the effect of particle size on the measured concentration and solids velocity profile using the FICA system and identifying the reasons for the possible effects.
6. Exploring the effect of concentration on the measured concentration and solids velocity profile using the FICA system. Also, identifying the reasons for the possible effects.
7. Highlighting the effect of transport velocity on the measured concentration and solids velocity profile using the FICA system and mentioning the reasons for the possible effects.
8. Estimation of the parameters that define stratified settling slurry flow, such as height of moving bed, height of stationary bed, height of shear layer, height of turbulent zone at the upper part of the pipe, identification of moving and stationary bed.
9. Comparison of In-situ and delivered solids concentration and establishing the relationship between the two parameters.
10. Identification of blockage (total stationary) in horizontal pipeline and estimation of mean solids concentration and mean solids velocity in the blocked pipe section.
11. Visualisation of four main flow regimes in horizontal flow through combination of concentration and solids velocity profile.
12. Automatic recognition of main flow regimes in horizontal flow through combination of concentration and solids velocity profile.
13. Error analysis of mean concentration and mean solids velocity obtained from the ERT system.
14. Investigation of the effect of Wave Velocity and any possible effect on the mean solids velocity in stratified flow.
15. Highlighting the rate of deviation of the ERT measured concentration at transport velocities up to 5 m/s.

4.3 Horizontal and vertical slurry flow loop layout

The experiments were carried out using a pilot scale re-circulating open flow loop, the schematic layout of which is presented in Figure 4.2. The major components are a mixing tank, slurry pump, horizontal and vertical pipeline

test sections, a switch or flow diversion system with a measuring tank (sampling tank), dual-plane Electrical Resistance Tomography sensors (ERT), an Electromagnetic Flow meter (EMF), pressure transducers and a thermocouple. The flow loop is laid on two floors in G.56, Houldsworth Building in the Institute of Particle Science and Engineering/ School of Process, Environment and Materials Engineering in the University of Leeds. The entire length of the loop is 22 m and has an internal diameter of 50 mm. The connecting pipes (DN 50) are from uPVC material (class E 15 bar BS EN1452) from Pipestock. The mixing tank has a capacity of 500 liter and is coupled with a three-blade mixer so as to obtain a homogeneous mixture before introducing it to the flow loop. Therefore, the main function of the mixing tank is to mix and hold the returning slurry from the flow loop before pumping it back to the flow loop. A bypass or a flush line is also connected to the mixing tank for initial lubrication of the pipeline before introducing the slurry of coarse particles, and also for draining purposes.

The loop is served by a 15 KW centrifugal pump (2/1/2 AH WARMAN PUMP), which is connected to a Digi-drive Frequency Converter (LEROY SOMER -15Kw) to control the mean slurry velocity. The two test sections of the loop, horizontal and vertical test sections, are placed in the straight lines so that the affect of bend and flow disturbances are avoided (Matousek, 1997). The length of both horizontal and vertical test sections is 2.40 m and 2.25 m respectively. The horizontal test section is equipped with two pressure sensors and a dual plane ERT sensor. According to Gillies (1991) and Pachowko (2004), the approach length must not be less than 50 pipe diameter. Therefore, the dual plane ERT sensor is placed directly 3.40 m away from the bend. Whereas the vertical test section is equipped with two pressure sensors, an Electromagnetic Flow Meter, a thermocouple and a dual plane ERT sensor. The dual plane ERT sensor, in the vertical section, was placed 2.5 m away from the bend. The returning limb connected to the top of the vertical section is 2.75 m and returns the slurry back into the mixing tank or the measuring tank if the flow is diverted. A flow switch mechanism is used for the flow diversion process. The measuring tank, which has a capacity of 90.5 liter is placed on a set of three load cells for measurement of weight and the level of diverted slurry into the measuring tank. The level of each diverted amount of slurry is determined through a graded glass tube, which is mounted on the measuring tank. A transparent pipe section of 1 m long is included into the horizontal section directly after the ERT sensor, which would enable visual observation of the flow and capturing photographic images for visual observations and validation

purposes. As slurry is opaque and murky, it was very difficult to capture the photographs of the flowing solid within the carrier liquid. Therefore, the observation section was coupled with a light box, which would enable to produce a clearer picture of flowing solid particles within the pipe section. Another transparent pipe section of 45 cm long is also included into the vertical section for the same purposes. Figures 4.1 and 4.2 showing the schematic diagram of the loop and some components of the flow system.

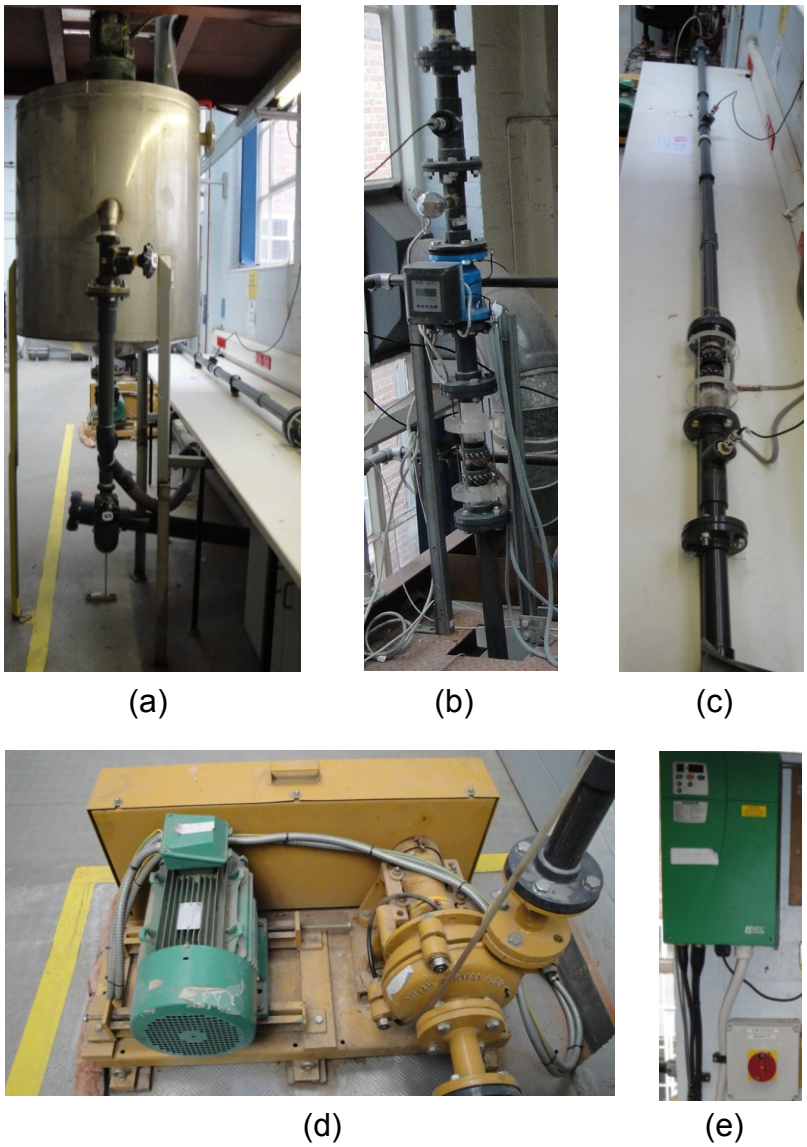

(a) (b) (c)

(d) (e)

Figure 4.1 Photographs of the flow loop with its associated instrumentations, showing (a) mixing tank with the flush line, (b) vertical test section, (c) horizontal test section, (d) centrifugal pump, (d) digi-drive frequency converter

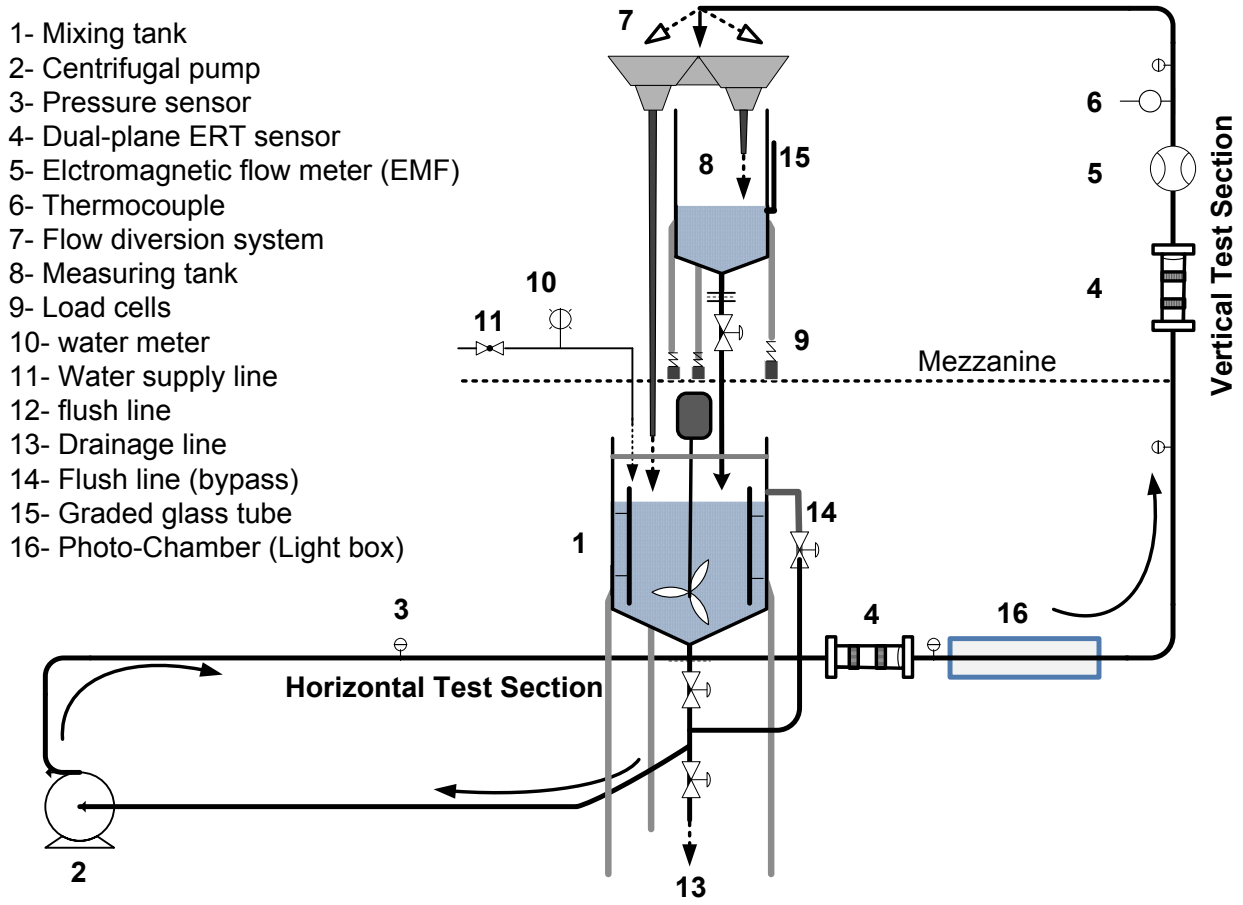

Figure 4.2 The schematic diagram of horizontal and vertical flow loop

4.3.1 Flow diversion technique

It is worth pointing out that the flow diversion system is one of the most important parts of the flow loop. This is due to the advantage of the system for measurement of several important flow parameters and verification of the data obtained from the ERT:

1. To establish delivered solids concentration.
2. To validate the mean slurry velocity measured by the EMF.
3. To validate local solids volumetric concentration obtained from the ERT.
4. To validate local solids axial velocity obtained from the ERT.

The flow diversion system consists of a switch system (or flow diversion system) and a sampling vessel (measuring tank), which is mounted on a set of three calibrated load cells, the actual photograph of the whole system is shown in Figure 4.3.

(a) **(b)**

Figure 4.3 Photographs of the flow diversion system, (a) measuring tank with the switch system, (b) graded glass tube mounted on the measuring tank

The flow switch system is coupled to the sampling vessel at the exit of the flow loop, through which the slurry would return to the mixing tank in a routine fashion. The bottom of the vessel has a conical shape, so as to facilitate the sliding of the solid particles at the bottom once the discharge valve is opened for the slurry to be placed back into the mixing tank. The flow diversion system was connected to the mixing tank through 100 mm uPVC pipe. In order to measure mean slurry velocity or delivered solids concentration, the flow is diverted to the sampling vessel for any given length of time. Obviously, during the diversion process, the valve at the outlet of the vessel has to be closed. A level graded glass tube was also mounted on the measuring vessel, through which the diverted slurry level could be monitored and measured. An electronic stop watch is used to measure the duration for which the flow is diverted. However, a great effort should be made to carry out the diversion process within a possible shortest time. This is due to two reasons, firstly so as to avoid settling solid particles at the bottom of the vessel, which could be a potential risk for blockage at the discharge point of the sampling vessel. Secondly, removing a given amount of slurry from the system would result in decreasing the suction head of the pump, which precipitate the instability of the flow. The procedure is to divert the slurry and allow a sufficient time for the slurry to reach a certain level, somewhere 50% of the measuring tank. Then switch the flow back to the mixing tank and record the slurry level and the duration of the diversion. As the cross-section area of the measuring tank was known, then the volume of the diverted slurry could be determined as well as the flow rate. After several seconds of diverting the flow to the measuring tank, it was noticed that the velocity shown on the Electromagnetic Flow meter (EMF) was gradually dropping. Therefore, the reading of the Electromagnetic Flow meter was recorded just before the slurry diversion. Although it was noticed that the EMF readings were slightly fluctuating, the velocity shown of the EMF just before the diversion was considered for the comparison process. As slurry flow is quite complex by nature, then this fluctuation is well expected. Both mean volumetric concentration and mean solids velocity from the ERT and the flow diversion technique was then collected for the comparison, as shown in the calibration section 4.5. It is worth mentioning that the validation of the local concentration using this technique could not be applied for all transport velocities, particularly low velocities, in horizontal flow, due to phenomenon of particle deposition at lower velocities. As at higher transport velocities the local concentration at any section of the flow loop is more or less the same. Therefore, the local concentration in

horizontal flow was validated only for flow of high transport velocities (4 m/s and above). On the other hand, as the slip velocity can totally be ignored for the slurry flowing through the vertical test section, the validation of in-situ solids volumetric concentration in the vertical line can be carried out using flow diversion technique.

4.3.2 High performance ERT system

The full ERT system was in house built (Online Instrumentation Laboratory/University of Leeds/UK). The main ERT system (Data Acquisition Hardware), this study employs a Fast Impedance Camera system (FICA) (or a high performance dual-plane electrical impedance tomography system), the software and hardware of which have been enhanced and consolidated by OLIL group (Online Instrumentation Laboratory/University of Leeds). It is worth pointing out that one of the advantages of this system is the efficiency of the hardware and simplicity of the operation of the control software. The principle of the hardware operating system and the operation of the control software is described in detail in Schlaberg *et al.* (2008).This development of the conventional EIT system could be considered as a response to the requirement of many industrial processes such as two/multiphase flow, where a higher (faster) frame rates is required to measure and monitor the flow behaviour. The Data Acquisition System (DAS) is based on the phase sensitive demodulation and both the amplitude and the phase of the measurement can be obtained. Once the system is connected it allows the Data Acquisition System to operate in two modes, continuous (on-line) and block mode.

In continuous mode, a single frame of data for one or two planes is acquired, captured, transferred and displayed in the selected format. This mode can capture data at a frame rate up to 50 dual-frames per second (dfps), which is equivalent to 20 ms; whereas block mode can capture data up to 8000 frames at a rate up to 1000 dfps. At the end of acquisition of each data block, it is then transferred and read by the PC, where it is processed and can be visualised or saved on an external hard drive for later analysis.

4.3.3 Visualisation and image reconstruction scheme

The ERT technique can also provide a visual result from the tomograms produced by the system. Each tomogram contains important information on the cross sectional distribution of constituent phases. For example, the conductivity of the domain or concentration of each phase (solid or liquid) can easily be determined on the tomograms. The time taken to construct an

image (tomogram) and its resolution, depend primarily on the type of algorithm used. The image reconstruction system can produce images for both amplitude and phase of the domain, by using one of the versions of Linear Back Projection (LBP) algorithm, which is called Sensitivity Back Projection (SBP) algorithm. The reconstruction algorithm (SBP) can provide further option of displaying images for real and imaginary part. In this study an alternating current of 15 mA with a frequency of 9600 Hz was injected. After mapping the conductivity of the media through each plane, the conductivity data was converted into the local concentration distribution using Maxwell relationship. Then the signals of the two planes were cross-correlated, using pixel-to-pixel correlation, to estimate the solids axial velocity profile. The principle of cross-correlation is described in section 3.2.4. The cross-correlation method, pixel-to-pixel, have been used in a number of previous studies such as Etuke and Bonnecaze (1998), Lucas *et al.* (1999), Mosorov *et al.* (2002), Wang *et al.* (2003), Henningsson *et al.* (2006). Furthermore, clear PVC sections are included into both test sections, in order to allow for visual observation of the flow, along with capturing photographs via a digital camera.

4.3.3.1 Maxwell relationship and solids concentration

The averaged concentration profile can be used to determine the distribution of the solid particles across the pipe cross section. The averaged concentration profile is obtained via measuring the voltage at the sensor location to determine the conductivity of the media. The conductivity is then converted to concentration based on Maxwell relationship (1881). The local conductivity value of each pixel can be converted to a solids concentration. Conductivity conversion to solids concentration is described in section 3.4.8.

4.3.4 The dual-plane ERT sensor

The dual-plane ERT sensor was in house built (Online Instrumentation Laboratory/University of Leeds/UK). The actual photograph of the dual plane ERT sensor is illustrated in Figure 4.4.

The ERT sensor was conFigured as a dual plane sensor in order to apply cross-correlation and measure the local axial velocity of the dispersed phase. The distance between the electrodes of one plane to the other plane was 70 mm. 16 stainless steel electrodes were mounted on the periphery of each plane at equal interval, flush with the inner surface of the pipe, where non-intrusively in contact with the media. The configuration of the electrodes

was based on the adjacent protocol, which produces N(N-3)/2 measurements (N denotes the number of electrodes).

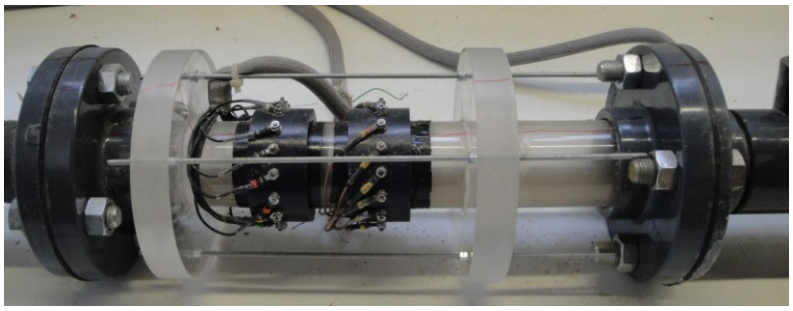

Figure 4.4 The actual photograph of the dual-plane ERT sensor within horizontal test section

4.3.5 Design of the photo-chamber (Light box)

A light box used to capture the photographs of the flow, the actual photograph of which is shown in Figure 4.5.The photo chamber has a rectangular shape with dimensions (1 m length, 0.3 m depth, 0.3 m width). All the sides are sealed with thin plywood, except the front side, which is covered with a matte black PVC coated cloth sheet. Two circular openings, which have similar diameter as that of outer diameter of the pipe section (63 mm), are on either side of the chamber. The cloth sheet can flexibly cover the front side of the chamber and has a lens sized hole in the middle, in front of which the camera is adjusted on a tripod. The top and the bottom of the pipe section inside the chamber were sealed with wooden panels covered to separate the lighting zone. The interior of the box is painted in matte black colour, as light and glossy paint can reflect the flash light and cause glare. The lighting system is attached firmly behind the pipe section and a hole is drilled to the side of the box for the wire to exit the box. In order to avoid the heat of the bulb, it is very important to keep the lighting source some reasonable distance away from the pipe. The distance between the light bulb and the pipeline is 150 mm in light box used in this study. However, this distance depends on the lighting supply. If low-heat LED source is used, then there is a little more leeway, but the lighting effect may not be sufficient for murky and opaque slurry. After testing several lighting sources, it was found that Halogen Work Light (500 Watt) with heavy duty wire guard is the most suitable for this project. It is worth pointing out that this type of light

source produces enormous amount of heat, which adversely affects some characteristics of slurry, such as conductivity of the mixture and as a consequence the ERT measurements. Therefore, in order to avoid overheating and possibility of burning, the light should be switched on only during the time when the photograph is taken. It was noticed that the maximum duration for capturing photographs of each condition was 5 seconds, which is not a long period to raise the temperature of the slurry flowing through the pipe section.

In order to better illustrate the track of solid particles, the photographs of each prevailing flow regime, which were captured by the digital camera, were inserted into the plot area of the measured profiles, the concentration and axial velocity. Despite using the light box, at certain conditions such as at high slurry velocity, some difficulties were encountered in distinguishing the solid particles in the murky carrier liquid. Therefore, the photographs were sent to the Microsoft Office Picture Manager and colour enhancement was applied. The reason for doing so was to avoid any light reflection and enhance the quality of the captured photographs. As it is apparent in the inserted pictures, some photographs required a specific colour so that the solid particles are well shown.

For the sake of clarity and validation, the photographs of flowing solids through the pipeline were captured using a digital camera. Due to opaque nature of slurry, naked eye observation is almost impossible. Therefore, the photographs were taken through 1 m transparent pipe section, which was confined in a photo-chamber (or light box) with a lighting source.

Figure 4.5 The actual photograph of the light box with the transparent pipe section

4.4 Experimental procedure and operating conditions

In order to fulfil the objectives of this study, it is paramount to establish an effective, comprehensive and flexible strategy for each measurement test carried out on slurry flow. Since the aim is to investigate the applicability of the ERT on slurry flow and the effects on measurement scheme, the effect of different variables on slurry characteristics, thus the choice of slurry components and the techniques used to measure each parameter accurately merit special considerations.

4.4.1 Slurry component selection and characterisation

Prior to the selection of the components of the slurry that is be under investigation, several characteristics of the solid particles have to be considered. Also, a careful decision has to be made to satisfy the objectives of this research. These could include particle density, particle size and shape, solubility, electrical properties, cost, safety and availability.

Since settling slurries exist, in nature and industry, in different sizes and shapes, therefore a uniform sized and shaped particle will be avoided in this study. It was decided to select particles that approach the real industrial scenario. Thoughts have been given to the mineral compounds, as they are widely encountered in nature and industry. Based on the above considerations, Glass sand (SiO2) was found to be the most suitable solid component of the slurry in this study. This is due to the advantages listed below:

1. Available in various sizes and shapes.
2. Cheap, (£60)/ton.
3. Non-harmful in case of exposure. Except the dust, for which the protectors will be used, such as goggles and mask.
4. Insoluble in water.
5. Non-conductive that makes it suitable for the ERT measurements.
6. Suitable density (2650 kg/m^3).

Since this study uses a system that handles a large amount of slurry, tap water was decided to be used as carrier liquid. Besides some other advantages, which are listed below, makes water the most suitable carrier liquid.

1. Water is a safe compound.
2. Availability.
3. It can easily be drained without breaching any governmental policy.

4. Good conductivity that makes it a suitable carrier liquid for the ERT measurements.
5. Suitable density and viscosity.

Thus the slurry used in this study consists of a mixture of water and a non-uniform shape and size sand with density of 2650 kg/m³. However, based on the objectives and the applicability of the methods used in this study, also in order to determine the influence of particle size and solids concentration on the measurement scheme, two sands were proposed, medium and coarse sand. Furthermore, the settling characteristics are the most important aspect of this study, which can easily be achieved with medium and coarse sand. On the other hand, two throughput concentrations, 2% (v/v) and 10% (v/v), were proposed for each of the sands to be used in the experiments.

4.4.1.1 Sand particle size analysis

The particle size distribution (PSD) for the two sands was obtained, by taking the sample and oven-dried to achieve each 500 g of dried sand. Sieving method was used, they were then sieved, using a laboratory test sieve, through a series of sieves of standard mesh size (2360, 1180, 600, 300, 150 and 75 μm). The sample fraction obtained in each sieve was weighted on a (Fisher brand, Model PF-6001) balance, ensuring that the final mass measured for each sieve is within 100% of the total solids put through. The fraction by mass was then recalculated to obtain a percentage of oversized particles that cumulated in each sieve. The results of these calculations are shown in Tables 1.1 and 1.2 for the both sands. The result was then plotted against the sieve mesh size to generate a particle size distribution curve, as shown in Figure 4.6.

Using the particle size distribution curve, various important statistics were found. It was concluded that sand 1 has a particle size range with d_{85} = 430 μm, median particle size (d_{50}) of 242 μm and d_{15} = 170 μm. Based on the above analysis, sand 1 can be classified as medium quite broadly graded sand. With regard to sand 2, it was found that d_{85} of which is 2240 μm, d_{50} is 480 μm and d_{15} is 270 μm. Therefore, sand 2 can be classified as coarse broadly graded sand.

Table 4.1 Showing sieve analysis for coarse sand based on 500 g

Nominal Aperture Size (µm)	Mass Retained (g)	Mass Retained (%)	Cumulative Undersize (%)
2360	71.2	14.24	85.76
1180	46.7	9.34	76.42
600	115.8	23.16	53.26
300	184.3	36.86	16.4
150	75.1	15.02	1.38
75	4.2	0.84	0.54
Pan	2.7	0.54	-1.11022E-15
Total	**500**	**100**	

Table 4.2 Showing sieve analysis for medium sand based on 500 g

Nominal Aperture Size (µm)	Mass Retained (g)	Mass Retained (%)	Cumulative Undersize (%)
2360	13.1	2.62	97.38
1180	0.7	0.14	97.24
600	7.1	1.42	95.82
300	166.5	33.3	62.52
150	290.2	58.04	4.48
75	20.8	4.16	0.32
Pan	1.6	0.32	-1.7486E-14
Total	**500**	**100**	

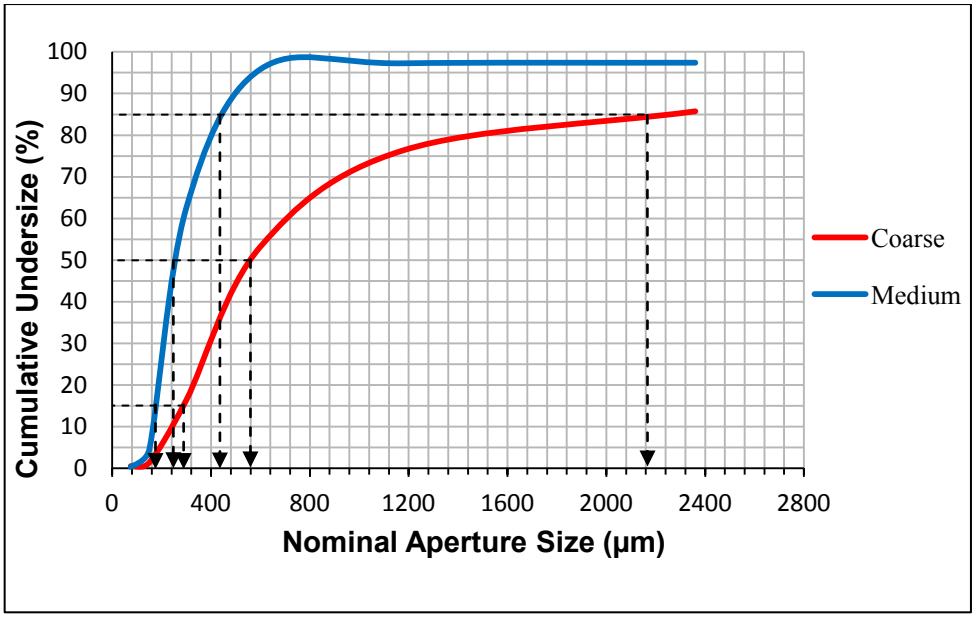

Figure 4.6 Showing the particle size distribution curve for the two sands

4.4.1.2 Density estimation of sand particles

Since the density of solid particles flowing through a pipeline affects solids settling characteristics and the pressure drop, therefore, the measurement of particle density is very important.

A pycnometric method was employed to determine the density of each of the sand used in the experiments. A pycnometer is a pre-calibrated glass bottle, which is used to determine a volume of dry solid particles of known weight. Initially the weight of empty and dry pycnometer was determined. The pycnometer was then filled (by 1/3 volume) with the desired sand particles and the total weight (Pycnometer and sand particles) was estimated. While the pycnometer contained sand particles, it was filled with distilled water. After completely emptying the pycnometer, it was then filled with only distilled water and the weight was determined. As the total volume of the pycnometer is known, then the volume of added water and full water in the pycnometer can easily be calculated. The volume of added water can be calculated theoretically (ratio of weight of added water and its known density). On the other hand, the volume of sand particles is the difference between the volume of water in the pycnometer, while containing sand particles, and the volume of only water in the pycnometer. Finally, the density of solid particles can be estimated through its known weight and calculated volume. The density of sand 1 and sand 2 was found to be 2650 kg/m^3.

4.4.2 Measured parameters and the measuring technique

A set of experiment was carried out at various flow conditions, in which different particle sand size and different concentrations were used. The flow was controlled by altering the mean slurry velocity and the measurements were carried out for each selected condition. The main focus was placed on the measurements of different slurry parameters such as pressure, temperature, flow rate (mean slurry velocity), in-situ and delivered solids concentration, solid's velocity and concentration profile. Since each parameter plays an important role in the evaluation procedure and analysis, therefore, it is very important to ensure that the instrumentations used to measure these parameters are reliable and accurate. This can be fulfilled by testing and calibrating each instrument prior to any experiment. The calibration procedure of the instrumentations is highlighted in the next sections.

4.4.2.1 Mean slurry velocity measurement

The mean slurry velocity was determined using an Electromagnetic Flow Meter (EMF) (Krohne-Aquaflux), which was mounted on the vertical test section. The photograph of the EMF is illustrated in Figure 4.7. Matousek (1997) reported that a reliable measurement can be obtained if the electromagnetic Flow Meter is installed on the vertical section of the flow loop. This is based on the experiment evidence that the slip velocity is negligible between the two phases, the dispersed phase and the continuous phase, within the vertical section. As a result the potential false readings are avoided.

Figure 4.7 Electromagnetic Flow meter within vertical test section

4.4.2.2 Solids volumetric concentration measurement

The measurement of two types of solids volumetric concentration were carried out for each test, in-situ solids volumetric concentration and delivered

solids volumetric concentration. The measurement strategy to determine each concentration is described below:

4.4.2.2.1 In-situ solids volumetric concentration measurement

In order to monitor the internal structure of the flow two-dimensional concentration profile of the local concentration were calculated across the pipe cross-section. Obviously the local chord concentration can represent a clearer picture of the distribution of solid particles and their movement in the vertical axis of the pipe cross-section. The Fast Impedance Camera System (FICA) was used to measure and collect a set of block data of 8000 frames for each mixture velocity. The measured conductivity data was then entered into the P2000 software to produce the conductivity map of the pipe cross-section. The conductivity map then imported into the software package called AIMFLOW, which stands for Advanced Imaging and Measurement for Flow, Multiphase Flow and Complex Flow in the Industrial Plant. The mean local concentration was produced by averaging a block of frames from the concentration map, and the solids concentration profile was extracted along the vertical centreline of the tomograms generated, which composed of 20 pixels. The size of each pixel was calculated as 2.5 by 2.5 mm for 50 mm diameter pipe. The tomograms reconstructed for each test were collected and analysed to determine the mean solids concentration and solids concentration profile across the vertical plane of each tomogram.

4.4.2.2.2 Delivered solids volumetric concentration measurement

Delivered solids volumetric concentration is a very important parameter, as it determines the capacity of a pipeline system (Brown and Heywood, 1991). Therefore this type of solids concentration was measured using a flow diversion technique, in which the slurry flow is diverted for a very short period of time into a measuring tank with a capacity of 250 litre. The delivered solids concentration was found to be an important parameter for validation of the in-situ solids concentration obtained from the Electrical Resistance Tomography system (ERT) and mean slurry velocity measured via the Electromagnetic Flow meter (EMF).

4.4.2.3 Local solids axial velocity measurement

To obtain the solids axial velocity distribution, FICA system was used in conjunction with the cross-correlation method. The data was acquired at a rate of 1000 frames per second for each plane. The measurements were taken and a set of block of 8000 dual images were reconstructed for each flow condition. Each dual image represents the conductivity distribution at

the upstream and downstream planes at a particular time. Then the relation between the two signals from the two planes was established using pixel-to-pixel correlation method, which has been developed into a software package (AIMFLOW) at the University of Leeds and Chinese Academy of Science. By importing the conductivity map, produced from the ITSP2000 software, into the AIMFLOW, the axial solids velocity, concentration and solids volumetric flow rate can be computed.

4.4.2.4 Temperature measurement

The measurement and monitoring slurry temperature is a crucial part of the experiments, as any change in the slurry temperature would affect the slurry behaviour, background conductivity of the slurry and as a consequence a dramatic effect on the results obtained from the tomography measurements. The temperature changes in the slurry were monitored via a K-type thermocouple (from Cole-Parmer) with a sensitivity 41μV/°C. Figure 4.8 showing the thermocouple mounted on the vertical test section. It was connected to the Data Acquisition System (DAS), where the slurry temperature is recorded every 5 seconds. The calibration procedure of the thermocouple is presented in section 4.5.

Figure 4.8 The thermocouple within vertical test section

4.4.2.5 Pressure measurement

The measurement of pressure differential between two points of a section of a straight pipe is one of the most important measurements for pipeline frictional head loss determination. Monitoring pressure changes over straight pipelines can provide valuable information regarding the condition of slurry flow. Therefore, pipeline pressure drops were measured over straight horizontal and straight vertical test sections. Four pre-calibrated pressure sensors (Danfoss flush diaphragm-model MBS 4010) were mounted on the

flow loop, two on the horizontal test section and the other two on the vertical test section. According to the manufacturer these pressure sensors are most suitable in connection with aggressive and non-uniform media with a measurement error of ±0.3%. The actual photograph of the pressure transducer mounted on the horizontal test section is shown in Figure 4.9.

Each pressure sensor was connected to the Data Acquisition System (DAS), where the data is generated in the form of current output, then this is converted to pressure data, knowing that the relationship between the current output and the pressure is linear. The calibration of these pressure sensors is described in section along with the qualitative calibration results.

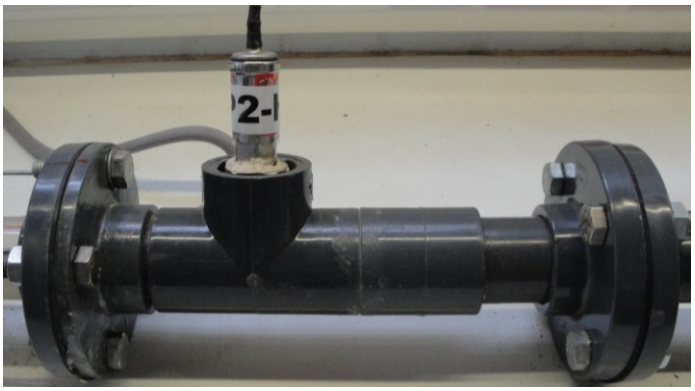

Figure 4.9 The Pressure transducer within horizontal test section

4.4.3 Operating procedure

Slurry transport is a complex operation that can easily divert from the steady state condition, which has a negative impact on the measurement scheme and the experimental data. Therefore, in order to make sure that a good quality of experimental data is obtained, a careful and effective experimental procedure has to be designed. Besides, the accuracy and reliability of the instrumentations used to measure the relevant parameters in each experiment are also paramount. The calibration procedure and the results of each calibration is described in section 4.5.

A series of experiments were carried out on each of the sands with different solids concentration, 2% (v/v) and 10% (v/v). At the start of each experiment the mixing tank is filled with tap water and the pump is continuously introducing water into the flow loop, knowing that the flow velocity is adjusted to a high velocity prior to adding the required sand. Then the conductivity of

water and its temperature is recorded, this will then be required for the ERT reference measurement. The pre-weighed desired sand is added into the mixing tank after switching on the mixer and adjusting the desired rotational speed. It is worth mentioning that while the sand is added into the mixing tank, the valve at the discharge point of the mixing tank is closed and the valve on the flush line is opened. This procedure would ensure continuous flow into the loop through the flush line. After adding the sand to the water, the slurry was initially well agitated in the holding tank so as to achieve a homogeneous mixture. The slurry was then introduced to the flow loop via the centrifugal pump from the mixing tank. The average superficial velocities were in the range of 1.5-5- m/s. The slurry flow was first established at the highest velocity of the pump, which was controlled via the digi-drive frequency converter, then reduced gradually from 5 m/s to 1.5 m/s. The reason for that was to cover all the flow regimes. However, this aim could not be attained for pseudo-homogeneous flow regime, particularly 10% (v/v) coarse sand, due to the limitations imposed by the pump capacity. Particular attention was paid to carry out every test at the steady state condition, through observing the fluctuation of pressure data via pressure graphs on the LabVIEW panel. For each condition and different sand with different concentration the ERT measurements were carried out using the Fast Impedance Camera System (FICA) by mapping the conductivity of the media under investigation. A digital camera was used to capture the photographs of the flow through the transparent pipe section confined in the light box. Since the photographic images of the flow are used to validate the flow regime visualisation, then it is very important to capture the photographs at the same time of the ERT measurement. After each ERT measurement and capturing photographs, the discharge measurements or flow diversion technique was performed, by diverting the flow to the measuring tank for a very short period of time, and then the level of the contents through the glass tube and its weight using the load cells were recorded. As previously mentioned, the diversion technique is a potential cause for flow instability, therefore, after diverting the slurry and returning it into the flow loop, a short period of time is required to ensure the steady state flow condition. Thereafter the next measurement test can be carried out as per previous procedure. Each test carried out for the horizontal flow was followed by the vertical flow measurement. All the measured data then collected via the LabVIEW and processed for future analysis.

4.5 Calibration procedure

In order to obtain reliable and accurate results, the calibration of the measuring instrumentations was carried out. These instruments include the conductivity meter, thermocouple, load cells, ERT testing, pressure transmitters, EMF. The calibration procedure of each instrument mentioned above is explained in the following sections.

4.5.1 Calibration of the thermocouple

The calibration of the thermocouple was carried out within a range of temperature from freezing temperature to boiling temperature. A glass mercury thermometer was also placed in the water alongside the thermocouple. They were initially placed in freezing water then the temperature was altered by adding boiling water to complete the range and reach the other extreme. The temperature indicated by the two devices was continuously recorded each time the boiling water was added. The qualitative data obtained from the calibration process is shown in Figure 4.10, while the quantitative data can be found in Appendix B.

By observing the data shown in Figure 4.10, it can be seen that the temperature values recorded by the thermocouple showing a linear relationship and is quite close to the predicted values. It is quite evident that some overestimation can be noticed and the operating error was established to be 2.5%, which is quite acceptable and no further action was required.

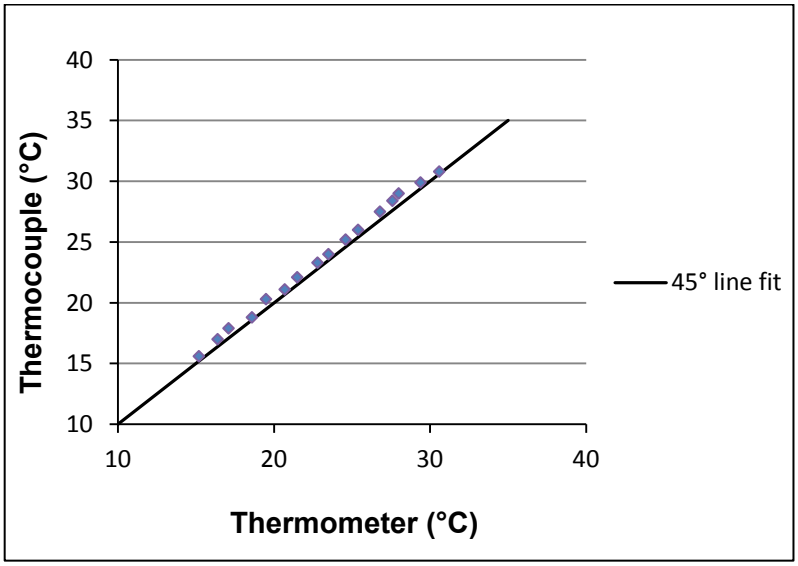

Figure 4.10 Measured temperature for the thermocouple and the thermometer

4.5.2 Calibration of pressure transducers

The calibration of the two pressure transducers mounted on the horizontal line, H1 and H2, and the two pressure transducers mounted on the vertical line, V1 and V2, were carried by recording static pressure against actual values. A long vertical pipe (5 m) was used, on which each pressure transducer could easily be mounted at the lower part of the pipe. The actual pressure (ρgh) was calculated at different level of water in the pipe. For each level the pressure was also recorded by the pressure transducers via LabVIEW software. The calculated actual pressure and the response of each pressure transducer, which was recorded via LabVIEW, are shown in Figure 4.11. A linear relationship can be noticed for each sensor, which confirms the functionality of the each pressure transducer. However, some deviations from the line fit can be seen for each transducer. The amount by which each transducer deviates was calculated and added to the reading of each transducer in the LabVIEW software. After correcting each pressure transducer, another calibration was then performed, the results of which is shown in Figure 4.12. The corrected and uncorrected data obtained from the calibration processes can be found in Appendix B. The observation of the corrected data can reveal a good line fit between all pressure transducers and actual values.

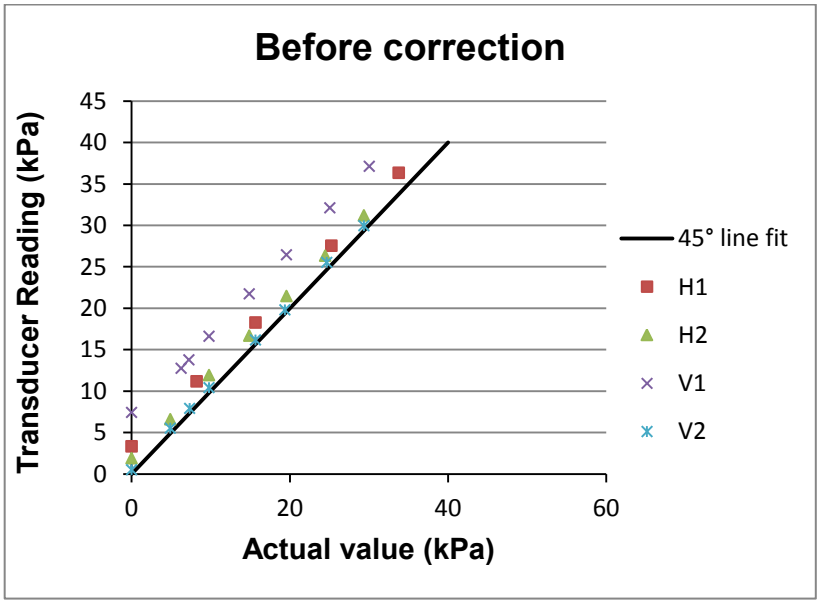

Figure 4.11 The transducers pressure readings against actual values before correction

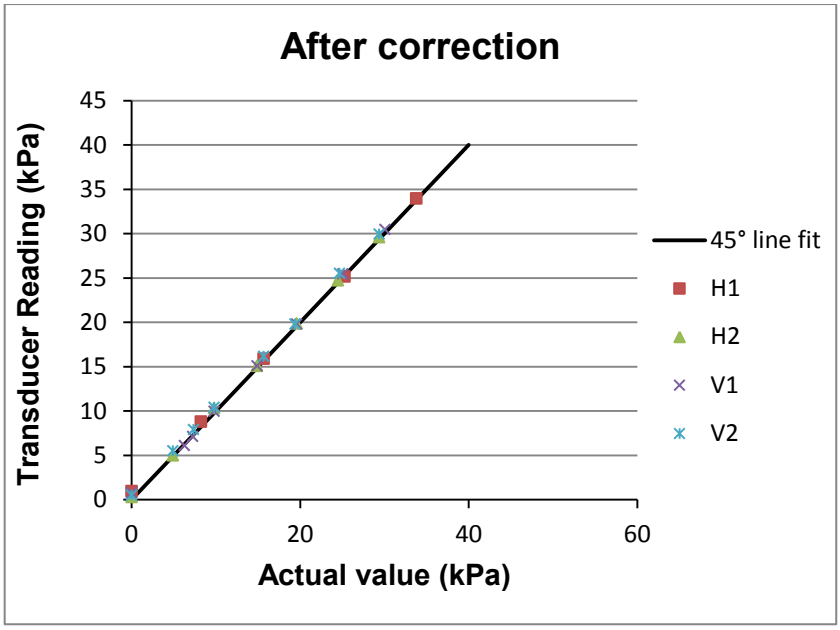

Figure 4.12 The transducers pressure readings against actual values after correction

4.5.3 Calibration of the conductivity meter

A handheld conductivity meter (Jenway 470) has been used for conductivity measurement of the slurry used in the experiments. In order to ensure the reliability of this device a calibration procedure against a pre-calibrated desktop conductivity meter (Cyberscan-PC6500 Desktop conductivity meter) from EUTECH Instruments was performed. The calibration process carried out by placing the probes of both devices into a brine solution (sand and water) at various temperature readings while the concentration kept constant. After analyzing the conductivity values of both conductivity meters, a linear relationship was observed and an average error of 0.45% was determined in the handheld conductivity meter. The comparison results of both conductivity meters is shown in Figure 4.13, while the quantitative measured data can be seen in Appendix B. Based on the value of the established error, the conductivity values obtained for the handheld conductivity meter was considered to be within the accuracy range and no further calibration was followed.

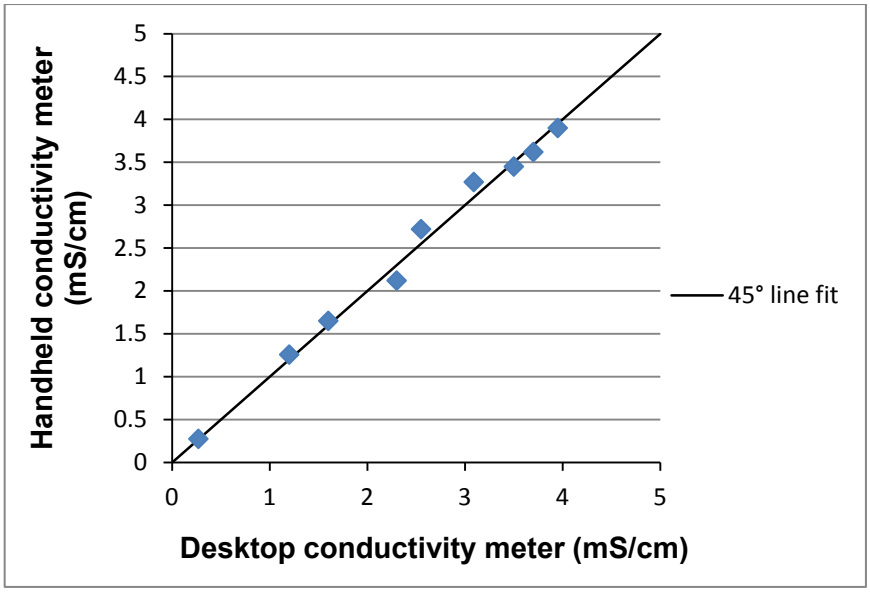

Figure 4.13 Comparison results of handheld and desktop conductivity meter

4.5.4 Calibration of the measuring tank

The measuring (sampling) tank, which is used to determine various important parameters in this study, was calibrated by gradually adding pre-weighed water and comparing the measured weight to the weight calculated based on density. Pre-weighed water, which was measured by a pre-calibrated scale, was added to the measuring tank and the level of water was recorded for each added amount of water. The volume of the contents of the conical section was determined, which is constant, and then the volume of the contents of the cylindrical section was calculated each time the water is added. Then the total volume of the tank content, contents of conical section and cylindrical section, was calculated as the water is gradually added. This way the measured weight of tank contents can be calculated based on known density and calculated volume of water in the tank. This measured weight was then compared to the readings of the pre-calibrated scale and a linear relationship was obtained, as illustrated in Figure 4.14. A good line fit was observed with establishing an average error of 0.65%, which is within tolerance level for the experimental measurement.

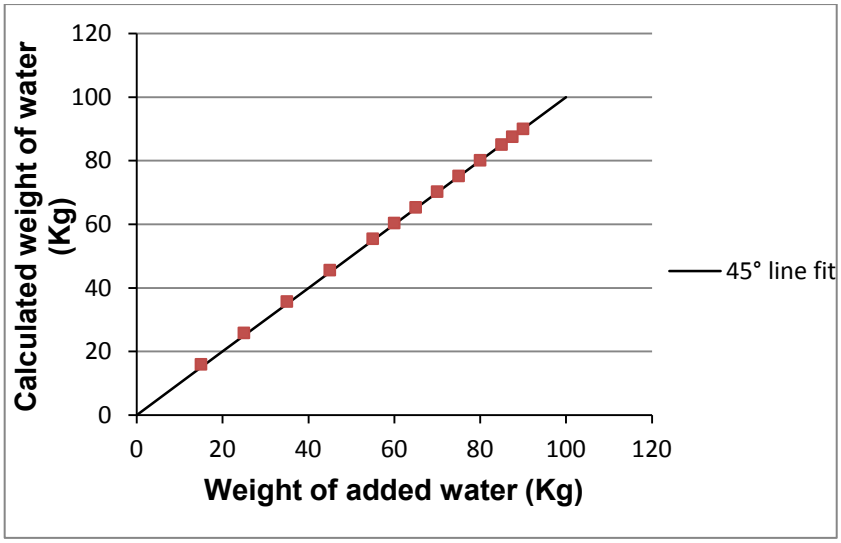

Figure 4.14 Showing the comparison between the weight of added water measured by the pre-calibrated scale and level based measured weight

4.5.5 Calibration of the load cells

The load cells play an important part in the experiments carried out in this study, as these transducers are used for load readings of the contents of the measuring tank. Therefore, a proper calibration is required to ensure their accuracy in recording the weights applied on them.

The full calibration of the load cells is carried out via two stage process calibration. The first stage involves loading the measuring tank with a pre-weighed object and adjusting the reading of the load cells based on the weight of the applied load. This stage can be done using the front panel of the software (Proview) used to conFigure and acquire the data read by the transducers. The second stage involves gradual adding of pre-weighed water to the measuring tank and simultaneous recording the response of the load cells. The calibration process of the load cells is similar to that of the measuring tank. Pre-weighed water is added to the measuring tank and the recorded weight via the load cells is compared to the total weight of added water in the tank. The result of comparison is depicted in Figure 4.15, in which an average error of 0.35% was established in the data recorded by the load cells. The recorded data is also shown quantitatively in Appendix B. By observing the data, shown in Appendix B, it can be seen that the response of the load cells to each amount of water added to the tank corresponds to the actual weight of added water within the range of 15 kg-60 kg. However, some overestimation in the readings of the load cells can be noticed. Since the amount of error is within an acceptable range in the

experiments carried out in this study and the weight of diverted slurry is no more than 60 kg in the measuring tank, therefore, no further calibration was performed.

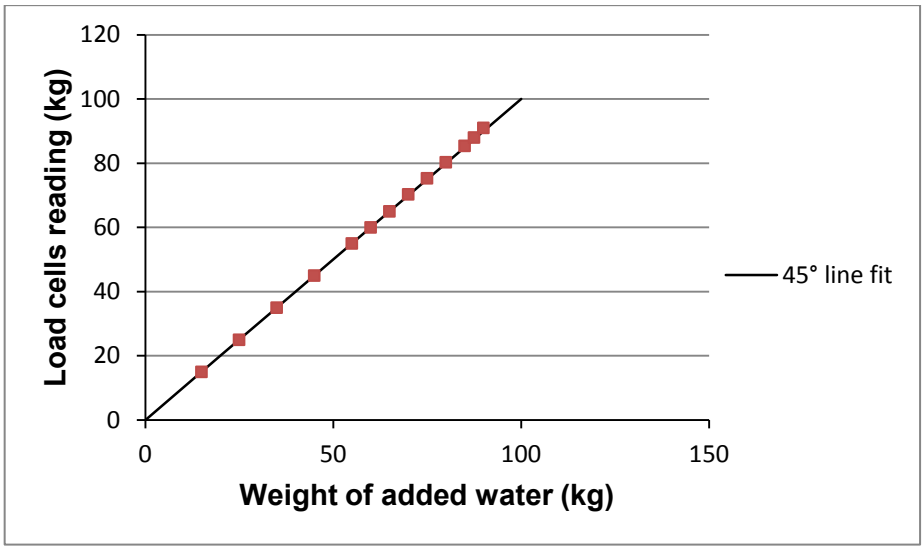

Figure 4.15 Showing the comparison between the weight of added water measured by the pre-calibrated scale and load cells readings

4.5.6 Testing and calibration of the ERT sensor

The calibration and testing of the ERT is very important to ensure the accuracy of the measurement and the reliability of the dual-plan ERT sensor. Therefore, the calibration of the ERT was performed in two-stage procedure. The first stage was to check the functionality of the electrodes mounted on each plane (1 & 2). The electrodes mounted were tested by moving a stimulus (plastic ball), approximately 25 mm diameter, within the sensing region in the water filled pipe. The concept of this test method was to check how much the sensors would record the change in conductivity (or resistivity) of the media and visualizing the result on the tomograms produced by each plane when a stimulus is applied. The result of the test is shown in Figure 4.16 for plane 1 and plane 2. It can be seen that the reaction of the two planes against the resistivity changes are similar in the presence of the stimulus. Figure 4.17 showing the reconstructed image (tomogram) obtained prior to placing the stimulus and during placing the stimulus. The plastic ball is demonstrated by blue colour, which occupies approximately 40-50% of the pipe cross section. Knowing that the pipe diameter is 50 mm and the plastic ball diameter is 25 mm, then a good

agreement can be concluded between the actual size of the ball and its size on the reconstructed image.

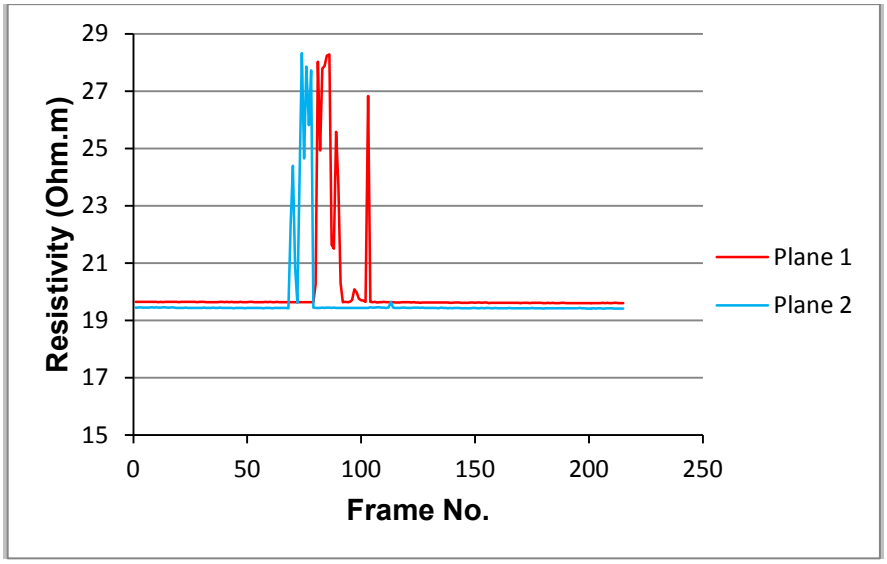

Figure 4.16 Changes in resistivity measured during the course of sensor testing

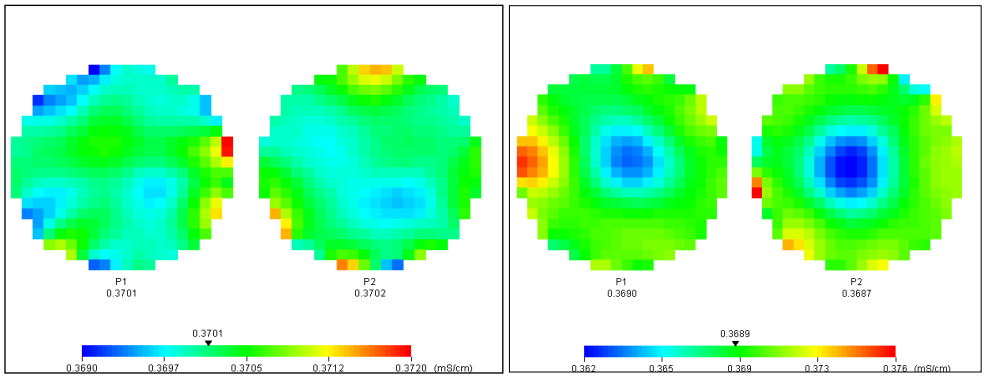

(a) (b)

Figure 4.17 Tomograms showing conductivity of the media: (a) prior to placing the stimulus (b) during placing the stimulus

On the other hand the second stage involved measuring the conductivity of brine solution (coarse sand and water) at different temperature while the concentration kept constant. Several measurement tests were carried out using a pre-calibrated conductivity meter (probe) and the ERT. The conductivity of the brine measured by both devices were recorded and compared. The comparison result is shown in Figure 4.18, in which an average error of 0.22% was determined in the ERT measurements. This,

however, can be considered as an acceptable rate, which is well tolerated in the experiments. Therefore, no further correction was performed.

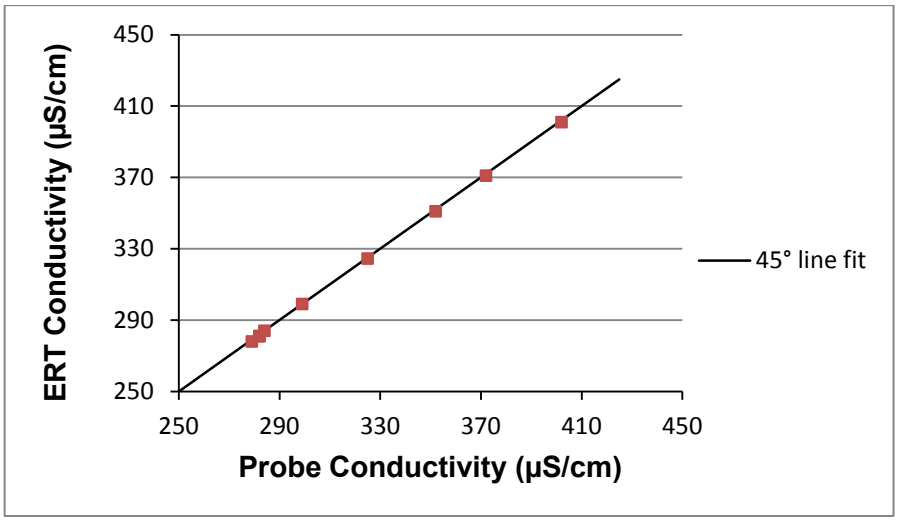

Figure 4.18 Comparison results of brine conductivity measured by the probe and the ERT

4.6 Conclusions

In this chapter, the horizontal and vertical flow loop layout is described, along with the associated instrumentations and techniques used to measure the relevant parameters in this study. The type and reasons for selecting the slurry components and the characterization of the solid particles are mentioned. The operating procedure and the calibration method for the main instruments are highlighted. Based on the calibration results, it was concluded that the thermocouple, the ERT, the conductivity meter, the measuring tank and the three load cells perform accurately within the experimental range. Therefore, based on the initial results of the calibration process, it was decided that the values measured by these instruments can directly be used for future analysis. However, it was revealed that pressure transducers require some corrections, so that the pressure values obtained by them can fall within the tolerance range.

Chapter 5
Horizontal and vertical flow results, discussions and important findings

This chapter presents the experimental results obtained from both test sections, horizontal and vertical, within the 50 NB flow loop. The experimental tests focus on the flow phenomenon of sand particles and its effect on the ERT measurement scheme. A detailed evaluation of the ERT is also presented through validation of the measured parameters obtained from the ERT.

5.1 Introduction

The results of laboratory experiments carried out on a 50 mm pipeline, with a horizontal and a vertical section are presented in this chapter.

The experiments were focused on the observations of both, the integral flow characteristics and the local flow characteristics of settling slurry pipeline. Since the measurement of the local flow characteristics is crucial for the identification of the mechanisms governing the process of slurry flow, then the ERT technique was employed to interrogate the internal structure of slurry flow in the pipeline under various slurry flow conditions. Besides, the ERT system was used to generate some of the integral flow characteristics, such as mean solids concentration and mean solids velocity across horizontal and vertical test section of the flow loop. Due to the dynamic and rapid change of the internal structure of slurry flow, it was believed that a fast measuring technique is required to provide continuous information about the development of slurry flow inside pipelines. Therefore, the Fast Impedance system was used in these experiments with capability of acquiring 1000 dual frames per second.

The following sections present the measurement technique used in the experiments together with the flow characteristics of the dispersed phase (sand) and continuous phase (water). The experimental data obtained from the ERT will be quantitatively and qualitatively analysed with highlighting the rate and potential cause of the occurring error in the measurement for both orientations. The visualisation of typical slurry flow regimes via both profiles, solids volume fraction distribution and solids axial velocity distribution, will be discussed and validated qualitatively. An analysis of stratified flow within

horizontal test section will be covered in this chapter, along with a presentation of a technique, by which the parameters relating to stratified flow can be estimated.

5.2 Experimental strategy

In order to achieve the objectives of this project, the adopted methodology consists of a three-fold strategy, which is outlined in Figure 5.1. This strategy is based on the achievement of the final target, which is evaluation of the measurement, visualisation and flow regime recognition scheme of settling slurry flow. The first approach is experimental measurement and visualisation, which is followed by a flow feature extraction through signal analysis of the ERT data for the purpose of automated flow regime recognition. The experimental measurement and visualisation involve intense utilisation of the ERT and the Electromagnetic Flow meter (EMF). The ERT is used to determine solids axial velocity and solids concentration along with the tomograms of the pipe cross-section for solids flow visualisation. On the other hand the EMF is used to measure the transport velocity (or superficial velocity). The measurement results are then used to characterise the flow of solid-liquid flow within the pipeline via generating the profiles, concentration and solids axial velocity. Also, in order to characterise slurry flow, a flow visualisation scheme has to be proposed.

Clearly each flow regime demonstrates distinct features, such as conductivity distribution, which is directly linked to the distribution of the solid particles across the pipe cross-section. Therefore, it is quite plausible to adopt a recognition scheme based on the specific flow features of each flow regime.

The final approach involves the validation of all the results obtained from the experimental measurement. This includes a comparison of the qualitative results against the obtained results from the flow diversion technique, which employs a bulk flow measurement vessel. Whereas the qualitative results obtained from the ERT is validated against the actual photograph of the flow, which synchronously captured with the ERT measurements.

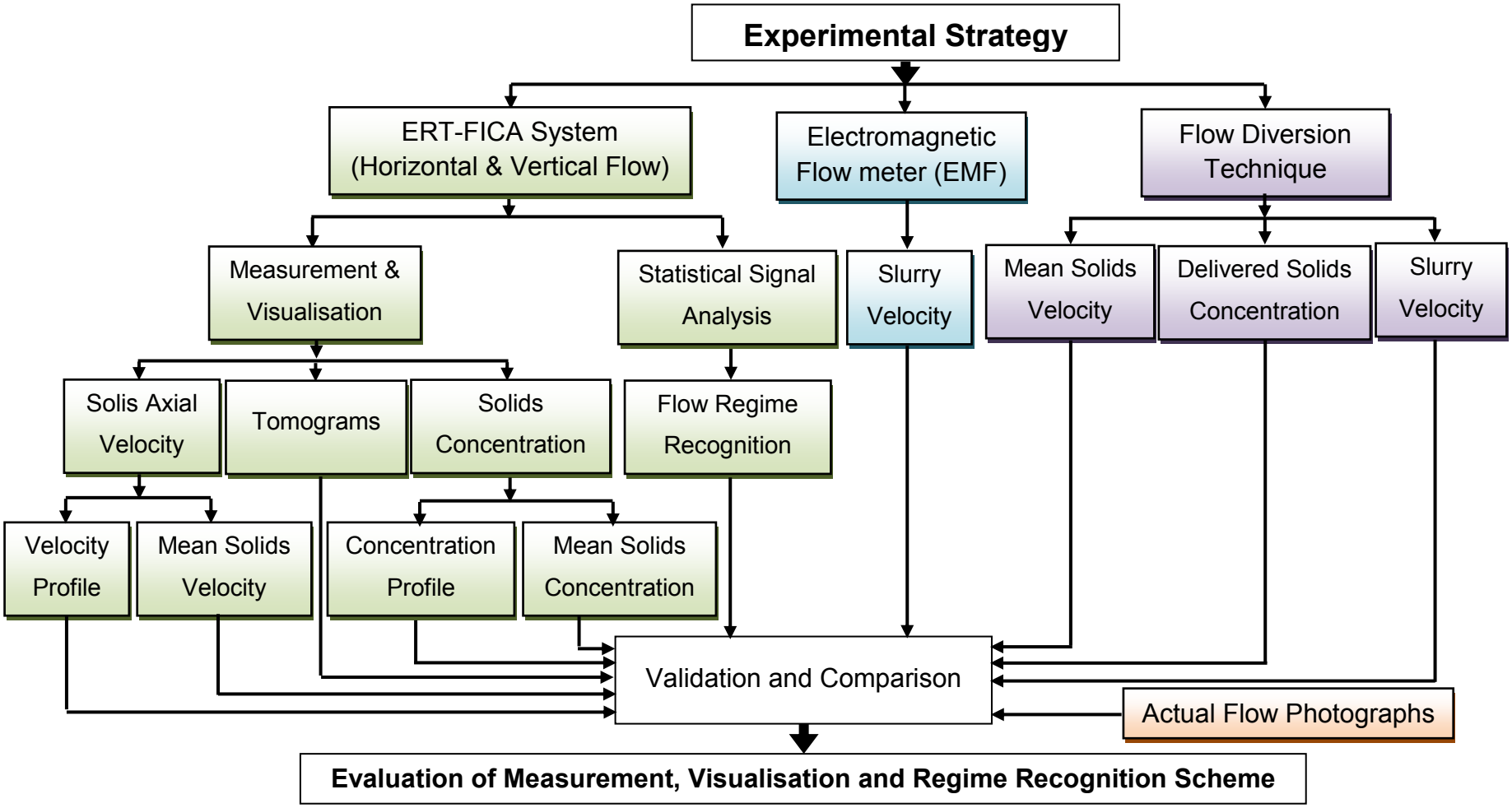

Figure 5.1 Schematic briefing of the methodology used in this study

5.3 Material and test conditions

Slurry flow through horizontal and vertical test sections of the flow loop shown in Figure 4.2 (Chapter 4) was studied. The loop consists of 50 mm diameter uPVC pipeline, the details of which can be found in Chapter 4. The material and test conditions are summarised in Table 5.1 shown below.

Table 5.1 A summary of material and test conditions used in the experiments

Slurry	Sand and tap water ρ_{water}= 998.2 kg/m^3 ρ_{sand}= 2650 kg/m^3
Particle size	Medium sand (75-900 μm) Coarse sand (150-2200 μm)
Throughput concentration	2%-10% (v/v)
Transport velocity	1.2-5.0 m/s
Pressure range	0.41-1.2 bar
Temperature range	20-28 °C
Pipeline	uPVC, Class E 15 bar (50 mm ID)

The slurry consisted of a mixture of tap water and a non-uniform shape and size sand with density of 2650 kg/m^3. Two types of sand were used, medium and coarse, with throughput concentration range 2%-10% (v/v) for each type. The average superficial velocities were in the range of 1.2-5.0 m/s. Transparent pipe sections were included into both, horizontal and vertical test sections, as observation chambers, which would enable visual observation of the motion of the solid particles within the pipeline and capturing photographs. The slurry was first established at the highest velocity, which was controlled via the Digi-drive frequency converter, then reduced gradually from 5 m/s to 1.2 m/s, at which the pipeline blockage occurred. The ERT measurements were carried out for each condition within a temperature range of 20-28 °C. Each horizontal flow measurement

followed by a vertical flow measurement and flow diversion measurement. Then the next measurement was carried out after allowing a sufficient time for the flow to stabilise. Attempts were made to capture the photographs of the flow at the same time of each ERT measurement. In order to reduce the rate of error in the flow diversion measurement, three level measurements were carried out, the average of which was then calculated against each corresponding ERT measurement.

5.4 Horizontal flow measurement and visualisation

In order to visualise the internal structure of the flow, concentration profile of the local concentration was calculated across the pipe cross section. Obviously the local chord concentration can represent a clearer picture of the distribution of solid particles and their movement in the vertical axis of the pipe cross section. The Fast Impedance Camera System (FICA) was used to measure and collect a set of block data of 8000 frames for each mixture velocity. It was noticed that the FICA system can offer an excellent speed in measuring the conductivity of the media and collecting the data. The FICA system was developed by OLIL group at the University of Leeds and is capable of measuring approximately 1000 dual frames per second, which makes it one of the very fast instruments amongst others. This can be considered as one of the primary advantage of the FICA system for visualisation and measurement of slurry flow, due to dynamic and instability of slurry flow over time. The measured conductivity data was then entered into the P2000 software to produce the conductivity map of the pipe cross section. The conductivity map then imported into the software package called AIMFLOW, which stands for Advanced Imaging and Measurement for Flow, Multiphase Flow and Complex Flow in the Industrial Plant. The mean local concentration was produced by averaging a block of frames from the concentration map, and the solids concentration profile was extracted along the vertical centreline of the tomograms generated, which composed of 20 pixels. The size of each pixel was calculated as 2.5 by 2.5 mm for 50 mm diameter pipe. The tomograms reconstructed for each test were collected and analysed to determine the mean solids concentration and solids concentration profile along with the mean solids axial velocity and solids axial velocity distribution across the vertical plane of each tomogram.

5.4.1 Solid flow visualisation

Since the ERT provides an image reconstruction scheme, then it can be used to monitor and visualise the internal structure of a pipe or a process. The aim of the image reconstruction scheme is to compute a tomogram, which is representing the electrical conductivity of the material flowing through the pipe. In the case of slurry flow, in which the solid phase is considered as dispersed phase, the value of in-situ solids volume fraction at a given location in the pipe corresponds to the local mixture conductivity using Maxwell relationship. It is worth mentioning that each measurement data generated is interpreted by an image reconstruction algorithm, in order to compute the cross-sectional image (tomogram) corresponding to the electrical conductivity field within the pipe. The image reconstruction scheme and the use of an appropriate algorithm are described in section 3.4.6. The cross-sectional image or the tomogram provides valuable information, which can readily be used for the purpose of visualisation. Flow visualisation using tomograms may be beneficial to the operator in industry if certain flow features are sought, such as bubbles, plug flow and formation of strata in horizontal flow. However, for detailed qualitative evaluation, both profiles, solids volumetric concentration and solids axial velocity, presented in the following sections, may be the best tool. The tomograms reconstructed in this study are used to monitor the distribution of sand particles across the pipe cross-section, which is described in the following section. These tomograms were generated using a non-iterative algorithm, Linear Back Projection (LBP), which was found to be suitable for the purpose of this study. The selection of this algorithm is based on its advantages, which are simple and fast which make it most suitable for on-line monitoring of solids flow within the pipeline.

5.4.1.1 ERT tomograms

Figures 5.2, 5.3 and 5.4 present the concentration tomogram obtained for flowing of medium and coarse sand particles with 2% and 10% throughput concentration at various transport velocities. The in-situ concentration measured by the ERT is also mentioned for both sands at various flow conditions. The cross-sectional area of the blocked horizontal pipeline is also illustrated along with solids in-situ concentration and the height of the stagnant bed. The in-situ concentration scale across the vertical line of the pipe cross-section is also indicated by a vertical gradient coloured bar below the tomograms for each sand and throughput concentration group. The actual corresponding photographic evidence of the flow, which is used to

validate the ERT tomograms, is also presented for each condition. Due to the vast amount of data the concentration tomograms shown here are only confined to several test conditions.

The tomograms represent the distribution of each phase within the pipe cross-section, and this is depicted by a colour gradient. The basic idea of each coulor code is to interpret the conductivity or the concentration distribution within the flow system. The tomograms illustrated here are based on the concentration distribution. The yellow colour shows the lower concentration of the dispersed phase (sand particles), while the blue colour represents its higher concentration within the carrier liquid.

From the tomograms shown in the aforementioned figures, it can be seen that the distribution of solid particles varies, for both sands, depending on the velocity throughput (i.e. the in-situ concentration increases with decrease of velocity). However, this is not the case for velocities above 4 m/s for both sands and both concentrations. This could probably be due to the entrained bubbles in the mixing tank at higher velocities, at which the returning slurry falls down into the mixing tank and produces bubbles.

At higher velocities the particles occupy not only the bottom half of the pipe, but also the upper half of the pipe and they are in suspension, while in lower velocities, especially at 1.5 m/s, the bed is formed and the particles clearly move either in the form of moving bed or contained in a stationary bed, some of which move in saltation (roll and tumble over the bed) or in a sporadic movement over the stationary bed. This phenomenon can clearly be seen in the corresponding actual photograph of the flow.

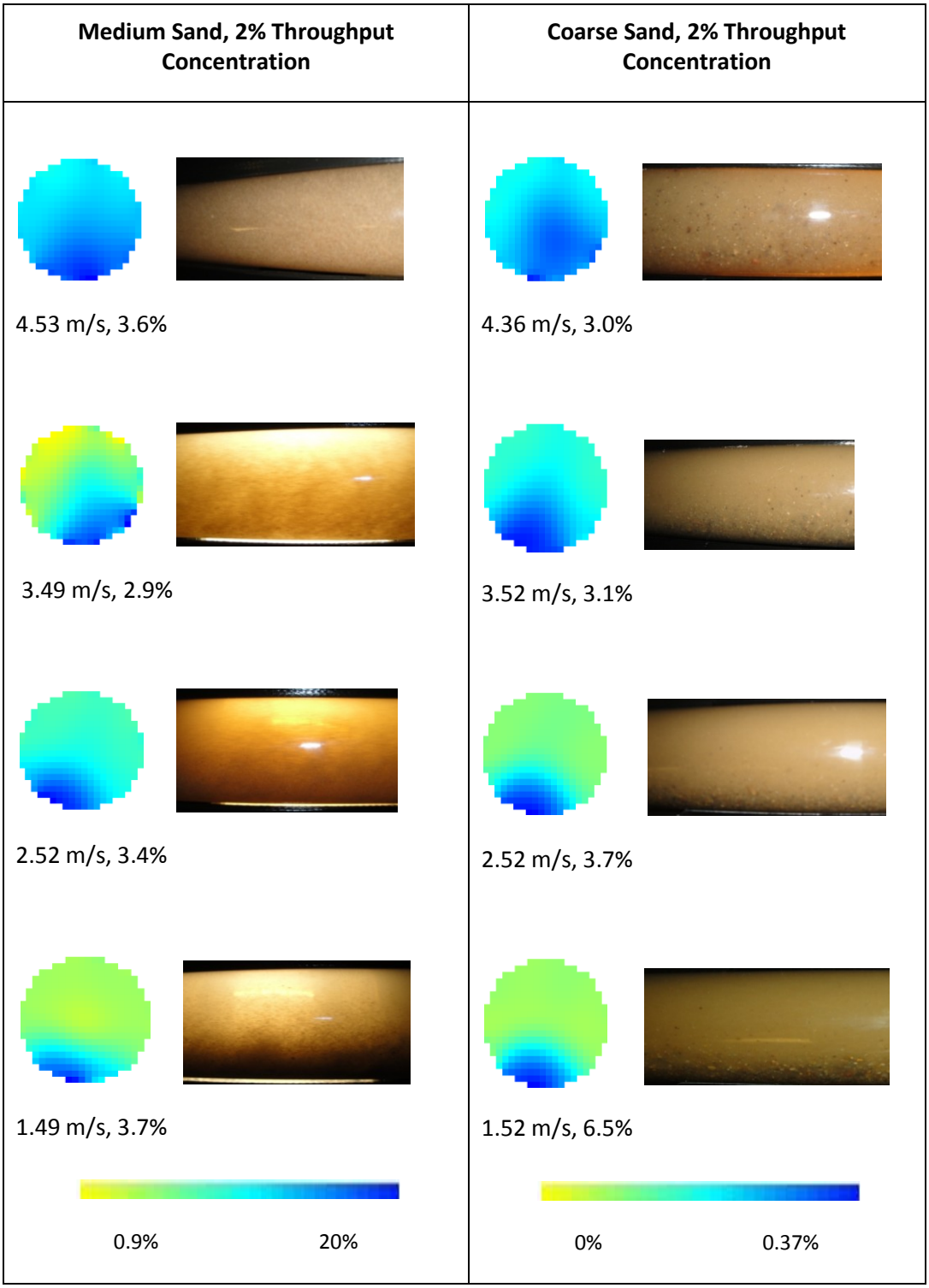

Figure 5.2 Concentration tomograms from the ERT (AIMFLOW) for medium and coarse sand at the shown transport velocity and mean local solids concentration across the pipe cross-section, along with the real photographs of the flow within the pipeline

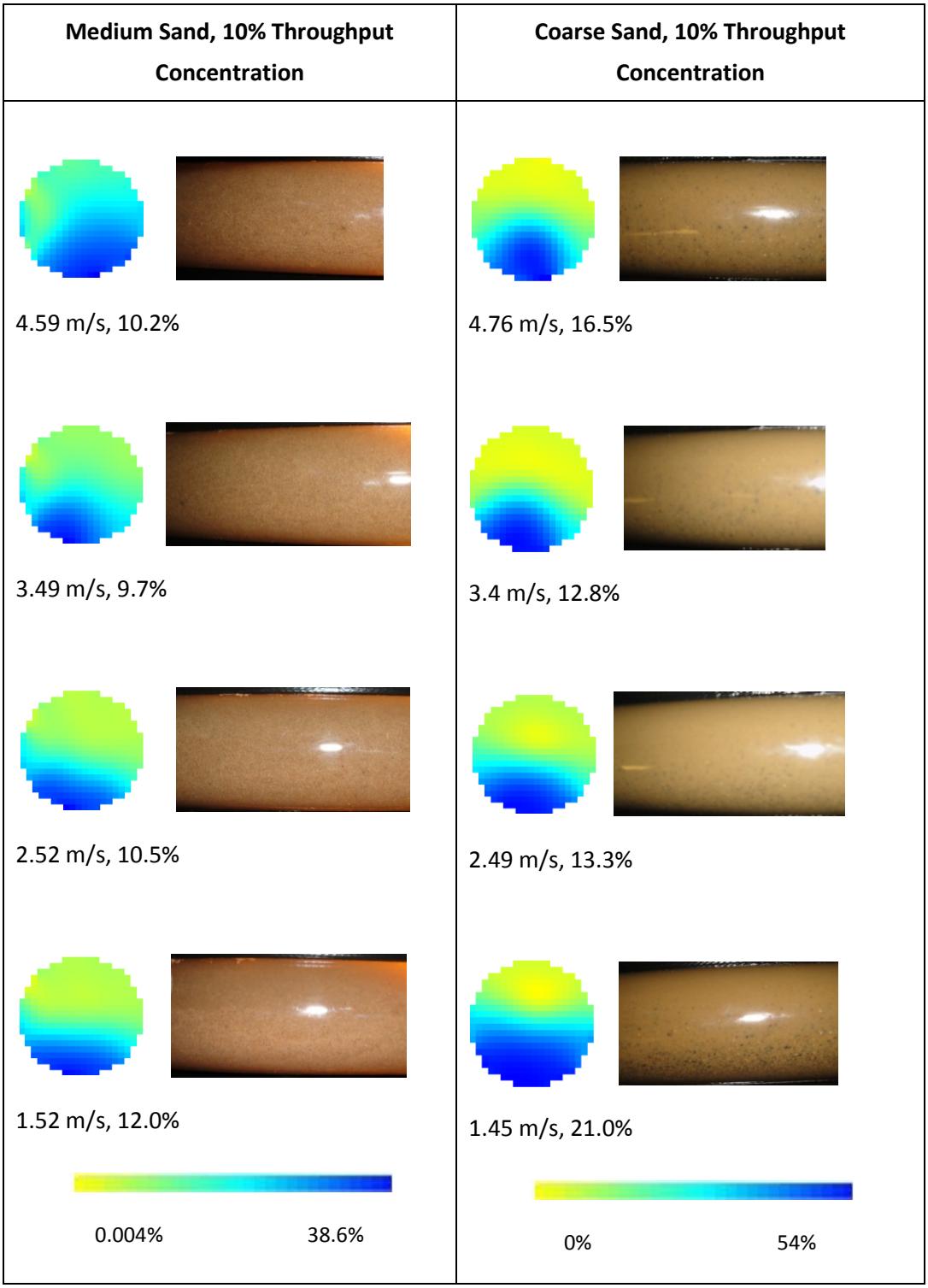

Figure 5.3 Concentration tomograms from the ERT (AIMFLOW) for medium and coarse sand at the shown transport velocity and mean solids concentration along with the real photographs the flow within the pipeline

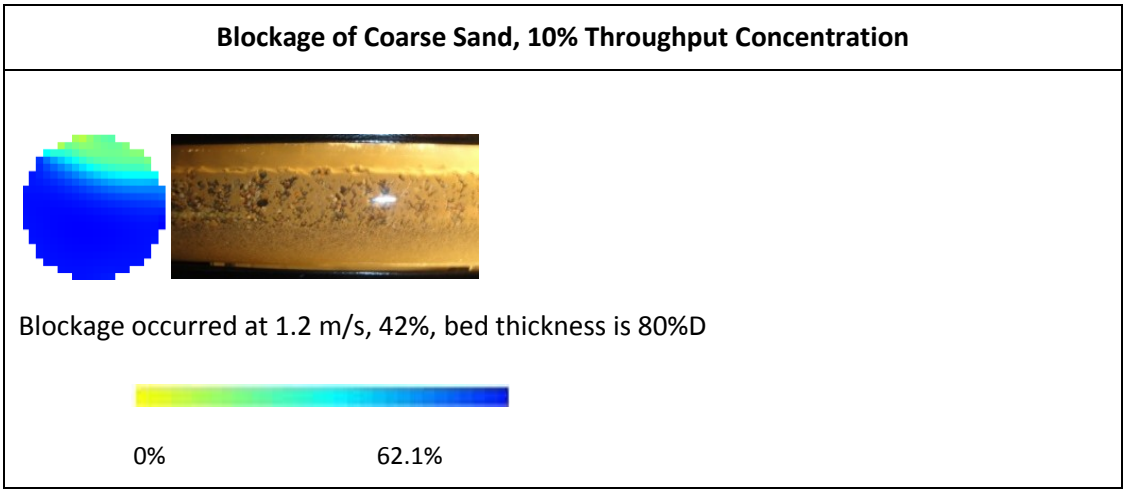

Figure 5.4 Concentration tomograms from the ERT (AIMFLOW) for medium and coarse sand at the shown transport velocity and mean solids concentration along with the real photographs of the flow within the pipeline

5.4.2 ERT solids volume fraction distribution

Figures 5.5, 5.6, 5.7 and 5.8 showing the profile of solids concentration as a function of transport velocity along the vertical axis of the 50 NB pipe cross-section. In order to determine the effect of concentration along with the particle size, two different sands, medium and coarse, were used at two different throughput concentrations, 2% and 10%. The y-axis represents the dimensionless vertical position (y/D) inside the pipe, while the x-axis represents the local volumetric solids concentration.

The generated concentration profiles represent the typical concentration profile of settling slurry flow. It can be noticed that, at velocities below 3.4 m/s, for the two sands the profiles composed of a concave (left-hand bend) curve in the upper part of the pipe and convex (right-hand side) curve in the lower part of the pipe. This behaviour can easily be noticed for all velocities used in the experiment, except for 2% medium sand at transport velocity 5 m/s, for which the distribution of sand particles is rather quasi-homogeneous with asymmetric distribution across the pipe cross-section.

The results for flowing medium sand with 2% throughput concentration, which is shown in Figure 5.5, illustrates a gradual distortion in the profile and changing its pattern from pseudo-homogeneous flow pattern to stratified flow with decreasing the transport velocity.

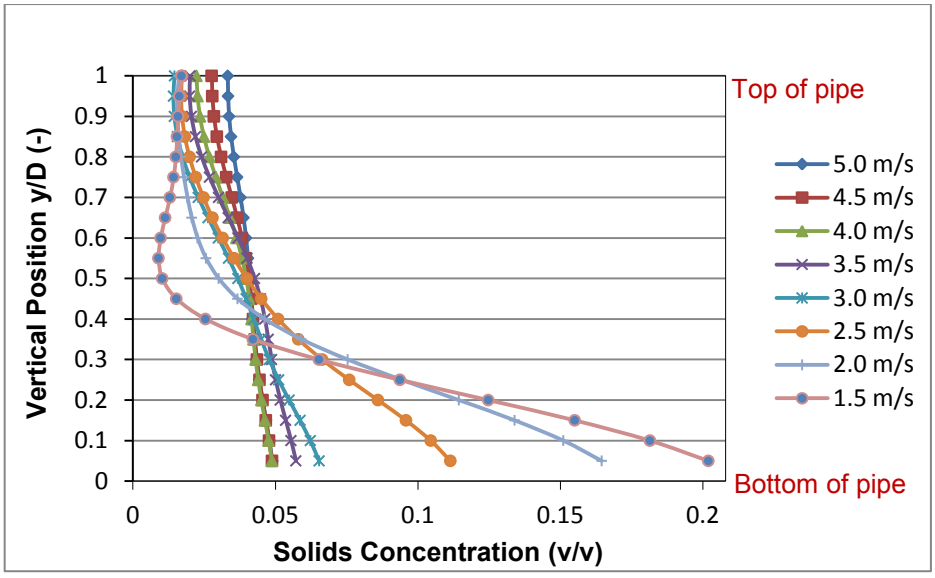

Figure 5.5 Concentration profile for flowing medium sand at 2% throughput concentration in the horizontal 50 NB pipe as a function of the transport velocity

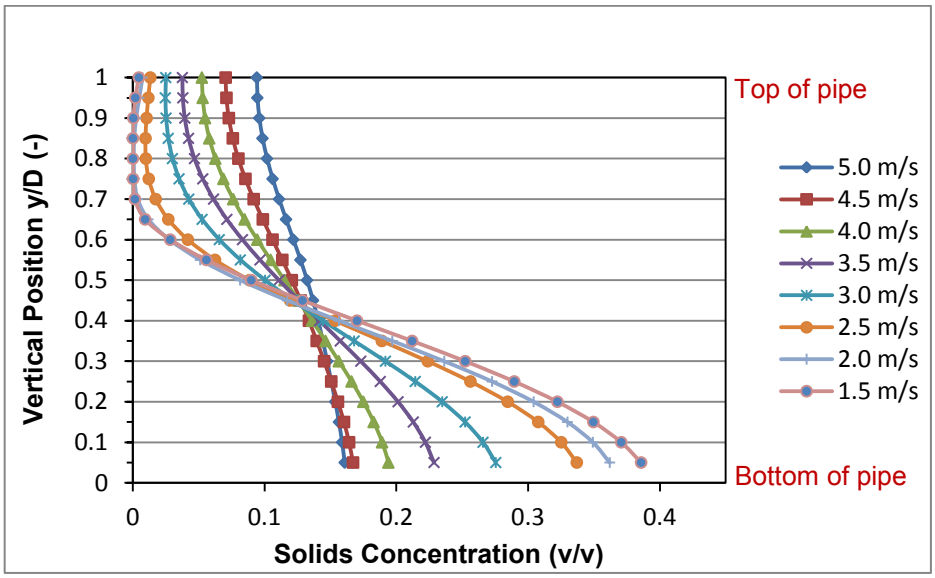

Figure 5.6 Concentration profile for flowing medium sand at 10% throughput concentration in the horizontal 50 NB pipe as a function of the transport velocity

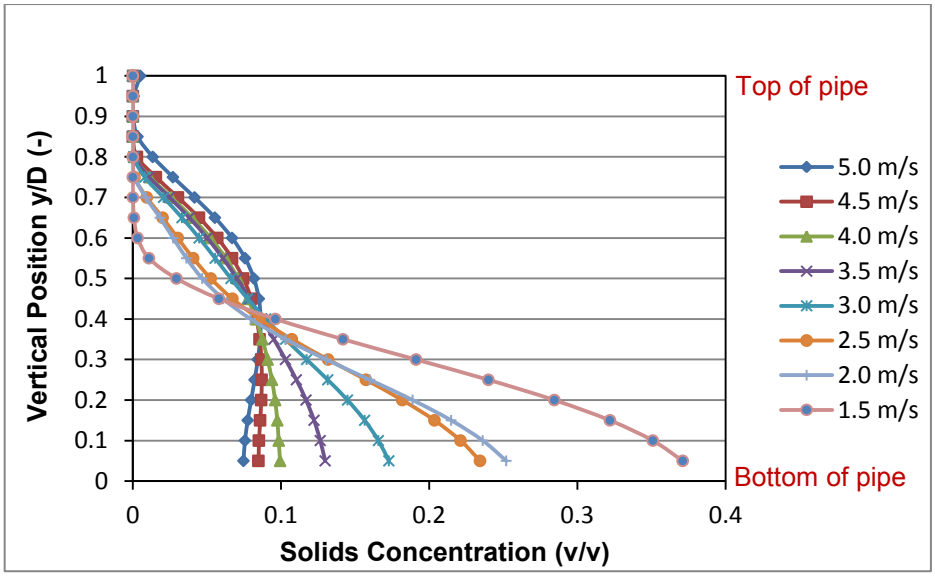

Figure 5.7 Concentration profile for flowing coarse sand at 2% throughput concentration in the horizontal 50 NB pipe as a function of the transport velocity

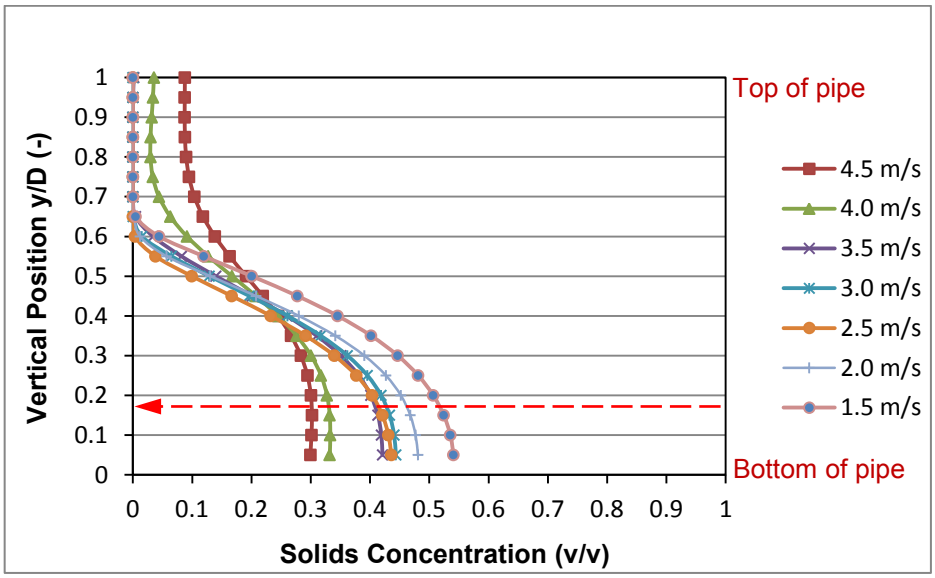

Figure 5.8 Concentration profile for flowing coarse sand at 10% throughput concentration in the horizontal 50 NB pipe as a function of the transport velocity. The red dashed arrow indicates the height of the bed at the bottom of the pipe

It can be noticed that the particles are suspended and fairly distributed in the carrier liquid within the range of higher velocities above the deposition velocity. This is due to turbulent eddies formed in the suspending liquid.

It is worth mentioning that the feature of off-wall hydrodynamic lift force, which has been observed for many heterogeneous slurry flows at velocities

well above the deposition velocity, is totally absent for all concentrations and particle sizes used in this investigation. This feature can clearly be seen in Gillies and Shook (1994), who observed the solids concentration profile near the bottom of the pipe, and found that the profile reaches the maximum concentration then it bends backward. It is worth mentioning that they noticed this phenomenon at 36% solids delivered concentration (C_v=0.36). Similar feature was observed by Matousek (1997) and Pachowko (2004), who also used more than 10% throughput solids concentration. Since this study uses a throughput concentration of up to 10%, which is less than that used by the above researchers, then this may be one of the attribution as to why the particle lift force is not seen in the above concentration profiles. The effect of concentration could be one of reasons. As with decrease of solids concentration, the particle-particle interaction and collisions become less effective. This results in less momentum transfer and the particles move in the form of loose-poured bed rather than highly concentrated bed. This observation is more consistent with wider particle spacing at low concentration, in which the turbulent is more effective. Another possibility for the absence of particle lift force, may also be due to generation of artificial errors by Linear Back Projection algorithm. However, the reason behind the absence of this phenomenon in this study merits a thorough investigation.

In the case of coarse sand with 2% throughput concentration, shown in Figure 5.7, similar trend was observed as described for medium sand with the same throughput concentration, but with higher degree of distortion, which was picked up by the ERT. This phenomenon indicating that the coarser particles cannot be suspended by the turbulent eddies in the suspending liquid in the upper region of the pipe at the highest velocity used in this study. As a consequence the coarse and heavy sand particles occupy the lower regions of the pipe, which result in producing a large shear stress at the upper surface of the contact bed by the pressure gradient acting on the pipeline. Therefore the flow at certain transport velocities tends to be more stratified for transport of coarser particles. The effect of solids throughput concentration has also been detected by the ERT. It can be seen that the profiles of both sands at 10% throughput concentration have higher degree of distortion than those of 2% throughput concentration at the given transport velocity. This can be attributed to the particle-particle interaction, the effect of which increases with increase of particle concentration.

5.4.3 ERT solids axial velocity distribution

To obtain the solids axial velocity distribution, FICA system was used in conjunction with cross-correlation method. The data was acquired at a rate of 1000 frames per second for each plane. The measurements were taken and a set of block of 8000 dual images were reconstructed for each flow condition. Each dual image is representing the conductivity distribution at the upstream and downstream planes at a particular time. Then a relation between the two signals from the two planes were established, using pixel to pixel correlation method, which has been developed into a software package (AIMFLOW) at the University of Leeds and the Chinese Academy of Science. By importing the conductivity map into the AIMFLOW, the axial solids velocity, concentration and solids volumetric flow rate can be computed.

The in-situ solids velocity in the slurry pipeline has been measured for various combinations of transport velocities, which was determined by the Electromagnetic Flow meter (EMF), and throughput concentration for 2% and 10% medium and coarse sand. The selection of slurry transport velocities was based on covering the predicted four flow regimes occurring in the horizontal slurry pipeline. The highest transport velocity was 5 m/s, which was enough to maintain all solid particles in suspension for both sands. The lowest transport velocity was 1.5 m/s, in which the effect of particle lift force approached zero and as a result the solid particles settled at the bottom of the pipe, where moving bed and/or stationary bed could prevail.

For each transport velocity, throughput concentration and sand type, velocity profile was measured along the vertical diametrical plane of the pipe cross-section. Along this plane the local solids velocity was measured at 20 locations. It is to be noted that once the mixture conductivity was measured by P2000 software, 20 x 20 grids were selected, and the grid locations falling outside the pipe cross-section were blanked out. Therefore, the number of remaining pixels within the pipe cross-section is 316. The mean solids local velocity was also determined by averaging the magnitude of solids velocity across 316 pixels.

For the sake of simplicity, the results of the velocity measurement presented here are limited and confined only to randomly selected sands and some operating conditions. Figures 5.9, 5.10 and 5.11 showing the solids velocity profiles along the vertical plane at a range of 1.5-5 m/s mean slurry velocity for coarse and medium sand at two throughput concentration 2% and 10%.

In the profiles shown below, for both sands and the two throughput concentrations, it can be seen that the shape of profile goes through continuous distortion as the mean flow velocity is further decreased. This is due to the fact that at low velocities the turbulent dispersing force decreases and the carrier liquid is no longer able to maintain the coarser particles, as a result the coarser particles migrate to the lower part of the pipe. This phenomenon causes an increase of solids particle concentration at the lower part of the pipe. In the case of medium sand at 10% throughput concentration, the velocity profile of which is illustrated in Figure 5.9, it can be noticed that with decrease in mean flow velocity the location of peak solids velocity shifts towards the upper part of the pipe. Simultaneously, the solid particles at the bottom of the pipe start to slow down. This slurry feature, which is clearly highlighted by the ERT, has been the subject of many previous studies (Kaushal *et al.*, 2002; Matousek, 2002). As the transport velocity decreases, the gravity force plays its role, in return the solids concentration increases at the bottom of the pipe. This increase in solids concentration causes a strong particle-particle interaction, which diminishes the momentum of the flowing solids, as a result the particles at the bottom of the pipe travel slower than those moving at the top of the pipe. The same trend was observed for coarse sand, at both throughput concentrations. However, an increase in the degree of asymmetry in the solids velocity profile was noticed to be higher than that of medium sand at the same throughput concentration and transport velocity. This behaviour could well be attributed to the particle size effect. As the particle size increases, the gravity effect dominate the turbulent eddies responsible for suspending solid particles in the carrier liquid, as a result the coarser particles are displaced to the bottom of the pipe. This effect enhances an increase in the solids concentration at the bottom of the pipe, where the particles face a strong interference between each other that cause them to slow down. At a given throughput concentration and transport velocity the degree of solids segregation at the bottom of the pipe is higher in coarse sand rather than medium sand; hence the velocity profile for coarse sand manifests a higher degree of asymmetry. Therefore, one can conclude that the degree of asymmetry in solids velocity profile dependent on the particle size.

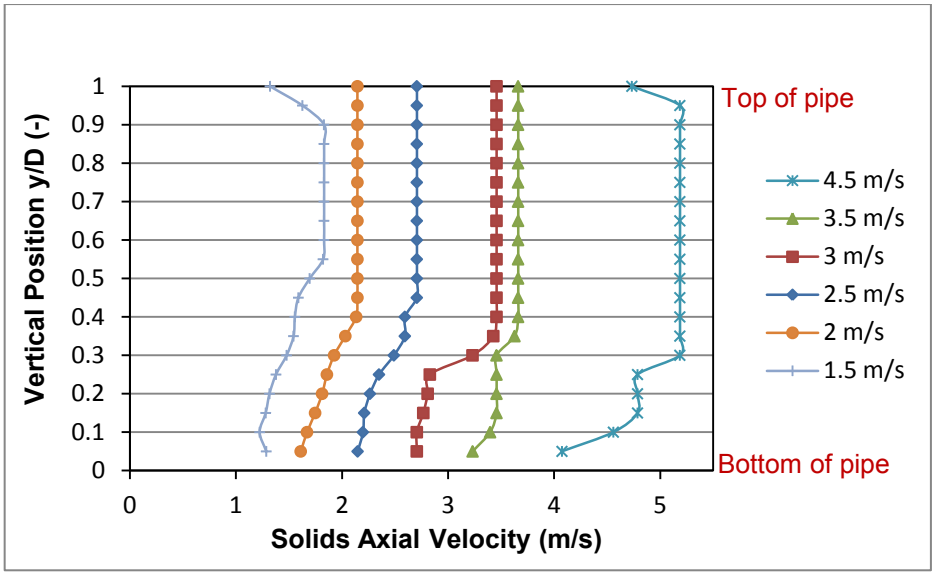

Figure 5.9 Solids axial velocity profile for flowing medium sand at 10% throughput concentration in the horizontal 50 NB pipe as a function of the transport velocity

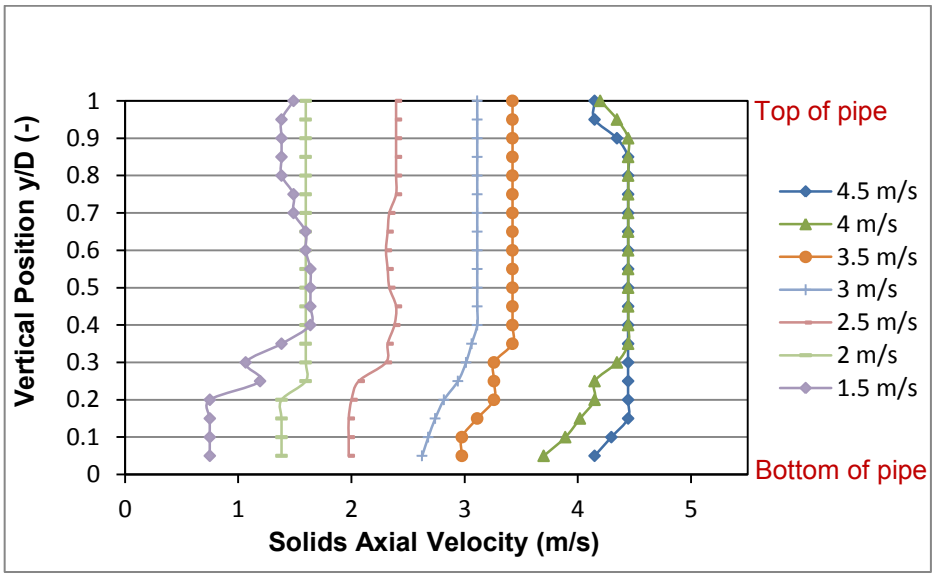

Figure 5.10 Solids axial velocity profile for flowing coarse sand at 2% throughput concentration in the horizontal 50 NB pipe as a function of the transport velocity

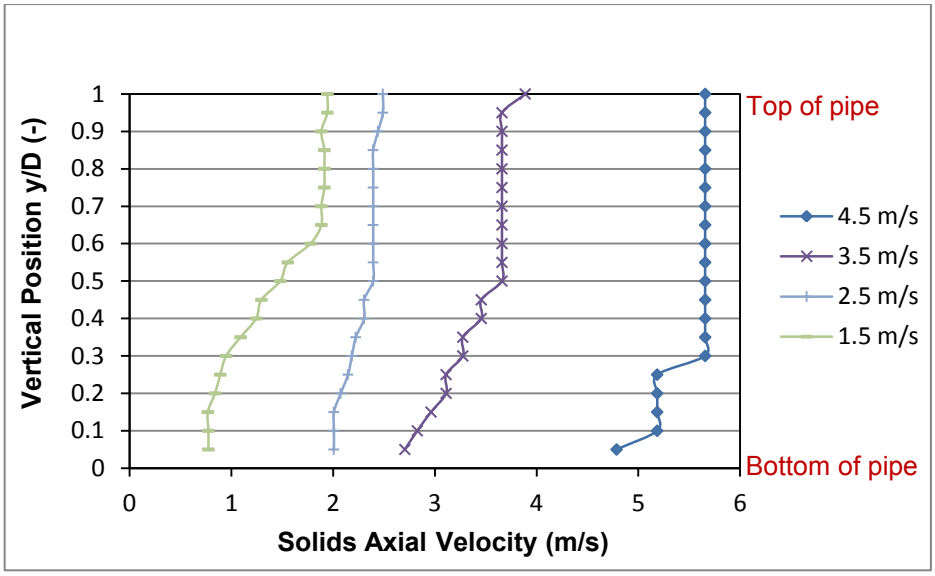

Figure 5.11 Solids axial velocity profile for flowing coarse sand at 10% throughput concentration in the horizontal 50 NB pipe as a function of the transport velocity

The observation of all solids velocity profiles measured by the FICA system can also clearly reveal that for the same particle size and transport velocity, the degree of asymmetry increases with increase of through put solids concentration. Again, the prime responsible is the particle-particle interaction, which widens the difference in the average solids velocity at the top and the bottom of the pipe. Therefore, the effect of solids concentration throughput can also be demonstrated by the ERT.

5.4.4 Methods of solid flow velocity visualisation

Apart from solids velocity profile, for which the data for 20 locations was taken and plotted against the 20 corresponding vertical location, the distribution of solids velocity across the pipe cross-section were also generated automatically by the AIMEFLOW software. After importing the conductivity data acquired by the FICA system and inputting several flow parameters for calculation of solids velocity, the reconstructed cross-sectionalsolids velocity profile can be visualised on the monitor. Some these cross-sectional solids velocity profiles are shown below. However, it was noticed that these profiles do not voluntarily provide sufficient information regarding the flow apart from mere monitoring of particles motion within the pipe. In addition, for certain flow conditions, the generated profiles associated with some noises, which would distort the profile and provide misleading information regarding the location, which is affected by the noise.

The reasons for this may well be attributed to the buried hardware noises. However, this issue has to be the subject of future investigation.

If we look at the profiles shown in Figures 5.12, 5.13, 5.14, 5.15, 5.16, 5.17, 5.18 and 5.19, a gradient of colours could be remarked. Each shade of colour represents the velocity level of the flowing solid particles. The yellow colour represents the highest velocity at the top of the pipe, whilst the blue colour refers to the lowest solids velocity at the bottom of the pipe. The velocity scale is also indicated by a vertical gradient coloured bar on the right hand-side of the profile. The right-hand side of each profile represents the bottom of the pipe, where the lowest solids velocity can be found.

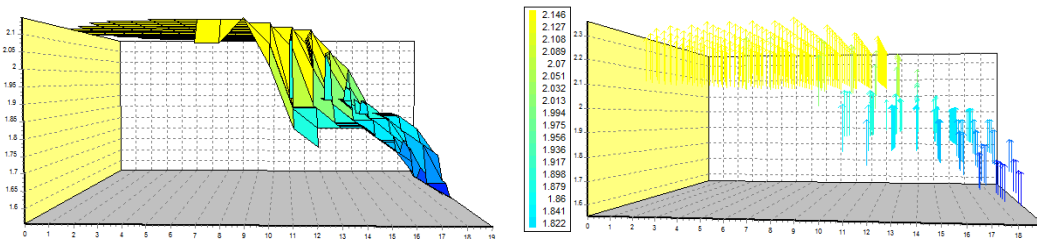

Figure 5.12 Solids velocity profile across the pipe cross-section for medium sand at 10% throughput concentration and 2 m/s transport velocity

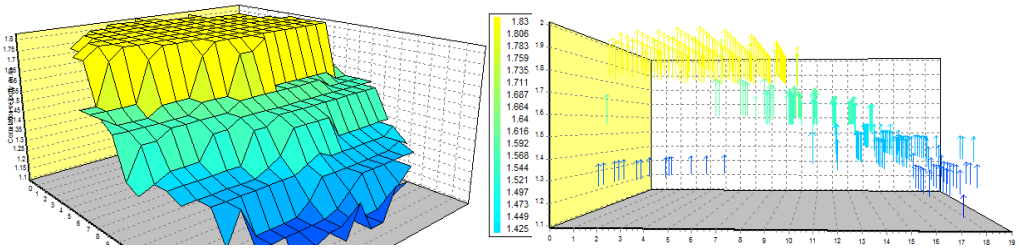

Figure 5.13 Solids velocity profile across the pipe cross-section for medium sand at 10% throughput concentration and 1.5 m/s transport velocity

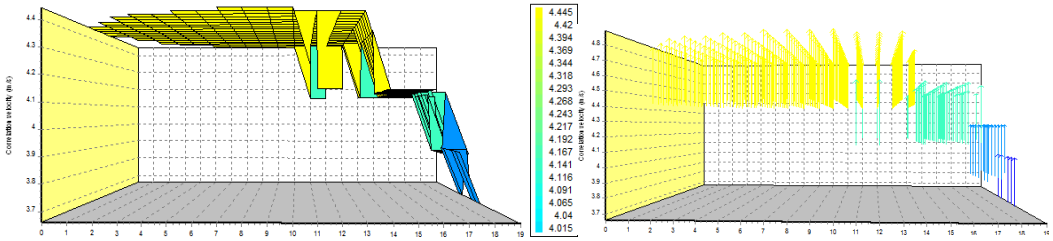

Figure 5.14 Solids velocity profile across the pipe cross-section for coarse sand at 2% throughput concentration and 4 m/s transport velocity

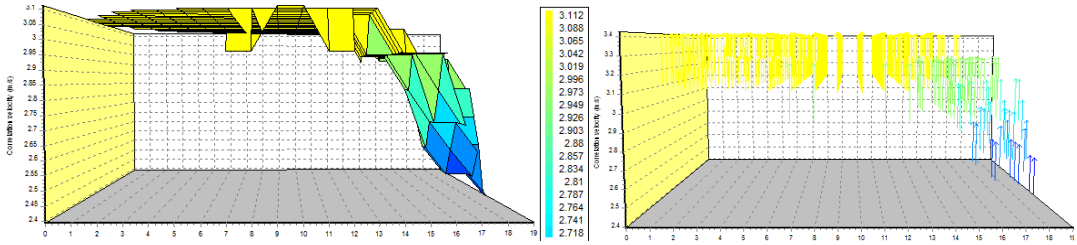

Figure 5.15 Solids velocity profile across the pipe cross-section for coarse sand at 2% throughput concentration and 3 m/s transport velocity

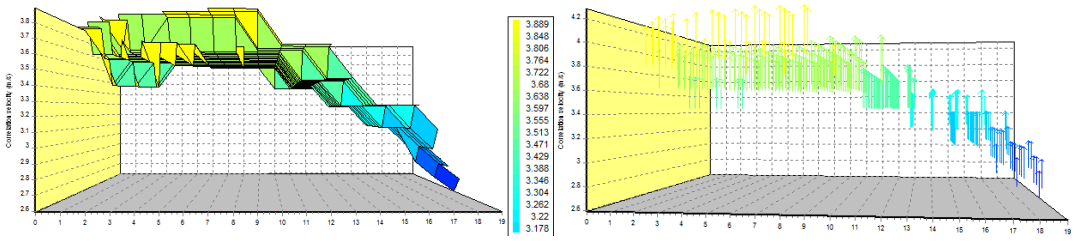

Figure 5.16 Solids velocity profile across the pipe cross-section for coarse sand at 10% throughput concentration and 3.5 m/s transport velocity

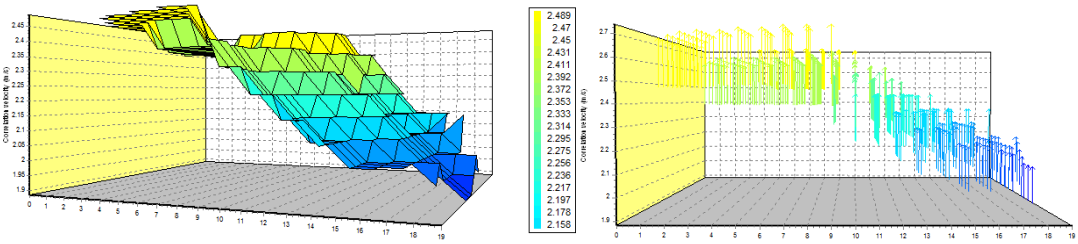

Figure 5.17 Solids velocity profile across the pipe cross-section for coarse sand at 10% throughput concentration and 2.5 m/s transport velocity

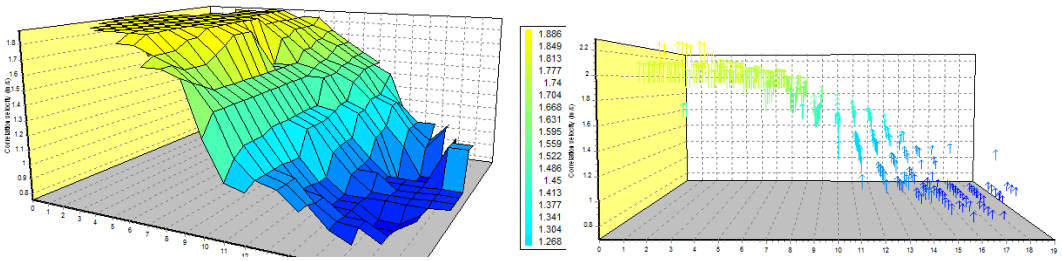

Figure 5.18 Solids velocity profile across the pipe cross-section for coarse sand at 10% throughput concentration and 1.5 m/s transport velocity

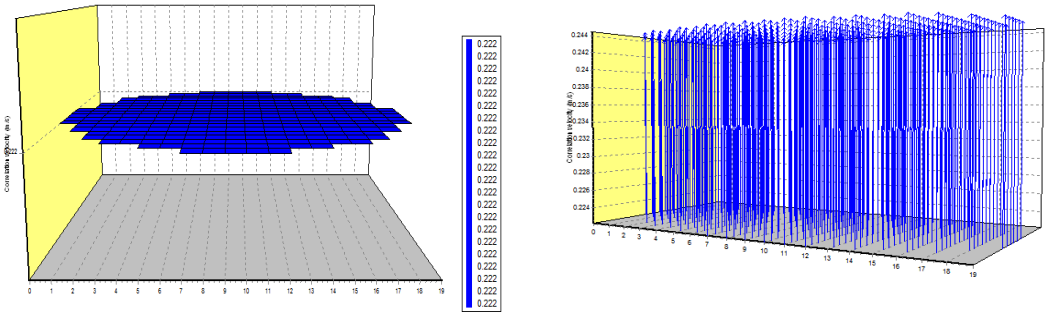

Figure 5.19 Solids velocity profile across the pipe cross-section for coarse sand pipe blockage at 10% throughput concentration

5.4.5 Slurry flow regime visualisation and characterization

Slurry flow regimes encountered in horizontal pipeline influence some parameters of system such as pressure drop, system instability, pipe erosion and some other performance characteristics. Therefore, monitoring characterisation and of these flow regimes are important tools for design and operation of pipelines conveying settling slurries.

This section presents a technique, by which the flow regimes in horizontal pipeline can be visualised and characterised. The technique is based on the analysis of solids concentration profile and axial velocity profile obtained from a dual plane Electrical Resistance Tomography (ERT) sensor, which was mounted in the middle of the horizontal test section of 50 NB flow loop. Careful selection of the transport velocity range (1.2-5 m/s) allowed the coverage of four main flow regimes along with pipe blockage. The flow regimes predicted via ERT compared to the photographic images of actual flow within the test section. An analysis of stratified slurry flow is also discussed and it is proposed that the tomography technique can be used for estimation of several parameters of stratified flow such as mean granular bed concentration and velocity, height of bed etc. The estimation of these parameters is based on the analysis of the grid of tomogram reconstructed with Sensitivity Back Projection (SBP) algorithm.

For the sake of simplicity the flow regimes illustrated here are only for coarse sand at 10% throughput concentration. However, due to the limitation in the pump capacity, the homogeneous flow regime for flowing 10% coarse sand could not be achieved; therefore, the pseudo-homogeneous regime of flowing coarse sand at 10% concentration throughput was selected. The flow regimes of flowing 10 % coarse sand shown here are pseudo-homogeneous, heterogeneous flow regime, moving bed and stationary bed. In addition, the concentration and velocity profile of the blocked horizontal pipeline is also highlighted. In order to cover all flow regimes, for each sand at a given throughput concentration, the transport velocity was decreased, starting from 5 m/s and ending at 1.2 m/s, where the continuous formation of stationary bed leads to pipeline blockage. For the sake of clarity and support for both concentration and velocity profiles, the photographs of each prevailing flow regime were captured by a digital camera and inserted into the plot area of the measured profile. Due to the murky nature of slurry, it was not easy to distinguish the solid particles in the murky carrier liquid. Therefore, the photographs were sent to the Microsoft Office Picture Manager, where colour enhancement was applied. As it is apparent in the

inserted pictures, some photographs required a specific colour for the solid particles to be shown. The photographs were taken through 1 m transparent pipe section, which was confined by a photo chamber details of which can be found in Chapter 4.

5.4.5.1 Pseudo-homogeneous flow regime

Figure 5.20, showing a pseudo-homogeneous flow regime, in terms of concentration and axial solids velocity profile, for 10% coarse sand at 4.5 m/s. On both profiles it can be seen that the particles occupying the pipe cross-section are more or less distributed symmetrically. However, the profile is slightly skewed at the centre of the pipe and changes its trajectory indicating the presence of finer particles with lower concentration and higher velocity. This distortion in profiles has been detected by tomography and it is apparent from the background inserted photograph, where the entire particles are suspended in the carrier liquid. Nevertheless, there is a possibility of presence of some gravels (5 mm diameter), which cannot be lifted, as gravitational attraction exceeds the fluid turbulence. These gravels were detected within the coarse sand, which initially added to the mixing tank.

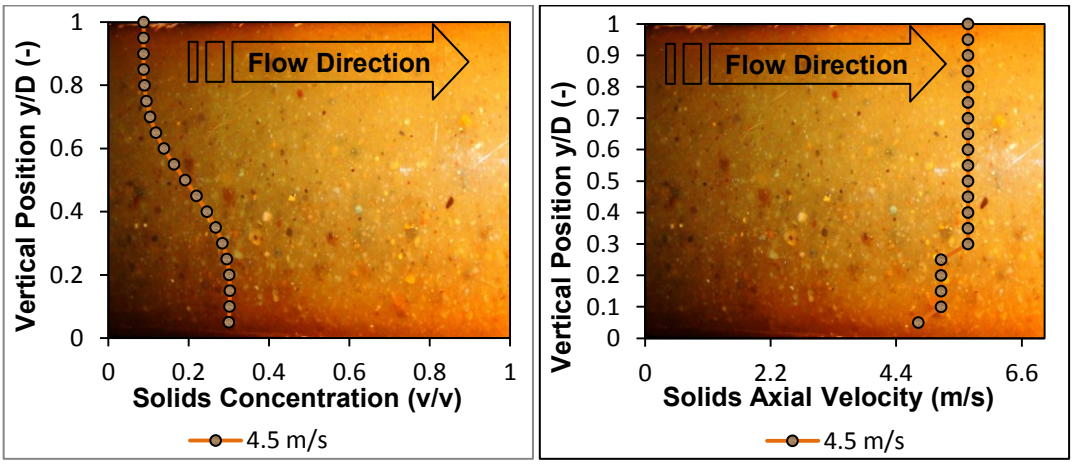

Figure 5.20 Pseudo-homogeneous flow regime for 10% throughput concentration of coarse sand at 4.5 m/s transport velocity shown on concentration profile (left) and solids velocity profile (right)

This is clearly seen in the velocity profile at the very bottom of the pipe, despite its disappearance in the concentration profile. The existence of such particles was very clear and could distinguishably felt during the experiment while travelling through bends and elbows of the flow loop. The reason for the distortion of both profiles could be attributed to the particle size and

shape. As totally even particle distribution can be applied only to materials with a rounded shape, which falls into a narrow size distribution. Therefore, this feature of uniformly distributed particles cannot be observed in our experiment at such transport velocity used and the coarse sand used here includes both fine and coarse particles.

5.4.5.2 Heterogeneous flow regime

Figure 5.21, illustrating the concentration profile (left hand-side) and the axial coarse solids velocity profile (right hand-side) at 10% throughput concentration and 4 m/s transport velocity. Both profiles showing the heterogeneous flow regime, which is by far the most complex as the characteristics of the extreme flow regime are embodied in the flow. It can be noticed that the finer particles occupy the upper part of the pipe, while the coarser particles only travelling at the lower part of the pipe. Nevertheless, some particles may be present in the form of a very thin bed or sliding deposit. It is quite noticeable that the two profiles agree with the real flow of solid particles in the photograph inserted in the plot area.

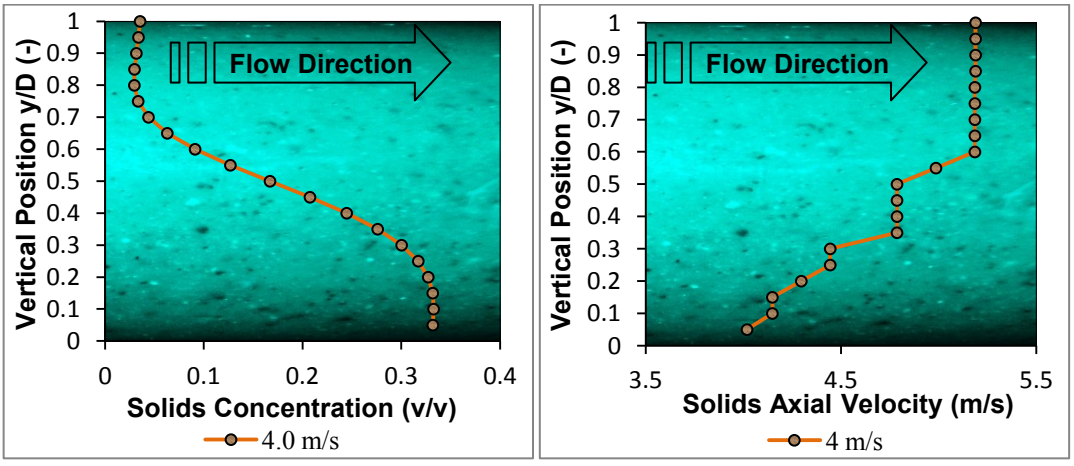

Figure 5.21 Heterogeneous flow regime for 10% throughput concentration of coarse sand at 4 m/s transport velocity shown on concentration profile (left) and solids velocity profile (right)

5.4.5.3 Moving bed

Once the transport velocity further decreased from 4 m/s, the solid particles then follows a smooth downward trajectory to form a moving bed, as it is highlighted by both concentration and velocity profile in Figure 5.22. The inserted real flow photograph into the plot area, at the very same velocity, supports this argument and agrees with the measured profiles by the ERT

that there is a granular bed. However, despite confirming the existence of moving bed by visual observations through a transparent pipe section, there is no sign that the granular bed is either moving en-bloc sliding bed or sliding layers. The velocity gradient along the vertical position of the bed shows no difference with the concentration or solids velocity profile measured at 1.5 m/s (Figure 5.23), where a stationary bed was formed. However, as per real time visual observation and the actual photograph of the flow, which shows a cloudy packed particle, the granular bed was moving along the bottom of the pipe.

By further observing the profiles it can be seen that the shear layer is further developed, which is associated with the variation of shear stress at the boundary where the shear layer is linked to the uniformly distributed granular moving bed. A wide variation in the velocity gradient can be observed within the shear layer, which is due to the difference in the local bed velocity and the mean slurry velocity. The high velocity gradient within the lower part of the shear layer causes a chaotic region over the bed, where the particles are lifted from the surface of the bed and supported again by the upward impulses of the turbulent eddies. They can also redeposit on the bed in the absence of fluid turbulence. This phenomenon of sporadic movement of particles continuously occur at the interface between the en bloc sliding bed and the upper turbulent region unless the variation in the transport velocity occurs, which has a direct effect on the lifting force. In fact this feature could well be attributed to an increase of the shear stress at the bottom of the shear layer, by the moving fluid stream in a momentary impulse fashion. The momentary jumping of the bed grains into the turbulent stream above the bed could contribute into the magnitude of the mean solids velocity, which in return cause an over estimation of the solids mean axial velocities, particularly those below the deposition velocity (i.e. with the velocity range, in which the bed is present). Another interesting feature could also be observed on the velocity profile, where the profile goes through a deformation through its course at the very top of the pipe (at y/D=0.85). The profile unfolds another region with higher velocity, comparable to the lower layers, and confined by another turbulent particle-rich layer and the pipe wall. The mean velocity of the particles moving within this layer is considerably higher than the rest of layers flowing below. This could be due to limited particle-particle interaction at the very top of the pipe. The background photograph of the real flow at the time of measurement clearly shows a particle-lean layer next to the upper wall. Since the effect of concentration has a direct link to the particle-particle interaction and the

motion of solid particles within the carrier liquid, then it is remarkable that this feature is absent in the solids concentration profile. However, this discrepancy merits a future investigation.

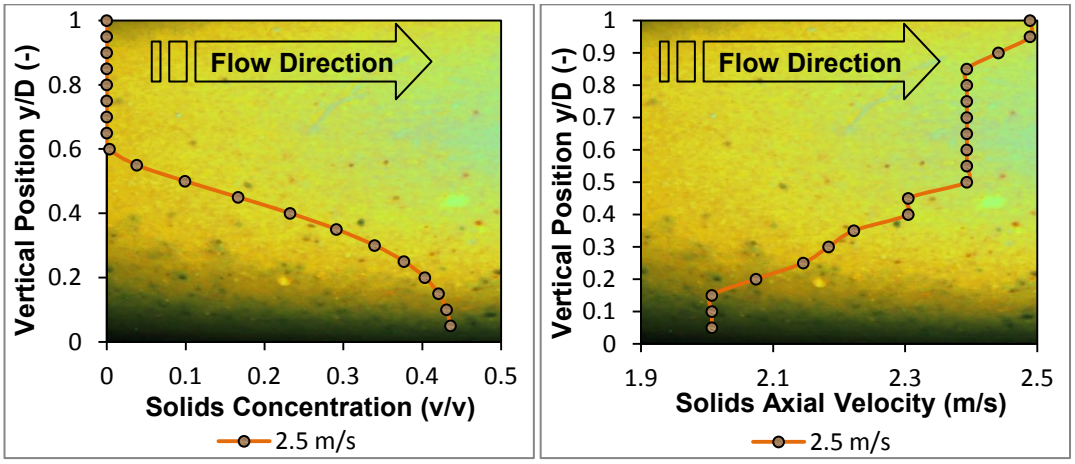

Figure 5.22 Moving bed flow regime for 10% throughput concentration of coarse sand at 2.5 m/s transport velocity shown on concentration profile (left) and solids velocity profile (right)

5.4.5.4 Stationary bed

During the experiment the flow was observed through the transparent pipe section and found that a stationary granular packed bed had been formed, on the surface of which a sliding thin layer was moving at the bottom of the pipe. The thickness of this stationary layer within the bed was measured using a ruler, and recorded as 7-8 mm from the bottom of the pipe. As the flow was extremely murky and the surface of the bed was in an unsteady-state condition, more precision could not be achieved in measuring the thickness of the formed stationary layer. By observing the both profiles, especially velocity profile, it is apparent that, for 10% throughput concentration of coarse sand at 1.5 m/s, the height of inter-granular contact bed is at y/D=2 at the vertical plane of pipe cross section, which makes 10 mm thickness and demarcated by a blue arrow, shown in Figure 5.23. Also, by further observing the velocity profile, no variation or gradient can be seen in the profile curve, where the minimum solids velocity occur. This phenomenon is an indication that each pixel lies within the bed region, is well saturated with solid particles and there is a mutual permanent contact between them, in return a stationary bed is formed. On the concentration profile it can be seen that within the bed height on the profile, the concentration gradient is hardly noticeable; hence, this suggests that the

particles are well segregated and fully packed within the bed. Similarly, the height of stationary bed can be indentified from the two profiles, particularly the velocity profile, which is measured to be y/D=0.15 (y=7.5 mm) from the bottom of the pipe and demarcated by a red line.

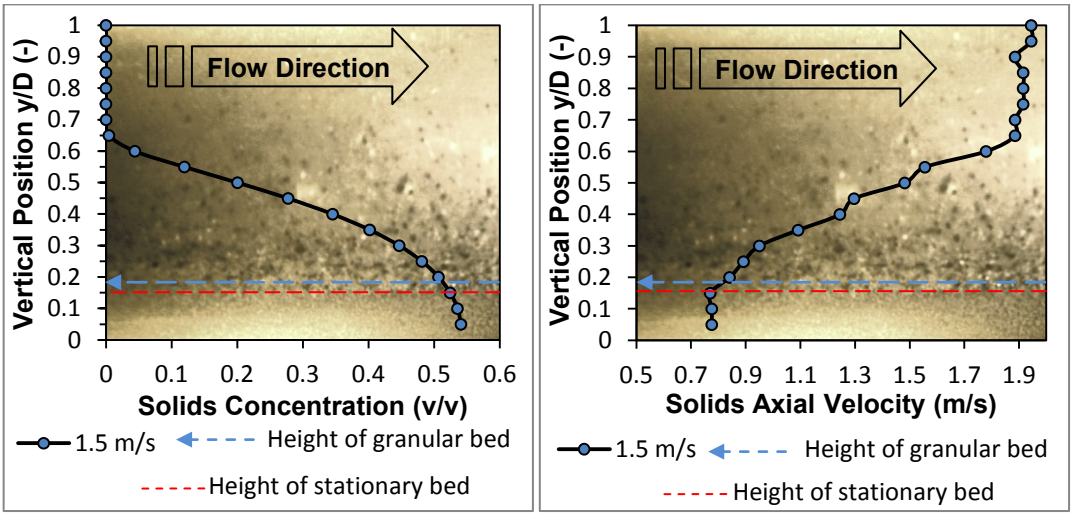

Figure 5.23 Stationary bed flow regime for 10% throughput concentration of coarse sand at 1.5 m/s transport velocity shown on concentration profile (left) and solids velocity profile (right). The height of granular bed is indicated by a blue arrow and the boundary of the stationary bed is indicated by a red arrow

If the height of the granular bed is 10 mm, and 7.5 mm out of which makes the stationary bed, then the rest (2.5 mm) makes the saltating carpet or rugged layer on the surface of the stationary bed. In other words, the thickness of the sliding bed on the surface of the stationary bed is 2.5 mm. However, as previously mentioned this moving layer on the surface of stationary layer is not well pronounced on either concentration or the velocity profile. Also, no or very little feature is provided by the profiles to indicate whether the bed within 10 mm from the bottom of the pipe is moving or stationary. As by observing the profiles in Figures 5.6 and 5.7, it is apparent that the profiles show no difference within the granular bed, whilst visual observation of flow through the transparent pipe section indicated a moving bed with 7 mm thickness at 2.5 m/s mean slurry velocity and a stationary bed with 10 mm thickness at 1.5 m/s. Therefore, it is still quite difficult to identify the state of granular bed, whether it is moving or stationary. However, the sporadic movement of particles above the granular bed may be identifiable on the two profiles, concentration and solids axial velocity, but

it is more pronounced on the velocity profile rather than concentration profile. An observation of the velocity profile can reveal that the velocity of the moving particles at the bottom of the shear layer goes through a narrow distribution. This is an indication of moving particles by saltation. Similarly, the real background photograph shows an agreement with that of suggested by the profile, and it is obvious that the shear stress at the surface of the bed produces elongated dune or ripples. It can also be noticed that the downstream face of these dunes have a greater slope than the face opposing the flow. These dunes have been created as a result of saltation and particle re-deposition on the bed. The effect of particles forming these ripples or dunes tempts the bottom pipe wall to overcome the driving force and the bed starts to gradually decelerate and comes to a momentary halt. The lift force in this condition is very sensitive to any decrease in the transport velocity. Any further decrease in the transport velocity would undoubtedly result in an increase of the formed dunes and solids hold-up in the pipe, which eventually restrict the water way above the stationary layer and pave the way for an imminent blockage.

5.4.5.5 Pipe blockage

The transport velocity was decreased by reducing the pump frequency through the Digi-drive. However, to reach the desired mean flow velocity and steady state it was rather difficult, as the velocity was constantly fluctuating. During the experiment, as the pump frequency was reduced to reach the desired flow velocity (1.5 m/s) for flowing 10% throughput concentration of coarse sand, the mean flow velocity unexpectedly reached the blockage zone (1.1-1.2 m/s), due to velocity fluctuation. As a result the flow of solid particles and the carrier liquid came to rest and the pipe was permanently blocked. This incident was then considered to be an opportunity, in which the ERT could be used for blockage observation. The main aim of this investigation was to evaluate the performance of the ERT while a thick coating of granular bed (up to 80% of the inner pipe diameter) exists on the electrodes of the dual-plane ERT sensor.

While the pipe was blocked, the conductivity of the domain was measured for calculation of concentration and velocity. After an investigation, it was found that the blockage occurred at the pump suction (pump inlet), and the pump was full of solid sand. However, by observing through the transparent pipe, which was mounted 6 m distance from the pump outlet, a block of solid bed at the bottom of the pipe and stationary water at the top could be seen. The thickness of the solid bed was measured by a ruler and found to be 75-

80% of the inner pipe diameter from the bottom of the pipe. The exact estimation could not be achieved, as the surface of the granular stationary bed was not totally flat, instead consisted of dunes and ripples, which had been formed as a result of waves created by the upstream liquid. Once the blockage occurred, there was no force to lift the slurry to the top of the vertical line; as a result it falls down again to the bend, where it is connected to the horizontal line. The coarser particles are expected to fall first, due to the gravity effect. This phenomenon was captured by a digital camera, through the transparent pipe section mounted at the bottom of the vertical line, as shown in Figure 5.24 for both test sections, horizontal and vertical.

(a) (b)

Figure 5.24 Showing the blockage of the pipeline, (a) blocked horizontal section (b) coarser solid particles in the blocked transparent pipe section mounted at the bottom of the vertical pipeline

Then the carrier liquid escapes through the gaps, formed between the coarser particles, into the horizontal line, where pushes the existing water at the top of the horizontal pipeline, until it reaches the other dead-end. Then it reverses back and agitates the existing stationary bed, where some of coarser particles are lifted and distributed into the surface of the downstream stationary bed.

Another photograph of a blocked transparent section of the ERT sensor was taken, so as to qualitatively compare to the profiles obtained by the ERT measurement. Figure 5.25 showing the concentration and particle velocity profile with a real photograph of the blocked pipe section inserted into the plot area. It is apparent that the highest concentration can be seen within the area occupied by well packed and granular stagnant bed particles, which is 0.62% at y/D=0.35 (y=17.5 from the bottom of the pipe). Consequently, the

velocity profile is indicated by a vertical line, where no velocity gradient could be seen, is indicating a total stationary flow. In this condition one would expect to have zero velocity along the vertical plane of the pipe cross-section, suggesting that the granular bed and the particle-free layer above it is in total stationary condition. However, this is not the case in the current velocity measurement; instead 0.2 m/s mean velocity was observed. This overestimation in the mean velocity could be explained by the movement of the carrier liquid, as mentioned above, and some particles on top of the bed in a sporadic fashion between the two planes of the ERT sensor. Nevertheless, there is no indication of the local velocity gradient along the vertical plane, this could be due to noise within the system hardware or even may have to do with ERT spatial resolution issue. Despite this slight discrepancy, the velocity estimation is still within the reasonable range.

By observing the concentration profile shown in Figure 5.25, a particle-free layer could be seen at the very top of the pipe, which occupies 20-25% of the pipe cross-section. This result totally agrees with the measurement of the thickness of the stagnant granular bed, which was measured during the experiment using a ruler, and found out to be 75-80% of the pipe cross-section. However, by further observing the concentration profile within the vertical line along the granular packed bed, a concentration gradient could be noticed at the top half of the bed. This phenomenon is probably attributed to the void and gaps between the non-uniform shape particles, in which the carrier liquid is accumulated. The coarser particles are the wider gap is created and the more carrier liquid is trapped. From the actual photograph inserted into the plot area, it is highly remarkable that the coarser particles are laying within the range of concentration gradient in the profile. The coarser particles are normally deposited at the very bottom of the pipe; however, these are due to the reverse flow of the carrier liquid as previously mentioned or descending the coarser particles of the vertical line at the time of blockage, when there was no force to lift them through the vertical pipeline. Another possibility of the occurrence of the concentration gradient across the height of the bed is due to difference in the density of the existing particles within the bed, alternatively they may be porous particles. This possibility is well based on the fact that the sand used in the experiment is a mixture of non-uniform shape and size, and could also well be in non-uniform density.

Another feature can be observed on the concentration profile, where the profile bends back at the very bottom of the pipe and indicates a decrease in

the local concentration. As the coarse sand used, containing some bigger size particles (gravels up to 5 mm diameter), which are the first to reach the bottom of the pipe once the turbulent eddies has no effect on them, then gaps could be formed, where the carrier liquid accumulates. By looking at the actual photograph of the blocked line, it is apparent that the coarser particles at the bottom of the pipe are completely covered by finer particles. From the above observations a conclusion can be drawn from the measurement of concentration and velocity profiles, that the ERT can undoubtedly detect the pipeline blockage and measure the mean solids concentration, solids axial velocity, and the thickness of the permanent granular bed in the blocked line, despite the coverage of the electrodes by a very thick granular bed.

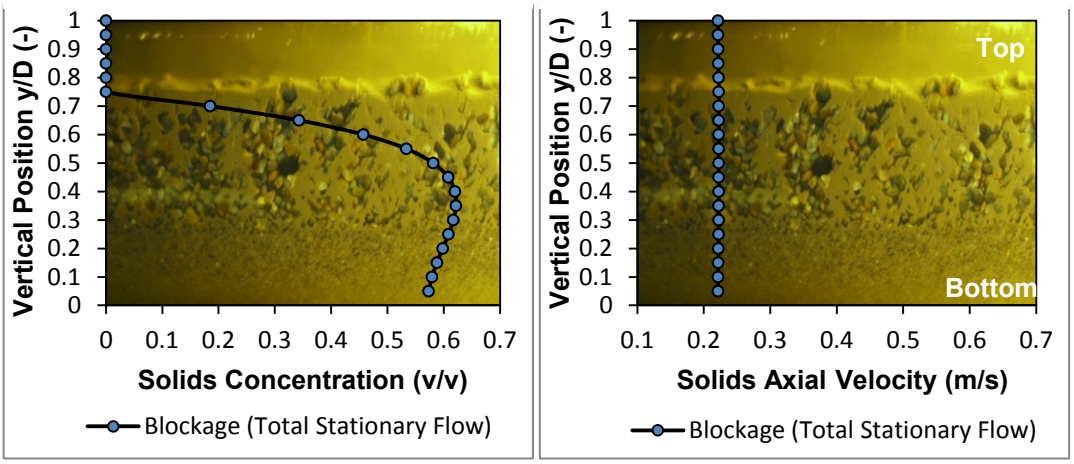

Figure 5.25 Pipe blockage for 10% coarse sand occurred at approximately 1.2 m/s shown on concentration profile (left) and solids velocity profile (right)

5.4.6 Formation of stratified flow

Once the transport velocity decreased, below the deposit velocity, the three zones, which were assumed by Wilson and Pugh (1988), were picked up by the ERT system. These are namely, a turbulent zone in the upper region of the pipe, a shear layer above the bed and the sliding bed in the bottom region of the pipe. Figure 5.26 highlights these three zones of the stratified flow through the distorted concentration and solids axial velocity profiles at 1.5 m/s transportation velocity.

The particles in the top layer are supported entirely by turbulence effect. In the shear layer there is a sharp gradient in both, the solids concentration and velocity profiles, in which all solids are fully suspended and supported by

turbulence and contact load effects. While in the bed there is no shear and solid concentration is that of a porous packed bed.

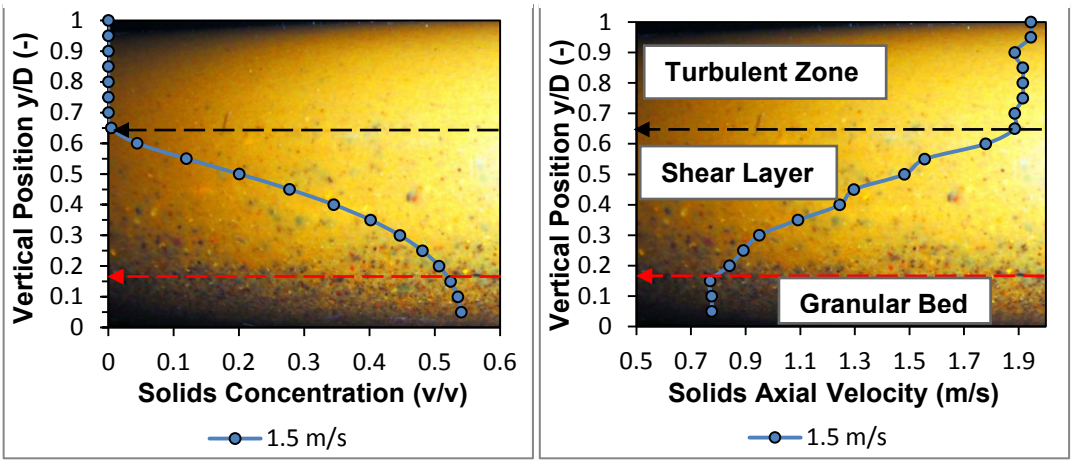

Figure 5.26 Showing the three zones of the distorted profiles, concentration profile (left) and solids axial velocity profile (right), in stratified flow at 1.5 m/s transportation velocity

Another phenomenon could also be observed for the two sands with the same condition, which is development of bed. The uniformly distributed bed can only be seen in the case of coarse sand with 10% throughput concentration, highlighted in Figure 5.26. This could be interpreted by the fact that in medium sand (2% and 10% throughput concentration), shown in Figure 5.27 and coarse sand (2% throughput concentration), shown in Figure 5.28, the distribution of the particles in the bed approach a limiting value in concentration (i.e. the concentration of the loose-poured bed has not reached the maximum concentration of the occupying pixel at the bottom of the pipe). Despite that, while observing the flow through the transparent pipe section for medium sand (2% and 10% throughput concentration) and coarse sand (2% throughput concentration) at low transport velocity (1.5 m/s), it was found that the loose-poured bed was moving in the form of *en-bloc* sliding (in mass).

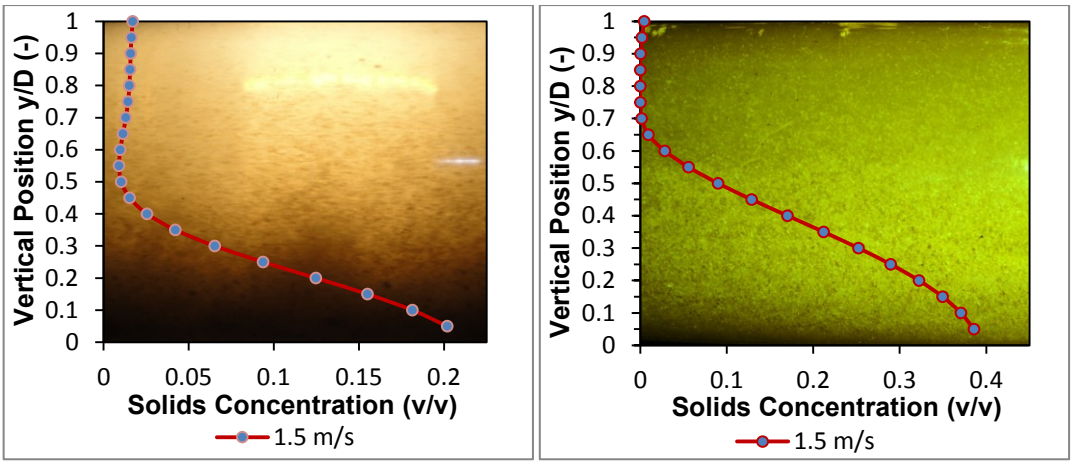

Figure 5.27 Showing sporadic movement of medium sand particles over the bed at 1.5 m/s transportation velocity and throughput concentration 2% (left) and 10% (right)

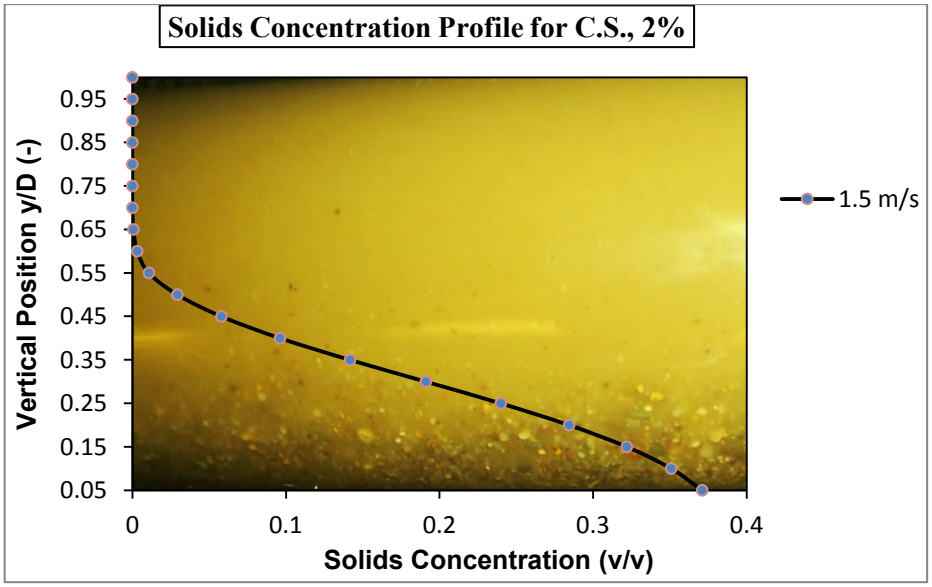

Figure 5.28 Showing sporadic movement of coarse sand particles over the bed at 1.5 m/s transportation velocity and 2% throughput concentration

It is worth pointing out that the profiles, generated by the ERT, correspond to the actual slurry flow illustrated in the background picture inserted into the plot area. This feature was also successfully picked up by the ERT system. This agreement between the profiles generated via the ERT and the actual photograph of the flow suggests the concentration distribution or solids axial velocity distribution, across the vertical plane of the pipe cross-section, could

be used for estimation of several parameters of stratified flow, which is discussed in the following section.

5.4.6.1 Estimation of parameters relating to stratified flow

The estimation of parameters relating to stratified slurry flow is paramount for slurry flow pipeline design and optimization. Therefore, based on the above findings the ERT can be utilised for estimation of such parameters through combination of solids concentration distribution and solids axial velocity distribution. The observation of both profiles and calculation of pixel height within the tomograms, the following parameters can be estimated:

1. Mean granular bed concentration.
2. Mean granular bed velocity.
3. The height of granular bed.
4. The height of shear layer.
5. The height of turbulent zone at the upper part of the pipe.

The height of granular bed can be demarcated at the point where the concave curve at the bottom of the pipe marks a sharp gradient in solids concentration or solids axial velocity distribution. This technique can be used to measure the height of granular bed only if the height of bed is greater than 2.5 mm in 50 mm inner diameter pipe, which is used in this study. In other words, this technique can only be used if the height of granular bed is greater than the ratio of pipe diameter to the number of pixels in the vertical plane of the tomogram. This can be expressed mathematically as:

$$The\ height\ of\ grannular\ bed > \frac{Inner\ Pipe\ Diametr}{No.of\ Pixles\ in\ the\ Vertical\ Plane} \tag{5.1}$$

However, the right hand-side of the above equation equals to the height of each pixel in the tomogram, then:

$$The\ height\ each\ Pixel\ in\ the\ Tomogram = \frac{Inner\ Pipe\ Diametr}{No.of\ Pixles\ in\ the\ Vertcal\ Plane} \tag{5.2}$$

The boundary of granular bed can be demarcated at the point where the profile changes its trajectory within the concave (left-hand side) curve in the

lower part of the pipe. As reported in literature (Dorn and Barnea, 1993; Matousek, 2002) the granular bed may be moving or stationary, or in some cases, as in three-layer, both moving and stationary layer may exist at the same time, where a moving layer is sliding over the surface of the stationary layer. Ideally, one would think that the height of stationary bed could be measured from the point where no further change is noticed in the solids concentration or solids velocity distribution within the granular bed. This is an indication that each pixel, from the concentration tomogram, is saturated with solid particles, although this is dependent on the shape of particles within the granular bed. Also in terms of solids velocity (as described in the following sections) within the granular bed, no gradient of solids velocity would be expected throughout the stationary layer, but a vertical line within the granular bed. However, none of the profiles (i.e. concentration and solids velocity profile) obtained from the ERT indicates moving or stationary bed at low velocities, but rather a packed granular bed. The reason for not being able to identify the two layers may be due to poor spatial resolution of the ERT or particle distinguish-ability problems associated with the ERT.

The observation of the profiles for 10% throughput concentration of coarse sand at 1.5 m/s slurry flow rate, as shown in Figure 5.26, reveals that it is apparent that the height of granular bed can be estimated as 10 mm from the bottom of the pipe (where y/D=0.2, y is the distance from the pipe bottom and d is the pipe diameter), as indicated by a red arrow.

Ideally, if the particle velocities found to be uniformly distributed within the bed height, then the bed is moving in the form of *en-bloc* fashion. However, this is only the case if no layer of the bed has zero velocity; otherwise the stationary layer has already formed within the bed layers. If the bed exhibits a velocity gradient along its height, then the bed is said to be moving in stream layers with different velocities, while the layer, which is in direct contact with the bottom pipe wall, could either be moving or stationary. These features regarding moving bed in the form of *en-bloc* fashion or sliding layers were not observed on the profiles obtained from the ERT. However, in the case of coarse sand the bed was observed at the time of the experiment that it was moving in the form of start-stop fashion at transport velocity just above 1.5 m/s, which is an indication of development of stationary bed, and sporadic movement of finer particles over the bed, as shown in Figure 5.26.

5.4.7 Reducing entrained bubbles

In order to reduce the amount of bubbles in the flow loop two measures were taken. The first was to reduce the acceleration of falling slurry at the discharge point, by placing several semicircle trays (plates) into the pipe wall of the vertical discharge pipe, in a way to occupy half of the pipe cross-section. Figure 5.29 showing the vertical discharge pipe with inserted plates. Since the flow does not cover the full bore of 100 mm discharge pipe, then reducing the pipe bore does not add up into the flow pressure. The plate spacing was arbitrary selected as 200 mm along the pipe section. The plates were placed in the pipe in an opposite sequencing fashion to ensure that the slurry flows down over the plates rather than through the passages (openings). In this manner, the pressure of down-coming slurry is reduced. In other words, the plates restrict the flow by approximately half and eventually reduce the gravitational force and flow pressure into the mixing tank.

(a) (b)

Figure 5.29 The vertical slurry discharge pipe into the mixing tank; (a) the Sanitary Tee connected to the outlet of the pipe; (b) the semicircle plates inserted into the pipe wall

The second measure was to separate the mixing region within the tank from the discharge zone, where the slurry returns to the mixing tank. The discharge zone made up approximately 20% of the tank and separated by welding a stainless-steel baffle to the tank wall. Figure 5.30 showing the baffle in the mixing tank.

It is very important to keep some distance of 300-350 mm between the baffle and the dead end of the mixing tank to allow the slurry to be transferred by the mixing effect from the discharge zone and reintroduced to the flow loop. In addition, a Sanitary Tee (100 mm ID) was connected to the end of the vertical discharge pipe to ensure that the slurry is smoothly returning into the discharge zone and retaining unavoidable bubbles deep towards the bottom of the mixing tank.

(a) (b)

Figure 5.30 The baffle in the mixing tank; (a) the discharge zone with the Sanitary Tee, (b) the mixing zone

After taking the above measures it was found that the amount of bubbles entering into the flow loop had significantly been decreased. Despite the above attempts, it was observed that unavoidable small bubbles were still present at high velocities, at which they are dispersed and homogeneously distributed across the pipe cross section. These unavoidable bubbles could clearly be seen at lower velocities, at which they flow at the upper part of the pipe. It is obvious that at higher velocities the rate of bubbles created are higher than that at lower velocities. This is due to the high momentum rate of returning slurry into the mixing tank and creation of vortices. The presence of small bubbles in the flow loop has been the cause for measurement errors in previous studies, and it is claimed that their reduction may be possible but their presence is unavoidable (Gillies, 1993; Matousek, 2005). Therefore, no further action was carried out.

5.4.8 Estimation of delivered solids volume fraction

The delivered solids volume concentration (C_v) calculated using the measuring tank, which is mounted on a set of three load cells, and the diverter system described in Chapter 4. The diverter system (switch system) was used to divert the slurry flowing out of the pipeline into the measuring tank for a given length of time. This period of time was recorded by an electronic stop watch. The volume of collected slurry in the measuring tank was determined using the level of the slurry in the tank and calculating the cross-sectional area of the measuring tank. Using the volume (v) and the total weight of collected slurry (wt), which was recorded via the load cells, the mixture density (ρ_m) can be determined, as shown in equation 5.4. Finally, knowing the solids density (ρ_s) and the carrier liquid density (ρ_l), the delivered solids concentration can be determined using equation 5.3.

$$C_v = \frac{(100\rho_{m-}\rho_l)}{(\rho_s - \rho_l)} \tag{5.3}$$

$$\rho_m = \frac{wt}{v} \tag{5.4}$$

5.4.9 Validation of the EMF velocity

The Electromagnetic Flow meter was installed in the vertical test section for regularly monitoring and recording the transport slurry velocity. The method used to validate the EMF consisted of using a switch system (or diverting system) and a measuring tank, which was mounted on a set of three calibrated load cells, the details of which is found in Chapter 4. After several seconds of diverting the flow to the measuring tank, it was noticed that the velocity on the Electromagnetic Flow meter was gradually dropping. Therefore, in order to avoid any false reading, the Electromagnetic Flow meter was recorded just before diversion of slurry. Both velocities from, the Electromagnetic Flow meter and the discharge level was then collected for the comparison, as shown in Table 5.2. The results of error analysis are illustrated quantitatively and qualitatively. Table 5.2 illustrating the comparison of velocity values obtained from the ERT and the discharge measurement for flowing medium and coarse sand with two different throughput concentrations (2% and 10%).

By observing the two data sets, it is apparent that the results, obtained within the range of velocities considered in the experiments, are in total agreement with each other. This conclusion was drawn from the results of error analysis carried out on the two velocities, EMF and discharge, for each sand at 2% and 10% throughput concentration and velocity range 1.5-5 m/s. The absolute error was calculated as the difference between the magnitude of the discharge velocity value and the observed EMF velocity value. However, in order to compare how incorrect the EMF is from the discharge values considered to be true, relative error was calculated between the discharge and the EMF, which is shown in percentage relative error (%). This calculation is shown in Equation 5.5, which is the product of absolute error, divided by the discharge value. As it is often expressed in percentage, then it is multiplied by 100:

$$\boldsymbol{Relative\ Error}\ \% = \frac{(V - V_O)}{V} \times 100 \qquad (5.5)$$

Where:

V= Discharge Velocity (actual) (m/s)

V_o= Observed (EMF) Velocity (Measured) (m/s)

V-V_o= Absolute Error (m/s)

The results are summarised and illustrated in the following table in terms of minimum deviation, maximum deviation and the average error within the range of velocities mentioned above.

For further investigation of relationships between the EMF readings and the calculated discharge, Regression Analysis was used as a statistical tool, for which a linear relationship was assumed between the two set of values. The results of this analysis are illustrated quantitatively in Figure 5.31, which in the meantime assesses the statistical significance of the estimated relationship between the two folds of data. The output results of the regression provide a range of important statistical information, which can be used for assessment of the relationship between the two variables, some of which are listed under the regression statistics heading, as shown in Table 5.3. The most important value here is the value of R square, which measures the degree of linear relationship between the velocity values measured by the EMF and those calculated by the flow diversion technique.

By observing the R square values in Table 5.3 for all conditions used, it is apparent that its values are not less than 0.99, which determines a well fit or a very good degree of linear relationship between the two measured and predicted velocity values. Nevertheless, the standard error shown in the aforementioned table can also indicate a good fit between the two data.

Table 5.2 The data obtained from the EMF reading and discharge calculation along with the rate of deviation at each given velocity.

EMF (m/s)	Discharge Velocity (m/s)	Absolute Error (m/s)	Relative Error (%)	Remarks
Medium Sand 2%				
4.97	**4.97**	0.00	0.01	
4.53	**4.49**	0.04	-0.86	
4.02	**4.08**	0.06	1.46	Min. Deviation = 0.01%
3.49	**3.49**	0.00	0.10	Max. Deviation = 3.13%
3.05	**3.05**	0.00	0.12	Average Error = 1.19%
2.52	**2.55**	0.02	0.97	
2.06	**2.12**	0.06	2.84	
1.49	**1.54**	0.05	3.13	
Medium Sand 10%				
4.96	**5.59**	0.63	11.27	
4.59	**4.47**	0.12	-2.79	
4.06	**4.00**	0.07	-1.69	Min. Deviation = 0.52%
3.49	**3.47**	0.02	-0.65	Max. Deviation = 11.27%
3.04	**3.19**	0.15	4.73	Average Error = 3.23%
2.52	**2.54**	0.02	0.67	
2.01	**2.02**	0.01	0.52	
1.52	**1.58**	0.05	3.49	
Coarse Sand 2%				
4.93	**4.82**	0.11	-2.29	
4.36	**4.53**	0.17	3.79	
4.11	**4.29**	0.18	4.14	Min. Deviation = 1.37%
3.52	**3.66**	0.14	3.90	Max. Deviation = 4.14%
3.11	**3.18**	0.08	2.48	Average Error = 2.81%
2.52	**2.45**	0.07	-3.00	
2.00	**2.03**	0.03	1.50	
1.52	**1.50**	0.02	-1.37	
Coarse Sand 10%				
4.76	**5.24**	0.48	9.18	
4.14	**4.61**	0.48	10.30	Min. Deviation = 3.38%
3.40	**3.62**	0.22	6.11	Max. Deviation = 12.7%
2.94	**3.36**	0.43	12.75	Average Error = 17.17%
2.49	**2.58**	0.09	3.44	
2.20	**2.09**	0.11	-5.05	
1.45	**1.40**	0.05	-3.38	

Table 5.3 The summary output of the statistical analysis of the two sands at 2% and 10% throughput concentration and 1.5-5 m/s velocity range

2% Medium Sand		**10% Medium Sand**	
Regression Statistics		*Regression Statistics*	
Multiple R	0.99993	Multiple R	0.99968
R Square	0.99986	R Square	0.99936
Adjusted R Square	0.83319	Adjusted R Square	0.8327
Standard Error	0.04048	Standard Error	0.08731
Observations	7	Observations	7
2% Coarse Sand		**10% Coarse Sand**	
Regression Statistics		*Regression Statistics*	
Multiple R	0.99978	Multiple R	0.99848
R Square	0.99955	R Square	0.99696
Adjusted R Square	0.83288	Adjusted R Square	0.79696
Standard Error	0.07274	Standard Error	0.17528
Observations	7	Observations	6

Qualitative results were also generated from the regression analysis, which show the deviations clearly for any given velocity. For the sake of clarity two relevant plots were generated for each flow condition, as shown in Figure 5.32. The line fit plot, which is shown on the left-hand side and the plot of residuals against the predicted velocity values measured by the EMF on the right-hand side. Each plot, especially the plot of residuals against the predicted values, can be used as a powerful diagnostic tool to identify the level of deviation and reveal valuable information throughout the range of velocities used. The deviations could also be seen on the line fit plot; however, these deviations are clearly highlighted and distinguished in the plot of residuals. In other words, it acts as an amplifier, which enlarges the level of deviation about the predicted (or estimated) velocity. For example in Figure 5.32, it is highly remarkable that the distribution of errors are random across the given velocity range and the EMF slightly overestimates the transport velocity, whereas for any velocity above 3.5 m/s there is an underestimation in the velocity values. However, these may not be manifested clearly. Despite a subtle difference between the residuals and the relative error, which is related to the reference data, they are not distinguished in this study. Therefore, the above equation for the calculation of the relative error could be employed to calculate the residuals.

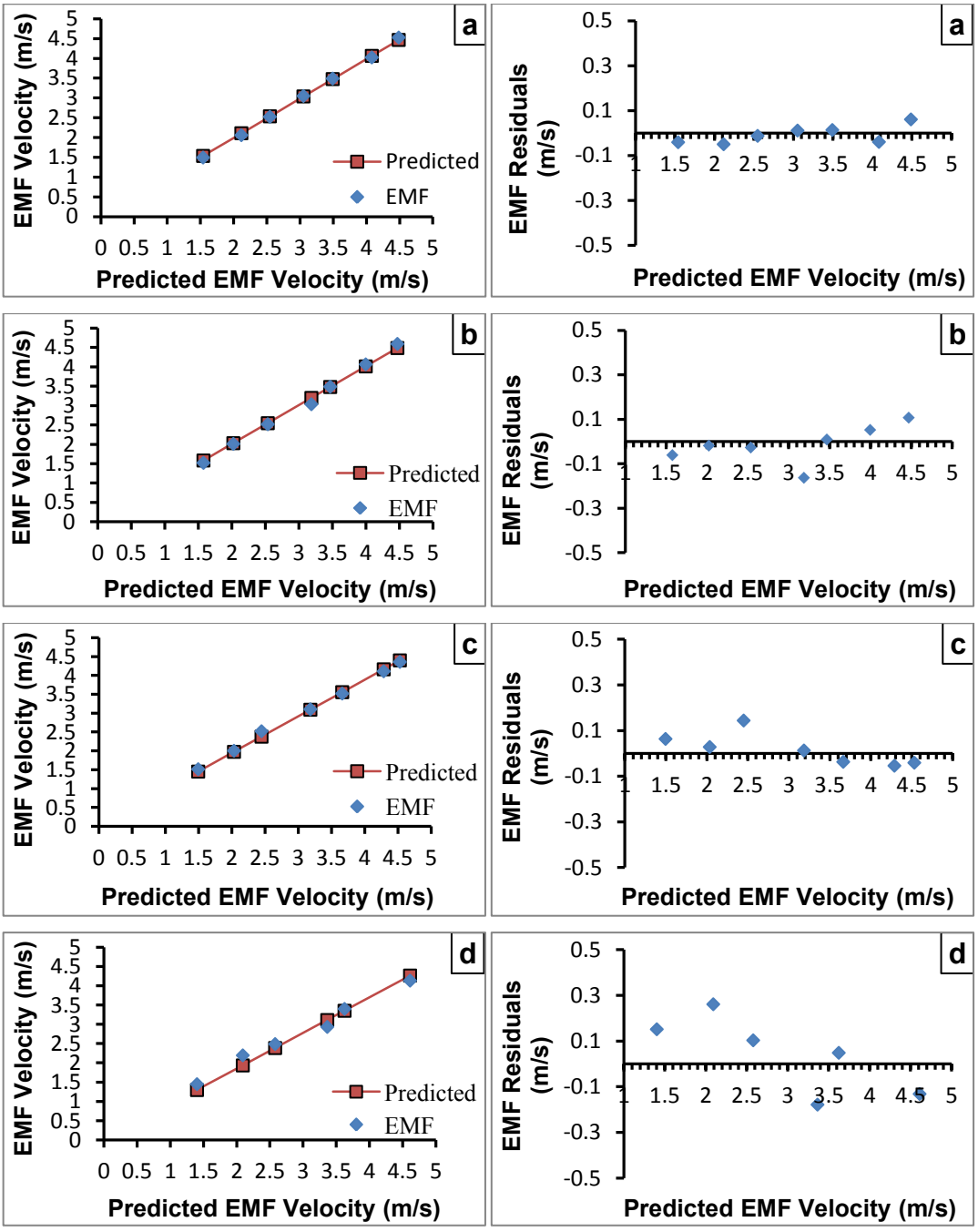

Figure 5.32 The EMF velocity line fit (left) and the residuals about the predicted velocities (right) for (a) medium sand at 2% throughput concentration; (b) medium sand at 10% throughput concentration; (c) coarse sand at 2% throughput concentration; (d) coarse sand at 10% throughput concentration

On the residuals plot, the abscissa (the distance cut off from the X-axis by a line drawn through it and parallel to the Y-axis) of any data point represents the magnitude of relative error. In this case, if the residual is a positive value, then the EMF measured velocity value is underestimated. Similarly, if the residual is a negative value, then the measured velocity value is

overestimated. In other words, any data point lies over the X-axis, in Figure 5.32 (right-hand side), represents the magnitude by what the velocity underestimated, and any data point under the X-axis represents the magnitude by what the velocity overestimated.

From the qualitative and quantitative results of the regression analysis, it can be concluded that the errors are random and the deviations are subtle. This implies that the errors are within the reasonable range. These errors may well be attributed to the degree of uncertainty of EMF or experiment. The experiment uncertainty could be related to the discharge measurement.

To further clarify this, while diverting the flow to/from the measuring tank, some of the diverted slurry splashed out of the switch system, especially at high velocities (3.5 m/s and above). As a result the level of slurry in the measuring tank would not correspond exactly to the duration of the diversion. Similarly, the duration of the diversion may have been overestimated, which caused by the lack of synchronisation between the diversion and the stopwatch. Therefore, it can be concluded that the two sets of velocity data are well fit and have a good agreement within the range of velocity used.

5.4.10 Validation of the ERT results

The estimated mean solids concentration and mean solids axial velocity values obtained from the ERT were compared to the corresponding values measured using the flow diversion technique. In the case of concentration validation, the ERT results were compared to the discharge concentration, obtained from the flow diversion technique, at different throughput slurry velocity. Since at velocities below the deposition velocity, the in-situ concentration values differ from the delivered concentration values due lack of turbulent eddies, which result in the deposition of solid particles and solids hold up in the horizontal pipeline. Therefore, the comparison is valid only at higher transport velocities above the deposition velocity. On the other hand the validation of solids axial velocity obtained from the ERT was carried out by assessing the linear relationship between the results of the ERT and that of flow diversion technique through output results of regression analysis (line-fit). The line-fit plot showing the relationship between the ERT measured values and the predicted values. The predicted values represent the values obtained from the flow diversion technique and are considered as a reference line for the ERT error analysis. Error analysis of the ERT results have been carried out for various flow conditions, flow orientation, particle size, solids loading concentration and transport velocity.

5.4.10.1 Validation of mean solids volume fraction

Tables 5.4 and 5.5 showing the comparison of in-situ concentration measured by the ERT and delivered concentration measured via the flow diversion technique, at different transport velocities. The comparison has been carried out only for concentrations within the range of higher transport velocities (3-5 m/s), shown within the shaded area within both tables. An analysis of the error is also presented along with an estimation of average error for each sand and throughput concentration. The average error was determined only for the range of concentrations falling into the shaded area in the either tables.

Through an observation of qualitative and quantitative results, it can be revealed that the occurring errors are random and the values differ from one condition to another. In other words, the rate of error is different from one transport velocity to another as well as particles size and throughput concentration.

Table 5.4 The comparison of solids concentration values for medium and coarse sand at 2% throughput concentration in the horizontal test section. The shaded area represents the values, only for which the comparison and error analysis have been carried out

	Medium Sand, 2% Throughput Concentration			**Coarse Sand, 2% Throughput Concentration**		
Velocity (m/s)	**In-situ Conc. %(v/v)**	**Delivered Conc. %(v/v)**	**Relative Error (%)**	**In-situ Conc. %(v/v)**	**Delivered Conc. % (v/v)**	**Relative Error %**
5	2.9	2.4	20.8	3.9	3	30
4	3.2	2.4	33	2.7	2.9	6.9
3.5	2.9	2.7	7	3.1	3.2	3
3	2.4	2.5	4	3.4	3.2	6
2.5	3.4	2.5	-	3.7	3.4	-
2	3.7	2.5	-	3.8	3	-
1.5	3.7	2.4	-	6.5	2.8	-
	Average Error=16.4%			**Average Error=12%**		

Table 5.5 The comparison of solids concentration values for medium and coarse sand at 10% throughput concentration in the horizontal test section. The shaded area represents the values, only for which the comparison and error analysis have been carried out

	Medium Sand, 10% Throughput Concentration			Coarse Sand, 10% Throughput Concentration		
Velocity (m/s)	**In-situ Conc. %(v/v)**	**Delivered Conc. %(v/v)**	**Relative Error (%)**	**In-situ Conc. %(v/v)**	**Delivered Conc. % (v/v)**	**Relative Error %**
5	11.6	8.4	38.37		-	-
4.5	10.2	9.3	10.11	16.5	11.4	44.58
4	9.7	9.1	6.21	13.9	12.1	14.98
3.5	9.7	9.6	0.88	12.8	12.8	0.07
3	9.8	9.3	5.77	13.8	12.4	11.71
2.5	10.5	9.5	-	13.3	12.7	-
2	11.0	9.7	-	16.2	13.4	-
1.5	12.0	9.6	-	21.0	12.8	-
	Average Error=12.3%			**Average Error=18%**		

Since the flow regimes dependent on these three parameters, then the distribution pattern of errors implies that the ERT measurement scheme is dependent on the flow regime present in the pipe. Therefore, an automated flow regime recognition technique is required so as to determine the prevailing flow regime, based on which the ERT measurements are corrected accordingly. However, it was observed that the ERT measurements give rather a reasonable estimation of the overall in-situ solids concentration, as shown quantitatively and qualitatively.

Nevertheless, some over estimation, relative to the delivered concentration, can be noticed for both sands at higher velocities (4 m/s and over), as shown in Figure 5.33 for different sands in different concentration. This is not a phenomenon that is predicted in slurry flow at higher velocities.

As at higher velocities the driving force can overcome the resisting force and there is no effect of slip velocity between the liquid phase and the solid phase (i.e. the velocity of the solid phase is equal to the velocity of the carrier liquid). This implies that there is no solids holdup in the pipeline, in other words the in-situ solids concentration is equal to the delivered solids concentration (C_i=C_v). However, the reason for this over estimation in the measured values of the in-situ concentration could well be due to the large amount of bubbles entering into the flow loop via the mixing tank and adding up more into the concentration of the dispersed phase (non-conducting

phase). These small bubbles have been created by dropping the returning slurry into the mixing tank at a considerable force through a 4" vertical pipe, which connects the discharge point to the mixing tank.

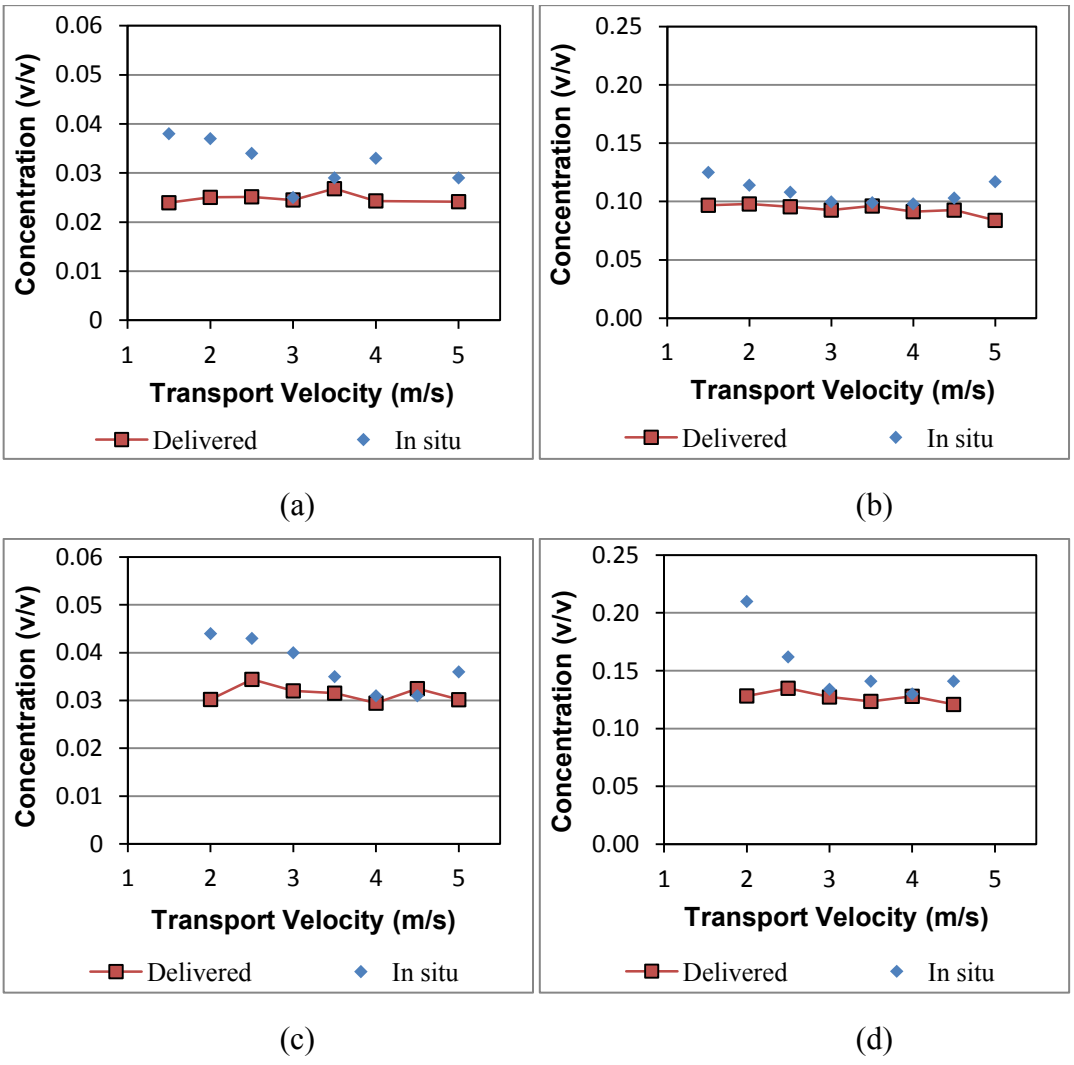

Figure 5.33 Showing the comparison between the in-situ solids concentration obtained from the ERT and delivered solids concentration obtained from the flow diversion technique in horizontal flow for (a) medium sand at 2% throughput concentration, (b) medium sand at 10% throughput concentration; (c) coarse sand at 2% throughput concentration and (d) coarse sand at 10% throughput concentration

Once the slurry falls at the discharge point into the mixing tank, it creates a chaotic condition, as a result small bubbles are trapped in the mixing effect and introduced into the flow loop. Attempts were made to reduce the amount of bubbles introduced into the flow loop, by placing several semi-circle trays along the vertical discharge section to reduce the momentum of the falling

slurry or reducing the vortex formed in the vertical pipe. In addition, a baffle was placed in the mixing tank to separate the mixing zone from the region of returning slurry. The methods used to reduce bubbles in the flow loop are discussed in section 5.4.7. This possibility is based on the fact that at higher velocities the slurry returning to the mixing tank through approximately 2 m length uPVC vertical pipeline (100 mm ID), at the end of which the slurry falling into the tank and creating a chaotic zone within the tank. As a result bubbles are entrained into the tank, whereby they are trapped by the mixing effect and introduced to the pipeline.

On the other hand, an increase in the In-situ concentration can be noticed at lower velocities (3 m/s and below), this is totally predicted for slurry flow as indicating the hold up of solids, which contribute into an increase in the local concentration and as a result the delivered concentration is decreased.

5.4.10.2 Validation of mean solids axial velocity

The technique used to validate the solids velocity results of the ERT is similar to that of the EMF, which is using the measuring tank and calculation of the discharge velocity. Since at the discharge point, there is no slip velocity, therefore, the solids velocity can be determined by the ratio of the discharge slurry volume flow rate to the discharge pipe cross-sectional area. Thereafter, comparing the two mean slurry velocity values (the discharge with that of measured by the ERT). The procedure was to measure the solids velocity by the ERT, then calculate the mean velocity across the horizontal pipe cross-section. Consequently, measuring the discharge velocity, considering all the implications that are associated with the slurry diversion, which is the driving force for flow instability. This procedure was repeated for both sands, each at 2% and 10% throughput concentration, including the blockage of coarse sand at 10% throughput concentration. The pre-calibrated EMF was used to monitor the mean slurry velocity within the range of 1.2-5 m/s. The two data velocities, the ERT and the discharge, were collected and compared against each other, as shown in Table 5.6. Error analysis was carried out for each condition and the results are highlighted quantitatively and qualitatively.

Table 5.6 The data obtained from the ERT measurement and flow diversion technique (discharge velocity) along with the rate of deviation at each flow condition for horizontal flow

EMF Velocity (m/s)	ERT Solids Velocity (m/s)	Discharge Velocity (m/s)	Absolute Error (m/s)	Relative Error (%)	Remarks
Medium Sand 2%					
4.53	**4.80**	**4.49**	0.31	-6.97	Min. Deviation = 3.44% Max. Deviation = 25.82% Average Error = 12.69%
4.02	**3.94**	**4.08**	0.14	3.45	
3.49	**3.80**	**3.49**	0.31	-8.87	
3.05	**2.70**	**3.05**	0.35	11.40	
2.52	**2.06**	**2.55**	0.48	18.91	
2.06	**1.83**	**2.12**	0.28	13.45	
1.49	**1.14**	**1.54**	0.40	25.82	
Medium Sand 10%					
4.96	**4.79**	**5.59**	0.80	14.37	Min. Deviation = 0.33% Max. Deviation =14.37% Average Error = 4.36%
4.59	**4.99**	**4.47**	0.52	-11.59	
4.06	**3.80**	**4.00**	0.20	4.90	
3.49	**3.51**	**3.47**	0.04	-1.25	
3.04	**3.17**	**3.19**	0.02	0.57	
2.52	**2.56**	**2.54**	0.02	-0.96	
2.01	**2.03**	**2.02**	0.01	-0.33	
1.52	**1.59**	**1.58**	0.01	-0.95	
Coarse Sand 2%					
4.93	**4.50**	**4.82**	0.32	6.64	Min. Deviation = 1.52% Max. Deviation = 35.97% Average Error = 12.81%
4.36	**4.41**	**4.53**	0.12	2.75	
4.11	**4.35**	**4.29**	0.07	-1.52	
3.52	**3.05**	**3.66**	0.61	16.78	
3.11	**2.79**	**3.18**	0.39	12.27	
2.52	**2.32**	**2.45**	0.13	5.40	
2.00	**1.60**	**2.03**	0.43	21.15	
1.52	**0.96**	**1.50**	0.54	35.97	
	Coarse Sand 10%				
4.76	**5.50**	**5.24**	0.25	-4.86	Min. Deviation = 3.25% Max. Deviation = 21.31% Average Error = 9.37%
4.14	**4.41**	**4.61**	0.20	4.31	
3.40	**3.51**	**3.62**	0.12	3.25	
2.94	**2.65**	**3.36**	0.72	21.31	
2.49	**2.31**	**2.58**	0.27	10.32	
2.20	**1.74**	**2.09**	0.35	16.75	
1.45	**1.47**	**1.40**	0.07	-4.80	
Blockage of Coarse Sand at 10% Throughput Concentration					
0	**0**	**0.22**	0.22	-	Absolute Deviation = 0.22 Relative Error = -0.22

The maximum, minimum and the average deviation are also highlighted for both, coarse and medium sand, at different throughput concentrations and velocity range mentioned above. Similarly, the error analysis was also carried out for blockage of horizontal pipeline, which is also highlighted in the aforementioned table.

The minimum deviation of (0.33%) between the discharge and the ERT velocities was observed at (10%) medium sand throughput concentration, whereas the maximum deviation of (35%) was noticed at (2%) coarse sand throughput concentration and 1.5 m/s transport velocity. While the horizontal pipeline was blocked, a transport velocity of 0 m/s was shown on the EMF. In addition, there was 0 m/s flow at the discharge. However, the mean slurry velocity measured by the ERT indicates 0.22 m/s, which makes -0.22 m/s error relative to the true value indicated by the discharge. Since the magnitude of the error is a negative value, then it is apparent that, based on the equation for the relative error, the ERT overestimates the mean velocity by 0.22 m/s.

However, if we look at the measured velocities it can be seen that the ERT measured values of solids velocity are reasonably close to the values of solids velocity measured by the measuring tank over the entire range of throughput concentration and transport velocities. The linear relationship between the ERT and the discharge velocities was also assessed through quantitative and qualitative output results of regression analysis. The quantitative results are shown in Table 5.7, in which it is apparent that the degree of linear relationship between both measured and predicted ERT velocity values are represented by R square. It is observed that the value of R square in all conditions employed in the experiment is around 99%. This value determines the suitability of using the predicted values of ERT to highlight the deviations for each velocity data point.

Table 5.7 Showing the summary output of the statistical analysis of the two sands at 2% and 10% throughput concentration and 1.5-5 m/s velocity range

2% Medium Sand	
Regression Statistics	
Multiple R	0.994
R Square	0.988
Adjusted R Square	0.788
Standard Error	0.327
Observations	6

10% Medium Sand	
Regression Statistics	
Multiple R	0.998
R Square	0.996
Adjusted R Square	0.830
Standard Error	0.211
Observations	7

2% Coarse Sand	
Regression Statistics	
Multiple R	0.995
R Square	0.991
Adjusted R Square	0.824
Standard Error	0.315
Observations	7

10% Coarse Sand	
Regression Statistics	
Multiple R	0.997
R Square	0.993
Adjusted R Square	0.793
Standard Error	0.255
Observations	6

In order to highlight the deviations of each data point clearly, four sets of plots were generated from the regression analysis, which are presented in Figure 5.34. Each set showing a line fit and a residual plot, indicating the deviation of the ERT data from the predicated values at each flow condition. The residual plots illustrate the rate of error in terms of magnitude, by which the solids velocity deviates. It is worth pointing out that there is a subtle difference between the relative error and the residuals. The relative error of a sample presents the deviation of a sample (the ERT velocities) from the true function value (discharge velocities); while the residual of a sample indicates the difference between the sample (the ERT velocities) and the estimated function value (estimated ERT velocities) based on the discharge velocity values. The estimation (or prediction) is well based on velocity data, the discharge and the ERT. Therefore, the predicted values are considered as the reference line and the basis of the ERT error analysis. The ERT line fit plot showing the relationship between the ERT measured velocities and the predicted velocity values. In this case the difference between the two values is the residual, which is highlighted by the plot of the predicted values against the residuals. In order to make an overall assessment of the ERT measured velocities, the residual plot is used as a diagnostic tool and analysis of each measured velocity. As previously mentioned the level of error may not be clearly shown on the line fit plot, therefore, the residual plot

is used, which clearly shows the deviation of each velocity data point about the predicted values.

An overall observation of the line fit plot in Figure 5.34, suggests a rather reasonable estimation of the ERT mean solids velocity values in all conditions. However, from both, the line fit and the residual plots, three observations can be remarked. Firstly, it is clear that the errors are quite random throughout the velocity range used in the experiments. This statement is valid for all conditions. Secondly, based on the discharge solids velocity values, it is obvious that the ERT velocities are mostly underestimated at low velocities (3 m/s and below), which is considered as stratified velocity region, where the bed exists (either moving or stationary) and the particles over it move in a sporadic fashion. Thirdly, an overestimation of the ERT solids axial velocities is well pronounced at high transport velocities (above 3 m/s). The occurrence of random errors can be attributed to the complexity of solid flow within the carrier liquid and the discontinuity of flow, whereby different flow regimes are manifested. Since the flow regimes are dependent on particle size and solids concentration, then the transitional velocities between flow regimes can differ for each concentration and particle size used in this investigation. Therefore, it is totally plausible for the errors to occur at different rate for each sand and concentration at a given transport velocity. From this a conclusion can be drawn that the ERT solids velocity measurement is dependent on the prevailing flow regime within the pipe. Therefore, in order to make a rather accurate ERT solids velocity measurement, automated flow regime recognition has to be developed to identify the prevailing flow regime, after which the ERT measurement correction will be applied based on the present flow regime within the pipe. This can be confirmed by the general distribution pattern of the errors on the line plots shown in Figure 5.34. At high velocities, where the particles are suspended in the carrier liquid, the solids velocities are overestimated by the ERT; whereas, at low velocities, within the range of which fully or partially stratification occurs, the solids velocities are underestimated. The change in the trajectory of the errors on the line fit is highly likely to be due to the phenomenon of particle wave speed. This is well related to the configuration of the dual plane ERT sensor (distance between the sensor planes). The optimum distance between the two planes is based on the transport velocities used in the pipeline. At low transport velocities the interval distance between the two planes requires to be shorter than that used for high velocities.

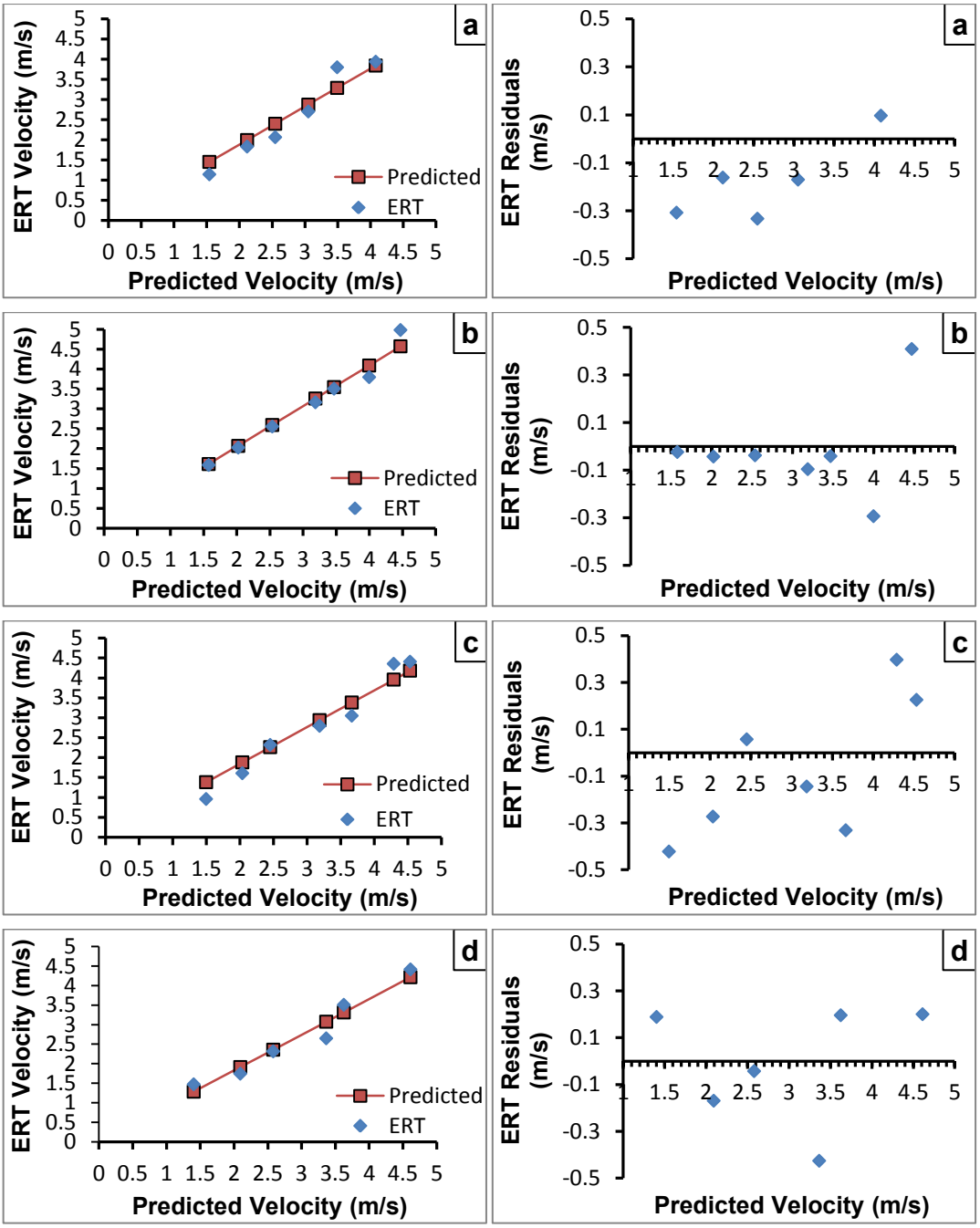

Figure 5.34 Showing the ERT velocity line fit (left) and the residuals about the predicted velocities (right) for (a) medium sand at 2% throughput concentration, (b) medium sand at 10% throughput concentration, (c) coarse sand at 2% throughput concentration, (d) coarse sand at 10% throughput concentration

The phenomenon of particle wave speed was also observed by Zafar *et al.* (2009), who conducted experiments on sand water flow and concluded that the phenomenon of particle wave speed can occur if the deviation is higher in heterogeneous flow regime as compared to stratified flow regime. The dual plane distance used in this study is 70 mm, which may be rather

suitable for high slurry velocity, but certainly not for lower velocities, where partially of fully stratification is present. In other words, the sporadic movement of the particles above the bed, as they are lifted from the top of the bed by the wave velocity of the carrier liquid, can be detected by one plane, however, due to long distance between the two planes, the second plane is unable to detect, as a result the cross-correlation fails. In some other cases, since the ERT suffers from particle distinguishability issues, the particles move above the bed may not be well close to each other for the ERT to detect them. Therefore, in this case the moving particle is not taken into account, as a result an underestimation of solids velocity occurs.

It is accepted in literature (Gillies, 1993; Matousek, 2005), that the prevailing mechanism of particle support, even within a short axial distance in the horizontal pipeline, is due to the interaction with turbulent eddies of the flowing stream. The same mechanism is applied for partially or fully stratified flow, where a portion of particles are lifted again from the surface of the bed by a lump of liquid and mixed with the stream flowing over the bed in a new location. The transfer of momentum and mass occur within the mixing length, the distance over which the lump of liquid transports its momentum and the particles caught in this length are migrated into the stream layers over the bed, (Perry *et al.,*1997). Once the particles are suspended in the carrier liquid, due to turbulent wave (or sporadic movement), they transfer their submerged weight to the carrier liquid above the bed. As a result a high shear-stress occurs above the bed, which slightly accelerates the rate of saltation (accelerates the rolling of particles over each other at the surface of the bed). This phenomenon creates a conflict between the driving force (the flowing stream) and the resisting force (the non-hydraulically smooth surface of the bed). In reality the condition over the bed is highly unstable, which imply that the conflict between the two forces, driving and resisting, is always present, unless the transport velocity is varied to a level, in which the pulse of liquid decrease or increase above the bed. In other words, while the particles move in continuous sporadic motion, an increase of the transport velocity would result in the increase of the turbulent eddies over the bed and cause the top granular layers of the bed to suspend in the carrier liquid. In this case the higher concentration of particles at the bottom of the shear layer causes particle-particle interaction and fluid-particle interaction, which both contribute into the mean solids axial velocity. Therefore, a conclusion can be drawn that the unsteady-state condition over the bed, which causes sporadic movement of a portion of particles at the surface of the bed, has effect on the magnitude of the mean axial solids velocity. In addition, the

ERT underestimation in stratified flow may have to do with low spatial resolution, due to which the moving particles at the surface of the bed cannot be detected, as shown in the velocity profiles for coarse and medium sand. In reality the particles of moving layer at the top of the bed roll over each other along the surface of the bed and picked up by the turbulent carrier liquid once they reach the bend, where they are taken upward through the vertical pipeline to the discharge point. As the ERT also suffers from particle distinguishability problem, then the particles moving within this region may not be detected. As a result the mean solids velocity is underestimated at stratified velocities.

It was observed that at high velocities (3.5-5 m/s) the ERT mostly overestimate the mean dispersed velocity by as maximum as 11.59% at 4.50 m/s transport velocity for 10% medium sand throughput concentration. Another reason for this overestimation could well be due to the presence of bubbles in the flow loop. These small bubbles have been created by dropping the returning slurry into the mixing tank at a considerable force through a 4" vertical pipe, which connects the discharge point to the mixing tank, as previously discussed.

5.5 Vertical upward flow measurement and visualisation

The same flow loop used for horizontal was also used for vertical upward flow measurement. The vertical test section was located directly after the horizontal section and connected to each other via a 90° short radius bend. The total length of the vertical section is approximately 4 m from the lower bend. The dual plane ERT sensor was mounted on the vertical section at approximately 3 m from the lower bend to ensure that the flow is fully developed at the ERT dual-plane sensor location. The Electromagnetic Flow meter (EMF) was mounted on the vertical line, 1 m above the ERT sensor, to monitor the slurry flow rate through the vertical pipe line. Two pressure sensors were also mounted on the same line, within the developed flow region at 2.5 m interval, for pressure measurement and calculation of the pressure difference across the test section.

The experiment procedure, for vertical flow measurement, was carried out the same as that of horizontal flow measurement and in a consequent fashion. In other words, after each horizontal measurement, consequently a vertical measurement was conducted at the same flow condition. The aim of carrying out the horizontal and vertical measurements approximately at the

time and the same flow conditions was to compare the results obtained for both orientations.

5.5.1 ERT solids volume fraction and solids axial velocity measurement

The data obtained for each test was recorded and collected for estimation of solids volume fraction and solids axial velocity. The qualitative results are shown in Figure 5.35, in terms of volumetric concentration profile (left-hand side) and solids velocity profile (right-hand side) across the vertical plane of the vertical pipe cross-section.

By observing the concentration profiles for flowing coarse sand, it can be seen that for higher sand concentration (10%) the bell-shape (or core peak) profile can clearly be manifested in the pipe. This phenomenon has been observed by early researchers such as Newitt *et al.* (1955). Hence in flowing coarse sand slurry through vertical counter-gravity radial particle migration occurs. The effect of radial particle migration is to move particles into the faster moving streams of the flow. However, the concentration profiles for medium sand suggest a totally different shape in contrast to the concentration profiles for coarse sand. In the case of coarse sand it can be seen that there is a particle-rich core at the centre of the pipe and a particle-lean annulus close to the pipe wall, whereas the phenomenon is vice versa for the flowing medium sand. Based on the ERT results, it can be concluded that the coarse particles move upward the vertical pipe in a core peak flow pattern, while the medium particles move in wall peak flow pattern. This means that in the case of medium sand the radial particle migration is towards the pipe wall. The phenomenon of wall peak flow has been observed by Karnis *et al.* (1966), who observed that for a more viscous carrier liquid the particles move close to the pipe wall. Therefore, it is highly plausible that the very fine particles in the medium sand are accountable for increasing the viscosity of the carrier liquid (water) used in this study.

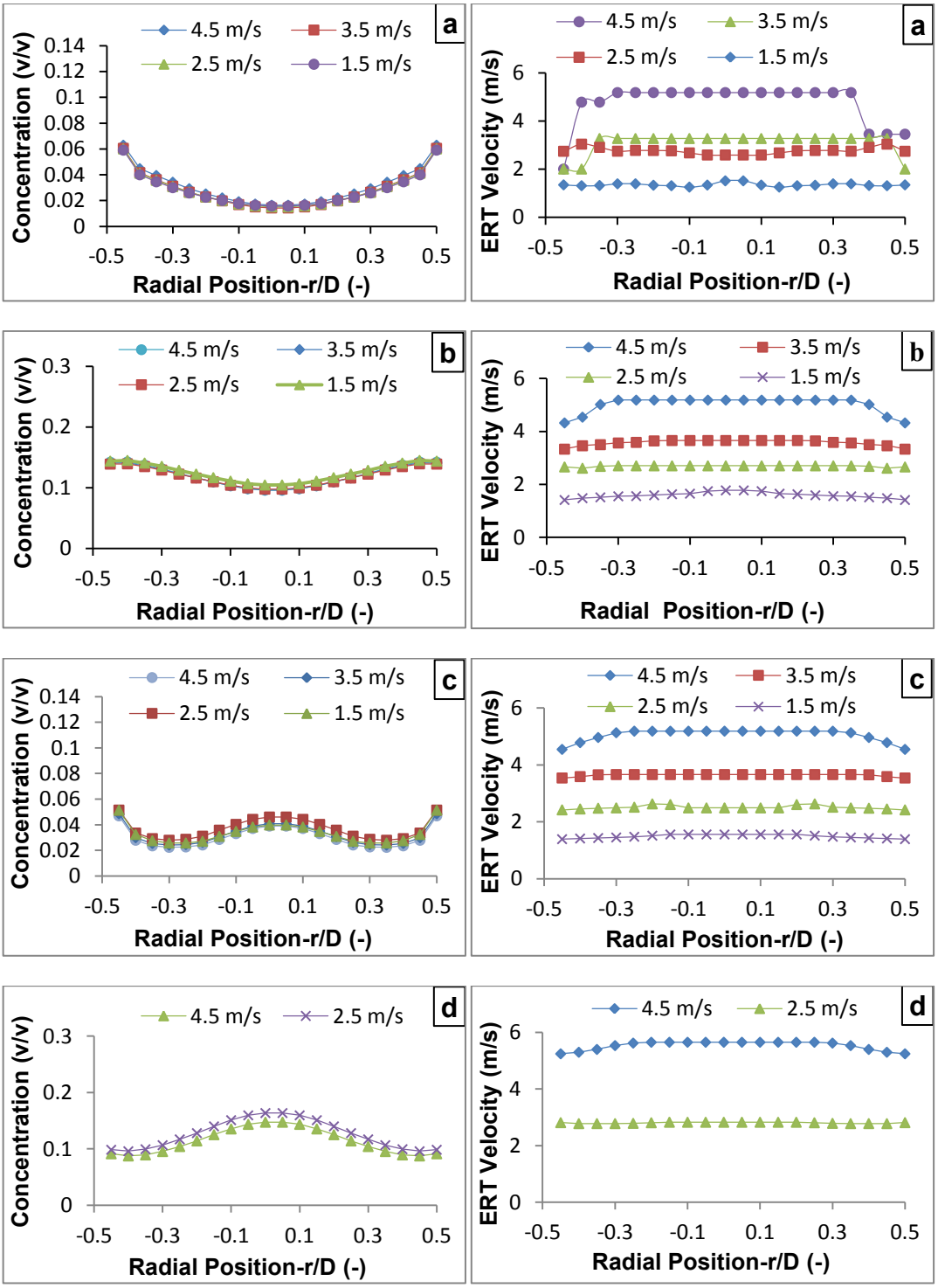

Figure 5.35 Concentration profile (left hand-side) and solids velocity profile (right hand-side) as a function of transport velocity in upward vertical flow for (a) medium sand at 2% throughput concentration, (b) medium sand at 10% throughput concentration, (c) coarse sand at 2% throughput concentration, (a) coarse sand at 10% throughput concentration

It is also apparent that the phenomenon of radial particle migration for coarse sand is not quite reflected in the solids velocity profile for all conditions, instead showing a blunted shape rather than an inverse bell-shape (or parabolic). The velocity of particles exhibits a uniform distribution throughout the centre region of the pipe cross-section. It is quite expected that the particles within the particle-rich core, for flowing coarse sand, move slower relative to the surrounding layer due to gravity effect (density difference) and particle-particle interaction. The flattened shape of velocity profile has been observed by some researchers, for example Koh *et al.* (1994), similar to the one obtained in this study using the ERT. They also noticed that with increasing delivered solids concentration, the velocity profile becomes increasingly blunted. This implies that at higher transport velocities, the shape of solids velocity profile becomes further flattened, as it can be observed in the solids velocity profiles shown in Figure 5.35. The results of Koh *et al.* (1994) also revealed another phenomenon, which is with increases in particle size the velocity profile become increasingly flattened. This phenomenon was also picked up by the ERT used in this study.

It is also apparent that by increasing the concentration and particle size, the particles move further towards the centre line region of the flow and the pick takes more towards the centre of the pipe cross-section. It was found that the results are in good agreement with those found by Lucas *et al.* (1999), using an electrical probe. Also, similar results were found by Koh *et al.* (1994), who measured the particle concentration and velocity profiles of particle size 1-5 mm in a Newtonian fluid through a vertical rectangular channel. Their results showed a non-uniform, bell-shaped concentration profile, with a maximum particle concentration at the centre line and a minimum particle concentration near the wall. Therefore, it can be concluded that the local solids concentration profile and the solids velocity distribution calculated using the ERT are a reasonably accurate representation of the true flow profile for flowing slurry through a vertical counter-gravity pipe at the particular conditions used in this investigation. However, there is only a significant feature, which is overestimation of velocities at the centre of the pipe, and this could well be attributed to the spatial resolution of the ERT and sensitivity gradient across the pipe cross-section.

5.5.2 ERT based slurry flow rate measurement

Due to the complexity of multiphase/two phase flow, particularly solid-liquid flow, it is enormously difficult to accurately measure the flow parameters of each phase individually using only one conventional flow meter. Currently

there is almost no multiphase/two phase flow meter practically available to majority of industrial applications (Munir, 2011; Li *et al.*, 2005; Thorn *et al.*, 1997). The most important parameters that characterise the flow of each constituent phase are, phase volume fraction, phase axial velocity and phase volumetric flow rate. In terms of industrial application the volumetric flow rate of the phases is very important flow parameter to the pipeline operator. The ERT can only provide the measurement relating to the dispersed phase and is unable to measure the continuous phase. Thus, a secondary sensor is required, along with the ERT technique, to determine the flow rate of the continuous phase. This research proposes an ERT based technique, which combines the Electrical Resistance Tomography (ERT) and the Electromagnetic Flow meter (EMF), to measure the volumetric flow rate of each phase and producing the total slurry volumetric flow rate. The schematic briefing of the technique is shown through three fold strategy in Figure 5.36.

Based on the constituent phases used in this study, solid and liquid, the ERT can successfully be used for the measurement of mean solids volume fraction (α_s) and mean solids axial velocity (V_s), as previously discussed. The combination of these two parameters yields mean solids volumetric flow rate (Q_s) across the pipe cross-sectional area (A), as shown Equation 5.6..

$$Q_s = V_s \alpha_s A \tag{5.6}$$

The accurate performance of Electromagnetic Flow meter for measuring two phase flow is highlighted in literature by numerous investigators, such as Wyatt (1986), who argues that the EMF can be used to measure multiphase/two phase flow only if the dispersed phase consists of uniformly distributed small particles, which create a macroscopically uniform isotropic suspension. This implies that the EMF can only be used to measure high transport velocities of the mixture, at which homogeneous flow regime prevails. However, the transport conditions used in this investigation can be seen as the scenario for many industrial applications.

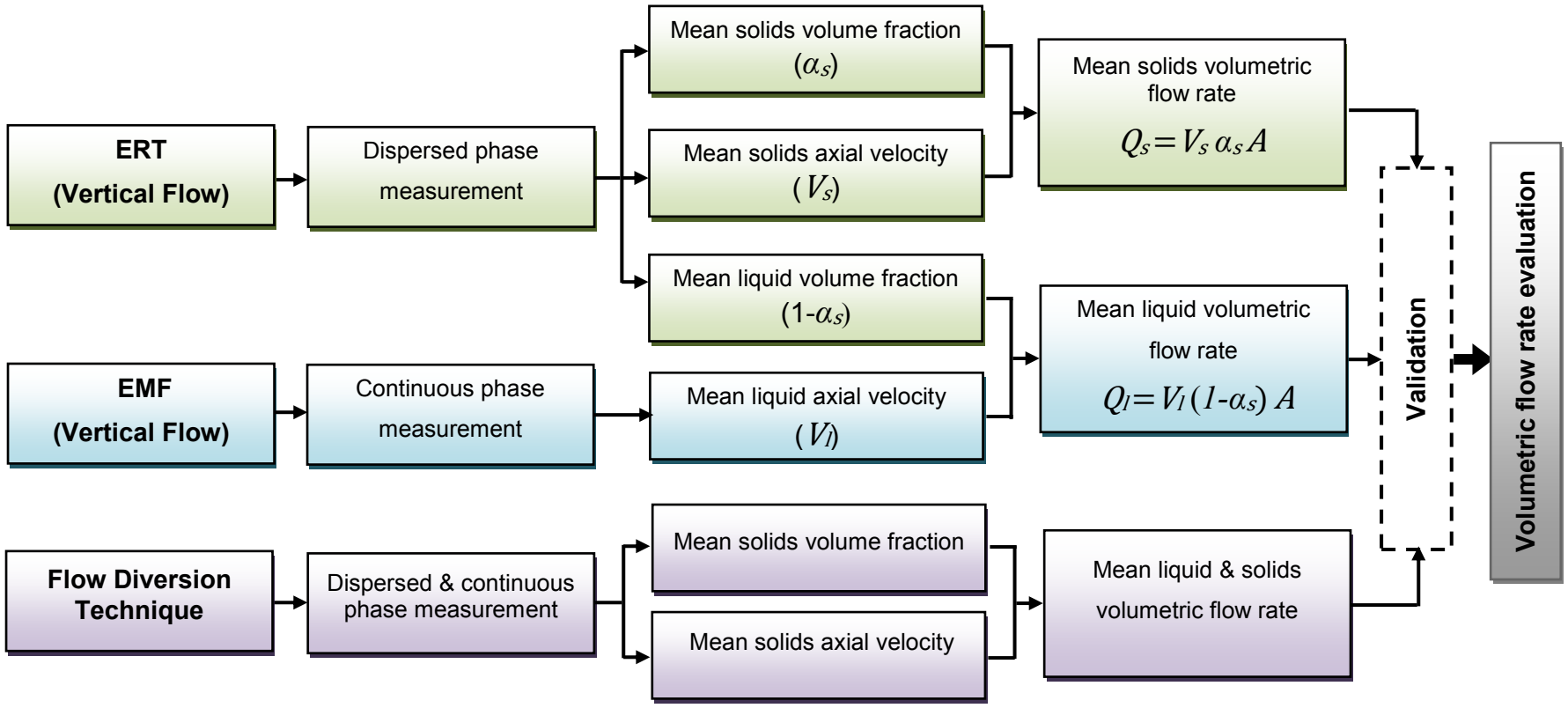

Figure 5.36 Schematic briefing of the methodology used in volumetric flow rate estimation

Currently, it is mostly assumed that the EMF measures the mixture velocity (superficial velocity), without taking the solids void fraction (sand) into consideration. Based on this assumption, the mixture volumetric flow rate is the same as that of the carrier liquid alone, as shown by equation 5.7.

$$Q_{EMF} = V_{EMF} A \tag{5.7}$$

However, it is apparent that the slip velocity, between the two phases is unavoidable, especially at low transport velocities, due to the density difference between the two phases. This suggests that the mixture flow rate cannot have the same value as that of the liquid. Therefore, the total slurry flow rate should be determined through the combination of both flow rates of the existing phases. In other words, for calculation of mixture volumetric flow rate, the solids void fraction within the mixture has to be taken into account. Based on this correction, the mean carrier liquid flow rate (Q_l) across the pipe cross-sectional area (A) can be determined through combination of the EMF velocity (V_l) and the volume fraction of the carrier liquid, obtained from the result of the ERT measurement, as shown in Equation 5.8.

$$Q_l = V_l(1 - \alpha_s)A \tag{5.8}$$

Now, the summation of both volumetric flow rates, the dispersed and continuous phase flow rates, can yield total mixture volumetric flow rate (Q_m), as shown in Equation 5.9. Since the consideration of the EMF measured velocity for the mixture velocity is always argued by many researchers, then the comparison between the mixture velocity taken as a direct EMF measurement with that determined via the combination of the ERT and the EMF, is also discussed.

$$Q_m = Q_s + Q_l \tag{5.9}$$

The solids volume fraction and solids axial velocity obtained from the ERT was combined to estimate the solids volumetric flow rate across the vertical pipe cross-sectional area. While the EMF readings were considered for calculation of the liquid volumetric flow rate. The results were then collected as shown in Table 5.8.

Table 5.8 Solid and liquid volumetric flow rate obtained through combination of the ERT and EMF, along with the mixture velocity and flow rate in vertical flow

Sand & conc.	*EMF velocity* m/s	*ERT mean solids volume fraction* v/v	*ERT mean solids axial velocity* m/s	*ERT solids volume flow rate* m^3/s	*EMF liquid volume flow rate* m^3/s	*Total slurry volume flow rate* m^3/s	*Slurry velocity* m/s
2% medium sand	4.53	0.0310	4.73	0.00028	0.0086	0.0089	4.5316
	3.49	0.0285	3.09	0.00018	0.0067	0.0068	3.4828
	2.52	0.0285	2.76	0.00015	0.0048	0.0050	2.5285
	1.49	0.0282	1.36	0.00007	0.0028	0.0029	1.4882
10% medium sand	4.59	0.1200	5.02	0.00118	0.0079	0.0091	4.6448
	3.49	0.1193	3.57	0.00083	0.0060	0.0069	3.4996
	2.52	0.1191	2.69	0.00062	0.0044	0.0050	2.5392
	1.52	0.1254	1.59	0.00039	0.0026	0.0030	1.5308
2% coarse sand	4.36	0.0304	5.05	0.00030	0.0083	0.0086	4.3800
	3.52	0.0324	3.64	0.00023	0.0067	0.0069	3.5245
	2.52	0.0368	2.51	0.00018	0.0048	0.0050	2.5217
	1.52	0.0333	1.49	0.00009	0.0029	0.0030	1.5154
10% coarse sand	4.76	0.1133	5.54	0.00123	0.0083	0.0095	4.8496
	2.49	0.1260	2.81	0.00069	0.0043	0.0050	2.5312

The qualitative results are also illustrated in Figures 5.37 and 5.38. These figures showing the track of solids volumetric flow rate against the carrier liquid volumetric flow rate for the two sands at 2% and 10% throughput concentration.

By observing the variation of solids volumetric flow rate in Figures, 5.37 and 5.38, it can be seen that each graph consists of a rather concave curve at the top and a convex curve at the bottom. It is apparent that these two curves are more pronounced at lower solids throughput concentration (2%) rather than higher solids throughput concentration (10%). The distorted shape of each line track can be attributed to the change in the transport velocity, which directly affects the solids volume fraction and the solids axial velocity within the pipeline. By looking at the line plot in Figure 5.37, for medium and coarse sand at 2% throughput concentration, it can be seen that solids volumetric flow rate manifests a linear relationship within the higher transport velocities (3.5 m/s and above), which are considered as non-stratified flow velocity range. This linear relationship between the solids flow rate and liquid flow rate is an indication of non-slip velocity between the two phases.

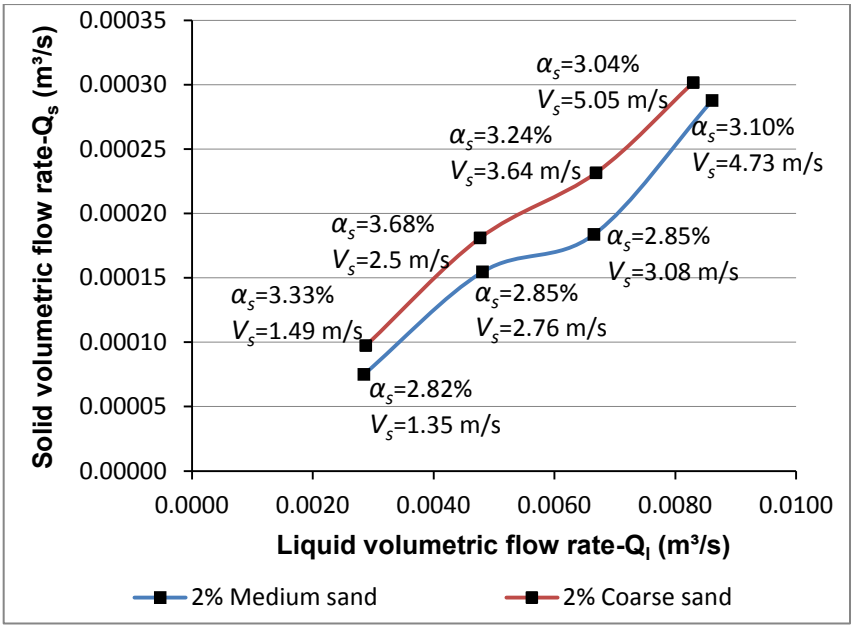

Figure 5.37 The variation of solids volumetric flow rate against the carrier liquid volumetric flow rate for flowing medium and coarse sand at 2% throughput concentration in upward vertical flow. Each volumetric flow rate data point is labelled with the corresponding mean solids volume fraction and mean solids axial velocity

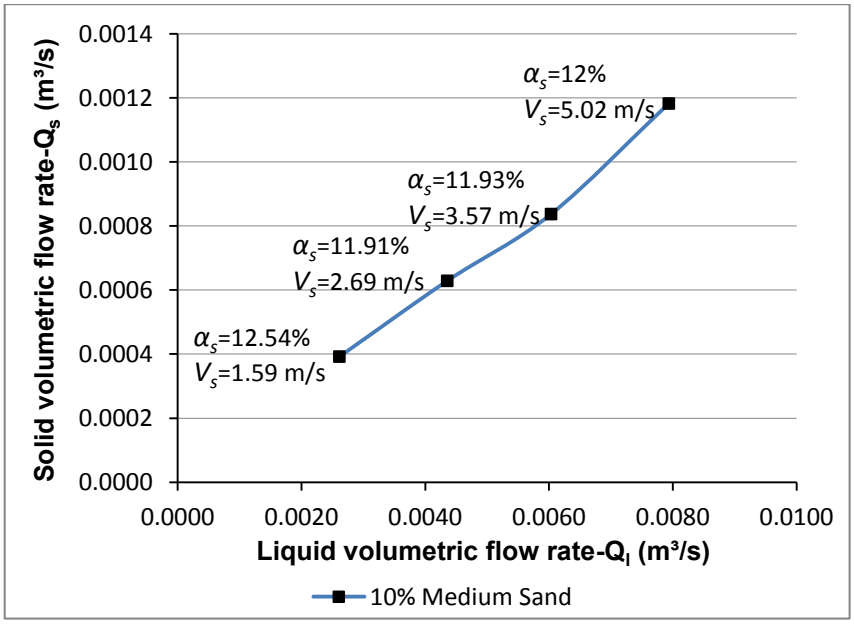

Figure 5.38 The variation of solids volumetric flow rate against the carrier liquid volumetric flow rate for flowing medium sand at 10% throughput concentration in upward vertical flow. Each volumetric flow rate data point is labelled with the corresponding mean solids volume fraction and mean solids axial velocity

In other words, within the range of velocities, at which all the solid particles are suspended in the carrier liquid and they move more or less at the same velocity as that of the carrier liquid, the track of solids volumetric flow rate continuous on a straight line. However, by decreasing the transport velocity the line changes its trajectory to produce a concave curve, then it bends down to form a convex curve. This is due to the density difference between the two phases. As the transport velocity decreases the solid particles slow down, which leads to the reduction of their flow rate. After the convex curve, further reduction of transport velocity leads to further reduction of solids axial velocity and deposition of solid particles within the horizontal pipeline. As a result the solids volumetric flow rate decreases in the vertical pipeline, which is clearly highlighted in Figures 5.37 and 5.38. Continuous reduction of transport velocity, towards pipe blockage condition, results in zero solids flow rate and obviously the carrier liquid flow rate too, as the flow of each phase comes to halt within the pipelines.

Another phenomenon can be noticed on each flow rate plot, on which the track changes rather sharply its trajectory to form the concave curve and the convex curve. The region between these two curves can be considered as a transitional region between the stratified flow and non-stratified flow. This argument is well based on the results of flow regime characterisation discussed previously in this chapter. Based on visual observation and photographic evidence, it was found that the stratified flow starts at around 3.5 m/s transport velocity. This region can be remarked between the two points, starting at the first point where the track goes through a rather sharp change to form the concave curve, and the second point where the curve goes through another change in its trajectory to form the convex curve. As previously mentioned this region is less pronounced for the flowing of sand at 10% throughput concentration. Despite that the diversion point from the linear track can be noticed.

Based on the above results and observations, it is apparent that the ERT can detect the variations of solids volumetric flow rate within the range of conditions used in this investigation. Also, based on the results obtained from the combination of the ERT and the EMF, to measure the solids flow rate and liquid flow rate respectively, the slip velocity between the two phases, can successfully be estimated. The evaluation of the technique, through highlighting the rate of associated error in each condition used in this study, is also discussed later in this section.

5.5.3 Validation of the vertical flow ERT results

The in-situ concentration, obtained from the ERT for vertical upward flow, was compared to that of flow diversion technique (discharge) similar to the comparison procedure described in horizontal flow measurement. With regard to the solids velocity, the quantitative (mean solids velocity) and qualitative (solids axial velocity profile) results were obtained from the AIMFLOW (statistical software package), as described in the previous section. The pre-calibrated EMF was used to monitor the mean slurry velocity within the range of 1.5-4.5 m/s. The solids axial velocity (in-situ) and solids volumetric flow rate were also validated against the discharge velocities calculated using the flow diversion technique. The validation of the ERT volumetric flow rate includes validation of total mixture volumetric flow rate, obtained from the combination of the ERT and EMF measurements of the carrier liquid and the dispersed phase volumetric flow rate. Since the vertical test section is followed by a short horizontal line, through which the slurry is returning into the mixing tank (or diverted to the measuring tank), and no solids hold up is occurred after the vertical test section, therefore it is predicted that the solids concentration in the vertical test section have similar value as that of discharge value. The solids axial velocity is also predicted to approach that of discharge, despite the existence of some resisting force (bends, pipe wall friction etc.). However, since the slurry is passing through only one 90° long radius bend and a rather short returning horizontal line, then these resisting forces on the slurry are neglected. The data obtained for each test was recorded and collected. These data then processed and compared against each other, as shown in Tables 5.9, 5.10 and 5.11. The error analysis is also described in the following section along with highlighting the rate and the potential reason for the occurrence of the error in each condition.

5.5.3.1 Validation of mean solids volume fraction

Tables 5.9 and 5.10 highlight the comparison results of both solids volumetric concentrations; the ERT and the discharge. Error analysis of solids volumetric concentration was carried out for each condition and the results are highlighted quantitatively, in the aforementioned tables, in terms of maximum, minimum and the average deviation. The comparison results are also illustrated qualitatively in Figure 5.39 in terms of line fit plots and residual plots.

It is apparent from the qualitative data and quantitative error analysis that the ERT provides reasonable estimates of solids volumetric concentration in

vertical counter-gravity slurry flow. However, the results of error analysis of the ERT concentration revealed that, for these particular conditions, the minimum deviation of 0.61% between the discharge and the ERT concentration was observed at 10% coarse sand throughput concentration, whereas the maximum deviation of 40.91% was noticed at 2% medium sand throughput concentration and at a transport velocity of 4.5 m/s. In addition, the average error, for all considered conditions, was found to be within 26%. From the qualitative results of error analysis it was remarked that, overall, the ERT tends to overestimate the local volumetric solids concentration, as shown in Figure 5.39

Table 5.9 Comparison of concentrations and occurring relative error for medium and coarse sand at 2% throughput concentration in vertical flow

	Medium Sand			**Coarse Sand**		
Velocity (m/s)	**ERT Conc. %(v/v)**	**Discharge Conc. %(v/v)**	**Relative Error (%)**	**ERT Conc. %(v/v)**	**Discharge Conc. %(v/v)**	**Relative Error (%)**
4.5	**3.1**	**2.20**	-40.91	**3.04**	**3.2**	5.00
3.5	**2.85**	**2.70**	-5.56	**3.24**	**3.1**	-4.52
2.5	**2.85**	**2.50**	-14.00	**3.68**	**3.4**	-8.24
1.5	**2.82**	**2.40**	-17.50	**3.33**	**2.8**	-18.93
Maximum Error = -40.91% Minimum Error = -5.56% Average Error = -19.49%				**Maximum Error = -18.93% Minimum Error = -4.52% Average Error = -9.17%**		

Table 5.10 Showing the comparison of concentrations and occurring relative error for medium and coarse sand at 10% throughput concentration in vertical flow

	Medium Sand			**Coarse Sand**		
Velocity (m/s)	**ERT Conc. %(v/v)**	**Discharge Conc. %(v/v)**	**Relative Error (%)**	**ERT Conc. %(v/v)**	**Discharge Conc. %(v/v)**	**Relative Error (%)**
4.5	**12**	**9.26**	-29.59	**11.33**	**11.4**	0.61
3.5	**11.93**	**9.62**	-24.01	**-**	**12.7**	-
2.5	**11.91**	**9.55**	-24.71	**12.6**	**12.7**	0.79
1.5	**12.54**	**9.68**	-29.55	**-**	**12.8**	-
Maximum Error = -29.59% Minimum Error = -24.01% Average Error = -26.96%				**Maximum Error = -0.79% Minimum Error = -0.61% Average Error = -0.7%**		

This overestimation can clearly be seen on the line fit plot of the ERT concentration vs. discharge concentration. The deviation of each data point is more clearly highlighted for each transport velocity in the plot of ERT deviation magnitude vs. discharge concentration. The reason for this overestimation may have to do with mechanical installation of 32 electrodes on the two electrode rings. In other words, one or more electrodes may not have been well tightened and as a result the electrical connection is affected, which affects the conductivity of the domain under investigation.

However, a future investigation is paramount to unveil the exact reason behind this overestimation. Nevertheless, it can be seen that for the flowing coarse sand, especially for 10% throughput concentration, an underestimation can be observed. The cause could be due to the gradient in sensitivity distribution across the radial plane on the sensitivity map (pipe cross-section), as the higher sensitivity can be found near the pipe wall rather than the centre of the pipe. This argument could well be supported by the shape of concentration profile, where a particle-rich core of solids can clearly be observed at the axis of the pipe surrounded by a particle-lean annulus. In other words, non-uniform concentration profile, which exhibits a maximum solids concentration at the centre line of the pipe, and minimum solids concentration near the pipe-wall, can be noticed, as shown in Figure 5.35.

As the concentration increases the bell-shape (or or core flow) profile can clearly be manifested in the centre of the pipe. Hence, in flowing coarse sand slurry through vertical counter-gravity radial particle migration occurs. Since most of the particles are segregated at the centre of the pipe, and the centre of the pipe presents the lowest sensitivity relative to the regions near the pipe wall, then it is reasonable to expect an underestimation of solids concentration profile at the centre of the pipe, which in return gives an overall underestimation of mean solids concentration across the pipe cross-section.

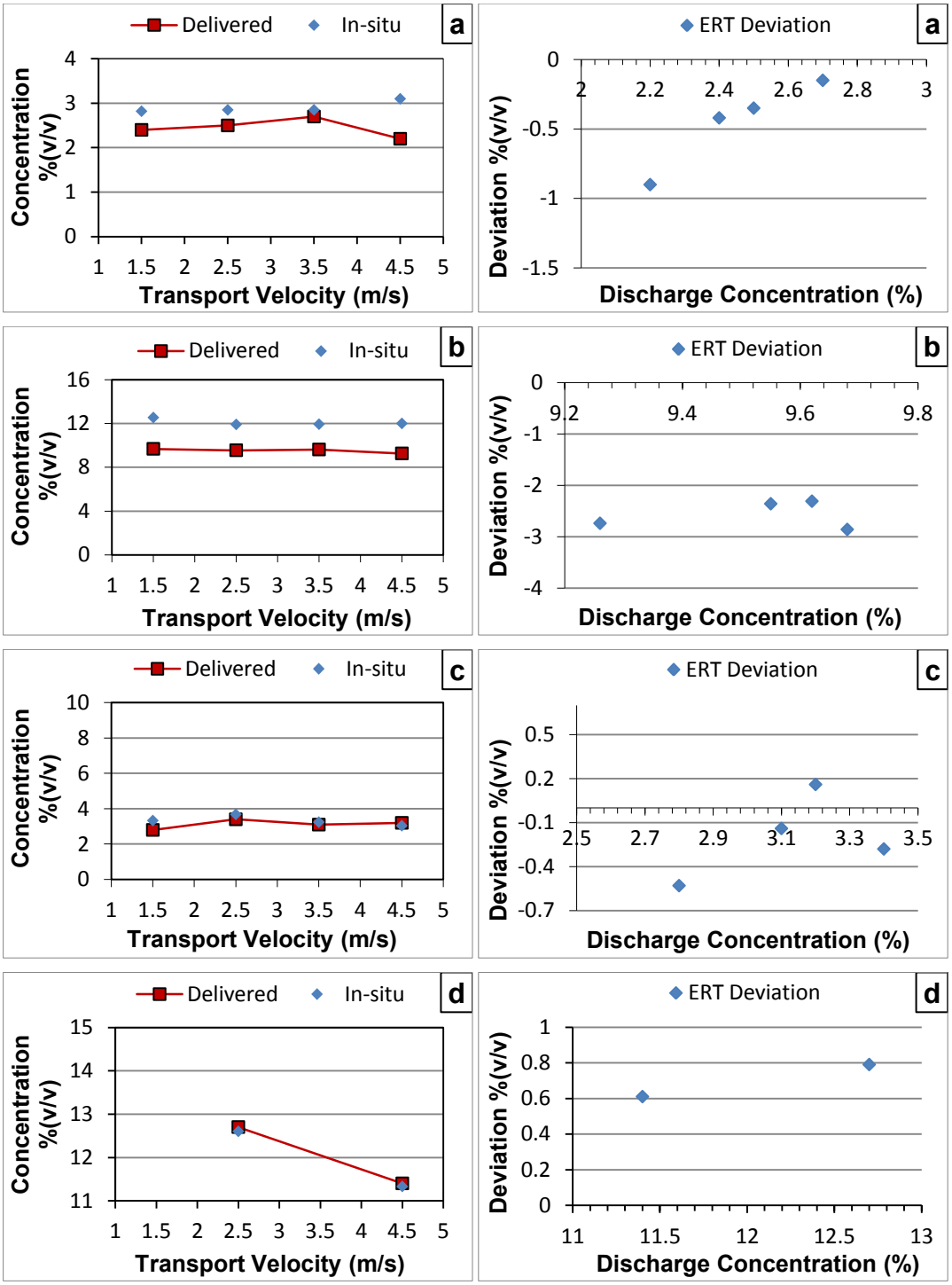

Figure 5.39 Comparison between in-situ (ERT) concentration and delivered solids concentration, through the line fit plot (left-hand side) and the residual plot (right-hand side), in vertical upward flow for (a) medium sand at 2% throughput concentration, (b) medium sand at 10% throughput concentration, (c) coarse sand at 2% throughput concentration, (d) coarse sand at 10% throughput concentration

5.5.3.2 Validation of mean solids axial velocity

The measured values of solids axial velocities using both techniques, the ERT and the discharge, are tabulated in Table 5.11. Error analysis was carried out for each condition and the results are highlighted quantitatively in terms of maximum, minimum and the average deviation for both, coarse and medium sand, at different throughput concentration and velocity range 1.5-4.5 m/s. The minimum deviation of 0.39% between the discharge and the ERT velocities was observed at 2% coarse sand throughput concentration, whereas the maximum deviation of 12.30% was noticed at 10% medium sand throughput concentration and at a transport velocity of 4.5 m/s.

Table 5.11 Showing the data obtained from the ERT measurement and discharge calculation along with the rate of deviation at each given velocity for vertical flow

Transport Velocity (m/s)	ERT Velocity (m/s)	Discharge Velocity (m/s)	Absolute Error (%)	Relative Error (%)	Remarks
Medium Sand 2%					
4.5	**4.73**	**4.51**	0.22	-4.80	Min. Deviation% = 4.80 Max. Deviation% = 12.01 Average Error% = 9.25
3.5	**3.09**	**3.49**	0.41	11.65	
2.5	**2.76**	**2.55**	0.22	-8.54	
1.5	**1.36**	**1.54**	0.19	12.01	
Medium Sand 10%					
4.5	**5.02**	**4.47**	0.55	-12.30	Min. Deviation% = 3.11 Max. Deviation% = 12.30 Average Error% = 5.66
3.5	**3.57**	**3.47**	0.11	-3.11	
2.5	**2.69**	**2.54**	0.15	-6.09	
1.5	**1.59**	**1.58**	0.02	-1.15	
Coarse Sand 2%					
4.5	**5.05**	**4.53**	0.52	-11.55	Min. Deviation% = 0.39 Max. Deviation% = 11.55 Average Error% = 3.72
3.5	**3.64**	**3.66**	0.02	0.62	
2.5	**2.51**	**2.45**	0.06	-2.32	
1.5	**1.49**	**1.50**	0.01	0.39	
Coarse Sand 10%					
4.5	**5.24**	**5.24**	0.30	-5.69	Min. Deviation% = 5.69 Max. Deviation% = 8.82 Average Error% = 7.26
2.5	**2.58**	**2.58**	0.23	-8.82	

By comparing the two velocity values, mean solids velocity obtained from the ERT and discharge velocity obtained from the measuring tank, it can be concluded that, for the particular flow conditions used in this study, the ERT provides a reasonable estimation of the solids axial velocity in vertical counter-gravity flow, despite some acceptable deviation from the EMF and

discharge velocity values. These deviations are due to similar reasons described in evaluation of solids concentration in previous section.

5.5.3.3 Validation of mean solids flow rate

Table 5.12 showing the volumetric flow rate of dispersed phase (sand) and continuous phase (water) measured using two techniques, the ERT based technique (in conjunction with the EMF) and the flow diversion technique (or discharge). The slurry velocity (superficial velocity) and total slurry flow rate were also determined via each of the above techniques. The error analysis was carried out and highlighted in terms of relative and average error for each condition used in the experiments.

The calculation of error analysis revealed that the ERT estimation of solids volumetric flow rate is associated with a maximum error of 34.19%, which occurred for flowing medium sand at 2% through put concentration. On the other hand a minimum error of 6.33% was estimated for flowing coarse sand at 10% throughput concentration.

The results of error analysis, in the prediction of solids volumetric flow rate, measured by both techniques, are also illustrated qualitatively through line fit plots, shown in Figures 5.40 and 5.41. By observing the line fit plots shown in the aforementioned Figures, it is apparent that, based on the discharge measurement, the ERT overestimates the solids volumetric flow rate in all conditions used in this study. It can also be noticed that the rate of overestimation increases with increase of transport velocity. Since the solids volumetric flow rate is determined as a product of mean solids volume fraction and mean solids axial velocity, which are both predicted by the ERT, then the occurred error could well be attributed to one of them. In other words, the overestimation of the solids volumetric flow rate is due to occurring some error either in the estimation of the solids volume fraction or solids axial velocity. However, the error analysis of solids volume fraction and solids axial velocity, in the previous sections, revealed that the ERT in general tends to overestimates these two parameters. The reasons for this overestimation is associated to the gradient in sensitivity distribution across the radial plane on the sensitivity map (pipe cross-section) or could possibly be due to mechanical configuration of the electrodes on the dual plane sensor. The higher overestimation of both parameters, solids volume fraction and solids axial velocity, was also found within the range of higher transport velocities (3.5 m/s and above), which is also reflected in the prediction of solids volumetric flow rate.

Table 5.12 Comparison of the volume flow rates obtained from the ERT and EMF with discharge corresponding values along with the rate of deviation at each condition in vertical flow

	ERT & EMF values				Discharge values				Error Analysis	
	Solids volume flow rate (m^3/s)	Liquid volume flow rate (m^3/s)	Slurry volume flow rate (m^3/s)	Slurry velocity (m/s)	Solids volume flow rate (m^3/s)	Liquid volume flow rate (m^3/s)	Slurry volume flow rate (m^3/s)	Slurry velocity (m/s)	Relative Error (%)	Average Error (%)
2% medium sand	0.00028	0.0086	0.0089	4.53	0.00019	0.0086	0.0088	4.48	45.51	20.35
	0.00018	0.0067	0.0068	3.48	0.00017	0.0067	0.0068	3.48	6.43	
	0.00015	0.0048	0.0050	2.52	0.00012	0.0049	0.0050	2.54	23.01	
	0.00007	0.0028	0.0029	1.48	0.00007	0.0029	0.0030	1.53	6.48	
10% medium sand	0.00118	0.0079	0.0091	4.64	0.00081	0.0080	0.0087	4.46	45.46	34.19
	0.00083	0.0060	0.0069	3.49	0.00065	0.0062	0.0068	3.46	27.93	
	0.00062	0.0044	0.0050	2.53	0.00047	0.0045	0.0049	2.53	32.32	
	0.00039	0.0026	0.0030	1.53	0.00030	0.0028	0.0030	1.57	31.04	
2% coarse sand	0.00030	0.0083	0.0086	4.38	0.00028	0.0086	0.0088	4.53	4.37	8.22
	0.00023	0.0067	0.0069	3.52	0.00022	0.0070	0.0071	3.66	2.09	
	0.00018	0.0048	0.0050	2.52	0.00016	0.0046	0.0048	2.44	9.37	
	0.00009	0.0029	0.0030	1.51	0.00008	0.0029	0.0029	1.49	17.04	
10% coarse sand	0.00123	0.0083	0.0095	4.84	0.00117	0.0091	0.0102	5.24	4.90	6.33
	0.00069	0.0043	0.0050	2.53	0.00064	0.0044	0.0050	2.57	7.76	

Despite this overestimation, the quantitative and qualitative results of solids volumetric flow rate measurement suggest that the ERT overall can predict a reasonably accurate solids volumetric flow rate in vertical counter-gravity slurry flow for the conditions used in this investigation.

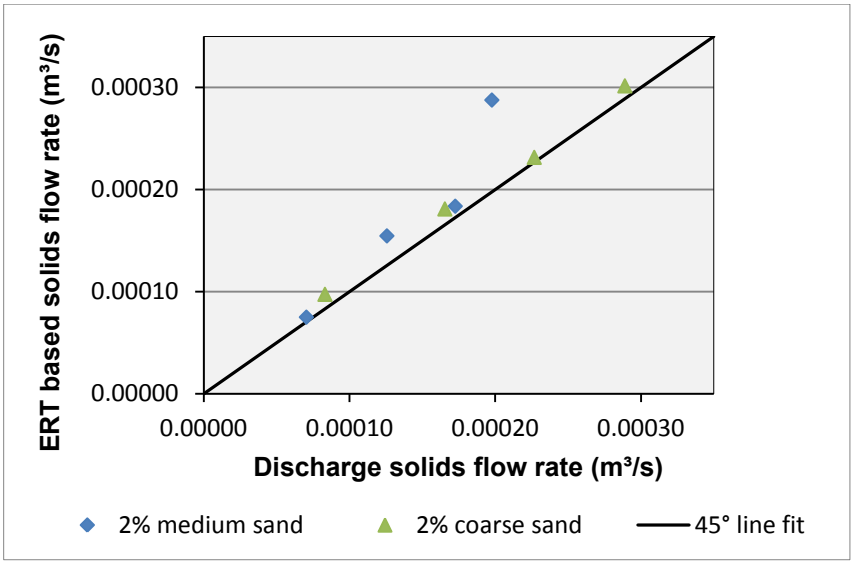

Figure 5.40 Comparison of solids volumetric flow rate predicted by the ERT in vertical pipeline with that of flow diversion for medium and coarse sand at 2% throughput concentration

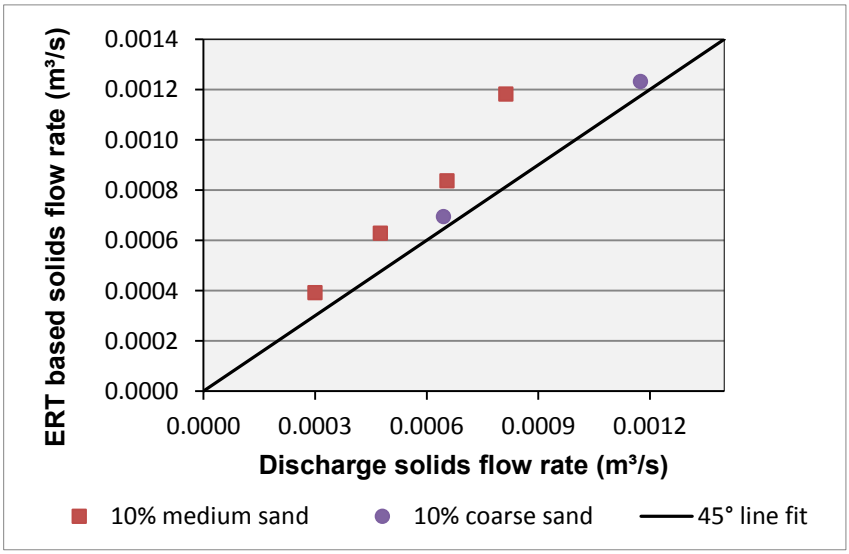

Figure 5.41 Comparison of solids volumetric flow rate predicted by the ERT in vertical pipeline with that of flow diversion for medium and coarse sand at 10% throughput concentration

The mixture flow rate was also determined, based on the flow rates of both phases predicted by the ERT in conjunction with the EMF, in which the solids void fraction was taken into account. The measured mixture flow rate then compared to that of discharge, as shown in Figure 5.42. It can be seen that error is quite random for the given conditions. However, a reasonable agreement can be noticed between the slurry flow rate measured by the ERT in conjunction with the EMF and the discharge.

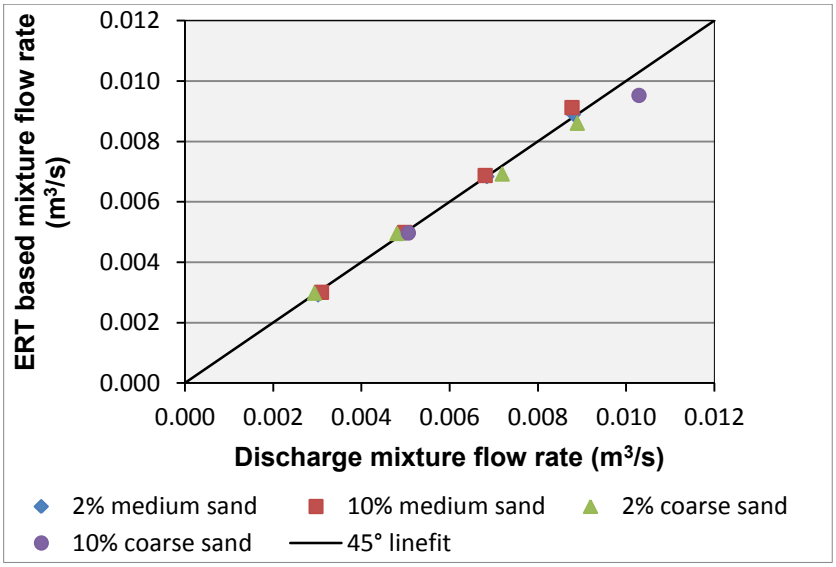

Figure 5.42 Comparison of slurry flow rate measured by the combination of the ERT and EMF in vertical pipeline with that of flow diversion

In order to further evaluate the ERT based volumetric flow rate measurement technique, in which the ERT is used in conjunction with the EMF, further comparisons were carried out, as shown in Figures 5.43, 5.44, 5.45 and 5.56. In these comparisons, the solid and liquid volumetric flow rate obtained from the ERT and EMF were compared to that measured by flow diversion technique. It is quite apparent that, in the aforementioned figures, the ERT can generate a reasonable qualitative track representation of solids volume flow rate for the range of the transport velocities used in this research. However, the overestimation again is quite pronounced for both sands and all conditions, especially at higher velocities above stratified velocity range (3.5 m/s).

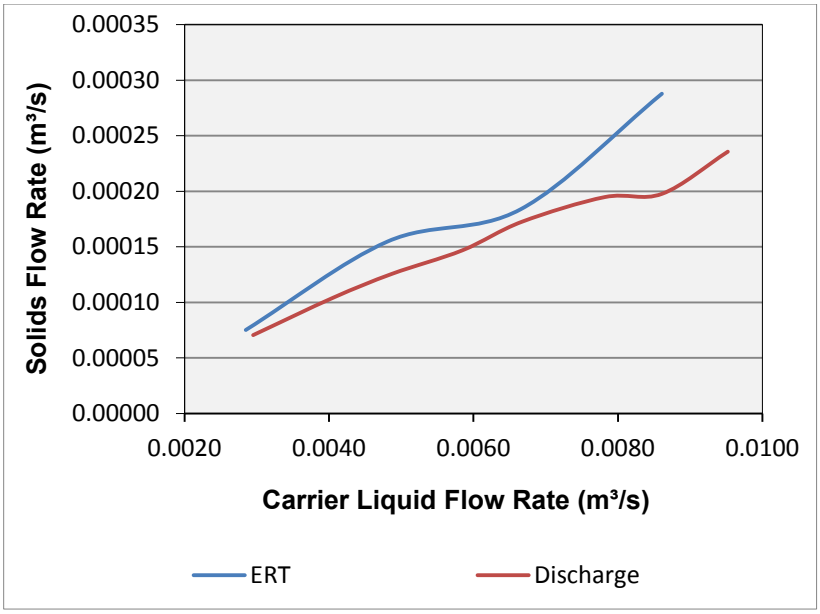

Figure 5.43 Comparison of the ERT solids flow rate in vertical pipeline with that of flow diversion for medium sand at 2% throughput concentration

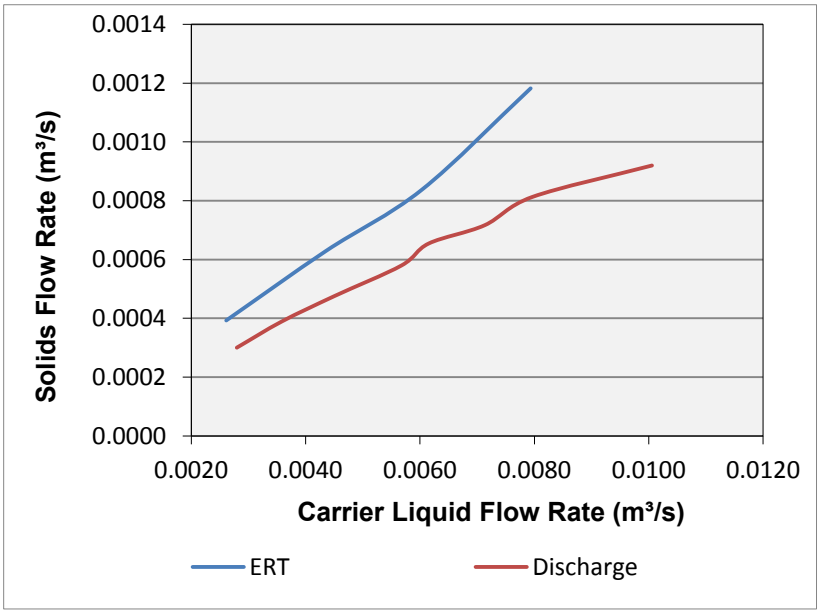

Figure 5.44 Showing the comparison of the ERT solids flow rate in vertical pipeline with that of flow diversion for medium sand at 10% throughput concentration

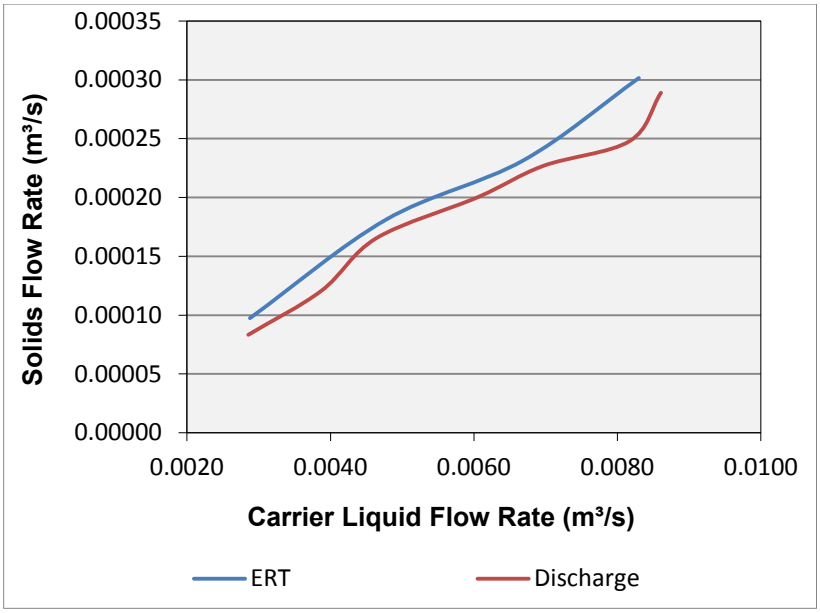

Figure 5.45 Showing the comparison of the ERT solids flow rate in vertical pipeline with that of flow diversion for coarse sand at 2% throughput concentration

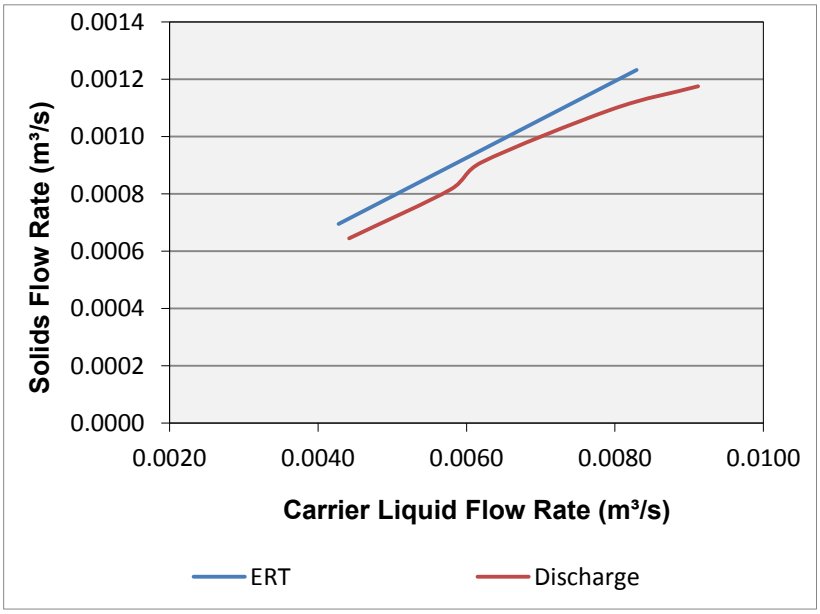

Figure 5.46 Showing the comparison of the ERT solids flow rate in vertical pipeline with that of flow diversion for coarse sand at 10% throughput concentration

5.6 Conclusions

A high performance dual-plane Electrical Resistance Tomography system (ERT) has been employed to interrogate the internal structure of horizontal and vertical counter-gravity slurry flow. The exceptional capability of this system enabled acquiring high frame rates (1000 dfps) in a non-intrusive fashion. The tomograms reconstructed for each test were collected and analysed to determine the mean local solids concentration and solids volumetric concentration profile across the vertical plane of the pipe cross-section. While the dual-plane ERT system was combined with the cross-correlation technique to obtain mean local solids axial velocity and solids axial velocity profile. The profiles, solids concentration and solids axial velocity, obtained from the ERT, was compared qualitatively with the actual photographs of the flow, which were captured during the ERT measurements. It was found that there is a good agreement between the two methods. Therefore, it can be concluded that the dual-plane ERT system could well be used for on-line monitoring slurry flow through pipelines. The estimated mean local solids volumetric concentration and mean solids axial velocity values measured by the ERT were also compared to the corresponding values measured using the diversion flow technique. Some deviations were noticed in the mean local concentration obtained from the ERT and have found to be quite random. However, the error analysis of the ERT results demonstrated that, overall, the ERT tends to overestimate the local volumetric solids concentration. The reason for this error was associated to the presence of bubbles in the pipeline. In vertical upward flow, the effect of radial particle migration has been picked up by the ERT system. Based on the solids volumetric concentration distribution across the vertical plane of the vertical pipe cross-section, it was found that the coarse sand flows in core peak flow, whereas the flow of medium sand demonstrated wall peak flow. On the other hand, it was found that the combination of the ERT and cross-correlation provides a reasonable estimation of mean solids axial velocity in both flow orientations. However, the velocities measured in horizontal flow were found to be underestimated by the ERT at low transport velocities (below 3 m/s). Therefore, a future investigation is required to unfold the reasons behind this error. Moreover, a novel ERT based technique has been proposed for measurement of total slurry volumetric flow rate in vertical upward flow. This technique combines the high performance ERT and the EMF to measure the volumetric flow rate of each phase individually, dispersed and continuous respectively, and

producing the total volumetric slurry flow rate. Based on the results obtained using this technique the slip velocity between the two phases can also be successfully determined. The evaluation of the proposed technique for volumetric flow rate measurement, through highlighting the rate of associated error in each condition used in this study, suggests that a reasonable qualitative track representation of volumetric flow rate of each phase, along with the total slurry volume flow rate, can be generated.

Finally, this study revealed that the high performance dual-plane ERT system can be used for monitoring slurry flow and estimation of volumetric solids concentration and solids axial velocity in horizontal and volumetric flow rate in vertical counter-gravity flow. However, particular attention should be paid to quantitative results obtained at high transport velocities.

Chapter 6
Design and construction of inclinable multiphase flow loop

This chapter describes the design of an inclinable multiphase flow loop with specific emphasis on slurry flow system. It attempts to provide a detailed coverage of the design analysis and acceptance criteria for every component of the system. The materials, fabrication, assembly, erection and testing are also described.

6.1 Introduction

In order to investigate the effect of different variables on multiphase flow characteristics and measurement scheme, a versatile, durable and accurate pilot scale flow loop is required. Therefore, it was decided to design and construct a pilot scale multiphase flow loop in the Engineering Building/G.56 in the university of Leeds. The aim was to build a durable and reliable flow loop, which would include all orientations, horizontal, vertical and inclined. It was also required to design the flow loop in such a way that could be used not only for slurry flow, but also for multiphase flow, which includes solid/liquid, gas/liquid, solid/gas/liquid, oil/liquid, oil/gas/liquid and oil/solid/gas/liquid. It is worth mentioning that due to space limitations and health and safety, the oil flow facility, such as storage vessel etc., has not been included into the design. However, it is proposed that an oil simulant, such as plastic beads with uniform shape and the same density of oil, could be used. It is also important to mention that as the loop will mainly be used for slurry flow and this type of flow is the most complex amongst the others, then most of design considerations and attention have been given to slurry flow rather than others.

The management of the design and construction, such as time and cost, was also considered to be one of the most important aspect of the project. A thorough examination was carried out for the selection and design of each piece of equipment, based on cost, objectives of the research and flexibility, along with producing a detailed working plan from conceptual design to the construction and testing. The working plan was developed in such a way in order for each task to be carried out efficiently and effectively.

This chapter details the methodology adopted to design and construct the multiphase flow loop, along with the equipment and instrumentations used to

achieve the design requirements. The final design of the constructed flow loop and each equipment is highlighted through schematic drawings and real photographs. A detailed operating procedure, start up and shut down, of the loop is also included in this chapter. The results of mechanical and hydrodynamic testing are also described.

6.2 Design requirements

In order to investigate the effect of different flow parameters on multiphase flow characteristics and flow measurement scheme, the flow loop must meet the following requirements:

1. The flow loop must be usable within the range of inclination angles 0° to 90° from horizontal.
2. A safe and remotely controllable lifting method must be used.
3. The instrumentation and working area must be well and carefully specified.
4. The piping material must be selected to suit the flow of solid particles and abrasives.
5. It must accommodate up to 40% by weight of the dispersed phase.
6. Must allow the mean flow velocity up to 5.5 m/s.
7. It must include the upward and downward flow.
8. The test sections must be within the developed flow region.
9. It must be functional for stratified and non-stratified flow.
10. Must meet health and safety requirements.
11. Must be robust, accurate and durable.
12. Flexibility in removing and mounting any instrumentation or section.
13. Must allow for visual observation of flow within the pipeline.
14. Can easily be operated by one operator.
15. Cost must be well balanced against accuracy, durability and robustness.
16. Include a bulk flow measurement and validation system.
17. Space and access (work area, walk way storage area, maintenance of equipment etc.) must be carefully considered.
18. Initial and later testing costs must be kept as low as possible, of course after achieving a well balance between cost and quality.

6.3 Design and construction project management

In order to achieve the final goal efficiently and effectively, a very well management of the entire project is paramount. Undoubtedly, a detailed

work plan is necessary to provide a framework for planning and controlling the project. Also the large number of tasks, which had to be carried out by different individuals and parties over a short period of time to reach the final stage, was the driving force for the outputs to be achieved. Therefore, a detailed work plan was introduced, amongst which the budget and schedule of work were clearly outlined.

In order to have a clear knowledge of the total cost of the flow loop, the list of material that had to be ordered was prepared, as shown in Table 6.1. Since the cost was the driving force, then a comparison of price and quality of each item, mentioned in the aforementioned table, was carried out between three suppliers. After achieving a good balance between the price and quality, the suitable supplier was chosen. Then of course every item had to be justified, therefore, a meeting had to be arranged with the budget holder to produce the documentations and justify the release of funds.

On the other hand, the schedule of the work plan, which was the most important element of standard management tool, was found to be rather more complicated. As previously mentioned, the number of tasks in the To Do list and the involvement of different individuals made it rather difficult to produce a rigid schedule of work. Therefore, the schedule produced for the completion of the flow loop had to be updated from time to time, a version of which is illustrated in Table 6.2. The scheduling strategy used for the completion of the loop, was that the entire work was split into goals, each of which had objectives for the goal to be achieved. It is apparent that the completion of all the target goals would mean the completion of the loop. In other words, a goal can never be achieved without achieving all the related specific objectives. The scheduling was designed in such a way that for each of stated objectives the completion date was listed in order with allotment of a reasonable length of time, while some tasks were in progress in a parallel fashion.

Table 6.1 List of items ordered for the flow loop

Item	Image	mm/each of Item	Net unit cost £	Net item total £	Supplier	Product no./Code	Product name	Comments
2" Clear Upvc Pipe (Transparent)		5 m	103.70/5m	103.7	http://www.pipestock.com/clear-pvcu-pipe/	PVCU.CLR5.0630	PVCu Clear Pipe 16 BAR 5m Length 63mm	This is metric it can go with metric fittings, but not with imperial fittings (eg, 2" flange)
2" Upvc Pipe (Opaque/black)		12 m	23.33/6m	46.66	http://www.pipestock.com/pvcu/pipe/class-e-inch/	PVCU.CLE.0630	PVCu Pipe Class E 15 Bar 6m 2"	
4" Upvc Pipe		6 m	80.48/6m	80.48	http://www.pipestock.com/pvcu/pipe/class-e-inch/	PVCU.CLE.1100	PVCu Pipe Class E 15 Bar 6m 4"	
Flexible Pipe		10 m	23.95/m[1]	287.4	Whitehouse Flexible Tubing Ltd. (quote will be attached)	See the quote	10 Mtrs X 63MM DIA, ARMOURVIN TYPE FLEXIBLE TUBING	
Flexible Pipe Clamps (Heavy Duty)		8 piece	2.53/piece[1]	50.528	Whitehouse Flexible Tubing Ltd. (quote will be attached)	See the quote	8 X SUPER HEAVY DUTY CLAMPS	
Flanges		30 piece	6.68/piece	200.4	http://www.pipestock.com/pvcu/flanges-flange-sets/flanges/full-face-pn1016-inch/	PVCU.FNA.0630	PVCu Full Face Flange Drilled BS EN1029-1 PN16 Plain 2"	
EPDM Flat Gasket		15 piece	5.81	87.15	http://www.pipestock.com/pvcu/flanges-flange-sets/epdm-gaskets/full-face-bs-en1029-1/	GFI.0630	EPDM Gasket For Full Face Flange BS4504 NP10/16 2" 63mm	
Nuts & bolts (M16 x 80)[2]		30 set	3.03/set	90.9	http://www.pipestock.com/pvcu/flanges-flange-sets/nuts-bolts/	BBZP.M16.0750	Bolt Set BZP 4 Pack M16 X 75mm	
Sockets (Plain)		6	1.73/piece	10.38	http://www.pipestock.com/pvcu/pipe-fittings/plain-inch/socket/	PVCU.MAA.0630	PVCu Socket Plain 2"	
Reducing Bushes (Plain: OD63X32ID mm)		2	1.21/ piece	2.42	http://www.pipestock.com/pvcu/pipe-fittings/plain-inch/reducing-bush/	PVCU.RCA.063D	PVCu Reducing Bush Plain 2" x 1"	
Reducing Bushes (Plain: OD32X25ID mm)		2	0.58/ piece	1.16	http://www.pipestock.com/pvcu/pipe-fittings/plain-inch/reducing-bush/	PVCU.RCA.032C	PVCu Reducing Bush Plain 1" x 3/4"	
Reducing Bushes (Threaded: OD25X20ID mm)		2	0.47/ piece	0.94	http://www.pipestock.com/pvcu/pipe-fittings/plain-inch/reducing-bush/	PVCU.RCA.025B	PVCu Reducing Bush Plain 3/4" x 1/2"	
Union		1	7.94/ piece	7.94	http://www.pipestock.com/pvcu/pipe-fittings/plain-inch/union/	PVCU.BOA.0630	PVCu Union Plain 2"	
Tee 90°		13	4.25/ piece	55.25	http://www.pipestock.com/pvcu/pipe-fittings/plain-inch/tee-90/	PVCU.TIA.0630	PVCu Tee 90 Plain 2"	
Tee 45°		2	10.65/ piece	21.3	http://www.pipestock.com/pvcu/pipe-fittings/plain-inch/tee-45/	PVCU.TYA.0636	PVCu Tee 45 Plain 2"	
Elbow 45°		1	3.73/ piece	3.73	http://www.pipestock.com/pvcu/pipe-fittings/plain-inch/elbow-45/	PVCU.GYA.0630	PVCu Elbow 45 Plain 2"	
Elbow 90°		1	3.32/ piece	3.32	http://www.pipestock.com/pvcu/pipe-fittings/plain-inch/elbow-90/	PVCU.GOA.0630	PVCu Elbow 90 Plain 2"	
Short Radius Bend 90°		8	9.53/ piece	76.24	http://www.pipestock.com/pvcu/pipe-fittings/plain-inch/short-radius-bend-90/	PVCU.CUA.0630	PVCu Bend 90 Plain 2"	
Solvent Cement[3]		2	14.12/ tin	28.24	http://www.pipestock.com/pvcu/accessories/pvcu-solvent-cement/	PVCU.RCO	Solvent Cement for PVC 500ml Tin	
Brushes		2	3.18/ piece	6.36	http://www.pipestock.com/pvcu/accessories/pvcu-solvent-cement/	FAIPBSY34	Brush 3/4"	
TFPE Tape		2	5.43/ pack	10.86	http://www.pipestock.com/pvcu/accessories/ptfe-tape/	PTFE.B	PTFE Tape 12m Roll Pack of 10	
Latex Gloves (L)		1 (pack of 100)	13.48/ pack	13.48	http://www.pipestock.com/pvcu/accessories/latex-gloves/	SCAGLOLATEXL	Latex Gloves Ambidextrous 100PK	
Digital Caliper		1	11.98 (inc VAT)	11.98	http://www.toolbox.co.uk/silverline-380244-digital-16488-85361	TBSL2911	Silverline 380244 Digital Vernier Professional Caliper	
Pipe Clamps[4]		30	1.75/ pack	52.5	http://www.thesitebox.com/britclips-girder-clips/pipe-clamps/sound-insulated-standard-r-pipe-clips.aspx	P/N: 1257060	59 - 62mm Sound Insulated Standard Pipe Clip M8 & M10 (1 item per pack)	This can be adapted to M8 and M10 threaded rod bar.
Threaded rod for pipe clamp (M8 x 100 mm)		10	2.25/ pack[5]	22.5	http://www.thesitebox.com/nuts-and-bolts/metric-studding/metric-high-tensile-steel-studding.aspx	P/N: STHTM81SC	Metric High Tensile Steel Studding 8mm x 1m (1 item per pack)	
U-Bolt clamp[6]		1	17.10/ pack[7]	17.1	http://www.thesitebox.com/nuts-and-bolts/u-bolts.aspx	P/N: UB75M12	Standard 'U' Bolt with nuts. 75mm nominal bore. M12 thread....	
Ratchet Strap (w:50mm, L:4m, Load: 4000KG)[8]		8	5.26/ piece	42.08	http://www.theratchetshop.com/ratchet-straps-lifting-systems-ratchets-c-26_28.html	LS02-04 (50mm)	Ratchet Strap-Blue	
Supply and Fit Tilted Table and frame supports		1	4500	4500	OG Fabrication		Supply and fit the table and frame	
Ultrasound Velocity Profiler (UDVP)		1	8500	8500	http://www.theratchetshop.com/ratchet-straps-lifting-systems-ratchets-c-26_28.html	UDVP-DUO (GAH100)	UDVP-DUO	two standard transducers (TX line model) with emitting frequencies 2 MHz and 4 MHz must be
Coriolis Mass Flow Meter		1	7432.79	7432.79	http://www.theratchetshop.com/ratchet-straps-lifting-systems-ratchets-c-26_28.html	OPTIMASS 7300	Mass flow sensor OPTIMASS 7000-T 50 straight single tube system (Titanium-Grade 9)	Wall mounting converter must be ordered, along with transitional pieces for leading edge protection
Coarse Sand (Sand 1)		20 bags	1.81/bag[9]	36.2	http://www.theratchetshop.com/ratchet-straps-lifting-systems-ratchets-c-26_28.html	SMBQSHS40	B&Q Sharp Sand Natural Large Bag	
Medium Sand (Sand 2)		20 bags	4.28/bag	85.6	http://www.theratchetshop.com/ratchet-straps-lifting-systems-ratchets-c-26_28.html	SMBQKDS40	B&Q Kiln Dried Sand Natural	
			Total	**21889.588**				

All the above prices are of 9th February 2012

[1]VAT 20% + Carriage are included into the total price
[2]Each set consists of a threaded bolt+2 washers+single nut.
[3]Each tin contains 500 ml (500 ml can cover 6
[4]Rubber lined pipe clamp with one fixing M.
[5]Price per pack ex VAT (Pack Size: 1x1m). This may not require ordering, checks have to ber made if there is any leftovers from the other
[6]Steel U-Bolt clamp for the flange to prevent the u-shape section from slipping down while the table is raised, especially at 90 degree.
[7]Price per pack ex VAT (Pack Size: 10)
[8]Break/load: 4000Kg, Colour: Blue, Width: 50mm, length: 4m
[9]If more than 10 bags ordered, the price comes to £1.18 per bag

Table 6.2 Schedule of work on the inclinable flow loop

Task	Description	RP	Completed by	Duration (Day)
1	***Project Management***			***33***
1.1	Budget (cost)	MW	MW + YF	33
1.2	Time & scope	MW	MW + YF	33
2	***Preinstallation***			***7***
2.1	Removing radiator	PD	Es	1
2.2	Alteration to lighting	PD	Es	1
2.3	Repositioning control (switch) panel	PD	Es	1
2.4	Installation of control panel box (with door)	PD	T + YF	1
3	***Inclinable Table and Frame Installation***			***19***
3.1	Installation and manufacturing of inclinable table	PD	OG + YF	19
4	***Pump Installation***			***2***
4.1	Positioning, drilling and installation of the pump	YF	YF + T	1
4.2	Connecting 3 phase power supply & control system	YF	YF + E	1
5	***Pipeline Installation***			***29***
5.1	Finalising pipeline design	YF	YF	5
5.2	Ordering flow loop parts	YF	YF	6
5.3	Construction of pump suction & discharge section (+ instrumentations)	YF	YF + T	1
5.4	Construction of U-shape line (+ instrumentations)	YF	YF + T	2
5.5	Construction of vertical line & returning line (+ instrumentations)	YF	YF + T	2
5.6	Support brackets to pipeline	YF	YF + T	0.5
5.7	Fitting 6 pressure sensors & 1 thermocouple	YF	YF + T	0.5
5.8	UDVP mounting position indication (vertical & inclined) & installation	YF	YF + T	1
6	***Mixing Tank, Measurement Tank & Flow Switch***			***10***
6.1	Repositioning & fixing mixing tank	YF	YF + BM +T	1
6.2	Cutting mezzanine section floor for flow and measurement tank discharge	YF	YF + BM +T	0.5
6.3	Drilling and alignment of girders to floor and load cell assembly positioning	YF	YF + BM +T	0.5
6.4	Repositioning & fixing measurement tank	YF	YF + BM +T	1
6.5	Improve the design of switching system	YF	YF + BM +T	1
6.6	Installation of flow switch diversion box	YF	YF + BM +T	0.5
6.7	Replace the flexible pipe from the switch system to a straight solid pipe	YF	YF + BM +T	0.5
6.8	Mounting a ruler onto measuring tank for level measurement	YF	YF + BM +T	0.5
6.9	Alteration of sight glass (measuring Tank) to a bigger one to avoid blockage	YF	YF + BM +T	0.5
6.10	Extension of drainage line	YF	YF + BM +T	1
7	***Gas/Water/Solid (Additional System)***			***28***
7.1	Design of Air/Water mixing nozzel[1] and pipe section	BM	BM + JZ	10
7.2	Fabrication of the nozzle & pipe section + ordering the cloth	BM	JZ + T	11
7.3	Ordering a gas mass flow meter[2]	BM	BM	10
7.4	Design of the oil simulant/water/gas mixing & flushing system[3]	BM	BM	13
7.5	Light solid/water/gas mixing system[4]	BM	BM	5
7.6	Search available particles[5]	BM	BM	3
8	***Process Sensors & Wiring***			***23***
8.1	2 ERT sensor assembly design (or modifying the existing sensors)	YF	YF	1
8.2	Reconstruct assembly of 2 ERT sensor (incline/vertical) & wiring	YF	YF	1
8.3	Testing ERT sensor connections	YF	YF	0.5
8.4	Updating LabVIEW programme	YF	YF	4
8.5	Connection of 6 pressure sensors, thermocouple & EMF to Field Point	YF	YF +E	2
8.6	Finalising wiring (cabling) design (main power & weak signal)	JJ	JJ + YF	1
8.7	Installation of 4 main power sockets and cable covering system	YF	YF + E	1
8.8	Arranging weak signal cables along the table using cable clicks	YF	YF + JJ	0.5
9	***Miscellaneous***			***33***
9.1	Making blank replacement section: ERT(1), EMF(2), PIV(2), Coriolis(2)	YF	YF	2
9.2	Pressure sensor & thermocouple base design and fabrication	YF	YF + T	1
9.3	Installation of bigger waterline (or adding another line)	YF	YF + T	1
9.4	Construction of slots on deck for fixing ERT & UDVP hardware using brackets	YF	YF	1
9.5	Providing support structure for the inclinable table	YF	YF + T	1
9.6	Design and installation of angle indicator (or slot)	YF	YF	1
9.7	Installation of a cone shape pipe to shoot sand from the mezzanine	YF	YF + T	1
9.8	Diffuser design & installation in the mixing tank (+ baffles)	YF	YF + T	1
9.9	Design & installation of a guarding system around the table	YF	YF + T	1
9.10	Design and fabrication of UDVP probe adjuster	YF	YF + T	10
9.11	Cleaning of G.56	YF	YF	1
10	***System calibration***			***3***
10.1	6 pressure sensor calibration	YF	YF	1
10.2	Thermocouple calibration	YF	YF	0.5
10.3	Measuring tank calibration	YF	YF	0.5
10.4	Load cells calibration	YF	YF	1
10.5	Gas/water/solid instrumentation calibration	BM	BM	0.5
10.6	UDVP calibration	YF	YF	0.5
10.7	ERT calibration	YF	YF	0.5
10.8	DP & temperature	YF	YF	0.5
11	***Final Process Testing***			***3***
11.1	Water flush the pipeline	YF	YF	0.25
11.2	Water leak test	YF	YF	0.25
11.3	Water mixing test	YF	YF	0.25
11.4	Min. & max. frequency water pump	YF	YF	0.25
11.5	Water switching system check	YF	YF	0.25
11.6	Table inclination test	YF	YF	0.25
11.7	Water pressure, temperature and flow rate check	YF	YF	0.25
11.8	Load cells switches check and sensor verification	YF	YF	0.25
11.9	Drainage system check	YF	YF	0.25
11.10	Check LabVIEW program	YF	YF	0.25
11.11	Gas/Water test	BM	BM	0.25
12	***Milestones and Deliverables***			**29**
12.1	Weekly progress report to MW		YF	7
13	***Final Completion Report***			**1**
13.1	Final completion report (including system & parts specification/ drawing/ recommendation etc.) by **ALL RP** by end of 29 Feb 2012		YF	1

January												*February*																				
16	*17*	*18*	*19*	*20*	*23*	*24*	*25*	*26*	*27*	*30*	*31*	*1*	*2*	*3*	*6*	*7*	*8*	*9*	*10*	*13*	*14*	*15*	*16*	*17*	*20*	*21*	*22*	*23*	*24*	*27*	*28*	*29*
M	*T*	*W*	*T*	*F*	*M*	*T*	*W*	*T*	*F*	*M*	*T*	*W*	*T*	*F*	*M*	*T*	*W*	*T*	*F*	*M*	*T*	*W*	*T*	*F*	*M*	*T*	*W*	*T*	*F*	*M*	*T*	*W*

[1] A top-fitted chamber with filtering cloth.
[2] The same type as that in G.21.
[3] It may still use the current flush pipe and the bottom drain pipe. However, the operation may be opposite to heavy solid/water.
[4] The structure of current mixing tank, baffle/separator should be reviewed.
[5] With density 0.9-0.96 and size range four size from 1, 2, 3, 4 mm.

RP : Responsible Player
MW : Mi Wang
YF : Yousef Faraj
PD : Peter Dawson
Es : Estates
T : Technician (Robert Harris or John Cran)
JJ: Jiabin Jia
E : Electrician
JZ : Jun Zhang
BM : Basit Munir
OG: O.G. Fabrication (Geoff)

6.4 Types of slurry flow loop

As slurry flow is a complex two phase flow, a properly designed flow loop system is necessary, so that it offers a greater flexibility and capability of generating data for wider range of conditions. Unfortunately, this wider range of conditions is required; if a good understanding of slurry flow and the effect of its behaviour is sought, especially in the case of flow measurement and visualisation.

According to Brown and Heywood (1991), flow loops are commonly used to determine and study and measure variety of slurry variables and their influence on the flow. Some of which are listed below:

- To determine the frictional pressure gradient for the flowing slurry.
- To determine the higher concentration limit for practical handling of slurry.
- To determine the slurries deposition velocity, at which the solid particles start to settle at the pipe invert.
- To determine velocity and concentration profile of the solid particles (radial and axial).
- To test and calibrate the flow meters and concentration devices.
- To assess pump characteristics and performance.
- To determine particle degradation.
- To determine the rate of pump and pipe erosion/corrosion of the system.
- To assess pipeline start/shutdown of a system, as in the case of inclined flow.

Normally, there are two types of flow loop that can be used to obtain the required data. These are the once-through and re-circulating flow loop. In the once-through flow loop the slurry (solid and the carrier liquid) is continuously fed to the flow loop during the course of the experiment. This implies that a lot of slurry is required if a meaningful data is desired. Therefore, this type of flow loop is ignored in this study and the other type (re-circulating flow loop) is considered. In the re-circulating flow loop the slurry is continuously returned to the pump, either directly or indirectly. In the direct method, the slurry is returned directly through the pipeline to the pump inlet, which forms a totally close flow loop. Whereas, in the indirect method the contents of the pipeline flows into a mixing tank (or holding tank) and continuously feeding the pump. Thus, the latter type can be considered as an open flow loop. Since the open loop contributes into the increase in the

suction head, therefore, it was decided that the open loop will be used in this study. In other words, the suction head increases with increase of slurry level in the holding tank. Therefore, the holding tank must always be monitored that the slurry level is sufficient, particularly when the flow is diverted into the measuring tank. Also, the slurry level must be high enough to avoid air entrainment in the mixture, which could enter into the pump and result in damaging the pump. Another reason of choosing an open loop is that samples can easily be collected, by diverting the flow via a switching system into the measurement tank.

6.5 Overall structural design

A long table with a steel frame were designed and build, on which the pipeline is laid. The table consists of two sections, the rigid section and the inclinable section, which are coupled using a pivot point. The inclinable table holding a U-shape pipeline, which consists of outgoing and returning limbs. Since one of the flow loop design requirements is to provide the flexibility of choosing any inclination angle between 0° to 90° from horizontal, then a lifting method is required. An electric winch is used to lift the inclinable table to a desired angle. The length of the U-shape pipeline (outgoing and returning) is 4 m long, which is enough to include all the required instrumentations within the developed flow region. Figures 6.5, 6.6 and 6.7 showing the schematic drawings of the inclinable flow loop system, which was built in the Engineering Building.

6.6 Flow loop design and component selection

In an open flow loop the slurry is discharged from the pipeline into a conical holding tank, which continuously feeding the pump through a connection at the bottom of the holding tank. However, to achieve a versatile flow loop, there are critical elements that must be carefully considered and selected. These elements can include piping length, test section length, and slurry instruments for measuring slurry parameters, such as velocity, concentration etc. These components will be discussed in the following sections, including the reasons behind the selection of each of them.

6.6.1 Structural design of the pipe-rack

A structural steel pipe rack is designed to support the pipeline, power cables, some of instrumentation and instrument cables on ground floor in the Engineering building/G.56. One of the design requirements is to include a

pivoted inclinable section within the structural steel framework, on which the U-shape inclinable pipeline is laid.

In designing the structural steelwork, the main emphasis was placed upon the stability, economics and practical aspects of the whole structure. The pipe rack (or pipe support) work consists of 3-stage process: design, fabrication and erection. The main considerations for the design aspect of the pipeline support are given to strength and stability, static and dynamic loads (pipeline, pipe costs and instrumentations) the intended function of the steel frame structure, cost and maintenance. The fabrication process involves cutting and preparation of each member to length, while the erection process includes rigging of all prepared members to their intended places in the pipeline support structure and making connections between all structural members.

At the earlier stage of the design, steel pipe rack (approximately 7000 mm long) was proposed to support the stationary horizontal lines and the inclinable U-shape section. It was decided that the rigid pipe rack section to be of a similar construction to the tilting section. Both sections are connected through a pivoted pin, which allows the U-shape pipeline support to be tilted, as shown in Figure 6.1. However, in order to complete the detailed design of both sections of the pipe rack, several documentations and information have to be reviewed and corrected. The following information is paramount for development of the design and constructing an economical and successful pipe rack.

1. Footprint plan and the pipeline layout (including the location of each equipment).
2. Access and maintenance requirement for each part of the flow line.
3. Drawing of the electrical cabling, showing the routing and location of electrical and instrumentation cables and/or support.
4. Information related to the concrete structure and foundations in the area of the piping table.
5. The lifting method used to lift the inclinable table.
6. Intention of any future provisions for piping system or related loading.

Once the above preliminary information is obtained, it is well documented for the next steps of the design. After collecting the required data for the development of the design, the following stages are conducted in chronological order:

1. Design load consideration.
2. Allowable deflection of the table.
3. Final framing of the pipe rack.

Normally, for pipe rack design, the loads considered are piping gravity load, electrical conduits and cables, self weight of the pipe-rack, live load, snow load, wind load, earthquake load, friction load (El-Reedy, 2011). Since the multiphase flow loop is built indoor, then this fact automatically eliminates snow load and wind load. Also, as the friction forces generated by hotlines sliding across the pipe support, thus the friction loading is considered to be negligible. The only loads that have to be considered are: piping gravity load, with its contents, electrical conduits and instrumentations on the deck and self weigh of the pipe rack.

The weight of all structural loads (except the support legging, on which the tables stand on) was calculated. However, since the loading on the tilting table is the most important to determine the capacity of winch used to lift it, the loading calculation was performed only for this part. The weight of all structural members of the tilting table was determined as approximately 200 kg. On the other hand, the piping gravity loads were determine by calculating the weight of empty pipeline with equipment and instruments, along with the weight of pipeline contents, for which slurry was considered. The weight of empty pipeline (the U-shape section) was determined by considering every individual component of the line, as shown in Table 6.3.

The result of weight calculation of inclinable table section with full pipeline is summarised as follows:

- Weight of the pipeline and instrumentation = 214 kg (based on 8.5 m length).
- Weight of slurry flowing through the inclinable section = 25 kg (this is based on 0.017 m^3 slurry flowing through 50 mm ID, 1350 kg/m^3 slurry density, 2650 kg/m^3 sand density, 1000 kg/m^3 water density and 40% concentration by weight).
- The total weight of inclinable U-shape pipeline with its contents = 214 +25 = 239 kg.
- By considering 25% safety margin (59.75) for future provisional addition to the pipeline, pipeline blockage etc, the total weight of the full U-shape section = 298.75 kg.

- Weight of all structural members of the tilting table = 200 kg (including bolts, nuts and washers).
- The total weight of the inclinable table with the pipeline and its contents = 498.75 kg.

Table 6.3 The weight of the U-shape pipeline on the inclinable table

Component	Weight (kg/each or kg/m)	No./m length available on the inclinable section	Total weight of each component (kg)
Flange	0.39	30	11.7
Straight Socket (Plane)	0.14	2	0.28
Pipe	1.045	7.5	7.8375
Flexible Pipe	0.6	3	1.8
Long rad. Bend	0.54	2	1.08
Pressure Sensor	0.23	4	0.92
Pipe Clamp (with threaded rod)	0.13	15	1.95
Bolt+Nut+2(washer)	0.16	64	10.24
EPDM Flat Gasket	0.07	16	1.12
Tee 90°	0.31	4	1.24
ERT Sensor	3	1	3
Coriolis Flow Meter	150	1	150
UDVP system	13	1	13
ERT system (P2000 or z8000)	10	1	10
Total weight of fitted pipeline (Inclinable Section)			**214.1675**

From the above load design calculation the lifting capacity of the winch can be determined. This implies that a winch with 500 kg lifting capacity can safely be selected for the intended application, even with some future addition to the pipeline (up to 25% of the actual weight of the whole inclinable section).

The maximum allowable deflection of the inclinable table also had to be determined. In terms of maximum allowable deflection, the focus was placed upon the inclinable section rather than the rigid section, due to load concentration on this section and longer span. The determination of maximum allowable frame deflection is important to avoid the occurrence of problems with the frame and the attached pipeline. These problems could be one or more of the following:

1. Inadequate drainage of the pipeline.
2. Flow disturbance and generating wrong measurement data.
3. Increase the rate of wear in pipes and fittings.

4. Broken seals at the joint locations.
5. Strain on the pipeline or fixings.
6. Damage or excessive strain at the connection points.
7. Surface distortion of the table.

Normally, for most buildings and structures various guidelines have been introduced based on the intended application to determine the maximum allowable deflection values of a structural member. Therefore, in order to find out the maximum allowable deflection value for the inclinable table, the recommended allowable deflection limit for beams is considered, which is L/360 of the span (El-Reedy, 2011). This means that based on the length of the longitudinal beam member of the table, the beam's maximum allowable deflection for the inclinable table can be determined using the following formulae.

$$d_a = \frac{L}{360} \tag{6.1}$$

d_a= Maximum allowable deflection.

L= The length of the span in mm.

360= Constant.

Thus, based on the above guideline a span of 4000 mm, which is the beam length of the table, has a maximum allowable deflection of 11,11 mm. In other words, the table beam subjected to the aforementioned load, bends from its original horizontal position by 11.11 mm. However, since the two beams are used and are connected by 5 transverse parallel flange channels, then the deflection value for the whole table is expected to be far less than 11.11 mm. Therefore, this deflection value can be accepted.

The framing of the pipe rack decks (inclinable and rigid) based on the pipeline layout, required safety and stability calculation and the intended application of each deck, was one of the most important aspect of the flow loop design and construction. As many factors had to be taken into account, most of these factors were case and project specific and are listed below:

- Some items had to be removed within the working area of the flow loop, such as the radiator at ceiling level.
- The heating pipeline running close to the ceiling had to be considered.

- The design and construction of the table could not be separated from the mezzanine, thus it was incorporated into the mezzanine redesign, which would result in the omission of some structural member of the mezzanine (column). Also at mezzanine level, there was a potential problem with regard to the fact that a support beam fouls the line of the inclinable table at 90%.
- A buffer stop or pushback had to be included to ensure the 90° angle is maintained and the table is lowered through some considerable force.
- The existing door at the end of the working area had to be kept accessible, and this obviously would affect the dimensions and installation of the table.
- Consideration had to be given to the flexibility of the pipeline at the pivot point.
- The mezzanine floor construction had to be amended, so as to allow the table to be raised to 90°.
- Some steel work had to be carried out for adjustment of the winch system, based on the level of the table at 90°.
- Locating the lifting point on the tilting table using a steel wire.
- Finalising the lifting method used to tilt the table and the associated work to adjust the lifting system. For example, based on using a winch system, some steel work had to be carried out to adjust it based on the level of the table.

After careful considerations and detailed design of the frame system, the following work had to be carried out to achieve an inclinable pipe rack, which can be tilted from 0° to 90°:

1. Manufacture and installation of L-shape support legs.
2. Manufacture and installation of a Universal Beam (152 x 89 x 16 mm) to support the mezzanine (2800 mm long).
3. Manufacture and installation of a tilting table (4000 mm long and 650 mm wide).
4. Manufacture and installation of a fixed table (3000 mm long and 650 mm wide).
5. Fixing 20 mm plywood to top surface of both tables.
6. Manufacture and installation of Universal Column (152 x 152 x 23 mm) (6000 mm high) bolted to floor and restrained to wall with another Universal Column (152 x 152 x 23 mm) (800 mm long).
7. Modification to the existing mezzanine to suit.

8. Installation of 0.5 ton remotely controlled electrical winch.

All the steelwork are painted red oxide primer and each structural member had been manufactured and prepared before full connections and installations on site. Based on the objectives and the final construction of the inclinable pipe rack system, the following plans had to be carried out:

1. Slab level plan.
2. Steel frame and deck level plan.
3. Plywood deck plan.
4. Mezzanine level plan.
5. Top level plan.

In the slab level plan, 3 L-shape support legs were fabricated and installed, two of which used to support the rigid table and the 3rd one to support the anchored end of the inclinable table. They were all designed in a way to raise the surface of each table by 1 m high from floor level. They are parallel flange channels (150 x 75 x 18 mm PFC), each end of which connected to a base plate (200 x 100 X 10 mm). One end is adjusted to the concrete floor using two M16 resin anchors, and the other end base plate to the wall using two similar anchors.

The 2800 mm long Universal Beam is used to support and increase the stability of the mezzanine after modification, and also to reduce the vibration during the experiment, as vibration affects the measurement carried out using the measuring tank. The bottom end of the Universal Beam is connected to a base plate and anchored to the concrete floor using two M16 resin anchors, while the other end is connected to the mezzanine. The 6000 mm Universal Column (152 x 152 x 23 mm UC) is also connected to a base plate (350 x 200 x 12 mm) and anchored to the concrete floor through four M16 resin anchors. The reason for installing this universal column is to fix one end of the horizontal UBC, which is restrained to wall to facilitate the winch installation.

The plan of steel frame at deck level comprises of 4000 mm long tilting table and 3000 mm long rigid table. Both tables fabricated from (150 x 75 mm) PFC and are connected through a pivot point. All members have steel-to-steel connections with M20 bolts and 6 mm fillet weld all round. The tilting table frame has two longitudinal beam (150 x 75 mm PFC) and three transverse beams (150 x 75 mm PFC) with 1000 mm spacing between them. Each cross members connected to 10 mm stiffener plate (6 mm) at either end and the plates are drilled to take bolts. In order to increase the

stability and strength of the frame, in addition to the bolts, each cross members (PFCs) are welded to the longitudinal beams. Similar connection method and structure is employed for the rigid table. The U-shape pipeline was designed in a way to have 400 mm spacing between both limbs. Based on this the width of the table has to have a width, onto which the pipeline could be laid without any pipeline extending out of the table sides. Despite the difficulties imposed by lack of spacing, the table was designed to have 650 mm width, which allows 11 mm leeway on either side of the flanges. In addition, the maximum spacing between the tilting table and the adjacent brick wall that could be left is 25 mm. Although, the concerns were raised as to whether the table would catch the adjacent brick wall during elevation by swaying side to side, 100% stability of the table was confirmed during mechanical testing. The rigid table is fixed at one end and connected to the tilting table on the other end through a pivot system. On the other hand, the tilting table pivoted at one end and anchored at the other, so the winch wire rope is connected through a D-shackle, which is shown in Figure 6.1. As previously mentioned, one support frame is fixed to the wall and floor to support the anchored end of the tilting table in horizontal position. In order to connect both tables via 20 mm diameter bright steel pin, 10 mm plates with 6 mm fillet welding are connected to the end of each table, as can be seen in Figure 6.1.

Figure 6.1 Actual photo of both ends of the inclinable table, pivoted end (left) and D-shackle at anchored point (right)

The plan of plywood deck, is to fix a flat surface on which the pipeline and required instrumentations could be laid. 20 mm marine plywood surface is fixed to the steel frame using screws at a maximum of 500 mm interval. The steel rubber lined clamps are mounted on the plywood through M10 threaded rod bars. Hole matrices are drilled between both limbs of the U-shape pipeline, so as to fix the instrumentation to the plywood on the deck using brackets and threaded rod bars, for which M10 nuts and washers are

used on either side (top & bottom) of the deck (plywood). Figure 6.2 illustrating the actual photo of the instrumentation fixture through hole matrices.

The mezzanine level plan involved some modifications to the existing mezzanine and using good propping method using 2800 mm Universal Beam, as previously discussed. Since the pivot point of the pipe rack is below the mezzanine level, in order to allow the tilting table to be raised to 90°, the mezzanine floor above the pivot point had to be cut by 1835 x 880 mm and removed.

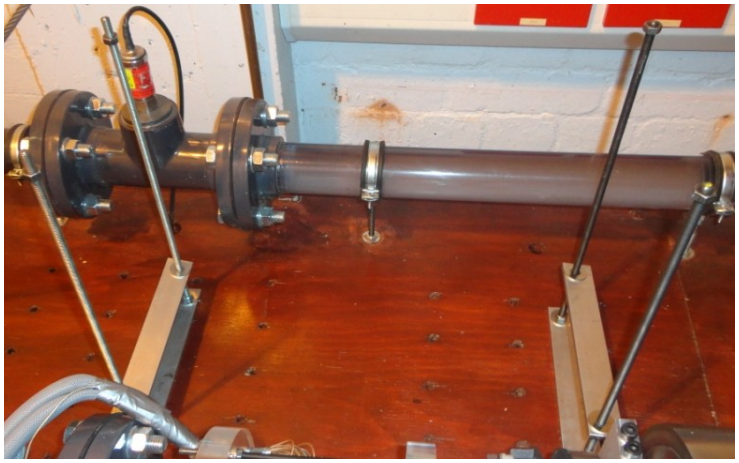

Figure 6.2 Actual photo of the instrumentation fixture and hole matrices on the inclinable table

Handrails are installed all round the cutting edges to provide a safe working area. Figures 6.3, 6.4, 6.5, 6.6 and 6.7 showing the inclinable pipe rack and pipeline at different level plan.

The top level plan was the last finishing touch to the inclinable pipe rack system. This plan involved the connection of 6000 mm Universal Column to the 800 mm Universal Column, on which the winch is mounted. In order to allow the table to be raised to exactly 90°, it is very important not to fix the winch exactly above it, but rather some offset to allow the table to be pulled diagonally, but not vertically. Also, some clearance of 500 mm is paramount between the winch and the raised table. Lifting shackles are installed on the winch side and one end of the tilting table to adjust the 6 mm bright steel wire rope. As there is a doorway at the end of the tilting table, it is very important that the access to this door is kept clear. Therefore, the lifting eye, which was initially mounted outward of the tilting table, had to be fixed inward to reduce the risk of injury to personnel.

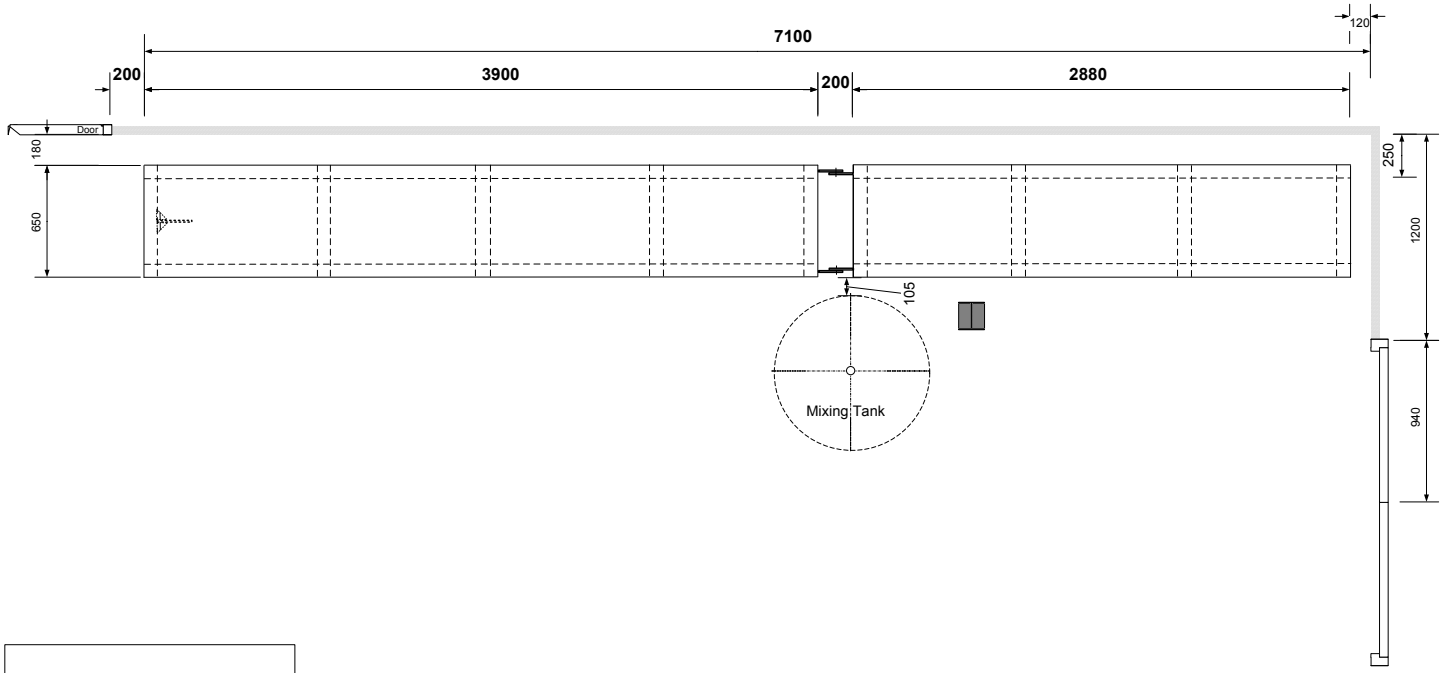

Inclinable Piperack-Top View (Ground Floor)		Dimensions are in mm			
	Company	**TIME IN REQUEST:**	**APPROVED BY:** *Prof. M. Wang*	**DWG NO.**	**© Copyright** This drawing and the copyright, design rights and all other intellectual property rights in it belong to the University of Leeds/ OLIL group. No licence or assignment of any such rights is granted hereunder. This drawing is not to be copied or divulged to a third party without written permission.
DRAWN BY: *Y. Faraj*	University of Leeds/ OLIL	15th March 2012	**SIGNATURE OF RT:**	17	
DATE: 11th March 2012	**SCALE** 1:20	**Material:** Steel	**SHEET** 1 of 3		

Figure 6.3 Schematic diagram of inclinable pipe rack (Top View-Ground Floor)

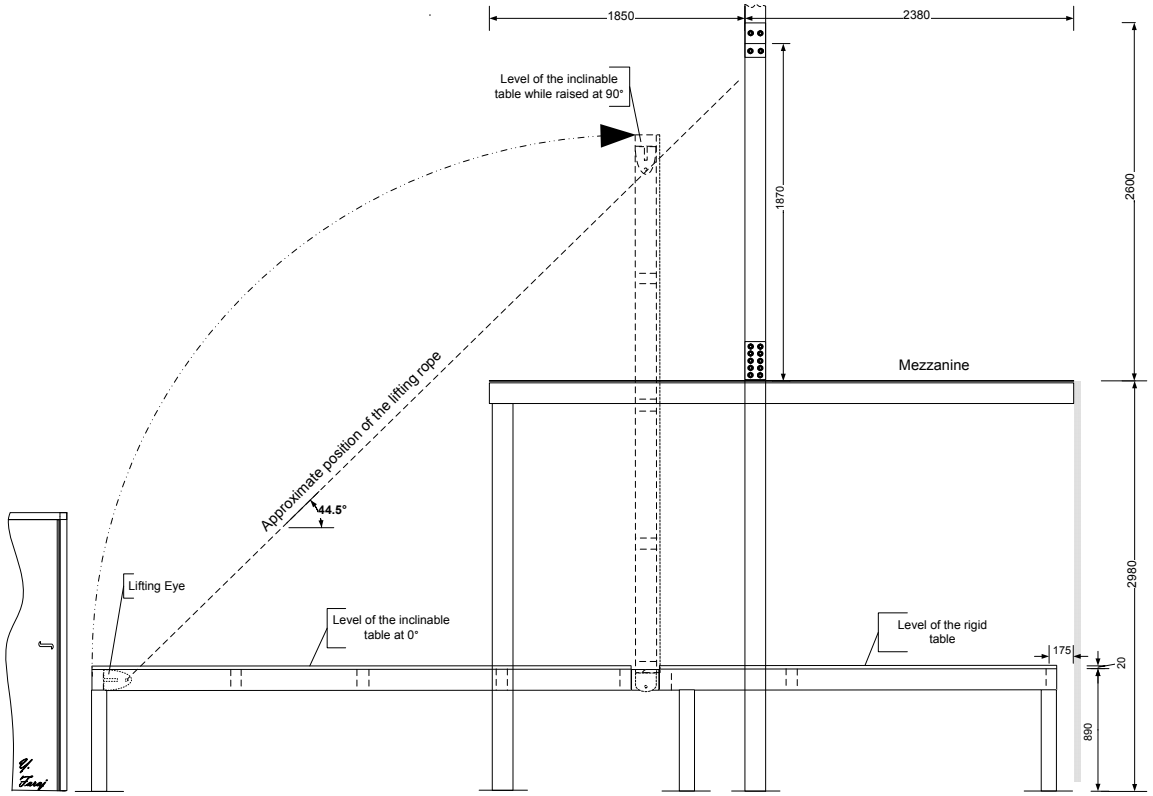

Inclinable pipe rack-side view (at horizontal and vertical level)	Dimensions are in mm					
DRAWN BY: Y. Faraj	**Company** University of Leeds/ OLIL	**TIME IN REQUEST:** 15th March 2012	**APPROVED BY:** Prof. M. Wang **SIGNATURE OF RT:**		**DWG NO.** 17	**© Copyright** This drawing and the copyright, design rights and all other intellectual property rights in it belong to the University of Leeds/OLIL group. No licence or assignment of any such rights is granted hereunder. This drawing is not to be copied or divulged to a third party without written permission.
DATE: 11th March 2012	**SCALE** 1:25	**Material:** Steel		**SHEET** 2 of 3		

Figure 6.4 Schematic diagram of inclinable table at horizontal and vertical level (East View)

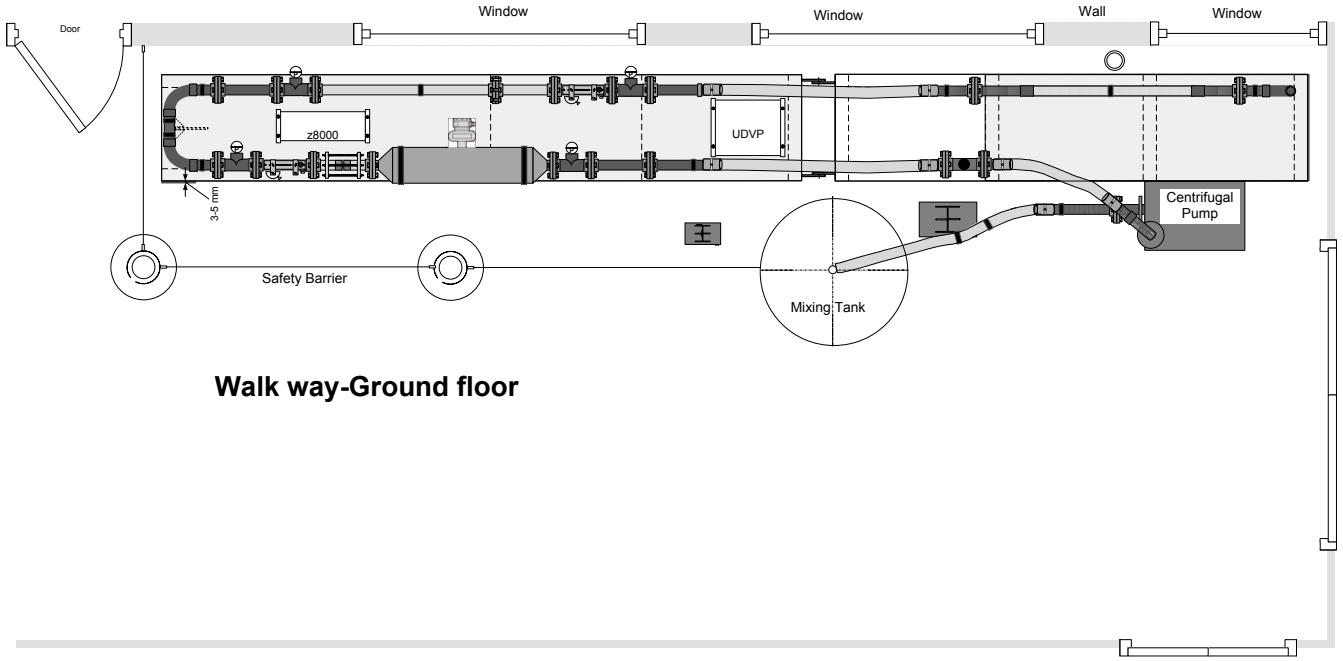

Inclinable Flow Loop-Ground Floor (Top View)		**Company** University of Leeds/ OLIL	**TIME IN REQUEST:** 15th March 2012	**APPROVED BY:** *Prof. M. Wang* **SIGNATURE OF RT:**	**DWG NO.** 17
DRAWN BY: *Y. Faraj*					
DATE: 11th March 2012	**SCALE** 1:20	**Material:** PVCu		**SHEET** 3 of 3	

Figure 6.5 Schematic diagram of inclinable section and rigid section (Top View-Ground Floor)

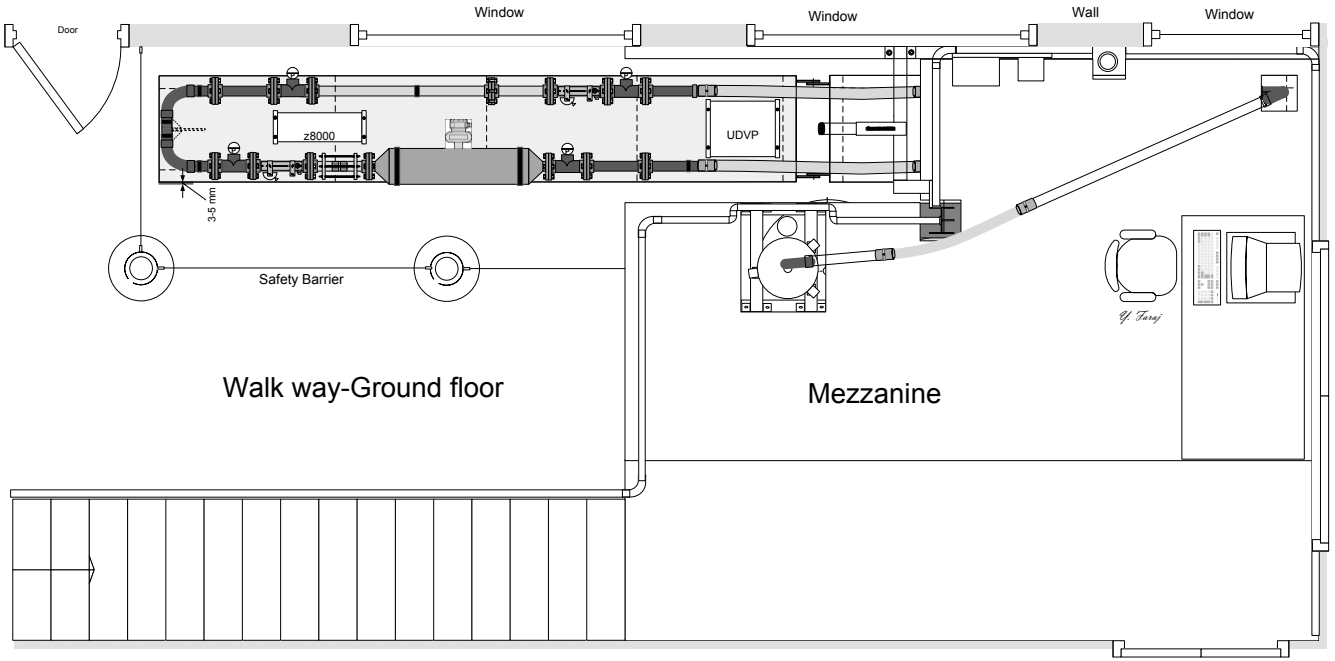

Inclinable Flow Loop-Mezzanine Floor (Top-view)		**Company**	**TIME IN REQUEST:**	**APPROVED BY:** Prof. M. Wang		**DWG NO.**
DRAWN BY:	Y. Faraj	University of Leeds/ OLIL	15th March 2012	**SIGNATURE OF RT:**		17
DATE:	11th March 2012	**SCALE** 1:20	**Material:** PVCu		**SHEET** 3 of 3	

Figure 6.6 Schematic diagram of inclinable flow loop (Top View-Mezzanine Level)

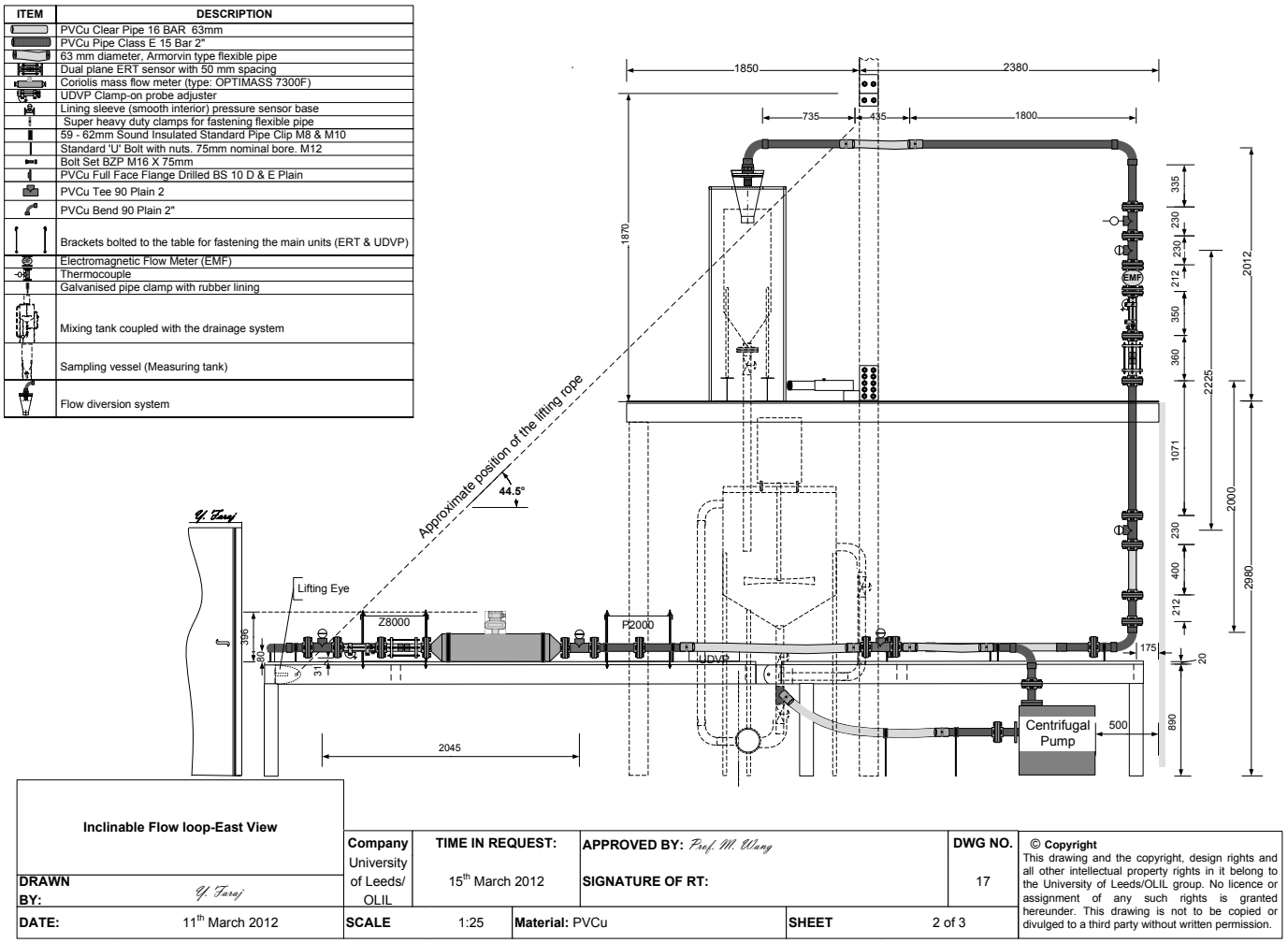

Figure 6.7 Schematic diagram of inclinable flow loop (East View)

6.6.2 Selection of lifting method

The selection of the lifting method to raise and to lower the inclinable table is one of the most important part of the design process. The selection process was based on four criteria: safety, efficiency, flexibility and economy. A journey through lifting equipment suppliers revealed that there is wide range of lifting equipments and methods available for almost any application, such as (www.electricwinchshop.co.uk). The lifting methods that could be considered in the selection process are hydraulic ram, hoists and winches. Each of these methods has to be carefully assessed against the criteria mentioned above.

The option of using hydraulic ram is totally eliminated in the selection list due to the following implications:

1. The ram position have to be designed carefully, as any position may not be mechanically acceptable due to space limitations.
2. Hydraulic ram housing was suggested, so that the ram direction would be more towards vertical rather than horizontal. The method of housing hydraulic ram was found to be an attractive one, as it would not interfere with the pipeline on the deck. However, the housing requires more steel work which increase the total cost and the total load on the deck.
3. Since one of the design requirements is to raise the table up to 90°, this suggests the requirement of a longer hydraulic ram, which complicates positioning of the ram. In addition, using telescopic cylinder can be another option, however, this type of cylinders are found to be very expensive. The required telescopic cylinder that suits the application in this project is very costly.
4. Since using hydraulic ram involves utilisation of 50 litre steel reservoir filled with oil, further problems are to be faced with positioning of the oil tank indoors due to lack of space in G.56-Engineering Building in the University of Leeds. Also having oil around, would certainly increase hazard in the working area and surrounding walkways through spillage or fire hazard. Although, attempts were made to place the oil tank outdoor, clearly this would increase the costs by adding flexible pipes and to protect the whole facility against extreme weather conditions.

Due to above implications using hydraulic ram as a lifting method was completely removed from the selection list.

The possibility of using a crane-type hoist system was also considered. After careful examination regarding the preliminary design of the hoist system, it was proposed that a crane-type hoist can be used in lifting beam as part of the whole system. This lifting beam is used as a mono-rail system along with the inclination angle (0° to 90°) along which the hoist would roll. This system would include a beam and a lifting block clamps over and it could move forward and backward using wheels. This, however, would overcomplicate the whole pipeline system by adding further steel work overhead. Also, fabrication and installation of the steel would increase the total cost. Therefore, this method was concluded as a costly and overcomplicated method, which was also eliminated from the selection list.

The last considered lifting method was a winch system, which can come in wide variety of styles and can be supplied from a choice of industrial and commercial suppliers. A budget choices also can be found within the supplied range that can deliver the job effectively.

As there are many different choices it can be very confusing to choose the specific type, which makes a good balance between the costs and effectiveness of the winch for the intended application. Therefore, the assistance has to be sought from professionals to make the right choice.

In order to make the right choice a few important considerations have to be taken into account, such as power and tension capabilities, size, reliability and costs. After balancing all of these factors it was finally decided to select an electrical wire steel rope winch (electric winch, BETA II, type Compact 1-BGV D8). Based on the total weight of the inclinable section (pipeline with contents and the steel frame) a 500 kg capacity was selected. In comparison to hydraulic ram and crane type hoists system, a winch system can offer several advantages: such as lower cost (unit and installation), simplicity of installation, it also uses no fluid.

6.6.2.1 The winch system

The winch system used to lift the inclinable table is an electric wire rope winch BETA II (type compact1-BGV D8), which is manufactured by PFAFF-Silberblau in Germany and supplied by Yorkshire Lifting Tackle Ltd, Figure 6.8 showing the actual photo of the electrical winch fixed overhead to the steel.

The BETA II-C1-BGV D8 is a compact winch that offers a good size, which is considered as an advantage due to lack of space in G.56 laboratory. The dimensions and specific technical data of the winch is shown in Figure 6.9 and Table 6.4 respectively.

Figure 6.8 Actual photo of the electric wire rope winch

The BETA II winch is a drum winch with spur gear (size 1.5), which holds the weight of the table in every position by an electromagnetic brake. The system is provide with a switch or braking limit, based on the desired lifting or lowering position. This function is clearly one of the design requirements of the whole inclinable flow loop system that allows the table to be tilted only within the range of inclination angle required in this study, which is between 0° and 90° inclination angle. Therefore, the braking system is adjusted at two levels, 0° inclination angle from horizontal and 90° inclination angle from horizontal. In other words, once the table is raised, it stops automatically at 90° and does not go beyond of that position. Similarly, while lowering the table in stops at 0° from horizontal.

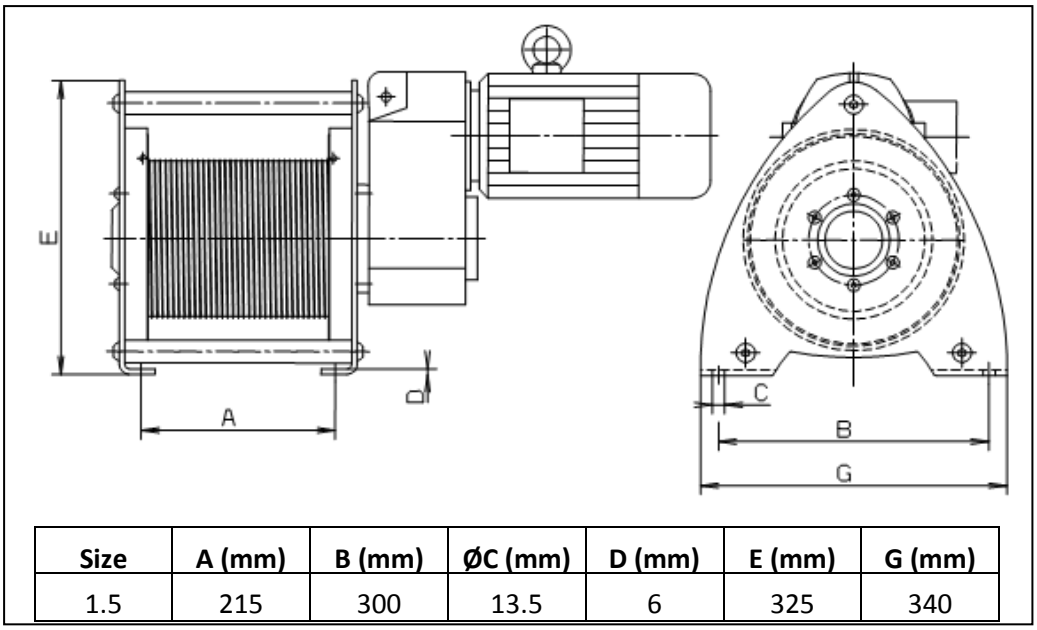

Size	A (mm)	B (mm)	ØC (mm)	D (mm)	E (mm)	G (mm)
1.5	215	300	13.5	6	325	340

Figure 6.9 Showing the electric wire rope winch main dimensions

Table 6.4 Technical winch BETA II specification

Drive group (DIN 15020)	1(Am)
Rope capacity (m)	8.4
Lifting capacity (kg)	500
Rope diameter (mm)	6
Minimum breaking force (kN)	23.14
Rope speed (m/min)	3.7
Load protection	Brake motor
Drive	Three-phase motor with built-on brake
Duty cycle (%)	53-40
Circuits/hour	120
Weight (without rope)	63
Operation temperature	-20 to 40 °C

The winch can be controlled by handheld remote control, which allows the operator to lift or lower the table via push buttons, along with the emergency

stop button in case of emergency. The schematic diagram of the handheld remote control is illustrated in Figure 6.10.

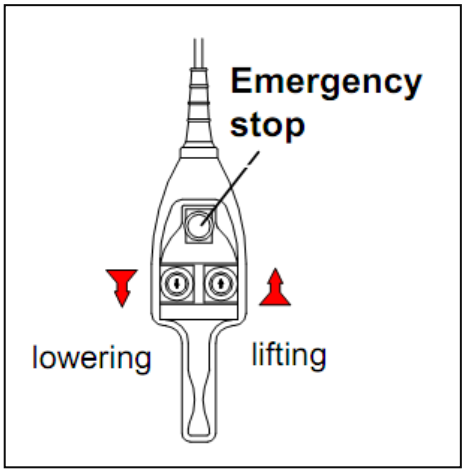

Figure 6.10 Winch remote control

In addition a main switch with external operating elements are also located at the mezzanine level, where they can quickly and easily be accessed. It is apparent that the remote control can provide more flexibility, and can be used at the ground floor level as well as mezzanine level. Nevertheless, it is recommended that while raising or lowering the table it is should be used in a location where the entire inclinable table and surroundings are overlooked from the operators position.

The winch is mounted on a steel structure (universal column-UC), and the whole structure is designed considering the sustainability of maximum force imposed by the winch, including consideration to the impact forces. In order to carry a safe mounting of the winch system, a proper mechanical fixing to be followed. After making sure that the mounting surface was flat, the winch was positioned against overhead steel structure and fixed with four M12 bolts (8.8 material grade). The galvanised steel wire rope (6mm diameter) is fixed to the left drum flange, within which the rope attachment is effectuated with two screws. The other end of the rope is connected to the lifting eye of the inclinable table via a D-shackle, which is pinned (threaded) so as to allow easy removal.

6.6.2.2 The telescopic table push-back system

Once the table is raised to a vertical position (90°), it is at the equilibrium position, based on Newton's First Law (Fowles and Cassiday, 1999). The only forces acting on the table are gravity force due to the load of the table acting on the pivot system and the pivot system exerts an upward force on

the table. Based on Newton's First Law the table's motion does not change unless a tangent or a horizontal force is exerted on the table. This implies that unless a force is exerted on the table, the table remains at rest even if the winch remote control lowering button is pressed.

Therefore, a telescopic push-back system was designed to create a horizontal force on the table, so as to push the table. The system comprises of a 300 mm long Square Hollow Section (SHS), 280 mm long Circular Hollow Section (CHS), 200 mm long carbon steel compression spring (60 mm diameter), 25 mm thick rubber pad (60 mm diameter) and an M10 hex-bolt. The actual photo of the push-back system is shown in Figure 6.11.

The circular hollow section is fitted into the square hollow section. A slot is made in the SHS by cutting a section (100 mm x 50 mm) on the top side along which the M10 bolt is travelling during compression and extension of the spring. The CHS is held in place (within the SHS) via an M10 bolt, which is tightened to the CHS through the slot. The compression spring is inserted into the SHS in such a way to push the CHS and SHS apart. In order to keep the elasticity of the spring, it is kept at its equilibrium position, unless it is compressed by the table (i.e. no force acting on the spring). The rubber pad is fitted to the outer end of the CHS, in order to prevent the table surface from scratch and damage. The whole system is secured by welding it to another steel SHS, which is bolted to the mezzanine structure.

Figure 6.11 Actual photo of the push-back system

The working principle of the system is that when the table is raised up to 90°, it starts to push CHS at some near vertical inclination angle (around 87°), while the spring is continuously compressed until the table remains at rest (90°). On the other hand, according to Hooke's Law, once the table is

lowered, by lowering the winch rope, the restoring force acts to restore the spring to its equilibrium state and the table is pushed back until one of the force components is created (Blake, 1985). Once the gravity force component (downward) is created, the table does not require the spring expansion force to push it back.

6.6.3 Piping design

Piping consists of pipe, flanges, fittings, bolting, gaskets, valves and other piping components, which are included into the pipeline for a specific requirement. Moreover, it also includes pipe support and other necessary elements to provide a safe, secure and effective pipeline. Therefore, piping refers to the line, where pipe sections are joined with fittings, valves and other items or mechanical equipment and are supported by supports.

In order to determine the most economical pipeline that responds to all the design requirements of the multiphase flow loop, it is paramount to consider several parameters of the pipeline, such as piping construction material, sizing, jointing method, pipeline layout, length and others. It is apparent that the economic viability of the pipeline can be defined through careful design or selection of the above parameters. Therefore, so as to understand the impact of each parameter and achieve a safe and economic pipeline design, this section discusses the design and selection of each parameter along with driving force for selecting some individual components or techniques used in the design of the flow loop.

Since ignoring any parameters mentioned above can have an adverse effect of the final design of the system, then careful selection and timely preparation is crucial for achieving an economical and successful design and installation of the flow loop piping. It is worth mentioning that throughout the whole design and installation process it is necessary to make careful and realistic compromises between the design features and costs, without ignoring minimum safety standards.

6.6.3.1 Piping construction material and diameter section

The selection of materials of construction for multiphase piping system is very important in designing a multiphase flow system. Since it is considered as an optimisation process, then the material selected must be chosen for the sum of its properties such as strength, ductile, corrosion resistance etc.

The selection of piping material is carried out in two stage process, in the first stage consideration should only be given to those piping materials that:

- Are allowed by code or standards.
- Are mechanically compatible with the fluid.
- Have rated pressure and temperature that meet the entire range of flow operating conditions; and
- Are compatible with environmental conditions such as external corrosion, ultraviolet degradation etc.

The second stage is the evaluation of considered materials for advantages and disadvantages such as cost, ease of fabrication and installation, support system complexity etc.

The piping material for the multiphase flow, including slurry, can either be metallic or thermoplastic piping system. The metallic piping that are commonly used for multiphase flow systems can stainless steel, carbon steel, ductile iron, alloys with iron, nickel, aluminium, copper, lead etc. On the other hand, thermoplastic piping systems, which are often referred to as plastic piping systems can be one of those shown in Table 6.5.

Table 6.5 Thermoplastic materials for piping system (US Army Corps Engineers)

Chemical Name	Abbreviation
Acrylonitrile-Butadien-Styrene	ABS
Chlorinated Poly(Vinyle Chloride)	CPVC
Ethylene-Chlorotrifluoroethylene	ECTFE
Ethylene-Tetrafluoroethylene	ETFE
Perfluoro(Ethylene-Proplylene) Copolymer	TEP
Polyethylene	PE
Perfluoro(Alkoxyalkane) Copolymer	PFA
Polypropylene	PP
Polytetrafluoroethylene	PTFE
Poly(Vinyl Chloride)	PVC
Poly(Vinylidene Chlride)	PVDC
Poly(Vinylidene Fluoride)	PVDF

Unlike metallic piping, plastic piping materials do not display corrosion rates and are cheaper, easier for fabrication and installation. Since the cost is the driving force and the technical criteria can easily be met with plastic piping systems, therefore it was decided that thermoplastic material would be used. Unplasticised Poly Vinyl (uPVC) Chloride was found to be the most attractive piping material amongst all the others. The selection of uPVC was influenced by its advantages and the required chemical criteria that is met for the project. The most common advantages of uPVC are:

- Environmentally sound.
- Providing strength and durability, which ensure long service life.
- Corrosion resistant.
- Easy for fabrication and installation.
- Light weight.
- Cost effective.
- Always recommended by manufacturers and widely accepted by codes.
- Available in different sizes.

According to manufacturers and contractors, the uPVC is a joy to work with and it is used in may piping system processes, such as sewers, water eservice line, Drain-Waste-Vent (DWV), irrigation, conduit and various industrial installation. Therefore, the uPVC pipeline was found to be the most suitable pipe for the multiphase flow loop.

6.6.3.2 Pipe sizing

The design criteria for sizing the uPVC piping system was to select the minimum acceptable diameter of the piping necessary to transport the mixture efficiently and the minimum pipe wall thickness to safely handle the internal and external exerted pressure. In order to determine the minimum acceptable diameter, the fluid flow design has to be carried out. The fluid flow design is carried out by determining the flow rate and pressure drops. However it is worth mentioning that before the determination of minimum internal pipe diameter, a review of flow conditions must be made to determine the operational conditions, such as transport velocity, or mean velocity, viscosity, temperature, solids throughput concentration, solids density and particle size analysis of the dispersed phase. Based on the above information related to the above parameters, the minimum inside pipe diameter can be determined. Due to tight cost controls, strict quality standards and working space limitations 50 mm (2") pipe diameter was selected.

On the other hand, the minimum wall thickness was determined depending on the pressure integrity requirements. The pressure integrity can be determined from calculation of the allowable stress and the commercial wall thickness tolerance for the selected pipe diameter (50 mm) pipe from Pipestock.com. After calculating the minimum wall thickness based on pressure integrity and referring to commercially available 50 mm uPVC pipe, a uPVC pipe with a nominal wall thickness of 4.2 mm was selected. Therefore, the sizing of the piping was determined and uPVC pipe (Class E 15 bar BS EN 1452) was decided to be used from pipestock.com with the following dimensions:

Nominal size (inch)	2 inch
Average outside diameter	60.3 mm
Average bore inside diameter	51.9 mm
Average wall thickness	4.2 mm

6.6.3.3 Section mechanical joints

Since a flexible and a versatile flow loop is required, then a special attention must be paid to the selection of mechanical joints of the piping system sections. Also, as the disassembly for maintenance will undoubtedly be required, for example in the case of blockage or replacing a pipeline section by another section within the flow loop, then flanged joints can make the right choice and the most suitable for fulfilment of the objectives. The flanges were supplied by Pipestock.com and its material of construction is the same as that of piping (i.e. uPVC material). They are uPVC full face flanges, drilled BS EN1029-1 PN16 2". The threaded flanges were not selected, as they were found to be not suitable for slurry application, due to accumulation of solid particles between the threads that make the connection and disconnection difficult. Therefore, plane flanges were selected, for which solvent cement was used as a jointing method. It was also paramount to select the appropriate gasket and bolting type to suit the application of the loop. EPDM gaskets (BS 4505 NP10/16 2") for full face flange were selected. While for bolting the flanges, Bright Zinc Plated (BZP) bolts (M16 x 75 mm), nuts and washers were used. The bolts are of Hexagon head part threaded bolt to DIN931 and are grade 8.8 high tensile steel.

6.6.3.4 Piping supports

Piping supports are normally used to support the weight of the pipe, equipments and the material flowing through the pipeline. The overall design and selection of pipe support is dependent on the loading and operating conditions. Since the multiphase flow loop uses plastic pipes, then the spacing of support is very crucial. This is because, unlike metallic pipes, thermoplastic (uPVC) pipes tend to deflect more under load. Based on this fact, the spacing support has to be closer than for metallic pipe. Also, the nature of uPVC pipes is that they can be repeatedly softened by increasing temperature and hardened by decreasing temperature, i.e. they can be more deflected if they are close to any source of heat. Therefore, special care must be taken to avoid laying the pipeline close to any source of heat, or reducing the support span if this is unavoidable. As in this study, in which the returning limb in the mezzanine had to be located close to the radiator, obviously the line is exposed to a higher temperature rather than the design value. Therefore an extra support was employed. As the multiphase flow loop, especially the U-shape inclinable pipeline, consists of a cluster of fittings and concentrated loads of instrumentations, an adequate piping support had to be used. Another requirement for the design of piping support had to be considered, especially for the inclinable pipeline, which was used not only for supporting the load, but also to anchor the whole pipeline and preventing it from slipping down while the table is raised. On the other hand, some heavy instrumentation mounted on the line, such as Coriolis mass flow meter, which weigh 150 kg, were supported exclusive of pipe sections.

After considering all the design requirement and specific consideration for the multiphase flow loop, steel (zinc plated) rubber lined pipe clamps were selected for suspension and support of the pipeline and associated equipments. 51 mm bore size sound insulated standard pipe clamps were selected, which could be coupled with either M8 or M10 threaded rod bar for suspending the pipeline above the surface of the table. Figure 6.12 showing the rubber lined pipe clamp used to support the pipeline. The advantage of the rubber line, or rubber gasket, is to prevent pipe rattling and vibration, as well as tight grabbing the inclinable U-shape section. The selected clamps are also easy to install and adjust to the desired height of the line.

Figure 6.12 Rubber-lined pipe clamp

6.6.3.5 Pipe jointing method

The method used to join the piping system components determine the integral part of the piping system. Therefore, as part of proper engineering design of a piping system, the type and effectiveness of the jointing method and the durability of the resulting joints have to be taken into account. There are many jointing techniques that can be used for jointing uPVC such as solvent cementing, threading, mechanical compression, grooved joints, flanged connectors and elastomeric seal. Each of the above techniques have advantages and limitations. Amongst all, the cementing method was found to be the most attractive and was employed for jointing the piping system. As this method is specially used for wet applications and can offer fast and effective jointing result. It is very important to carry out the cementing procedure in a well ventilated, free of naked flames and dry area, as the cement and cleaner produce harmful vapours. The jointing procedure is outlined below:

1. Each pipe section was cut square to the required length using special cutting machine.
2. The burrs at the cut end of the pipe were removed and 3-4 mm of the leading edge was chamfered to an angle of approximately 30°-40°. An electrical Dremel (model 225) was used for chamfering the end cut, as shown in Figure 6.13c. There were two reasons for chamfering the leading edge of the pipe, firstly for preventing the solvent cement being wiped from both components, fittings and pipe, when pushed together, secondly to eliminate any gap between the pipes of two consecutive flanged sections. Once the flanges are connected, a gap is left between the pipe ends of each section, as the pipe is stopped by the pipe stopper at the end of each flange socket. Obviously, this gap at each flange connections disturbs the flow and contributes into an increase in pressure drop and accumulation of solid particles. Therefore, chamfering the leading edge of the pipe allows the pipe to

go further through the flange socket until the end, Figure 6.13a and 6.13b showing the coupling of a pipe section with the flange, before and after chamfering.

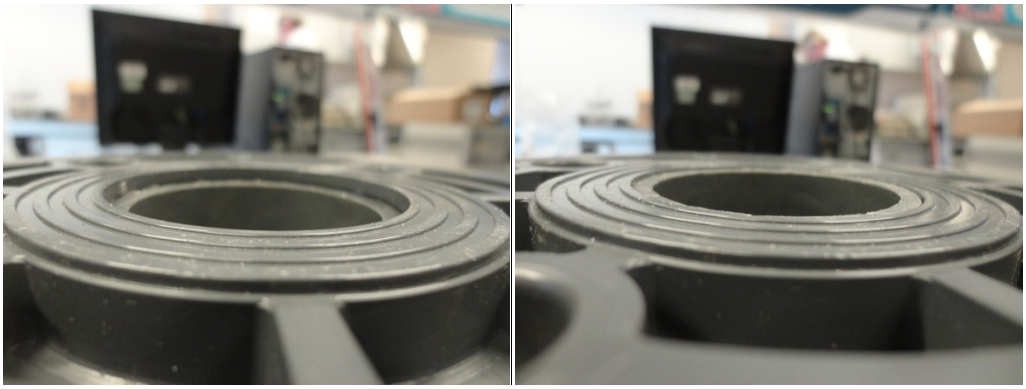

(a) (b)

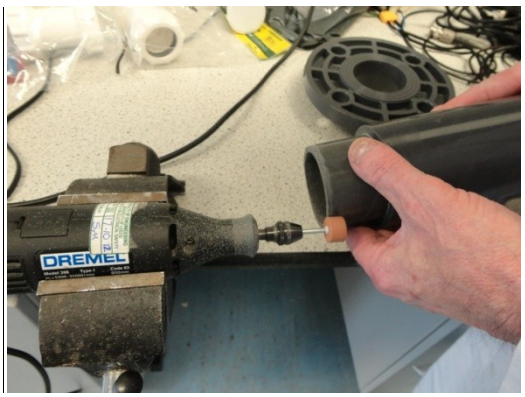

(c)

Figure 6.13 Chamfering the pipe end cut, (a) before chamfering; (b) after chamfering; (c) chamfering the leading edge using Dremel

3. The depth of the pipe fitting socket was measured by dry-fitting the pipe into the pipe fitting socket and drawing a line around the pipe at the edge of the socket.
4. The shiny surface of the pipe, up to the indicator mark, must be taken off using a file or sandpaper. However, the roughing process of both surfaces must not be to the extent that would result in increasing the clearance between them.
5. MEK Cleaner (from pipestock.com) was used for fully cleaning both jointing surfaces with a lint free cloth. It is very important to allow the cleaner to evaporate before applying the solvent cement.

6. An appropriate sized brush (1" flat brush for 50 mm nominal pipe bore size) was used to apply the uPVC solvent cement directly from the tin. First to the fitting socket and then to the pipe using longitudinal strokes, then both, the pipe and fitting, must be pushed together while the cement is wet, ensuring that the roughed area is completely covered with an even layers of cement. It is very important to carry out this step neatly and quickly, as the cement dries up very quickly.
7. After pushing the fitting and pipe together, both pieces must be held for approximately 30-40 seconds (longer time for pipes larger than 2″ bore size). It is crucial to wipe the bead and excess cement from the outer join of the pipe, as this can weaken the wall. It is important not to disturb the joint for 10-15 minutes. The cement within the join is dried after 8 hours under normal conditions (temperatures above 10 °C). However, the manufacturers recommendation is to leave the join for the full period of 24 hours, after which the pipe system can be fully pressure tested.

6.6.3.6 Piping layout

Since piping is a major expenditure and important in the design and construction of flow loops, especially when one considers material costs, fabrication and field costs. Therefore, proper planning and execution of the design and routing of the pipeline have a major impact on controlling the total cost. Piping design and its associated equipment arrangement are interrelated and must both be taken into account in the pipeline design. Of course both of them depend on a sound mechanical engineering as well as chemical engineering background. The pipeline designer must well understand the pipeline layout, equipment and instrumentation arrangement and the functionality of the system. Moreover, the designer requires a good knowledge and understanding of each element within the pipeline, such as piping materials, valves, pumps, tanks, mixers and other equipments that are included into the design.

In this project, proper planning was an important activity performed in the early stages of the design. The whole system was evaluated in the preliminary stages of the design, so as to achieve space conservation and a symmetric piping arrangement. Piping layout was carried by designing dimensioned routings from one point to another point, as shown in Figures 6.14 and 6.15. One of the most important considerations in the piping layout process is to consider the cost of piping material, by keeping the lines as

short as possible, as well as maintaining proper piping flexibility and engineering standards. In addition, some other factors have to be considered in the process of piping layout, such as interference piping flexibility, cost of material, pipe supports, operation, maintenance and safety and construction requirements. One of the most challenging aspects of piping layout was the avoidance of interferences with other facilities within the working area in G.56 Engineering building, such as structural steel and concrete (wall), heating systems (radiator) etc. This is obviously due to space limitation in G.56 laboratory. The voidance of interferences was tedious and time consuming. At the early stages of the design it was necessary to search mentally and visually for interferences and find an appropriate interference-free-rout.

Despite the avoidance of using too many valves in the pipeline, particular attention was given to the placement of valves in the piping system. As improper application and location valves can be detrimental to the flow loop function. It was made sure that the valves are not installed upside down. As a general guide a minimum of 100 mm clearance for all valve hand-wheels and possible removal of the valve.

The routing of piping at the centrifugal pump was also carefully planned, since the pipeline of the pump, particularly the suction section, can adversely affect the operation and life expectancy of the pump. Poorly designed suction line can cause cavitation, as a result of entrainment of air into the pump. The cavitation obviously displaces liquid from within the pump casing, which causes vibrations and the pump out-of-balance. The out-of-balance of the pump causes a slight eccentric shaft rotation, which at the end wears out the bearings and seals. It is worth mentioning that the cavitation results in severe erosion of the impeller. On the other hand, the discharge line was also carefully routed, depending on the efficiency of the pump and system functionality.

The discharge point was designed in such a way so L-shape (or elbows) would be avoided, which contributes an increase into the pressure drop. Instead a heavy duty flexible pipe was connected to the discharge point, so as to achieve a smoothly curved line to follow the rest of pipeline on the table, as shown in Figure 6.16.

In addition, when the pipeline at the pump was designed, several engineering rules, which are mostly recommended by the manufacturers, had to be followed such as:

- The suction and discharge sections were supported independently of the pump, so as to decrease the amount of load transmitted to the pump casing.
- Since the suction section is in horizontal plane, then a minimum of 3-4 pipe diameter is provided between the pump suction point and the bend below the mixing tank.
- In order to avoid any loop or L-shape in the suction line a heavy duty flexible pipe is connected to the discharge point of the mixing tank and pump suction point.

The engineering of pipe supports was carefully considered in the piping layout process. The pipelines are supported and located in close proximity of the tables, the inclinable and rigid table. However, the pipeline was raised by approximately 80 mm, which would allow the space of 31 mm between the bottom of the flanges in the horizontal line and the table. Considering the allowance of an adequate space between the pipeline and the table in the design process was very crucial for installing and dismantling the flanged sections, as well as facilitating the installation of equipments and instrumentations, especially those that have bigger outer diameter than the pipe diameter. In order to achieve this, the supports used are connected to threaded steel rod with allowing an additional length to allow raising and lowering the pipeline.

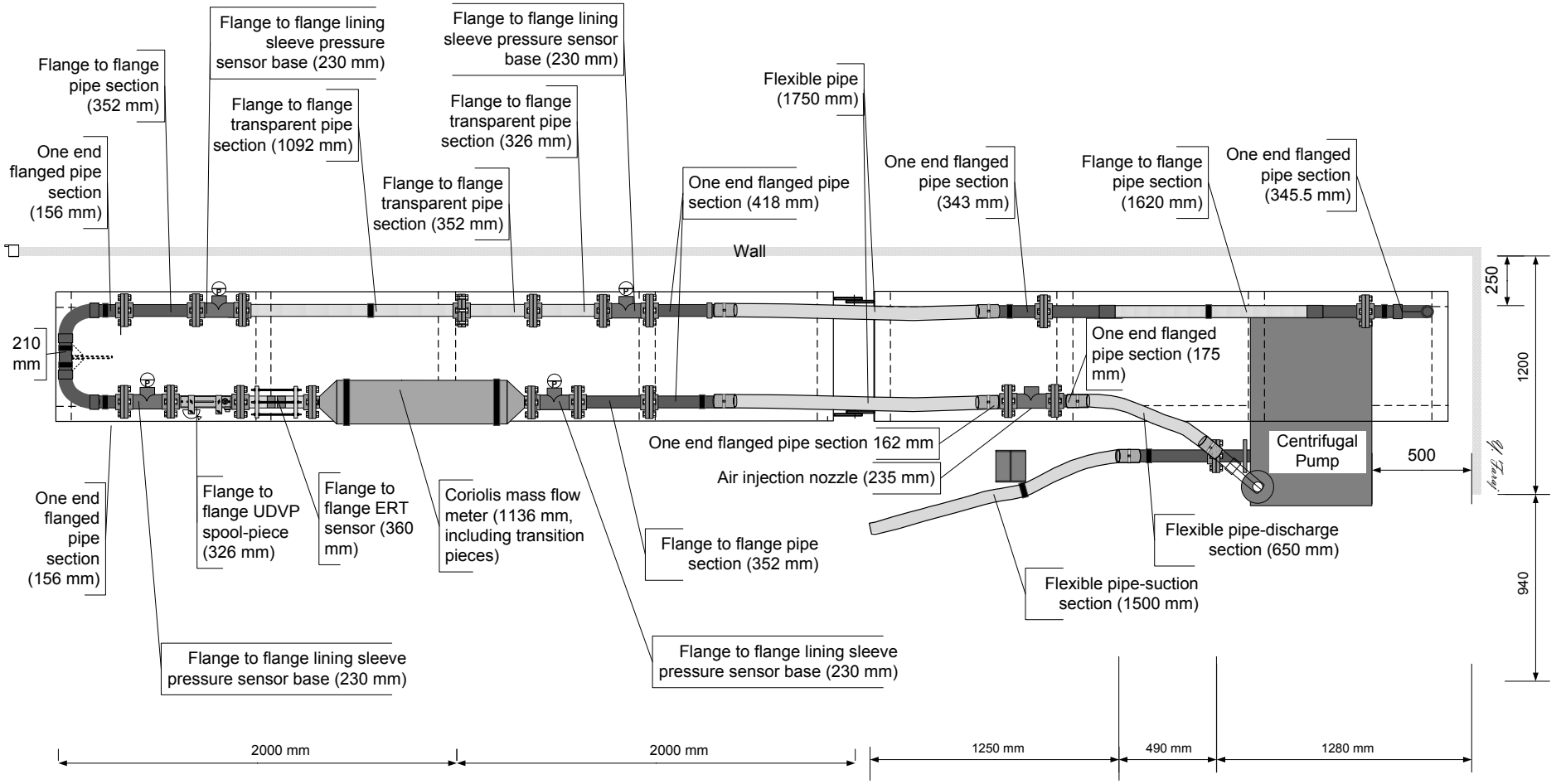

Figure 6.14 Horizontal and inclinable U-shape piping layout, including suction and discharge sections

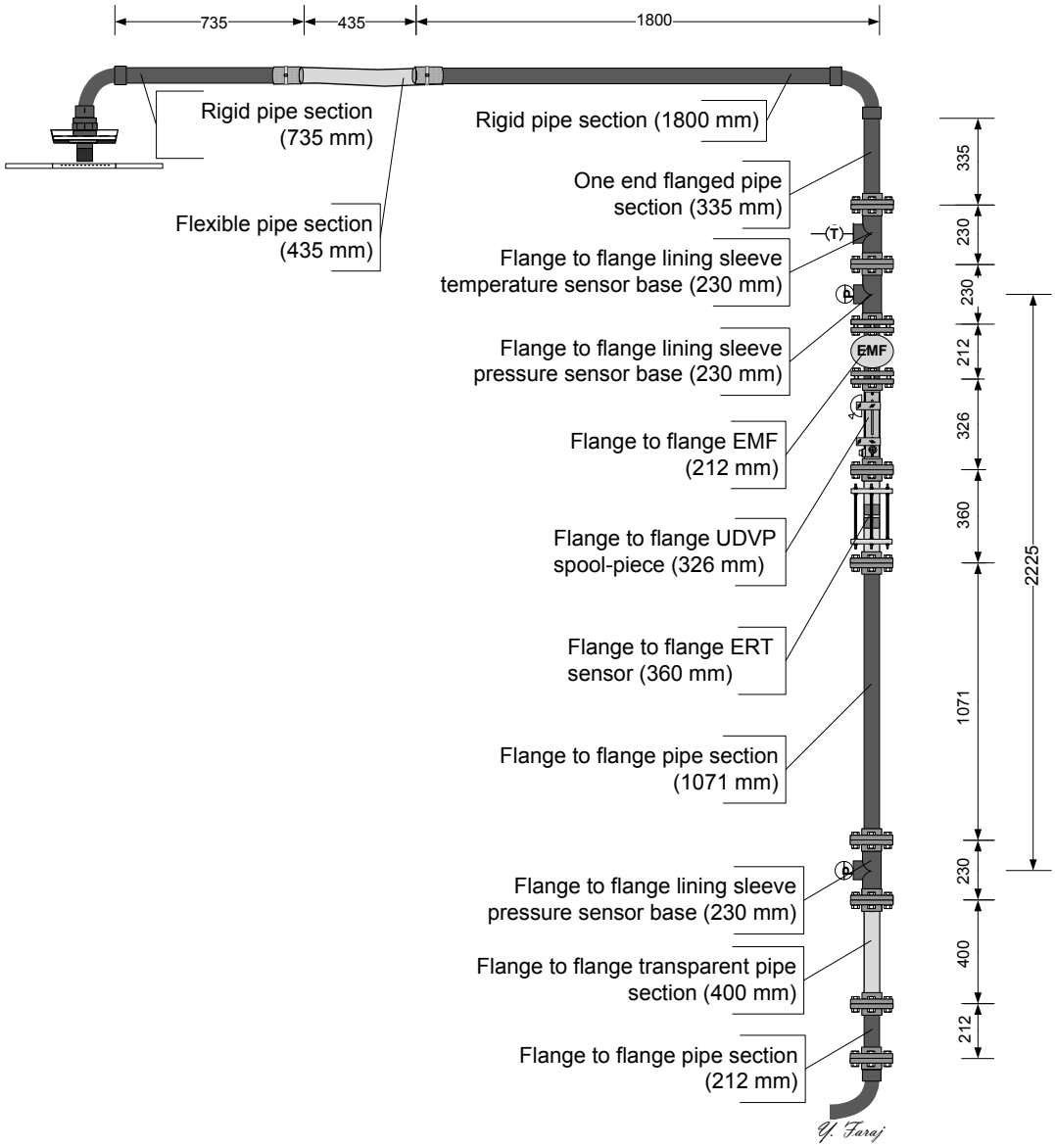

Figure 6.15 Vertical piping layout including returning limb

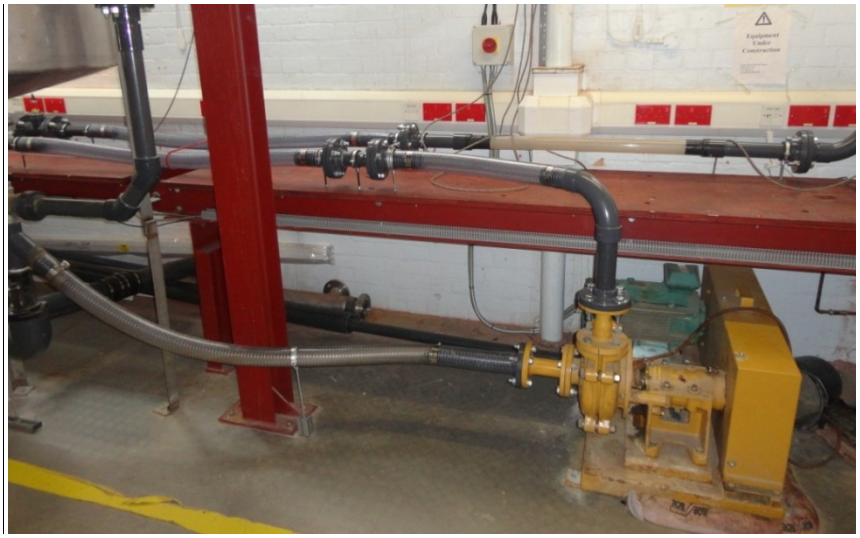

Figure 6.16 The suction and smoothly curved discharge section

Special attention was also given to the aspect of operability, maintenance, accessibility and safety. The operability here refers to the ability of the operator to operate the loop in a an efficient manner within the working area. This design requirement was achieved with consideration for the frequency of operation and the degree of operator's physical effort needed to perform operation. Clearly, due to space limitation, it was not possible to make every section and points of flow loop accessible, but the main focus was upon the parts, which require frequent operation. The ease of maintenance and accessibility of the equipment had to be well considered at the earlier stages of the design. For example, the pump had to be placed under the rigid table close to the wall, but it was necessary to allow sufficient space (approximately 500 mm) away from the wall for maintenance and potential repair. These space locations included removal and installation spaces of the pipeline and its associated instrumentations. In terms of safety in the design and piping layout, special attention should be give from the stand point of the operator. For instance, the equipment or any element of the flow loop that require frequent operation should not be located in such level that the operator would need to stand on a ladder or a platform to reach it. There is a number of codes and standards relating to health and safety had to be followed.

6.6.3.7 Flexible pipe

In order to connect the pipeline on the rigid table to the U-shape pipeline on the inclinable table, two flexible pipe sections are required, so as to keep the flexibility of the line during raising and lowering the inclinable table. Clearly,

these two sections of the pipeline are very important parts of the whole pipeline, as connecting the inclinable U-shape section to the rest of flow loop sections and the flexibility is required for handling the required situation, i.e. some careful consideration in regards to the flexibility and motion expected of the sections. Therefore, in order to select the most suitable type of flexible pipe several important factors has to be considered, which are listed below:

- Sizing.
- Flow temperature and pressure.
- Media.
- Motion type and the amount of motion (bending radius).
- Internal structure.
- Length of the flexible pipe.
- Connection.

The size of the flexible pipe was determined based on the existing piping on either tables. Since the size of existing uPVC is 50 mm, then the size of flexible pipe should fit the aforementioned pipe size. Therefore, the inside diameter of the flexible pipe was selected as 63 mm.

The pressure rating for each type of flexible pipe depends on flow conditions used. As rule of thumb, the maximum operating pressure should be 25% of the nominal burst pressure. The nominal pressure here is referred to as the pressure at which the pipe can be expected to burst. Based on the flow loop specification, the design pressure that corresponds to the maximum pump frequency is 2 bar. Accordingly, it was decided that the flexible pipe should have a working pressure more than the flow loop design pressure, and clearly the nominal pressure is quite above the working pressure. The decision was made that a flexible pipe would be chosen with 4 bar working pressure and not less than 10 bar nominal pressure. On the other hand, as the slurry temperature is expected to correspond to ambient temperature, considering cold weather in winter and hot in summer, and also elevation of temperature as a result of heat generation from the pump. Since the flow loop is build indoor, thus the slurry temperature range is expected to be 1°C in cold weather and 30°C in hot weather. However, with some design tolerance, it was decided to choose a flexible pipe with temperature range -5-50°C.

In terms of the media, or material, since slurry is considered, then it is associated with corrosion and abrasiveness. Therefore, the main consideration in specifying a flexible pipe to select a material, which has a high resistance to the media transported through the pipe. Based on the

nature of aqueous slurry, it was decided to select a flexible pipe with a material that has a high corrosion resistance and abrasion resistance.

Normally, flexible pipes are used depending on the specified application and requirements, such as to avoid excessive vibration, pipe alignment, flexibility of motion and handling the situation etc. The selection of the proper pipe requires careful consideration based on the intended application. In this project, the main reason for using flexible pipe is flexibility of the pipeline during raising or lowering the inclinable U-shape section. The most important factor that determines high degree of pipe flexibility without affecting the process or damaging the flexible pipe (kinking) is the minimum bending radius. Minimum bending radius is the radius, which is measured to the inside of curvature when bending the pipe without damaging or kinking the pipe, as shown in Figure 6.17. Clearly, the minimum bending radius ensures more flexibility of the flexible pipe. Since the range of flow loop inclination angle between the inclinable section and the rigid section is designed to be between 0°-90° from horizontal, then the selected flexible pipe must have a minimum bending radius that allows the flexible pipe to connect the inclinable section, while it is raised to 90° from horizontal to the rigid pipeline section without kinking or damage to the flexible pipe or the connected rigid pipeline. However, it is important not to choose such length that would create a short radius bend, as previously mentioned, using or creating a short radius bend can increase the rate of pipe wear and restrict the flow. Thus it can be concluded that the flexibility factor and the pipe length are interrelated. In order to select the optimum bending radius of the flexible pipe for easy bending without damage and without putting any strain on the connected rigid pipes, an optimum length must be designed. Therefore, a journey through manufacturer's websites revealed that the selected flexible pipe must have a minimum radius between 140-145 mm, and the optimum length was designed as between 1700-1800 mm, while the pipeline is in horizontal orientation. Also, in order to avoid kinking, it was decided to select a reinforced flexible pipe. However, once the table is raised the flexible pipe is not bent to a straight angle, instead it is bent as a curve, which connects the two pipeline sections. The further the table is raised the shorter the distance along the curved pipe trajectory is required. This means that the original connection point is extended by some length, which was found to be 20%-25% of the pipe length. Since both connection ends are not movable, then the extra length must shape another bend to a specific direction. Clearly, this extra bend is not desired and may put one of the connection ends at enormous amount of strain. Therefore, in order to merge the

resulted bend due to extra length with the original bend due to inclination, 1 m section of the fixed plywood on the rigid table is cut, as can be seen in Figure 6.18, so that once the table is raised the flexible pipe bends downwards between the two frame beams.

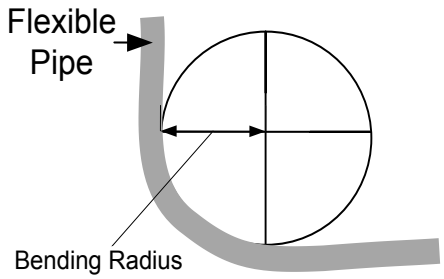

Figure 6.17 Minimum bending radius of a flexible pipe

Figure 6.18 Actual photo of the opening section on the rigid table

Another factor that has to be considered is the internal structure of the flexible pipe. Since any disturbance within the pipe affects the flow and contributes into further pressure drop, especially for slurry flow, then a non-intrusive smooth bore flexible pipe has to be selected.

Based on the factors considered for selection of the most suitable flexible pipe, it was decided to select Armorvin flexible pipe, which is shown in Figure 6.19, to connect the inclinable U-shape pipe section to the rigid pipeline sections of the flow loop. Armorving flexible pipe is supplied by Whitehouse flexible tubing Ltd. (flexible-tubing.com) in standard length of 20

m. It is manufactured from thick flexible PVC and reinforced with a high tensile steel spring.

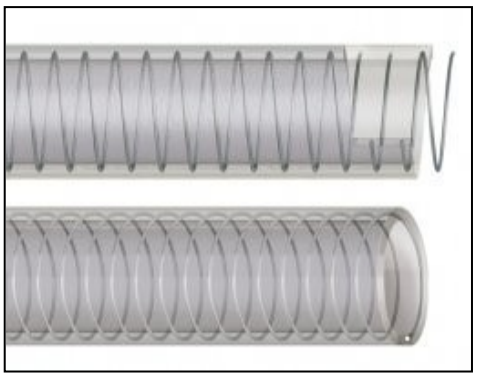

Figure 6.19 Armorvin flexible pipe (Whitehouse flexible tubing)

The selection of Armorvin was influenced by the following technical specifications and advantages, which fulfil all the design requirements for the intended application:

- 60 mm internal diameter.
- 6 mm wall thickness.
- 140 mm inside bend radius.
- 1.8 kg/m weight.
- -10 to 65 °C operating temperature range.
- Reinforced with centrally positioned high tensile steel spring helix, which offers an excellent vacuum throughout and prevent the pipe from being kinked.
- Suitable for dry and wet applications.
- Non-toxic.
- Good abrasion resistance.
- Smooth internal and external bore, which make the flow non-intrusive.
- High impact resistance.
- Good chemical resistance.
- Excellent transparency, which facilitates visualisation of flow.

With regard to connection method, clamps are selected to connect the flexible pipe to the rigid pipe. In order to prevent leaking and a full circle grip of the flexible pipe to the uPVC rigid pipe, super heavy duty clamps were chosen, which are supplied by Whitehouse flexible tubing Ltd. These clamps are manufactured from stainless steel strip and have bevelled edges.

The installation of Armorvin flexible pipe was carried out by cutting the pipe to the desired length using a hacksaw in water. Once the hacksaw reached

the steel spiral wire, the wire bent out and cut with a bolt clipper. However, as the wire protrudes after cutting, as a matter of safety and prevent injury, a pair of pliers was used to bend the wire into the rubber.

6.6.3.8 Pipeline length and test section length

Selecting the piping length is an important aspect of the flow loop design. Since too long flow loop will result in large sample requirement and costly experiment, whereas too short flow loop will not be able to generate an accurate data as a result of non-developed flow. Therefore, a careful consideration has been given to the approach and the test section length. According to Gillies (1991) and Pachowko (2004), the approach length must not be less than 50 pipe diameter, and the test section can be any length between 60-100 pipe diameter. Following the above recommendations, for our 50 mm (2") pipe diameter, the flow loop used in this research must have an approach length not less than 2.5 m and a test section between 3-5 m. Therefore, outgoing limb of the inclinable U-shape section has an approach length of approximately 2 m, while the table is raised and 3 m, while the table is at rest horizontally, and the test section is approximately 3 m.

It is worth mentioning that the above recommendation is only applied to horizontal and near-horizontal sections. For instance, the vertical section does not necessarily have to have an approach length of 50 pipe diameter. This is clearly due to the existing simpler flow patterns in vertical flow. The approach length in the vertical section was chosen to be 20-25 pipe diameter.

The length of the outgoing and returning limbs was designed to be 16 m in total and vertical height of 5 m from the floor and 4 m from the top of the table, which giving a total pipe length of approximately 21 m.

6.6.4 Pump selection

Slurry pump can be considered as the heart of any slurry transport system, as an industry pumps main duty is to introduce to downstream pipeline and unit operations. Also, in flow loop studies, such as the one used in this study, the pump is the main element of the whole pipeline, to which the slurry is pumped and introduced to the rest of pipe sections and equipments.

Slurry pumps are used to transport mixtures of solids and liquids in many industries with the wide range of applications, such as dredging, mine drainage, drilling mud etc. Slurry pumps are normally used for the purpose of pumping a medium with abrasive particles, hydraulically transporting solids or pumping the final product of a process.

There is a large number of pump types available for pumping slurries. All of these types fall into the scope of two main categories, centrifugal pump and positive displacement. However, by far the common type of slurry pumps used are centrifugal pumps. The centrifugal pumps use the centrifugal force, which is generated by the pump impeller to impart energy to the slurry being transported.

In order to size a centrifugal slurry pump a number of factors have to be taken in to account. In the mean time, it is very important to avoid an overestimation of the system resistance (Warman Slurry Pumping handbook), otherwise it will lead to the following consequences:

1. The pump provides a larger flow than it is required.
2. More power consumption.
3. Overloading the motor and causing damage.
4. Creating of cavitation due to poor suction conditions.
5. Increase of wear rate.

Therefore, for sizing the centrifugal pump in this study attempts were made to make the best estimate of system head and the final required pump power was calculated with an addition of safety margins. It was then decided that for the multiphase flow loop, which is mainly used for slurry, a centrifugal slurry pump to be used. The decision of using the centrifugal slurry pump was based on the abilities of centrifugal pumps that are listed below:

1. The ability to handle larger flow rates.
2. The ability to handle larger solid particle size.
3. The ability to withstand high discharge pressure.
4. Smoother pressure characteristics.
5. Longer wear life.
6. Relatively lower cost than for positive displacement pumps.
7. Having heavy duty pump bearings.

On the other hand, one of the disadvantages of centrifugal slurry pumps is the operation of the pump at a constant flow rate, i.e. it is very difficult to alter the discharge flow rate of a centrifugal pump. Despite that, this limitation can be overcome by either throttling the pump to the desired flow rate or using variable speed drive, which allows variable speed output. In the flow loop used in this study, the centrifugal pump is fitted with a variable speed drive, which allows the total discharge pressure, and thus the flow rate to be controlled and adjusted. The variable speed drive can also provide the ability to maintain particular output to compensate of pump and pipeline

wear. The results of calculations for sizing the pump are highlighted in the following subsections.

6.6.4.1 Pump performance

Assuming that the flow loop is a fixed control volume, on which a shaft work is produced by the pump in a steady state condition. Mass of slurry flowing at a certain rate through a single planer entrance (the surface of the tank) and a single planar exit (at the point the slurry is discharged into the holding tank, as shown in Figure 6.20.

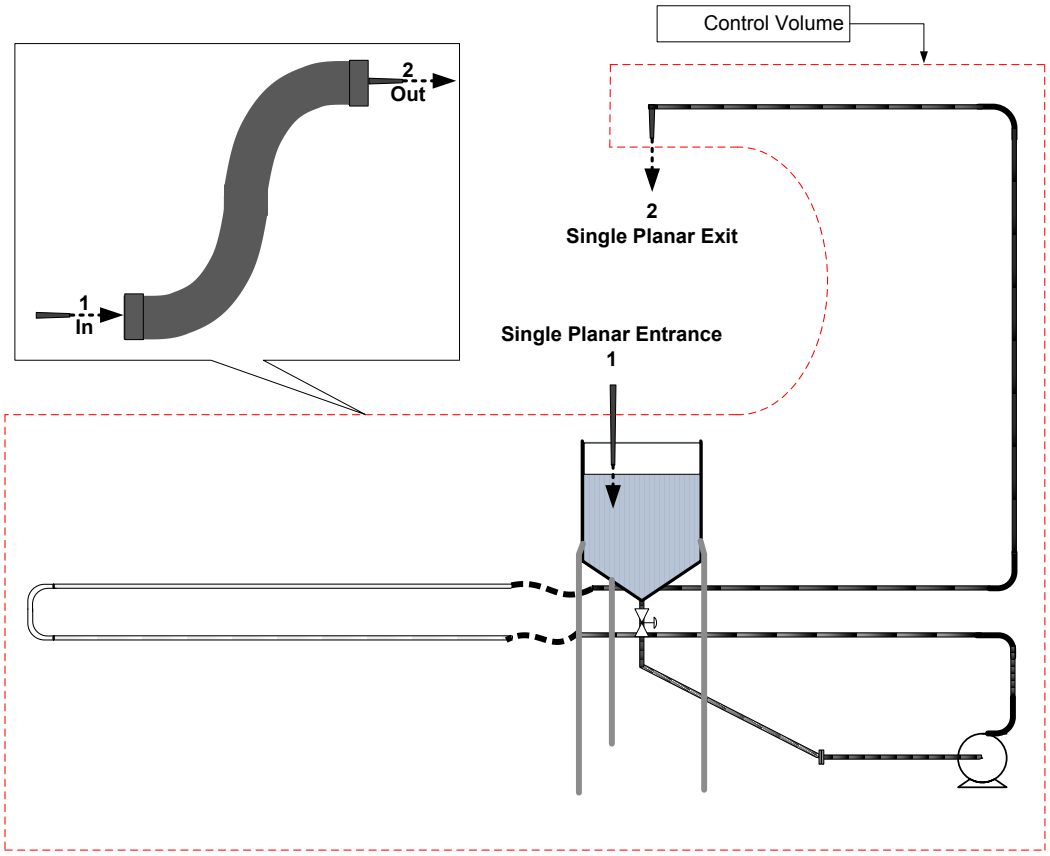

Figure 6.20 The flow loop as a fixed control volume

A balance equation for the sum of kinetic and potential energy on the control volume can yield Mechanical Energy Balance (or Bernoulli Equation). The Bernoulli equation, or sometimes called Engineering Bernoulli Equation, for incompressible flow can be written as (Perry, 1997):

$$\frac{P_1}{\rho} + \alpha_1 \frac{V_1^2}{2} + gZ_1 + \sum W_s = \frac{P_2}{\rho} + \alpha_2 \frac{V_2^2}{2} + gZ_2 + l_v \quad (6.2)$$

Rewriting the equation in a customary form, as shown in Equation 6.3.

$$\frac{P_1}{\rho g} + \alpha_1 \frac{V_1^2}{2g} + Z_1 + \sum \frac{W_s}{g} = \frac{P_2}{\rho g} + \alpha_2 \frac{V_2^2}{2g} + Z_2 + \frac{l_v}{g} \quad (6.3)$$

Where, P_1, V_1, Z_1 denote the pressure, slurry velocity at inlet and the elevation of inlet level respectively. Similarly, P_2, V_2, Z_2 are related to the exit planar. *g* is the gravitational acceleration (9.806 m2/s), ρ is the density of the mixture. The factor α is the ratio of the cross-sectional area to the cube of the average velocity. In turbulent flow α is usually equal unity and for a circular pipe flow it is typically about (1.07). $\sum W_s$ is the summation of the work done by moving solid boundaries. Here, in this project, the work is done by the pump impellers and it is called shaft work. The last term, l_v, is the rate of viscous energy dissipation. In other words, the viscous or frictional loss term that accounts for the pipeline and its associated fittings, such as elbows and valves.

The slurry density (ρ_m) can be calculated using the following equation from Abulnaga (2002):

$$\rho_m = \frac{100}{\frac{C_w}{\rho_s} + \frac{(100 - C_w)}{\rho_l}} \quad (6.4)$$

Where, C_w is the slurry concentration by weight that has already been assumed as 40%. This amount has been assumed on the basis that the flow loop may also be used for a high slurry concentration. ρ_m is the slurry density, ρ_l is the liquid density, which is water, and equals to (1000 kg/m^3). ρ_s is the density of the solid phase (sand) and it was found to be (2650 kg/m^3)(or the specific gravity of 2.65). Using the above data the slurry density was calculated as 1331 kg/m^3.

Since the volumetric flow rate Q is the product of average velocity and the cross sectional area, then the slurry velocities, V_1 and V_2, at the entrance and the exit of the system can be calculated using Equation 6.5:

$$V = \frac{Q}{A} \tag{6.5}$$

For a flow rate of 35.28 m^3/hr (0.0098 m^3/s) through the tank cross-sectional area (0.63 m^2), the velocity V_1 was calculated to be 0.015 m/s. As the same amount discharging from the system through a pipe cross-sectional area of 0.00196 m^2, then the velocity V_2 was calculated to be 5 m/s.

Since the atmospheric pressure of inlet and discharge point (P_1 and P_2) of the flow system are similar, then they will be eliminated at either sided of the Engineering Bernoulli Equation.

Z_1 and Z_2found to be 2.70 and 2.80 respectively.

The frictional loss term is the product of the summation of the total head loss due to friction in pipes and the total head loss due to fittings. Therefore, it can be written as Equation 6.6:

$$\frac{l_v}{g} = \frac{\sum h_L}{g} + \frac{\sum h_f}{g} \tag{6.6}$$

The total head loss due to friction for incompressible flow in sections of straight pipe of constant diameter, using fanning friction factor, can be determined by the Equation 6.7 (from Perry,1997):

$$\sum h_L = \frac{2fV^2L}{Dg} \tag{6.7}$$

Where, L is the length of the pipe, D is the pipe diameter, f is the fanning friction factor, which can determined from the friction factor as a function of pipe surface roughness and Reynolds Number (Re_m) (Perry, 1997). However, in turbulent flow, the friction factor for rough pipe follows the

smooth tube curve for the range of Reynolds Number, as shown on the friction factor graph (or Moody Diagram) in Appendix C. The mixture Reynolds number can be determined using the following equation:

$$Re_m = \frac{\rho_m V D}{\mu_m} \tag{6.8}$$

Where, ρ_m is the mixture density, V is the mixture velocity through the pipe diameter D with a viscosity of μ_m .The mixture viscosity can be determined using Thomas equation (1965) (from Abulnaga, 2002):

$$\frac{\mu_m}{\mu_l} = 1 + K_1 C_v + K_2 C_v^2 + A\, e^{B C_v} \tag{6.9}$$

Where, μ_m is the absolute (or dynamic) viscosity of the slurry, μ_l is the absolute viscosity of the carrier liquid, K_1 is the Einstein Constant (2.5) and K_2 has been found to be in the range of 10.05-14.1 (from Abulnaga, 2002), $\mathrm{C_v}$ is the solids concentration by volume, A & B are constants and they have values of 0.00273 and 16.6 respectively.

However, the value of $\frac{\mu_m}{\mu_l}$ can be determined from the graph shown in Figure 6.21, in accordance with the Thomas equation (1965). This graph is widely accepted in the industry for heterogeneous mixture of a Newtonian Rheology.

The solids concentration by volume, C_v, can be calculated using Equation 6.10 (from Abulnaga, 2002):

$$C_v = \frac{C_w \rho_m}{\rho_s} \tag{6.10}$$

C_v was calculated to be 20% by volume. Then based on solids concentration be volume (20% v/v) the ratio of mixture viscosity versus viscosity of carrier liquid ($\frac{\mu_m}{\mu_l}$) was determined, from the graph shown in Figure 6.21, as 1.978. If the viscosity of carrier liquid (water) is 1.002 x 10-3 pa.s (at 20°) then the mixture viscosity would yield 1.974 x 10-3 pa.s.

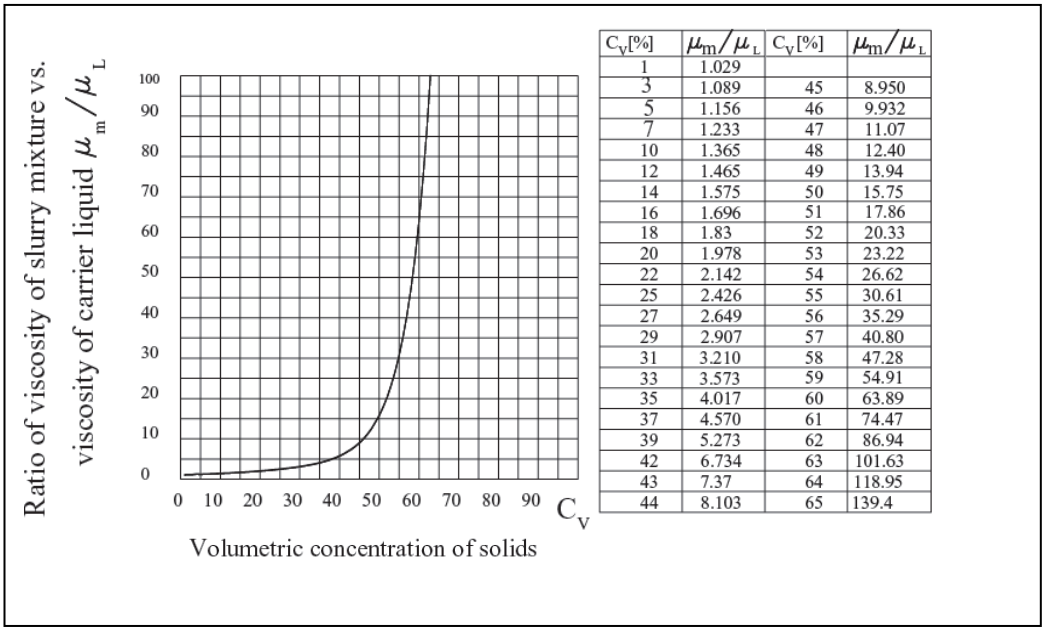

C_V[%]	μ_m/μ_L	C_V[%]	μ_m/μ_L
1	1.029		
3	1.089	45	8.950
5	1.156	46	9.932
7	1.233	47	11.07
10	1.365	48	12.40
12	1.465	49	13.94
14	1.575	50	15.75
16	1.696	51	17.86
18	1.83	52	20.33
20	1.978	53	23.22
22	2.142	54	26.62
25	2.426	55	30.61
27	2.649	56	35.29
29	2.907	57	40.80
31	3.210	58	47.28
33	3.573	59	54.91
35	4.017	60	63.89
37	4.570	61	74.47
39	5.273	62	86.94
42	6.734	63	101.63
43	7.37	64	118.95
44	8.103	65	139.4

Figure 6.21 Ratio of viscosity of mixture versus viscosity of the carrier liquid in accordance with Thomas equation for settling slurries (Abulnaga, 2002)

In order to take into account any design errors or uncertainties, then a high viscosity value is to be chosen by an extra of 30%, which would make it 0.0025 pa.s. Therefore the mixture Reynolds Number would be approximately 133100.

The surface roughness for uPVC pipe (category E class, Plastic and Perspex) was found to be 0.0025 mm, then the relative roughness ($\frac{\varepsilon}{D}$) was calculated to be 0.05. Then, the friction factor was found, on the Moody Diagram, as 0.001.

The total head loss due to friction in pipes for 20 m pipe length yields 1.4 m. Similarly, the head loss due to fittings can be calculated using Equation 6.11 (from Perry, 1997).

$$\sum h_f = \frac{\sum KV^2}{2g} \tag{6.11}$$

Where, K is the additional frictional loss (which is equivalent number of velocity heads). There is one diaphragm valve and six 90° elbows (long

radius) in the flow system. The K value was found from Perry (1997) for diaphragm valves (assuming fully open) as 0.44. Also the K value for the elbows mentioned earlier was found to be 0.45. By adding up all K values and calculating the above equation, the total head loss due to fittings was determined as 0.6 m.

Calculation of Equation 6.2 yields the shaft work per unit of mass ($\sum W_s = \frac{W_s}{\dot{m}}$) flowing the flow system, which was calculated to be 33 kw/unit mass. Multiplying this value by the slurry mass flow rate would produce the power required by the pump, which would be (13.2 kw). However, it is very important to take any design uncertainties into account. Therefore, 10% was added to the actual value and yielded the power requirement approximately (15 kw).

6.6.4.2 Suction limitations

Every pump requires a minimum suction head to operate properly. This is called the Required Net Positive Suction Head $(NPSH)_R$, (Perry, 1997; Brown and Heywood, 1991; Pachowko, 2004). This parameter is usually published by the manufacturers and it should be equal or less than the Net Positive Suction Head Available $(NPSH)_A$, so that the cavitations are avoided. Cavitations occur, when the absolute pressure of the pump is below the vapour pressure of the liquid in the slurry at the operating temperature. As a result the vapour bubbles appear and release the energy, which cause damages to the pump components, such as keys, loosing of rotor and shaft breakage.

Therefore, the $(NPSH)_A$ must be calculated at the design stage and has to be equal or greater than $(NPSH)_R$ for the desired capacity. The $(NPSH)_A$ can be calculated as:

$$(NPSH)_A = h_a + h_s - h_{vp} - h_f - h_i \qquad (6.12)$$

Where h_a is the atmospheric head and is equal to 10.34 m, as the holding tank is vented to atmosphere. h_s is the static head in (m), which was found to be 2.35 m. h_{vp} is the vapour pressure head of water at 20 °C and is 0.19 m. h_f is the frictional losses and was calculated from Darcy's formula with the help of equivalent length table for fittings and valves. h_f was calculated to be 1.08 m. h_i denotes the safety factor of 0.7 m as a compensation to the losses

after the fluid entering the pump. Finally, $(NPSH)_A$ was estimated as 10 m with considering any design uncertainties.

According to Pachowko (2004) in order to avoid cavitation phenomenon, the $(NPSH)_A$ is usually taken to be 0.5-1 m less than $(NPSH)_R$.

The total dynamic head was also calculated using the following equation from Perry (1997):

$$\Delta h = (h_d)_t - (h_s)_t \tag{6.13}$$

Where $(hd)_t$ is the total discharge head and is calculated from:

$$(h_d)_t = (h_s)_d + \left(h_f\right)_d \tag{6.14}$$

Where $(hs)_d$ is the discharge static head and $(hf)_d$ is the head loss in piping and fittings, which was calculated from the Darcy's Equation and estimated as 12.6 m. The total discharge head was calculated as 30 m. Similarly, the total suction head was estimated to be 9 m. By combining these two values the total dynamic head was calculated as 21 m.

From the above calculations, it was concluded that a 15 kw pump would be satisfactory to overcome the total head difference. As the cost is the main point of consideration, therefore, it was decided to use the existing pump, which is in G.56 laboratory/Engineering Building and used by the previous researcher and meets the requirements. This decision was made based on the fact that this pump meets the required pump capacity of our design and it has been designed for heavy duty slurry pumping. It was also decide to use the same (15 kw) Digi-drive frequency converter, in order to control slurry flow rate.

6.6.5 Equipment design

A properly designed and arranged equipments of any pilot plant flow loop will undoubtedly provide an excellent flexibility and capability of the loop to generate a promising data over a wide range of conditions. Some of these equipments may be used for different purposes, such as the measuring tank and the flow diversion system, which are used for calibration purposes and producing one of the important parameters delivered solids concentration. Therefore, it is crucial to design a proper tank to fulfil the objectives and cover the whole range of intended conditions. Another important piece of

equipment within the flow system is the holding or mixing tank, which can have an adverse effect on the loop operation and the data generated from the loop, if it is not carefully designed or located within the whole system. For example, when designing the mixing tank it is very important to consider the level of slurry within the tank. If the level of slurry in the mixing tank is not kept high enough, it results in air entrainment in the mixture and introduced to the pump. Also low slurry level within the tank have a negative impact on the suction head. Therefore, the design functionality and layout of the main equipments used within the multiphase flow system are described below. These equipments are mixing tank, measuring tank, flow diversion system, drainage system, slurry valves and the ultrasound probe holder.

6.6.5.1 Mixing tank

The holding tank has to be designed with a conical section rather than a flat base. As this will prevent the accumulation of solid particles at the dead ends of the tank and facilitate the drainage system at the end of each experiment. To ensure that enough suction head is provided to the pump, the volume and level of the slurry in the holding tank are very important to be carefully designed. Pachowko (2004) successfully designed a holding tank with a capacity 10 times the volume of the pipe work of his flow loop (24 m). By following Pachowko's design procedure we should have a holding tank with a volume 10 times the volume of the 21 m pipeline length. If the volume of 21 m pipeline length with 50 mm diameter is 0.04123 m^3 (41.23 litre), then 10 times of the above value would make the volume of the holding tank, which is 410.23 litres.

When the flow is diverted into the measurement tank, the slurry level would decrease by the amount added to the measurement tank. This would have a negative impact on the suction head. The holding tank volume has to be designed with adding some extra volume to compensate the amount of slurry added to the measuring tank. Therefore, the holding tank volume was designed to be 500 litres, some of which replace the amount of slurry diverted to the measuring tank.

The total height of the holding tank can be calculated, if assumed that the diameter of the cylindrical part is the same as its diameter. Also, assuming a slope of 20% (11°) at the base of the conical part, which can provide an easy surface for the solid particles to slip down the tank, makes the height of the conical part 0.1 of tank diameter. Figure 6.22 showing the schematic drawing of the holding tank. The height of the tank can be determined using

the following equation, in which the first and second term on the right hand side refers to the cylindrical and conical part respectively.

$$V = \frac{\pi D^2 H_1}{4} + \frac{\pi D^2 H_2}{12} \tag{6.15}$$

Where V is the volume of the mixing tank, D is the tank's diameter; H_1 and H_2 are the height of the cylindrical and conical part respectively.

Using the above equation, the diameter and the height of the cylindrical part was found to be 900 mm and the height of the conical part is 100 mm. However, if the height of the cylindrical part was increased to 1 m, to avoid splashing, then the total height of the tank would be 1100 mm.

The result of holding tank design shows that the dimensions are almost similar to that of the existing holding tank in Engineering building, which has been used by the previous researcher. Therefore, in order to reduce the cost of the project, it was decided to use the existing tank along with its three blade impeller. The mixer is known to be the best mixer with lowest power consumption and is totally suitable for slurry mixing. The tank is also fitted with four equi-spaced baffles, which are useful for avoiding the formation of vortices in the tank during the experiment.

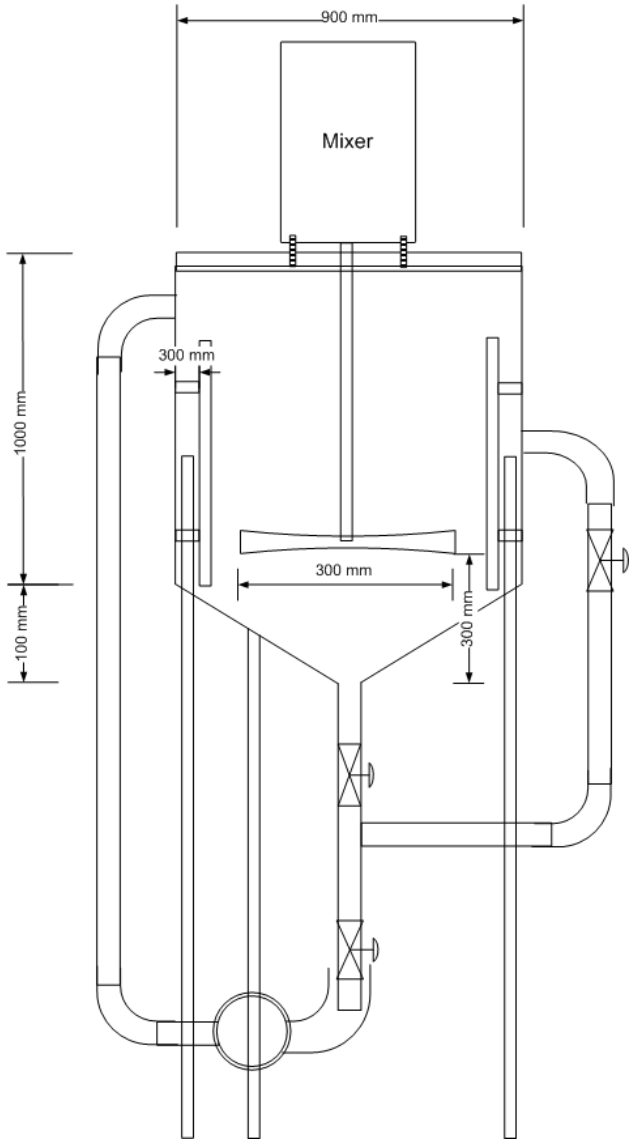

Figure 6.22 The schematic drawing of the holding tank

6.6.5.2 Measuring tank

The measuring tank, which is an important element of the flow loop, is mounted on three load cells and used to measure several parameters of bulk slurry flow. The most important parameters that are measured using this tank are highlighted bellow:

- Slurry density
- Delivered solids concentration
- Slurry velocity at the discharge point
- In-situ solids concentration at high transport velocity
- Slurry flow rate

The principle of using the measuring tank is to collect the diverted slurry and determine the relevant flow parameters. Clearly a diversion system is required to direct the slurry into the tank. The design and functionality of the diversion (or flow switch system) is described separately in the following subsection. The schematic drawing of the tank along with the flow diversion system is shown in Figure 6.23.

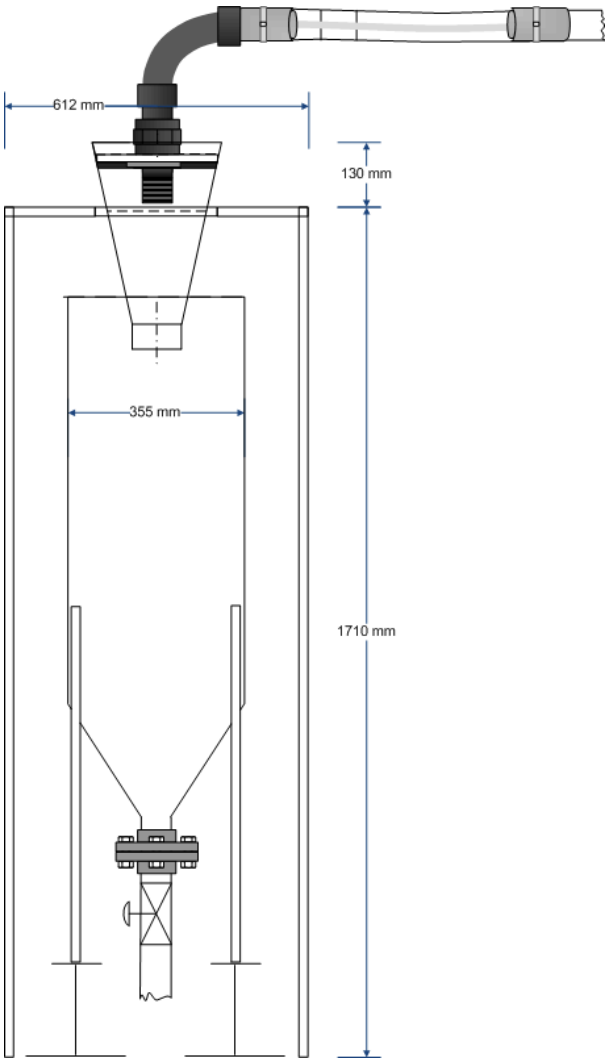

Figure 6.23 Schematic drawing of the measuring tank

The measuring tank is constructed from steel and has a cylindrical section, which is 850 mm high and has 35.5 mm internal diameter, and the conical section which is 200 mm high. The conical section is conned by 45° to prevent the accumulation of solid particles at the bottom of the tank and allows them to be easily drained at the end of diversion process. The total capacity of the tank is 90 litre. The total height and capacity of the tank is

very important to be taken into account in the design process. Therefore, some leeway was aloud for the tank to avoid splashing and overflow while diverting the slurry. In order to determine the slurry level within the tank a graded glass tube is mounted at the half point of the cylindrical section. A diaphragm valve is also installed at the bottom of the tank (at the discharge point of the tank) for easy collection of diverted slurry during the diversion process and drainage at the end. The measuring tank is located above the mixing tank to avoid any extra bend in the pipeline and allow the slurry to be drained through a straight part section into the mixing tank.

6.6.5.3 Flow diversion system

In order to facilitate the flow diversion process and obtain more accurate data, a flow diversion system was designed, the geometry and dimension of which is shown in Figure 6.24.

The main part of the system is a steel container which is split in to two port circular sections with 99 mm outer diameter, each of which fits into 100 mm (4 inch) PVC pipe. One of the sections directs the flow into the mixing tank and the other one into the measuring tank. On either side of the steel container two tracts are fixed, through which a 50 mm thick Perspex sheet slides. Both tracks are extended on either side of the steel container by 160 mm, which accounts for the distance between the centre lines of the two sections. In order to avoid accumulation of the solid particles and splashing, the bottom of the steel container at the outlet of each section was designed as a curved shape, on which the solid particles roll down. In other words, any flat dead end within each section is avoided. 600 mm long flexible pipe is used to connect the main pipeline to a pipeline fitting section, which is going through the sliding Perspex sheet. A union system is used to fix the line at the Perspex sheet point. The length of the Perspex sheet has carefully been designed, so as to allow a flexible and easy switching of the flow between the two sections. The length of the pipe section, which is connected to the bottom of the sheet and through which the flow is discharged into each section, must be long enough to avoid splashing. However, some distance (0.15 mm) must be kept between the discharged pipe section and the split plate inside the steel container, so that the pipe does not catch the plate while sliding the Perspex sheet.

It is also very important to use some type of stoppers at the end of the two tracks, to keep the Perspex sheet in place within the track. Therefore, welded hinges (two wings and welded bush) are used in the switch system in this study. The bush is welded to an L-shape metal bar (8 mm diameter),

which pivots 360° and it is used to stop the Perspex sheets to slide out of the track under the influence of flow pressure, while the flow is discharged into the mixing tank. The whole system is designed in such a way that the centreline of the discharge pipe section is aligned to the centreline within the pipe section, by sliding the Perspex sheet all the way through to the end. A drawer handle is fixed to one end of the Perspex sheet which enables the operator to easily switch the flow by pulling and pushing the Perspex sheet through the track.

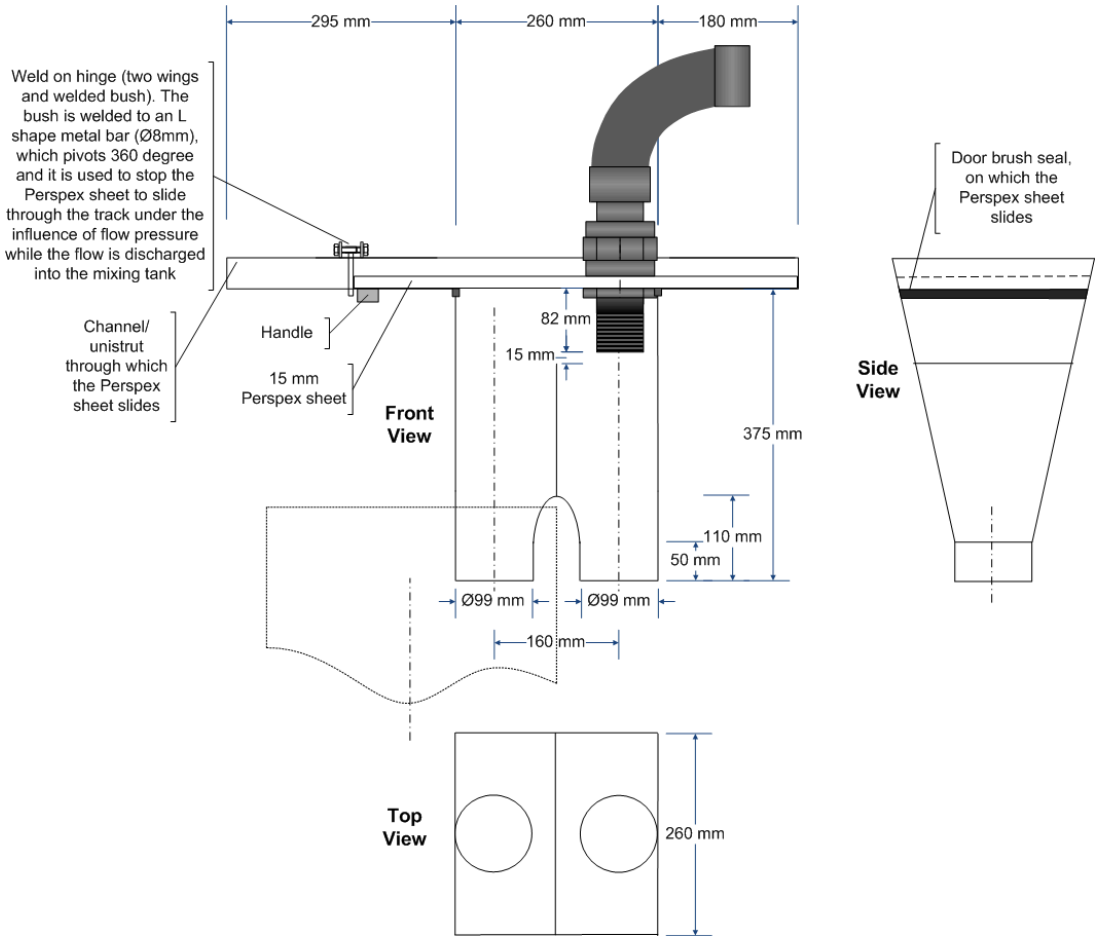

Figure 6.24 Schematic drawing of the flow diversion system

In order to avoid splashing and spillage two door brush seal sections were fitted to the steel container perpendicular to the sliding direction and they are in total contact with the Perspex sheet. The whole system is supported by a unistrut support frame structure, in a way that has no contact with the measuring tank. As any contact with the measuring tank will result in incorrect readings of the load cells.

The testing of the system concluded that diversion of the flow through sliding of the Perspex sheet provides a convenient means of controlling the flow, thus obtaining a good quality measuring data.

6.6.5.4 Drainage system

A drain-line is a necessary feature of the open loop. The drainage system can be used for removing the slurry directly from the bottom of the holding tank, at the end of each experiment.

The drainage system used, as a important element of the whole flow system, consists of three tanks (large, medium and small), the actual photograph of which is shown in Figure 6.25. The three tanks are connected to each other via extended pipelines at the top and bottom level. The top connections are permanently open, while the bottom connection lines can be controlled via three diaphragm valves. This technique is based on settling characterisation of solid particles. As the drainage line goes through the three tanks, the solid particles settle at the bottom of the tanks successively, while the carrier liquid (water) flows into the next tank and finally to the drain. During each draining procedure, while the mixing tank is drained, all of the valves are closed, so that the solid particles are trapped within the tank. This way, once the slurry enters into the first tank, the solid particles settle at the bottom of the tank due to gravity and the carrier liquid flows into the next tank and so on. Based on previous experience, after each drainage procedure, a very few coarse solid particle within (very fine particles in water) were noticed in the third tank. This clearly confirms the efficiency of the system. The settled solid particles then can easily be collected from the three tanks and disposed off in accordance with health, safety and environmental standards.

Figure 6.25 Actual photograph of the drainage system

6.6.5.5 Slurry valves

According to Brown and Heywood (1991) the first rule on application of valves in slurry systems is to avoid using them, if possible. This is due to potential leakage and blockage.

The common valves used in slurry systems, based on the type of slurry, are knife gate, diaphragm, pinch, plug, ball and butterfly valves. However, based on the economical aspect and suitability, the diaphragm (straight through type) is used throughout the flow loop in this research. Relative low cost and ease of maintenance make the diaphragm an excellent choice in this project.

6.6.5.6 Ultrasound probe holder

The ultrasound transducers used in the multiphase flow loop are non-wetted transducers, i.e. they are not in direct contact with the flowing slurry. This is obviously due to abrasiveness of slurry and avoidance of the transducers to be subjected to wear. Therefore they are used as clamp-on transducers. This implies that they are clamped on to the pipe and send their ultrasonic pulses through the PVC pipe wall. In order to avoid vibration of the transducer and determine a good fixture on the pipe wall, along with obtaining a good quality of data a robust and flexible clamp-on probe holder has to be designed. This would also ensure an easy installation of the transducer on any section of the flow loop.

The clamping transducer fixture consists of a solid PVC bar section (250 mm x 55 mm x 15 mm), and the two pipe clamps are fixed on either end of the PVC bar to suit 50 mm pipe, as shown in Figure 6.26.

In order to ensure a good coupling, robustness and versatility of the system, it is split into two sections. One of the sections (variable angle region) is used to fix the transducer non-intrusively, with a rotating variable angle section. The transducer can be adjusted along the spoolpiece section, by sliding another PVC bar (93 mm x 30 mm x 10 mm) variable angle section (125 mm long). The sliding PVC bar can easily be tightened or loosened with a BZP wing nut, which enables the operator to adjust it without using tools.

On the other hand, a solid circular PVC section (50 mm long and 20 mm OD) is attached to the sliding PVC bar to slide along the variable angle section. A hole is drilled across the circular PVC bar, so the transducer can go through and reach the pipe wall, along with another hole perpendicular to the transducer hole for a screw pin to tight fix the transducer. Since accurate determination for the Doppler angle is a key issue for many UDVP application (Geisler, 2001). Therefore a protractor is also fixed across the

circular PVC section in such a way when the circular PVC section is rotated, so the protractor too to determine the Doppler angle. In order to provide a more robust system which would facilitate the use of transducers with different diameter, several circular PVC sections were fabricated and could easily be replaced via the BZP wing nuts. On the other hand all the elements of the second section (90° angle section) has similar structure as that of variable angle section, except that the transducer, which is fixed on this section can only provide 90° Doppler angle. It is believed that this section can be used if an investigation regarding the solid bed in stationary and sliding bed flow is sought. However, it will not render any sign of axial velocity, as the axial velocity component is zero. In addition, two bubble levels (spirit level or bulls eye level) are attached to the clamp-on fixture system to determine whether the pipe surface test section is horizontally levelled or not. Since the ultrasound measurements are intended to be carried out non-intrusively on the multiphase flow loop, then the transducer should be mounted on the pipe surface. However, it is very important that the face of the transducer is totally in contact with the flat surface of the pipe wall. Otherwise the sound signals are attenuated or side scattered due to interaction of air and emitted ultrasonic waves, thus affecting the measuring solids velocity (Wang *et al.,* 2003).

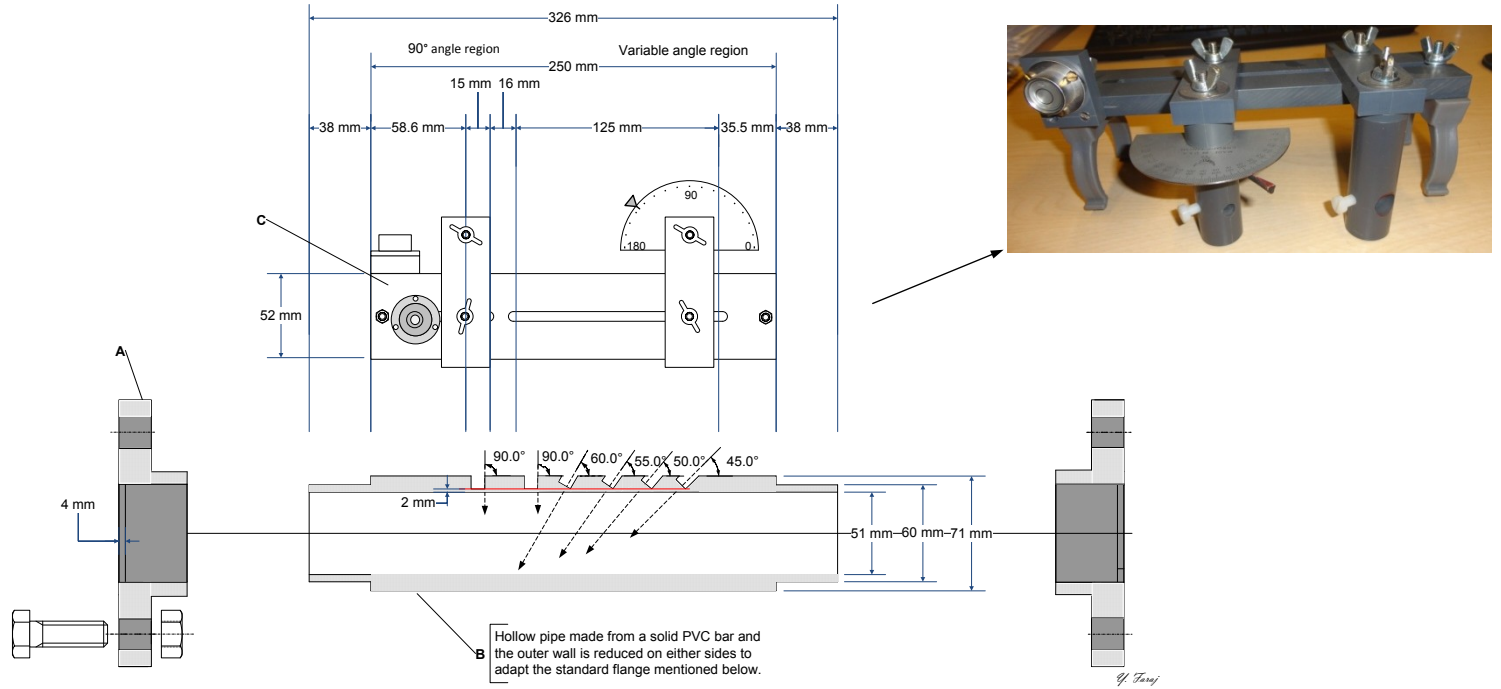

UDVP probe holder and flanged 2" ID spoolpiece		**Company**	**TIME IN REQUEST:**	**APPROVED BY:** Prof. M. Wang	**DWG NO.**	**ITEM**	**QTY.**	**DESCRIPTION**
DRAWN BY:	Y. Faraj	University of Leeds/ OLIL	1 week	**SIGNATURE OF RT:**	2	A	2	PVCu Full Face Flange Drilled BS 10 D & E Plain 2"
						B	1	PVCu Pipe, Wall thickness reduced from 10 to 4.5 mm
DATE:	2 March 2012	**SCALE**	1:2	**MATERIAL:** PVCu	**SHEET** 1	C	1	Clamp-on UDVP probe holder (PVCu)

Figure 6.26 Showing the UDVP probe fixture and 50 mm ID flanged spoolpiece

Based on this phenomenon, it was decided to drill two holes into the pipe wall, where the transducers are placed. However, the Doppler angle (the Doppler angle is the one over which the probe is tilting) plays a very important role in the measurement of solids velocity, as it provides the component of true solids flow velocity vector. Also, depending on the application, an accurate determination of this angle is always a problem for the ultrasound application. For example, the lower the angle is the higher resolution can be achieved. However, with lower Doppler angle a very long penetration is required until the best sound reaches the outer end of the pipe wall. With higher solids concentration the sound burst may not reach the other end (pipe wall) due to half way echoing, thus, a higher angle must be used. Normally, a good quality of data can be obtained with the Doppler angle between 45° and 60°. The selection of Doppler angle depend on ultrasonic application (Camarasa *et al*., 1999).

Considering the facts shown above it was decided to drill the pipe wall test section, to achieve four slots with Doppler angles 45°, 50°, 55° and 60° for the transducer fixed on the variable angle section and a 90° hole for the transducer fixed on the 90° angle section. However, due to thickness limitation (4 mm) of the PVC pipe, the difficulty was recognised to drill holes with the dead end of each of them 100% flat and enough deep for the transducer to fit, especially for slots with lower angles such as 45°. Therefore, it was decided to design and fabricate a flanged spoolpiece, which is a hollow pipe made from a solid PVC bar with a larger outer diameter than the rest of PVC pipeline in the flow loop. In order to adapt the fabricated hollow pipe section of the spoolpiece, the outer wall was reduced on either sides to suit the standard flanges used on the flow loop. The flanged spoolpiece is shown in Figure 6.26. The length of the spoolpiece (flange to flange) is 340 mm, on which the clamping transducer fixture can easily be mounted. After making the hollow pipe section from the circular solid PVC, the spoolpiece wall was found to be 20 mm, which was drilled to obtain six slots with different Doppler angles. For example, one of the transducers (4 MHz) has an outside diameter of 8 mm, and in order to achieve the best fit, it was decided to make each slot with 8.1 mm diameter. Also, after drilling each slot it was found that the thickness of the spool-pipe wall, between the transducer face and the pipe contents, to be 2 mm, the limit of which is shown by a red line in Figure 6.26. Since the spoolpiece is flanged, thus it makes the whole system robust and versatile. In other words the system can be mounted on any section within the flow loop via its flanges. Nevertheless, an accurate ultrasonic velocity measurement and

performance depends on the location and alignment of the transducer. Based on the engineering rules, the chosen location for the installation must be at least 10 pipe diameter of straight line, undisturbed flow upstream and 5 pipe diameter of straight, undisturbed flow downstream from the measurement point (GE sensing, 2007).

In general, non-wet transducers operate with coupling gel between the transducer face and the pipe wall. This is to insure an acoustically conductive path between the transducer face and the pipe wall surface. This means that any air interface between the transducer face and the pipe wall reflects all the ultrasonic energy, because air or gas has a very low acoustic impedance. Therefore, the use of coupling gel is paramount.

6.6.6 Instrumentations used to measure the relevant parameters

The final selection of each instrumentation used to measure the relevant and important parameters of flow within the multiphase flow loop was made after a thorough examination and consideration of several factors such as flexibility, cost, application and functionality. The following subsections detail the selection and driving force for using each specific instrument mounted on the flow loop.

6.6.6.1 Mean velocity measuring device

For determining slurry flow rate, several commercial instrumentations were considered, kinetic energy meters (venturi meters, flow nozzles and wedge meters), electromagnetic flow meters and acoustic velocimeters. Finally it was decided to use an Electromagnetic Flow Meter (EMF Krohne Aqua-flux) to measure the flow rate. This decision was influenced by the advantages that the EMF can offer over the other flow meters. It is considered as a reliable and relatively cheap flow meter. According to Brown and Heywood (1991), Matousek (1997) and Pachowko (2004) the reliability of EMF is without any doubt. However, Matousek (1997) has reported that to achieve a reliable measurement, the EMF must be installed on the vertical section. This is due to slip velocity between solid particles and the carrier liquid.

6.6.6.2 Solids concentration and axial velocity measuring device

There are two types of solids concentration, in-situ and delivered solids concentration. In a definitive slurry flow loop, in order to extract productive features, both in-situ and delivered solids concentration have to be determined. In-situ solids concentration demonstrates the local conditions of solid particles within the pipeline. This type of concentration is determined by the dual-plane ERT sensor, which measures the conductivity of the pipe

contents, and the conductivity data is then converted to solids volume fraction using Maxwell relationship. The dual-plane ERT sensor in conjunction with cross-correlation method is also used to determine the solids velocity profile in the carrier fluid. Two dual plane ERT sensors were designed, the geometry and dimensions of which is shown in Figure 6.27. They both are housed in the U-shape and vertical sections of the flow loop.

In-situ solid's concentration can also be determined by sampling of slurry at the discharge point, if no solids hold up occur in the pipeline. To ensure that there is no hold up, the sampling must be carried out in very high velocity. This high velocity is required to overcome the frictional loss, as a result the whole slurry behaves as a single liquid.

Delivered solids concentration is a very important parameter, as it determines the capacity of a pipeline system (Brown and Heywood, 1991). This type of solids concentration is determined from the multiphase flow loop using a pre-calibrated measuring tank, which is mounted on calibrated three load cells that determine the weight of the slurry in the tank. In order to perform this, the full pipe flow is diverted temporarily into the measuring tank via a flow diversion system.

6.6.6.2.1 Design of 360 mm dual-plane ERT sensor

The dual plane ERT sensor, shown in Figure 6.27 consists of two 16-electrodes planes, which are connected to three Perspex pipe sections (50 mm ID) in such a way to obtain a smooth internal section at the connection points, to avoid any disturbance to the flow. The Perspex section A (140 mm long) is connected to the left of plane 1 (P1), whereas the Perspex section C (140 mm long) is connected to the right side of plane 2 (P2), while both planes are separated by the third Perspex pipe section B (30 mm long). As the length of each plane is 40 mm, then this gives the distance between the centres of each electrode plane 50 mm. Considering the slot depth at the end of each plane, in which the Perspex pipe section B placed, the apparent separating the two electrode planes is 10 mm. In order to achieve a secure section and good coupling, two Perspex flat flanges (D & E) are mounted at the centre of both Perspex pipe sections (A & C) using PVC solvent cement.

The two flat flanges used as clamping fixtures via four M8 threaded rod bars, which are going though the four pre-drilled holes in the flanges and pulling the whole section together by tightening four M8 nuts at the end of each rod bar. It is apparent that over-tightening the nuts can pull both flat flanges together and separate them from the Perspex flat sections at the joint point.

Each end of the whole section is flanged, using the standard flanges used in the loop (uPVC full face flange drilled Bs 16/10 PN plain 2 inch). Connecting all the sections together gives a total length of the dual plane sensor 360 mm (flange to flange). This clearly makes the dual plane ERT censor a very compacted and robust equipment, which can be coupled with any flanged section within the flow loop.

The design of 16 electrodes at the periphery of each plane is one of the most important aspect of the whole sensor design. The design of electrodes followed the most common type of geometry and layout, in which the equisized electrodes are arranged around the pipe's inside diameter in an equispaced fashion. In order to avoid impedance problems, the electrodes have to be more conductive than the flowing fluid within the pipe. Since the main carrier liquid used within the flow loop is mainly water and conductivity difference between stainless steel and water is very high (GE Sencing 2007; kayelaby.npl.co.uk, hypertextbook.com), therefore, stainless steel was chosen as material of construction for the electrodes. In addition, some other factors such as good ability to resist chemical attack, cost, protection against fouling of the electrodes by solid particles make stainless steel the prime material of construction amongst all.

Based on typical values of the number of nodes per electrodes (Nd), the number of boundary nodes (NB), the number of electrodes in each plane (16 electrodes in this study), and the electrode angle 13.8°, the width of each electrode was determined as 6 mm for 50 mm pipe diameter. On the other hand the length of each electrode sized as 20 mm. This would make the final electrode size mounted on each plane 20 mm x 6 mm. Each electrode has been manufactured from M6 stainless steel rods, by cutting them in half to give semi-cylindrical shape. 16 electrodes are mounted on a predrilled circular PVC plane, in such a way to give an angle of 22.5° between centre of an electrode to the centre of the next one.

Each electrode welded to 24 mm long stainless steel rod (M4), which is inserted into the hole at the circumference of the uPVC plane. Each electrode is placed in a slot within the PVC plane, which enables the electrodes to be flush mounted in the interior without any disturbance to the flow.

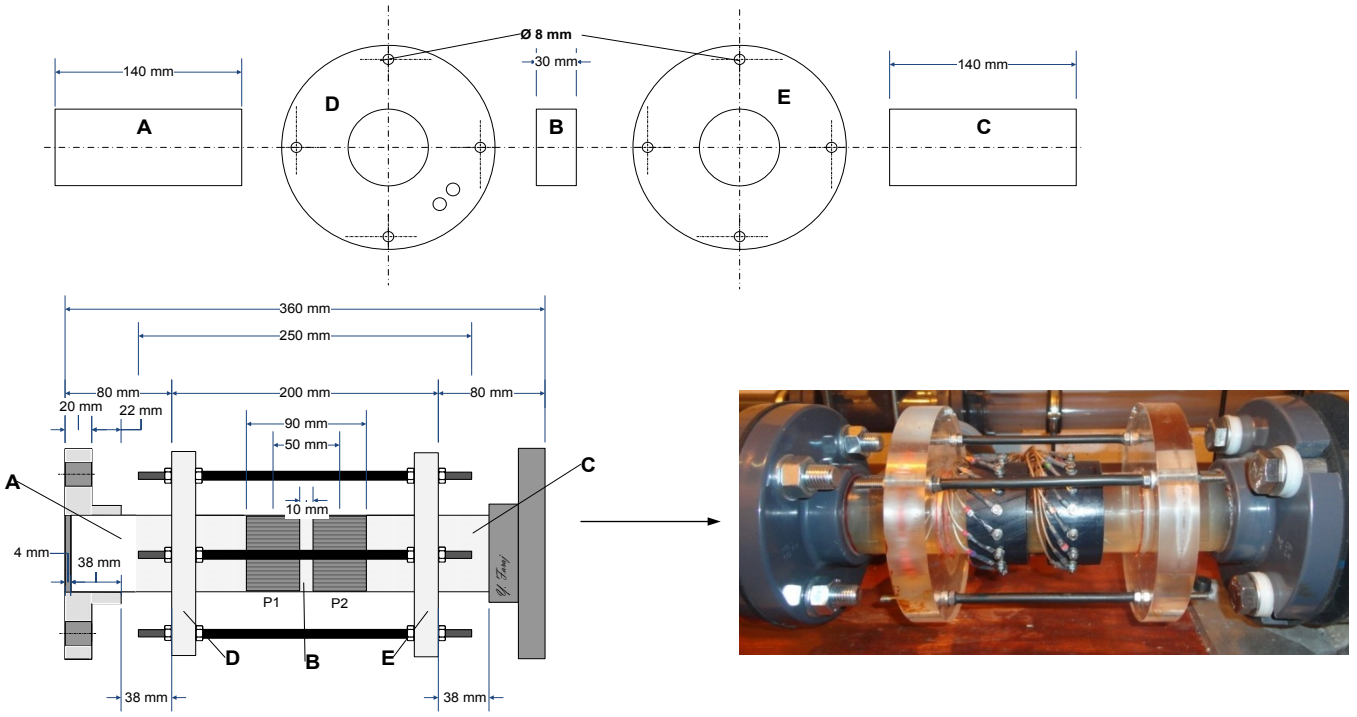

Dual Plane ERT Sensor					
DRAWN BY: Y. Faraj	**Company** University of Leeds/ OLIL	**TIME IN REQUEST:** 1 week	**APPROVED BY:** Prof. M. Wang **SIGNATURE OF RT:**	**DWG NO.** 2	© **Copyright** This drawing and the copyright, design rights and all other intellectual property rights in it belong to the University of Leeds/OLIL group. No licence or assignment of any such rights is granted hereunder. This drawing is not to be copied or divulged to a third party without written permission.
DATE: 2 March 2012	**SCALE** 1:2.5	**MATERIAL:** PVCu	**SHEET** 1 of 1		

Figure 6.27 Schematic drawing of the dual-plane ERT sensor

The welded M4 rods extend out of the plane by 11.5 mm to allow the connection of cables using solder tags. The cables are connected to the electrodes using solder tags and fixed each of them with M4 nuts and washers. Co-axial cables are used to connect the electrodes to the data acquisition system (DAS) and are sheathed so as to reduce the electromagnetic interference. The geometry and dimensions of the 16-electrode plane is shown in Figure 6.28. In order to prevent leakage at the coupling point of each plane with the Perspex pipe sections, slots of 3 mm wide have been made on each plane, into which 2.63 mm (3/32 inch) O-ring can be placed.

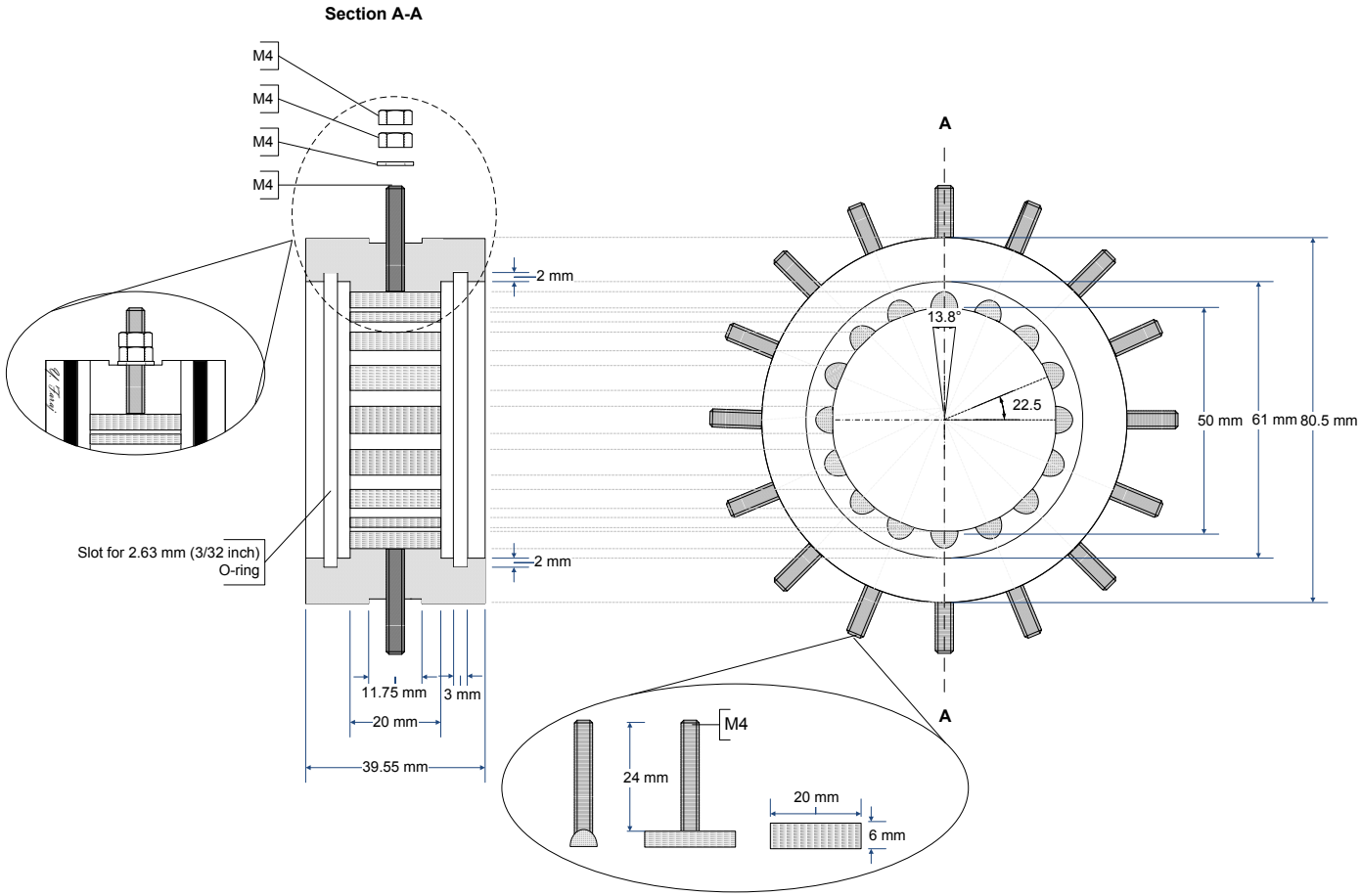

Figure 6.28 Schematic drawing of the 16-electrode ERT plane sensor

6.6.6.3 Mass flow rate measuring device

Although measuring volumetric flow is sufficient, mass flow rate measurement is often required by many industries such as Chemical industry, pharmaceutical industry etc. (Yoder, 2008). Measuring mass flow is one of the most important feature of Coriolis meter. Therefore, Coriolis mass flow meter was chosen for mass flow measurement in the flow loop. The choice of Coriolis was based on total cost, accuracy, maintenance and versatility. By comparing Coriolis mass flow meter to some other flow meters, such as turbine flow meter and differential pressure flow meter, it can be noticed that amongst all, Coriolis has a relatively high purchased price (approximately £8000) and low total cost of ownership. This is clearly due to the fact that Coriolis mass flow meter does not require periodic maintenance. This is due to not having moving parts except vibrating tubes, which means they are more reliable and require minimum maintenance. By contrast, turbine flow meters and DP have moving parts and subject to wear, which results in high cost of ownership. Moreover, Coriolis flow meters are the most accurate type of mass flow meters, with ±0.1% range (www.endress.com).

Based on the above advantages offered by Coriolis mass flow meter, it was decided to select Coriolis mass flow meter, which provides the measurement of mass flow rate density and temperature directly. On the other hand, it enables the measurement of total of mass and volume flow. In addition, to its high accuracy, it can be used for data validation of other instrumentations used to measure the same parameters such as validation of solids volume fraction measure by the ERT.

After consulting several supplier's websites, such as Endress + Houser (www.endress.com), KROHNE (www.krohne.com), it was found that each of them has a special style of Coriolis tube. Some of them supply single-bent tubes, some dual-bent tubes and some others such as KROHNE, who became the first company to supply straight tube Coriolis mass flow meter.

It was decided to select OPTIMASS 7000 series straight-tube Coriolis mass flow meter from KROHNE. The factors that influenced the selection of the aforementioned type of the flow meter are highlighted bellow:

- Unlike bent-tube meters, straight-tube Coriolis flow meters cause less pressure drop.
- Easier to clean and to be drained.

- Can offer four tube materials of construction (Titanium, Stainless Steel, Hastelloy or Tantalum).
- Excellent zero stability.
- Fast signal processing, even with changes in concentration or temperature.
- Can be used in many applications, such as non-homogeneous mixtures, slurries, product with entrained solids or gas, products requiring low flow velocities etc.

KROHNE OPTIMASS 7300F (field housing for wall mounting) is installed on the U-shape outgoing pipe section just before the dual-plane ERT sensor. The straight signal tube system made of Titanium (Grade 9) with mounting length 1101 mm. The flow meter converter type is MFC300F (field housing for wall mounting). It has an accuracy of ±0.15 of MV and uses PACTWARE operating software. When installing the meter it was paramount to make sure that the pipe work is supported behind the flanges, so as to avoid placing any stress to the meter flanges. Also, as part of manufacturers recommendations for slurry applications, transition pieces were used on the inlet port and the outlet of the tube for leading edge protection.

It is worth pointing out that the heavy weight of the meter (approximately 150 kg) on the inclinable steel structure raised the concern that the whole pipeline may slide down the table, while the table is raised, especially at 90°.It was essential to insure rigid and stable connection to the mounting steel structure. Therefore, Split Plummer Blocks were designed and fabricated for firm fixture of the heavy meter to the inclinable deck. Each Plummer Block consists of two aluminium plates (12 mm thick), which are welded to form an L-shape to support and clamp either flange parts of the meter, as shown in Figure 6.29. Four M10 bolts were used to firmly fix the meter to the steel beam and four M8 bolts were used to clamp and anchor the meter.

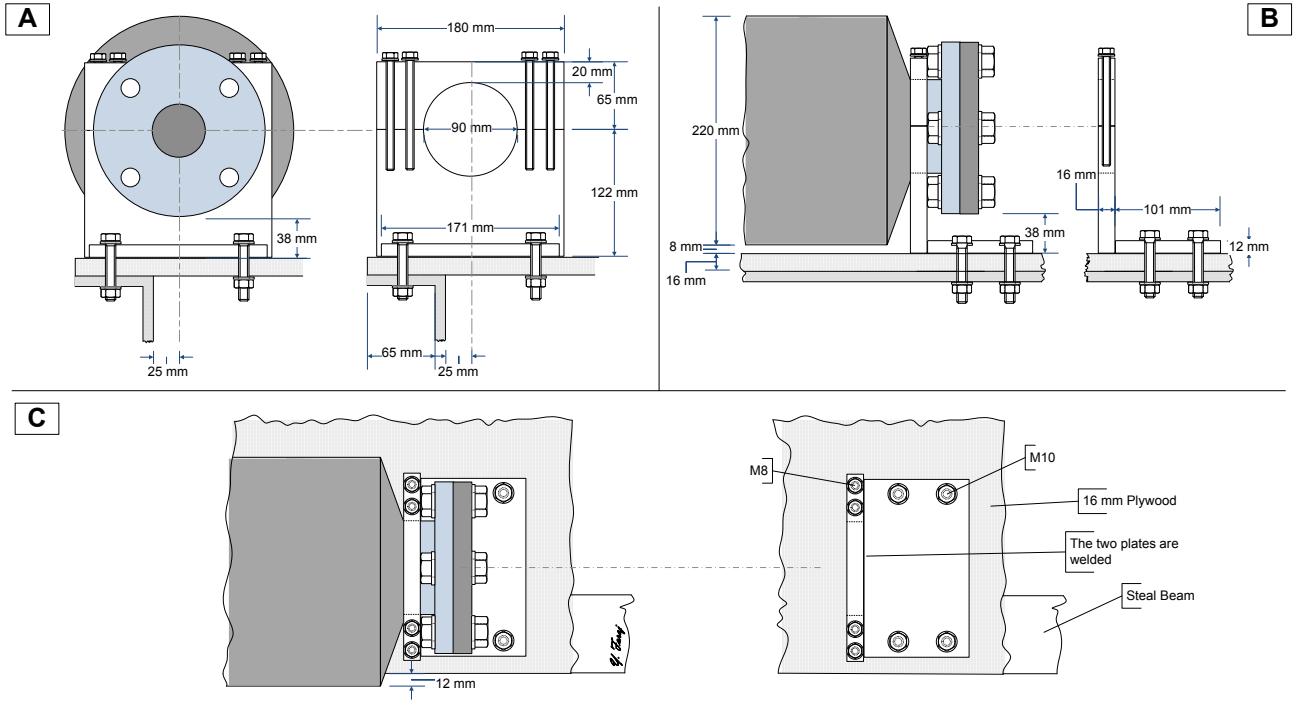

Split Plummer block for fixing coriolis mass flow meter							
DRAWN BY: Y. Faraj	**Company** University of Leeds/ OLIL	**TIME IN REQUEST:** Max. 2 weeks	**APPROVED BY:** Prof. M. Wang **SIGNATURE OF RT:**	**DWG NO.** 1	**ITEM**	**DESCRIPTION**	© **Copyright** This drawing and the copyright, design rights and all other intellectual property rights in it belong to the University of Leeds/OLIL group. No licence or assignment of any such rights is granted hereunder. This drawing is not to be copied or divulged to a third party without written permission.
					A	Front View	
					B	Side View	
DATE: 14 June 2012	**SCALE** 1:3	**Material:** Aluminium	**SHEET** 1		C	Top View	

Figure 6.29 Schematic drawing of the Split Plummer Block

6.6.6.4 Additional local velocity measuring device

The decision was made that another local velocity measuring device would be used and mounted on the U-shape inclinable flow loop. The remarkable advantage and driving force for the decision was to use this device for measuring solids local velocity, mean solids velocity and solids velocity profile, and thus validating solids local velocity obtained from the combination of the ERT and cross-correlation. After a thorough research for finding an instrument for Ultrasonic Doppler Velocity Profile measurement, two versions were considered. The first instrument was the UDVP-DUO (GAH100), which is manufactured by Met-Flow and supplied by Dantec (www.dantec.com), while the other one was DOP velocimeter, which is supplied by Signal-Processing (www.signal-processing.com). From an objective prospective and measurement point of view, UDVP and DOP, offer more or less the same functionality. However, the cost was the driving for selecting UDVP-DUO from Met-Flow. Figure 6.30 showing the UDVP, which is currently used in OLIL laboratories in the University of Leeds. The whole system consists of three main parts:

1. *Measuring unit*, which performs signal processing and digitalisation.
2. *Transducers*, which transform electrical signals in ultrasonic acoustic signals.
3. *User interface,* which provides data analysis and storage.

It is worth mentioning that all configurations are set via user interface, but not from the main measuring unit. The main unit has a reasonable dimensions (340x130x400 mm), which can be adjusted on the inclinable table between the two limbs of the U-shape pipeline, and can easily be handled due to its reasonable weight (9.3 kg). The main unit operates with a set of TX-line transducers, each with five emitting frequencies (0.5, 1, 2, 4 and 8 MHz), which are connected to the main unit via an integrated multiplexer. As recommended by the manufacturer (Met-Flow), 4 m long cables are used for the transducers, so as to achieve reliable operation. In other words, providing the best compromise between the installation of the probe and attenuation of the signal.

For the detail description and technical specifications, relating to any part of UDVP-DUO system, the author recommends a journey through manufacturer's website (www.met-flow.com).

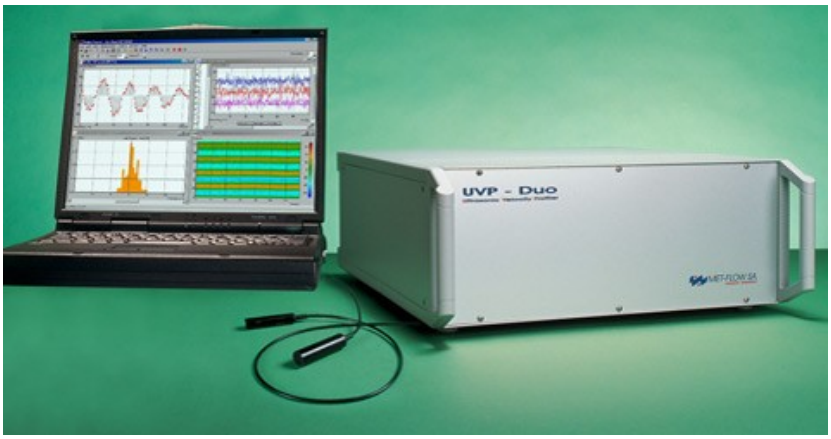

Figure 6.30 Showing the UDVP-DUO system from Met-Flow

6.6.6.5 Pressure measuring instrumentation

The measurement of pressure differential between two points of a section of a straight pipe is one of the most important measurements for pipeline frictional head loss determination.

Monitoring the pressure changes over straight pipelines can provide valuable information regarding the condition of flow. Therefore, it was decided to mount six pre-calibrated pressure sensors on three sections of the flow loop (vertical and ascending inclined section and descending inclined section) at 2 m intervals between the two pressure sensors mounted on each section. In order to avoid solid particles and entrained air entering the sensors, six Danfoss flush diaphragm pressure transmitters (type MBS 4010) were selected, which could measure the pressure within the range of 0-10 bar. These transmitters can perform an accurate measurement for all conditions of testing and it is designed for use even under harsh environmental conditions. Also according to the manufacturer (CSE Industrial Electrical Distributers) the measurement error is ±0.3% and has an excellent vibration stability and robust construction.

In order to make a robust pressure transmitter system, which can easily be mounted in any section within the flow lop, a flanged lining sleeve was designed an fabricated, as shown in Figure 6.31. The whole system consists of a 50 mm ID pipe section, which is pressed into a 90° Tee to provide a smooth internal surface and flanged at either ends using solvent PVC cement. The Tee is machine treated for easy insertion of the pipe section. A tapped cylindrical solid PVC bar is pressed into the vertical opening of the Tee and sealed with PVC solvent cement to prevent leakage. The remarkable advantages of this lining sleeve is that it allows easy connection

and disconnection of pressure transmitter by fitting it into the tapped solid PVC bar and can be joined to any desired section within the flow loop via the flanges. Similar lining sleeve is used for the connection of temperature transmitter in the vertical test section.

Each pressure transmitter is connected to the Data Acquisition System (DAS), which sense the deflection of each transmitter by the flowing slurry and the data is generated in the form of current output. The data then can be converted to pressure data due to linear relationship between the current output and the pressure.

6.6.6.6 Temperature measuring device

Monitoring the operating temperature is an important task of any slurry flow. As any change in slurry temperature can affect the slurry viscosity and as a result this may have a dramatic effect on the slurry flow behaviour.

In this study, a K-type thermocouple is used and mounted on the vertical section. It is also connected to the DAS, where the slurry temperature data is recorded. The working principle of this type of thermocouple is based on generating voltage, which is a function of temperature. The K-type thermocouple is very common and widely used. They are cheap and can be used to monitor the temperature range 0-100 °C (Pachowko, 2004).

However, controlling the temperature was found to be costly and needles, as the time taking for each experiment was found to be rather short. Also the heat, which is produced by the dissipation energy input to the pump, was found to be very little and could not have a dramatic effect on the slurry's viscosity. Moreover, pumping a chilled heat transfer fluid through the annulus of a double pipe heat exchanger can increase the cost of each experiment and occupy a significant area. Therefore, based on the above reasons, it was decided not use any heat exchanger in this study. However, as a safety precaution, the slurry temperature will still be monitored via the thermocouple.

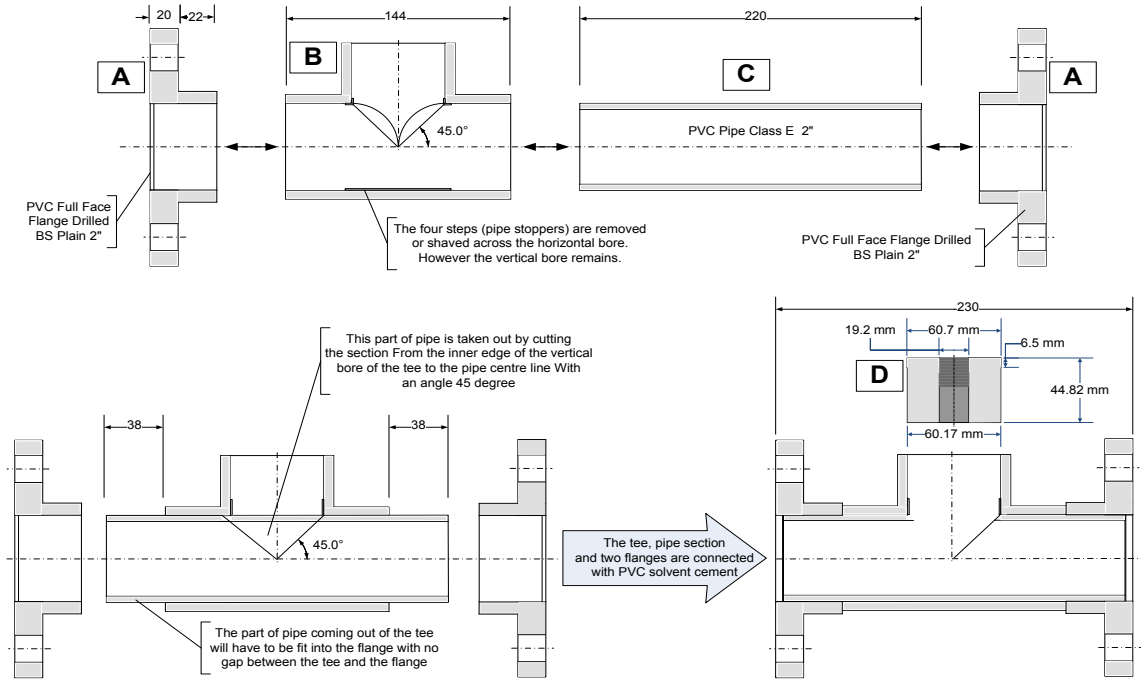

Pressure and temperature transmitter spoolpiece					
DRAWN BY: Y. Faraj	**Company** University of Leeds/ OLIL	**TIME IN REQUEST:** 1-2 weeks	**APPROVED BY:** Prof. M. Wang **SIGNATURE OF RT:**	**DWG NO.** 1	
DATE: 28 March 2012	**SCALE** 1:2	**Material:** PVCu	**SHEET** 1		

ITEM	QTY.	DESCRIPTION
A	2	PVC Full Face Flange 2"
B	1	PVC Pipe Class E 2"
C	1	PVC Tee 90 Plain 2"
D	1	Tapped PVC solid bar

Figure 6.31 Pressure and temperature transmitter spoolpiece

6.6.6.7 Data Acquisition System (DAS)

A Data Acquisition System is used to acquire the real time measurement of the relevant parameters and quantities and presenting them on a personal computer.

A National Instrument Field-Point (FP @ 129_11_241_2\FP-AI-111, 40-20 mA) is used, which is connected to the Electromagnetic Flow meter (EMF), OPTIMASS Mass Coriolis Flow meter, six pressure transmitters and the thermocouple. The current output is powered by the Field-Point (FP-1600), 10.100MPs Ethernet network interface power point, which collects the data and present it in a Front Panel, a screen shot of the front panel is shown in Figure 6.32.

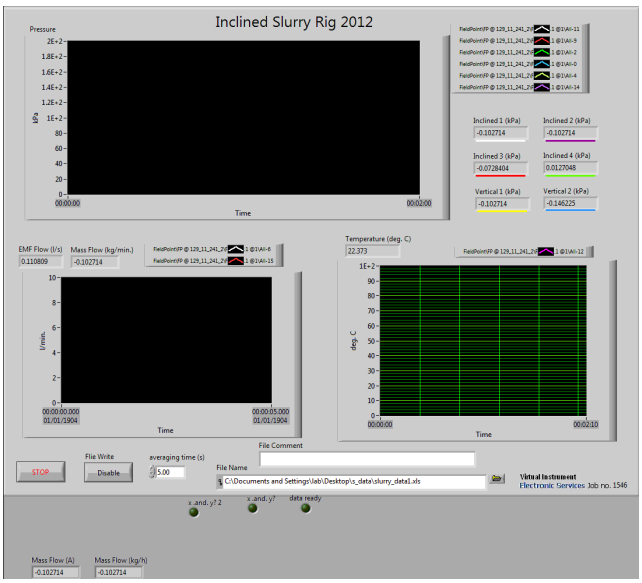

Figure 6.32 Showing the LabVIEW front panel

In order to receive the current input from the above instrumentations and convert to the desired measured parameters using scaling factor, a LabVIEW programme was written, as shown in Figure 6.33. It is worth mentioning that, for the conversion of the current input to the desired variables, it is assumed that all the instrumentations have a linear response. The current input of the EMF converted to slurry velocity (m/s), the current input of mass flow meter to slurry mass flow rate (kg/min), pressure sensor current input to slurry pressure (kPa) and the thermocouple current input to slurry temperature (°C). In each experiment the data is collected every 5 seconds, they are then averaged at the end of each experiment. All the data is recorded in a data file that can be reviewed later and used for the analysis.

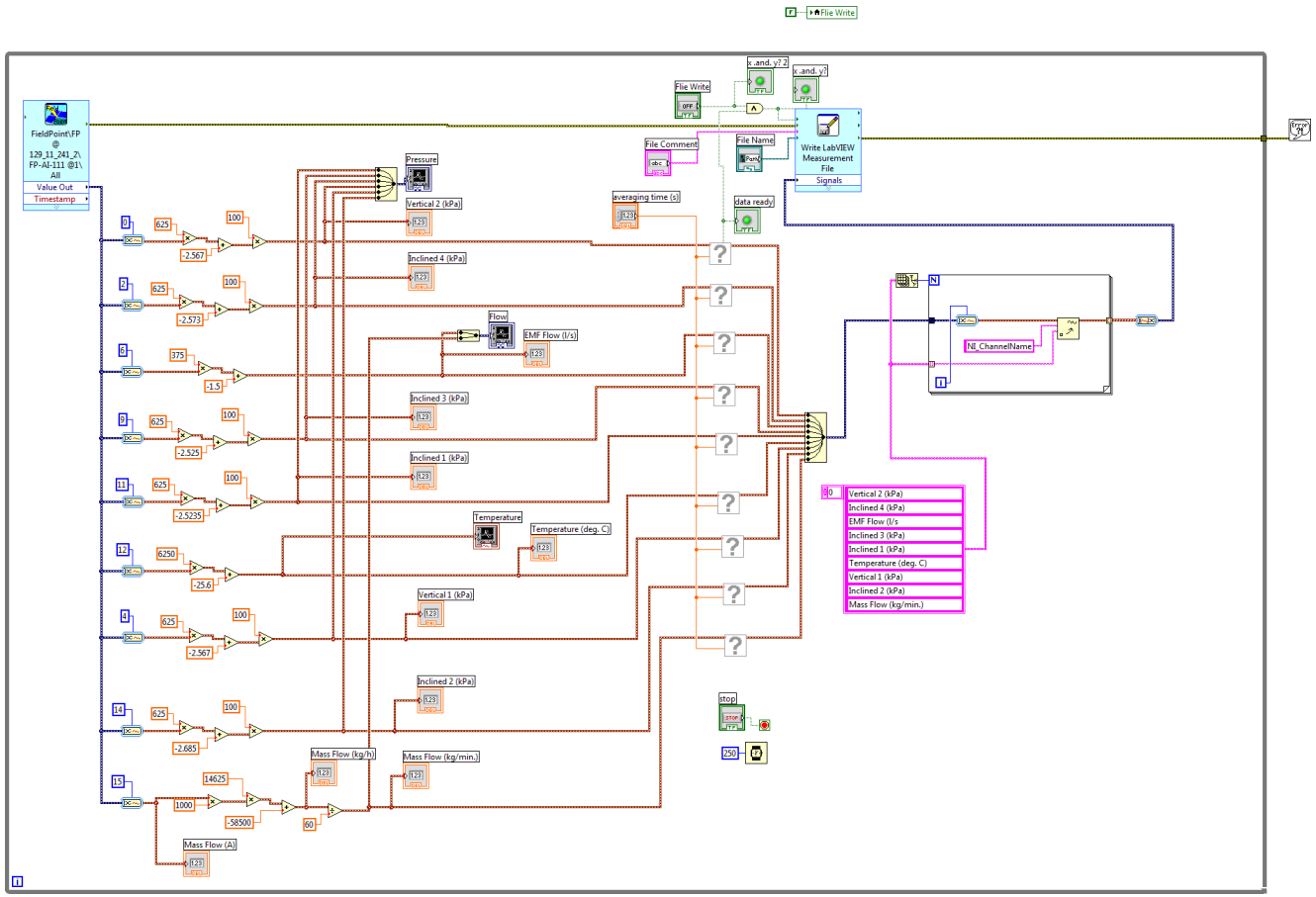

Figure 6.33 Showing the LabVIEW programme

6.6.7 Flow loop operation procedure

Slurry transport is a complex operation that can easily divert from the steady state condition, which has a direct influence on the experimental data. In order to make sure that a good quality of experimental data is obtained, a careful operating procedure (or experimental method) has to be designed. According to Sundqvist (1996), slurry parameter measurements have to be carried out when the flow system has reached a steady state condition. In addition, as the flow loop is inclinable, the likelihood of arising problems is higher than when only a rigid horizontal or vertical line is used. Especially during shut down procedure, when the risk of blockage is higher, due to accumulation of solid particles at the pivot point. As previously mentioned, the main focus will be on the measurements of different slurry parameters such as pressure, temperature, flow rate (mean slurry velocity), in-situ and delivered solids concentration, solids velocity and slurry mass flow rate. Therefore, it is very important to ensure that the instrumentations used to measure these parameters are reliable and accurate. This can be fulfilled by testing and calibrating each instrument prior to any experiment. The general operating procedure (start up and shut down including draining procedure) is described below, the location of each controlling valve within the flow loop is highlighted in Figure 6.34

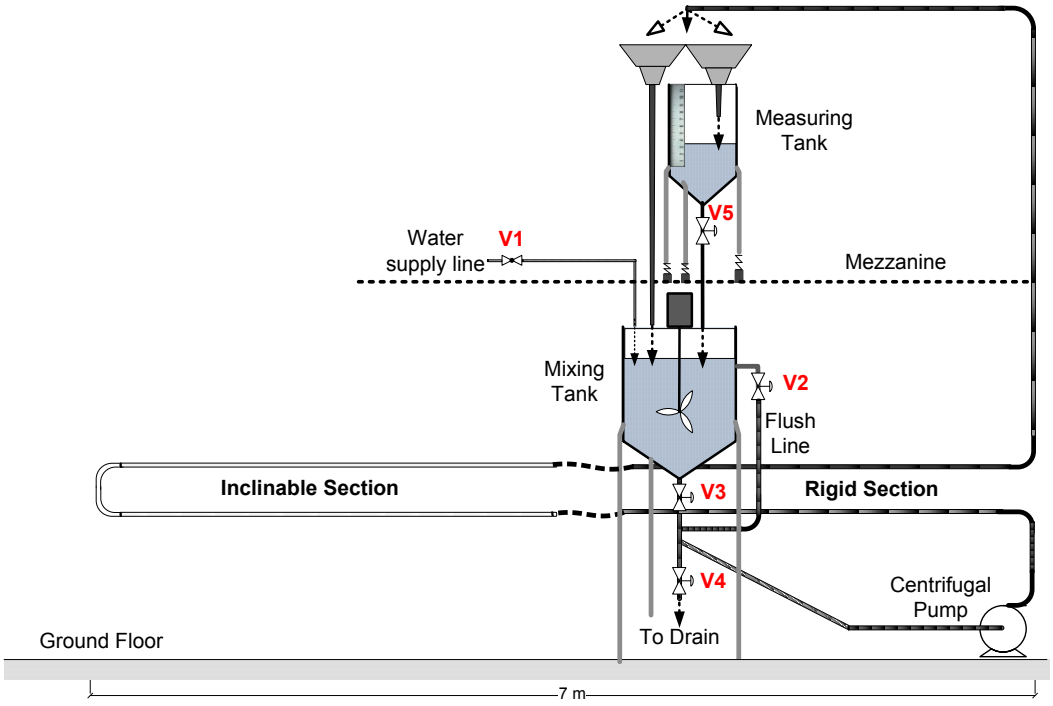

Figure 6.34 Schematic diagram of the inclinable loop piping

1. The inclinable section is set at 0° inclination angle from the horizontal.
2. Assure that both valves V3 and V4 are closed.
3. Open the gate valve V1 and fill the 500 litre mixing tank with 100 litre of water, via the water flow meter
4. Once the loop lines are open then it is possible to release valve V3
5. Once valve V3 has been opened, start the centrifugal pump at a low flow rate via the Digi-drive frequency converter to allow the pump to reach its optimal conditions.
6. Shut off valve V3 and then after a few seconds shut off the pump
7. Open valves V3 and V4 and drain the contents of the tank
8. Close valve V3 and V4 and refill the mixing tank with water, by opening valve V1 and record how much water has been added to the tank. Once the desired volume has been reached, close valve V1 and allow the level of the water to stabilise.
9. The conductivity measurement of water, in the mixing tank, will be carried out, as this will be required for ERT reference measurement.
10. Weigh about 25 kg of solid in a bucket.
11. The stirrer is started at a low speed via the Digi-drive frequency converter (around 80-100 rpm) and Pre-weighed sand is added to the mixing tank, in a controllable fashion, to achieve the desired concentration.
12. The solids have to be added in 25 kg increments, ensuring that a uniform solid concentration is generated
13. The stirrer speed is increased (up to a maximum of 400-450 rpm) until the particles are suspended homogeneously, and at the same time the solids are continuously added until the desired solid concentration is reached.
14. Once the desired solid concentration is reached, valve V3 can be opened, and then the pump is switched on. The slurry is introduced to the flow loop and return to the mixing tank or measuring tank. However, a different procedure will be applied for each sand particle size, if sand used as solid particles, depending on the particle size distribution:

    - *For medium sand:* The exit valve to the mixing tank V3 is opened and the centrifugal pump is started via the Digi-drive frequency converter.
    - *For coarse sand:* The flush line will be opened (V2) first and the centrifugal pump is started via the Digi-drive frequency converter. Then after a few seconds the exit valve to the mixing tank (V3) will

be opened and the flush line valve (V2) will be closed. Carrying out this procedure, for coarse sand, ensures that the blockage in the suction line is avoided. As the finer particles flow through the flush line and lubricate the line beforehand, then the coarser particles will be following. In either case, when the centrifugal pump is started, the electrical power supply to the pump must be adjusted to the highest velocity mentioned in this study, so that a homogeneous flow in the flow loop is achieved.

15. While the flow is circulating through the flow loop, the desired inclination angle is set via the winch remote control.
16. Once the slurry reached the other end of the flow loop, it can either be returned to the mixing tank or diverted to the measuring tank. However, the flow must not be diverted to the measuring tank until the steady state flow is reached, as the accuracy of the data, particularly the delivered solids concentration and the flow rate may be in doubt.
17. For the purpose of calibrating the flow meter and determining solid concentration, the measuring tank will be used; meaning the slurry is diverted to the measuring tank at the discharge point using the flow diversion system. Once the diversion process has finished and the level measurement is complete the contents are allowed to flow into the mixing tank via valve V5.
18. Slurry flow rate (mean velocity), Pressure, temperature, slurry mass flow rate are recorded via the LabVIEW and the ERT measurements are carried out.
19. It is important that initial tests are carried out at higher transport velocities, then gradually reduced to the lowest. The procedure of decreasing the mean slurry velocity is continued until the stationary bed is totally formed. However, the last measurement must be carried out as quickly as possible to avoid the blockage. Also, for each measurement taken, the slurry flow must be visually inspected through a transparent pipe section along with taking photographs if it is desired. However, it is expected that visual inspection will be almost impossible, as the media is totally murky.
20. If another solids concentration is due to be considered in the test matrix, then more sand is added into the mixing tank, and the above procedure is repeated. However, each set of measurements must be carried out at different velocities, concentration and inclination angle, so that the influence of each parameter is determined.

21. Once all the tests have been carried out, the inclinable table is lowered back to 0° (horizontal) and the shut down procedure starts.

The shut down and draining procedure is as important as start up procedure, it may even be more sensitive, due to clogging at the inlet of the inclinable U-shape section. The shut down and draining procedure is described below in a chronological order:

1. At the end of all the tests, the inclinable table must be lowered to the horizontal position.
2. Open V2 and V5, while the remaining valves (V2, V3 and V4) are closed.
3. The flow velocity is adjusted to 2.5-3.0 m/s and the mixer is switched off, in order for the solid particles to settle at the bottom of the mixing tank. This way only the brine is flowing through the flow loop via V5 and the solid particles are flushed from the loop into the mixing tank.
4. Once the level of the mixing tank contents about to reach the flush-line inlet, V2 is fully opened to fill up the tank again with fresh water.
5. The same flushing procedure is continued (2-3 times) until a clear flow is seen through the transparent pipe section of the flow loop.
6. The pump is switched off, V1 is opened, V2 is closed and the mixer is switched on to achieve a reasonable homogeneous mixture in the mixing tank. The mixing process may take 2-3 minutes.
7. V3, V4 and V1 are opened, while the mixing continues. At this step the first draining is carried out.
8. Once the contents level reaches 2/3 of the tank height both valves, V3 and V4, are closed, so the tank is filled up again with water to obtain a diluted mixture.
9. Step 7 is repeated for the second draining process. The number of draining process depends on the solids throughput concentration. Based on previous experience, it was found that 2 times draining would be sufficient for 10% throughput concentration.
10. At the last draining process, the tank must be well washed from the settled fine particles at the dead end of the mixing tank using the water supply hose. However, at this step the mixer has to be switched off.
11. This step may not be necessary, however, it is preferable to fill up half of the tank with fresh water, while all valves are closed, except V1. Then the pump is switched on, V3 is opened for final flushing process,

including the measuring tank by diverting the flow for a couple of seconds.

12. The pump is switched off, V1 is closed, V3 and V4 are opened to empty the mixing tank and washing it.
13. All the electrical instrumentations and equipments are switched off and secured.
14. The deposited sand within the drainage system must be disposed off considering health and safety and environmental codes.

6.6.8 Hydraulic and mechanical testing

Before full operation of the whole flow loop, it is important to ensure that the system is functional in accordance with the design requirement, and also safe enough in accordance with the health and safety codes. Therefore, the hydraulic and mechanical testing of the flow loop, particularly the mechanical structure of the inclinable table and the flow through it, was performed. The structural testing was carried out by raising and lowering the inclinable table several times, considering the two extremes 0°, when the table is at horizontal position and 90°, when the table is at vertical position. In addition, several randomly chosen angles, within the aforementioned range, were also included into the test.

However, it was very important to adhere to health and safety of everyone working or walking in the vicinity of the working are. Therefore, 48 hours before testing the whole system, the faculty staff and students were notified. Moreover, guards and warning signs were used during the test process. Each test involved the following checks and observations:

- Visually checking the whole inclinable table, for swaying, deflection, strain at the pivot point, the connection point of the wire rope and general checking regarding the stability of the table in a raise and stop and lower and stop fashion.
- The winch position and controlling the lifting and lowering process had to be well checked.
- Examining the hooks for deformation and cracks.
- Checking the telescopic push/stop system.
- Visual inspection of the running rope.
- The cables running along the table.
- The flexible pipe and strain on the rigid pipes connected to it.
- The bend in the flexible pipe and look for potential kinks throughout the designed inclination angle range.

- The stability of the pipeline on the table, especially at higher inclination angles 45°-90°.

The hydraulic tests were initially carried out focusing mainly on leak test throughout, while the table was in horizontal position. Then the hydraulic testing was carried out at various inclination angles and various flow velocities, including the highest velocity, at which the highest pump frequency could be reached. All instrumentations, pressure transducers, thermocouple, Electromagnetic Flow meter, Coriolis mass flow meter, measuring tank and flow diversion system and the UDVP, were tested and the randomly measured data was recorded. The flow measurement test included the inspection and operation of the data acquisition system.

The whole results of the testing procedure was found to be promising and it was finally concluded that the whole flow loop, including instrumentations and equipments, is perfectly safe and functioning with meeting all the design requirements and objectives for the intended application.

6.7 Conclusions

This chapter has highlighted the procedure and strategies used in the design and construction of inclinable multiphase flow system, including the detailed design of various equipments and instrumentations used to measure the desired parameters of flow. The selection of each instrumentations and their location within the flow loop have been based on slurry flow. The design and layout of the whole piping system have been described with consideration to the project design requirements and engineering rules. The structural design, fabrication and erection of tables, rigid and inclinable, have been presented in detail to generate a design procedure, along with associated work to facilitate the process of inclination up to 90° (vertical). The design and fabrication of pressure and temperature transmitter lining sleeve have been detailed, along with the design and fabrication of the UDVP spoolpiece to suit any potential future application. A general start up, shut down and draining procedure, based on slurry flow, has also been discussed. Finally, the mechanical and hydraulic testing of the whole system concluded that all the design requirements for the intended application have been met providing total functionality and safety for the future applications.

Chapter 7
Automated horizontal flow regime recognition using statistical signal analysis of the ERT data

This chapter presents a new method of flow regime recognition based on statistical signal analysis of the ERT data, along with writing a script using MATLAB so as to facilitate an automated recognition. An evaluation of the recognition scheme is also described with highlighting the success rate based on different sands and different flow conditions.

7.1 Introduction

Flow regime recognition is not only useful for characterization of the flow, but also for the purpose of modelling and for flow meters, as most of flow meters, especially the ERT as discussed previously in Chapter 5, are flow regime dependent. In order to develop a flow meter, it is paramount to determine the flow regime present in the pipeline, which enables accurate measurement and selection of the optimal method for flow measurement.

This investigation aimed at developing a method for recognition of slurry (sand/water) flow regimes occurring in the pipeline and coding a program based on the proposed method. Nevertheless, the modelling aspect to correct the ERT measurement is not dealt with in this study.

Usually the flow regimes are recognised and distinguished using either direct or indirect recognition method. The direct methods involve a visual observation of the flow through a transparent pipe section and/or the reconstructed images or real photographs of the flow within horizontal pipeline. It is quite clear that as slurries are usually opaque and contained in opaque enclosures, thus, the direct methods are very difficult if not impossible. Also, even if the pipeline operator is able to visualise the flow within the pipeline, the distinction between the flow regimes is dependent on the operator bias. Therefore, the recognition of the prevailing flow regime requires an indirect method, which moves away from the operator bias and based upon a measurement scheme and flow feature extraction, which related to the distribution of solid particles across the pipe cross-section whether the pipe wall is transparent or opaque.

A new indirect method for recognition of the active flow regime using statistical signal analysis of the ERT data (conductivity) has been proposed.

The zoned average conductivity of five zones, along the vertical centreline of the tomogram is considered. Mesh (21 cells) of the regionisation scheme, which is embedded in the p2000 software, described in Chapter 3, is selected. The ERT data can undoubtedly reveal key flow features, which would enable the recognition of the prevailing flow regime. The main features are extracted from both, time domain signal and frequency domain of the signal. Statistical spectrum analysis of the signal, such as Power Spectral Density (PSD) of the signal, is rendering significant flow features. Besides, a direct recognition method was attempt. The direct method involved the observation of flow through a transparent pipe section, mounted in the horizontal pipeline, along with the real photographs of flow captured using a digital camera. It is worth mentioning that the direct method is used as a mean of comparison for the proposed indirect method.

MATLAB has been used for coding the program to facilitate automatic recognition of the active flow regime. The method has been evaluated and the recognition rate has been determined at 90.32%. An automated visualisation of the solids volumetric concentration has been included into the main program, through which the local solids distribution can be visualised and mean solids concentration is automatically calculated and displayed.

7.2 Test strategy

A set of experiments were carried out using a pilot-scale slurry flow loop shown in Chapter 4. The horizontal line of the flow loop made the test section of the experiments, in which different flow regimes were generated by altering the slurry velocity. In order to cover most of typical slurry flow regimes, a relatively wide range of superficial velocity were selected to pump two sands, medium and coarse, each with different throughput volumetric concentration, 2% and 10%. At the beginning of each test the transport velocity (mean slurry velocity) was nominally set to 5 m/s, then it was incrementally decreased until the transport velocity reached 1.5 m/s. After a steady state pressure gradient was observed on the LabVIEW front panel the use of Fast Impedance Camera System (FICA) is attempted to measure a cross-sectional pipe tomogram by collecting blocks of 8000 frames for each flow condition. Since the data collection speed for FICA system is around 1.15 ms/frame, then 9.2 seconds are required for collection of 8000 frames in real time. A 1.2 m transparent pipe section were included into the test section, so as to visually inspect the active flow regime and note all the

phenomenon occurring in real time, such as type of flow regime seen, measuring the height of the bed etc. Also for each measurement test photographic images of the flow were captured for later comparison and evaluation of the proposed method.

7.3 Automated flow regime recognition

In order to achieve automatic recognition of the prevailing flow regime in horizontal slurry flow, two key stages had to be taken. First is developing a recognition method, for which statistical signal analysis of the ERT data has been proposed, second is coding a program; which would facilitate automatic recognition of the prevailing flow regime.

The following typical slurry flow regimes were considered into the recognition scheme:

1. Homogeneous.
2. Pseudo-homogeneous.
3. Heterogeneous.
4. Moving bed.
5. Stationary bed.

Statistical analysis of the conductivity data within each zone were carried out to provide a quantitative comparison of the flow regimes, thus reducing the subjectivity associated with recognising each flow regime. In order to achieve this objective the following stages were adopted:

1. Experimental ERT measurement and generating 21 cell zoned average scheme.
2. Statistical signal analysis and flow feature extraction.
3. Threshold indication for each flow regime.
4. Decision making.
5. Program coding.
6. Running and testing the new technique, and also determining the recognition rate (error analysis).

7.3.1 Experimental ERT measurement

The ERT measurements were taken for each of the sand used in the experiments at two different throughput concentration, 2% and 10%, and at different slurry velocity so as to generate a range of flow regimes considered in the investigation. Since each measurement block yields a huge amount of

data (i.e. 8000 frames each frame at 316 data pixel), then it was decided to use mesh/21 cell zone scheme, as shown in Figure 7.1, which made the basis for the statistical analysis of the conductivity data. The 21 cell averaged conductivity tomogram were exported using P2000 software. Since the flow regimes in horizontal settling slurry flow are influenced by gravity then it was decided to consider only the vertical 5 cells on the central axis of the tomogram. The analysis of only these 5 zones will obviously produce all of the characteristics relevant to the active flow regime. Upon the ERT measurements, two files were exported (zave.csv & conc.csv), which would later be used for automated flow regime recognition and visualisation and measuring mean local solids concentration respectively.

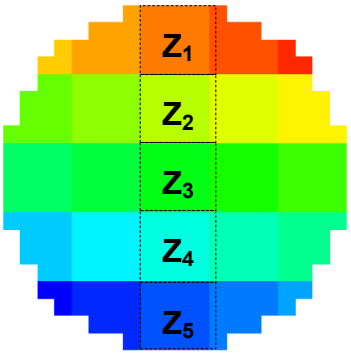

Figure 7.1 Mesh/21 cell zone scheme

7.3.2 Statistical signal analysis and flow feature extraction

7.3.2.1 Signal analysis in the time domain

The analysis of the data for each cell mentioned above was carried out by considering the change in conductivity relative to the reference. The signal, which is buried in a noisy time domain were plotted for each condition, an example of which is shown in Figure 7.2.

From the relative conductivity data within each zone at different slurry velocity shown above it is somehow difficult to extract any specific feature that would facilitate the recognition of the prevailing flow regime. Nonetheless, it can be seen that by reducing the slurry velocity the difference or gap between the conductivity of slurry at the top of the pipe and the conductivity at the bottom half of the pipe increases.

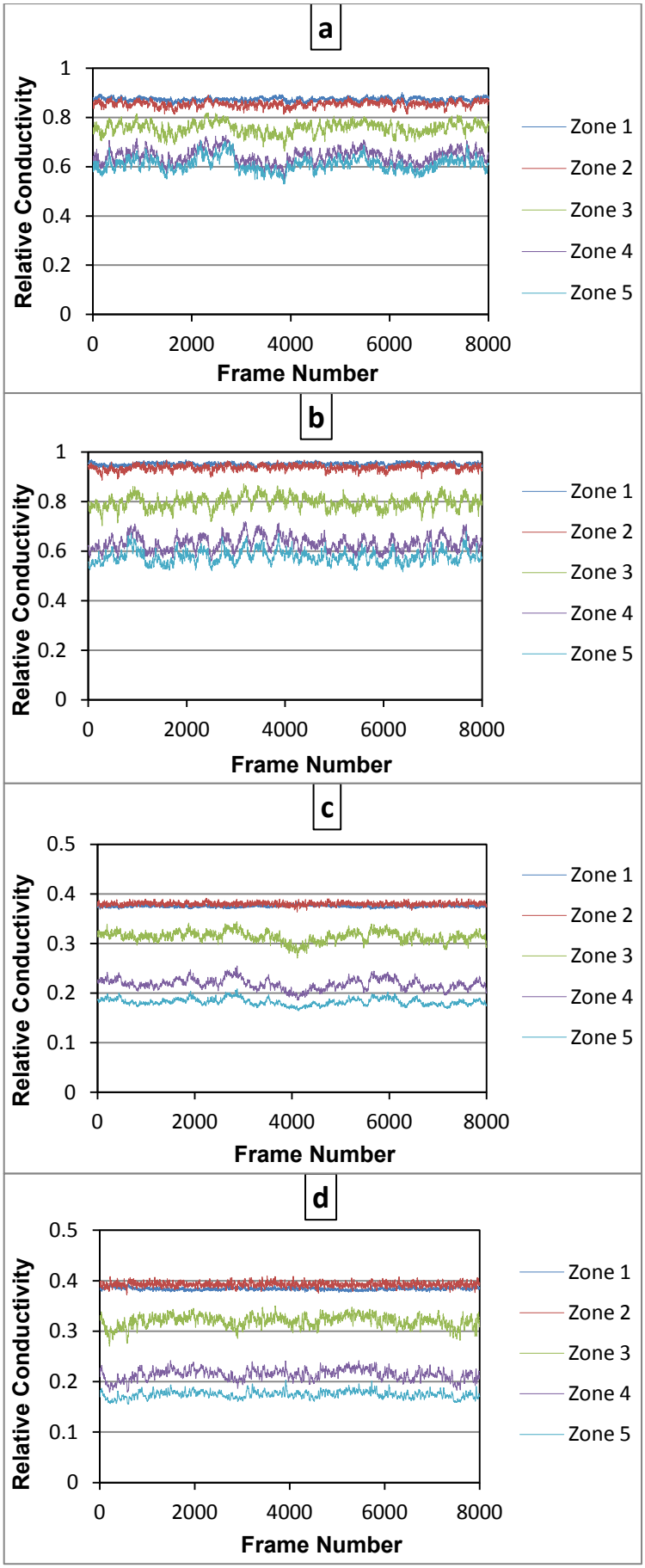
a
Relative Conductivity
1
0.8
0.6
0.4
0.2
0
0
2000
4000
6000
8000
Frame Number
Zone 1
Zone 2
Zone 3
Zone 4
Zone 5
b
Relative Conductivity
1
0.8
0.6
0.4
0.2
0
0
2000
4000
6000
8000
Frame Number
Zone 1
Zone 2
Zone 3
Zone 4
Zone 5
c
Relative Conductivity
0.5
0.4
0.3
0.2
0.1
0
0
2000
4000
6000
8000
Frame Number
Zone 1
Zone 2
Zone 3
Zone 4
Zone 5
d
Relative Conductivity
0.5
0.4
0.3
0.2
0.1
0
0
2000
4000
6000
8000
Frame Number
Zone 1
Zone 2
Zone 3
Zone 4
Zone 5

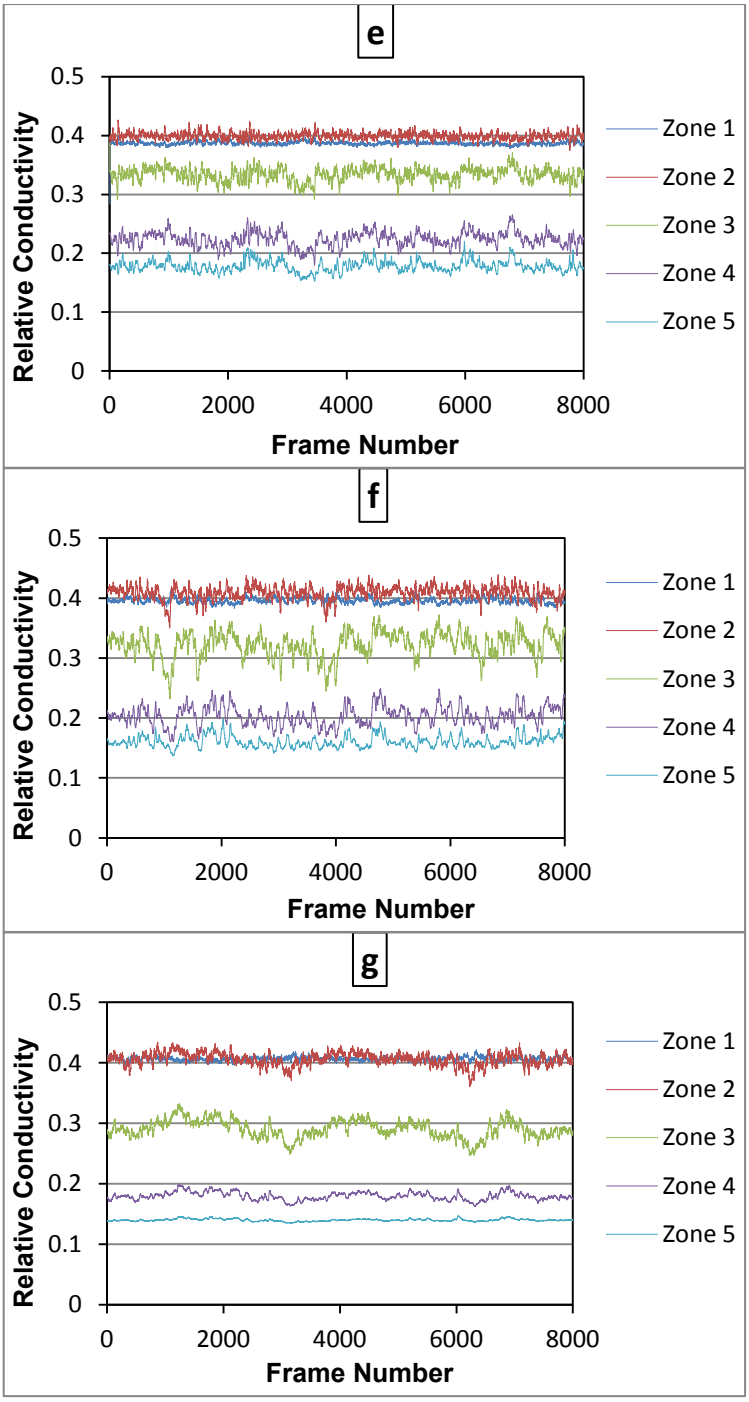

Figure 7.2 Showing the time domain signal of the ERT measurement for coarse sand at 10% throughput concentration: (a) 4.5 m/s, (b) 4.0 m/s, (c) 3.5 m/s, (d) 3.0 m/s, (e) 2.5 m/s, (f) 2.0 m/s, (g) 1.5 m/s

In other words, by altering the transport velocity the mean conductivity goes through changes in each zone. It is apparent that the mean conductivity of each zone is related to the solids volume fraction. This is due to the fact that by reducing the velocity the solid particles migrate towards the bottom of the pipe, which results in higher conductivity at the top half of the pipe and lower at the bottom half. Based on this phenomenon, this feature could be considered as an element in the recognition scheme. Moreover, it is quite

evident that at 1.5 m/s slurry velocity; the signal of zone 5 decreases its fluctuation significantly. It can be seen almost as a straight line. It is worth pointing out that the visual observation of the flow during the experiment revealed that there was a packed stationary bed at the bottom of the pipe, the thickness of which was measured to be 7.5 mm. It can then be concluded that, based on the form of the signal in zone 5 at 1.5 m/s, the flow regime is stationary bed. By further analysis of the signal of zone 5 it was found that the standard deviation decreases with decrease of velocity. This is an indication of reduction of turbulent fluctuation in the conductivity. For example, for the velocity range 1.5-4.5 m/s the standard deviation range was found to be within 0.0019-0.2. Therefore, a threshold can be assigned for stationary bed, based on the standard deviation of zone 5. Also, the relative difference between the slurry conductivity at the top half of the pipe and the bottom half of the pipe could be used as a threshold for every flow regime, as shown below:

$$\mathrm{A} = \frac{Z_1 + Z_2 + \left(\frac{Z_3}{2}\right)}{3} \tag{7.1}$$

$$\mathrm{B} = \frac{\left(\frac{Z_3}{2}\right) + Z_4 + Z_5}{3} \tag{7.2}$$

$$C = \frac{A}{(A + B)} \tag{7.3}$$

Where:

A= Average slurry conductivity at the top half of the pipe.

B= Average slurry conductivity at the bottom half of the pipe.

C= Ratio of average conductivity of the top half of the pipe to the average conductivity across the pipe cross-section.

Z_1= Average conductivity in zone 1.

Z_2= Average conductivity in zone 2.

Z_3= Average conductivity in zone 3.

Z_4= Average conductivity in zone 4.

Z_5= Average conductivity in zone 5.

As the significant feature and relevant information regarding every flow regime is also contained in zone 3, therefore, this zone, which splits the pipe cross-section in the middle, has also been taken into account in the analysis. One half of zone 3 is included into the top half of the pipe, whereas the other half is incorporated into the mean conductivity of the bottom half of the pipe. Therefore, based on the value of C, a threshold can be assigned for the flow regimes under consideration. However, in order to assign the value of C to every flow regime some initial information regarding the boundaries between the investigated flow regimes is required. In order to define these boundaries it is paramount to know the transitional velocities for the condition used in this investigation. Therefore, this information regarding the boundaries of flow regimes was experimentally obtained, through visual observation of slurry flow and photographic evidence of the active flow regime for each condition. It is worth mentioning that the identification of these boundaries, at which one flow regime changes to another, can be quite difficult by conventional visual observation of flow through a transparent pipe section. This is obviously due to the opacity of slurry and complex nature of slurry flow. Therefore, the transitional regime boundaries were arbitrary widened (±0.3 m/s) to include the velocity at which one flow regime changes to another.

7.3.2.2 Signal analysis in the frequency domain

In order to remove or at least reduce the subjectivity in recognizing the active flow regime, it was decided to extract further features of the signals, which would make another condition in decision making within the flow recognition scheme. It is evident that the signal in the time domain does not reveal enough information regarding the frequency component or characteristics of the signal. Therefore, Fast Fourier Transform (FFT) of the noisy original signal was taken to display the signal in frequency domain. MATLAB was used for the FFT analysis of the signal and the code is shown below:

```
T = 0.0015; % Sample Time
Fs = 1/T; % Sampling Frequency
L = 8000; % Length of Signal
% Sum of a 50 Hz sinusoid and a 120 Hz sinusoid

NFFT = 2^nextpow2(L); % Next power of 2 from length of y

V = fft (Z1,NFFT)/L; % Zone 1
W = fft (Z2,NFFT)/L; % Zone 2
X = fft (Z3,NFFT)/L; % Zone 3
Y = fft (Z4,NFFT)/L; % Zone 4
Z = fft (Z5,NFFT)/L; % Zone 5

f = Fs/2*linspace(0,1,NFFT/2+1);

% Plot single sided amplitude spectrum
plot(f,2*abs(V(1:NFFT/2+1)),f,2*abs(W(1:NFFT/2+1)),f,2*abs(X(1:NFFT/
2+1)),f,2*abs(Y(1:NFFT/2+1)),f,2*abs(Z(1:NFFT/2+1)))

plot(f,2*abs(V(1:NFFT/2+1)))
plot(f,2*abs(W(1:NFFT/2+1)))
plot(f,2*abs(X(1:NFFT/2+1)))
plot(f,2*abs(Y(1:NFFT/2+1)))
plot(f,2*abs(Z(1:NFFT/2+1)))
title('Single-sided amplitude spectrum of noisy ERT signals-2.0
m/s')
xlabel('Frequency (Hz)')
ylabel('Amplitude')
ylabel('|Y(f)|')
axis([0 50 0 0.06])

legend('Zone 1','Zone 2','Zone 3','Zone 4','Zone 5');

legend('Zone 1')
legend('Zone 2')
legend('Zone 3')
legend('Zone 4')
legend('Zone 5')
fprintf('%8.3f, %8.3f\n',f, 2*abs(V(1:NFFT/2+1)));
```

The frequency components of each zone for each condition were determined, and an example of coarse sand at 10% throughput concentration and 4.0 m/s is shown in Figure 7.3.

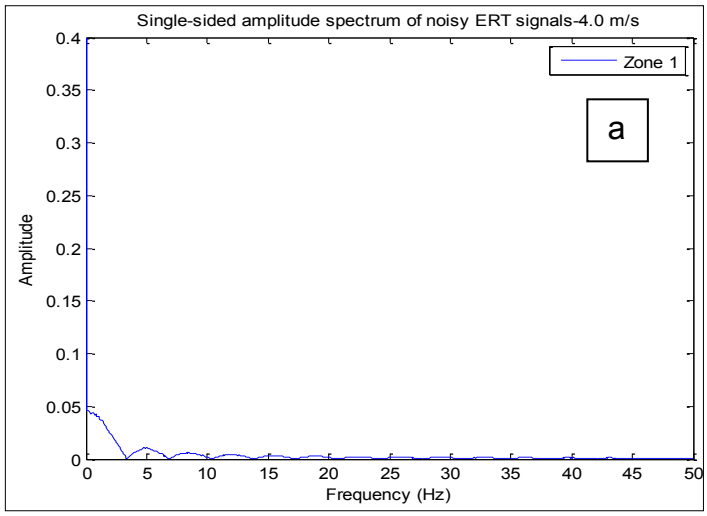
Single-sided amplitude spectrum of noisy ERT signals-4.0 m/s
Zone 1
a
Amplitude
Frequency (Hz)
0.4
0.35
0.3
0.25
0.2
0.15
0.1
0.05
0
0 5 10 15 20 25 30 35 40 45 50

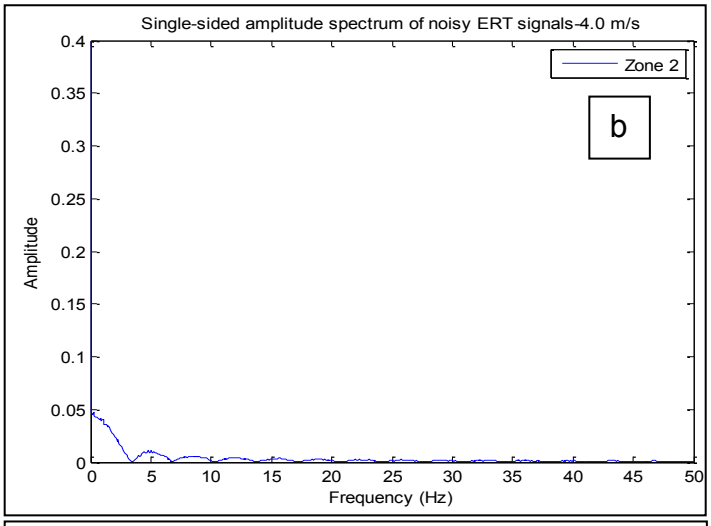
Single-sided amplitude spectrum of noisy ERT signals-4.0 m/s
Zone 2
b
Amplitude
Frequency (Hz)
0.4
0.35
0.3
0.25
0.2
0.15
0.1
0.05
0
0 5 10 15 20 25 30 35 40 45 50

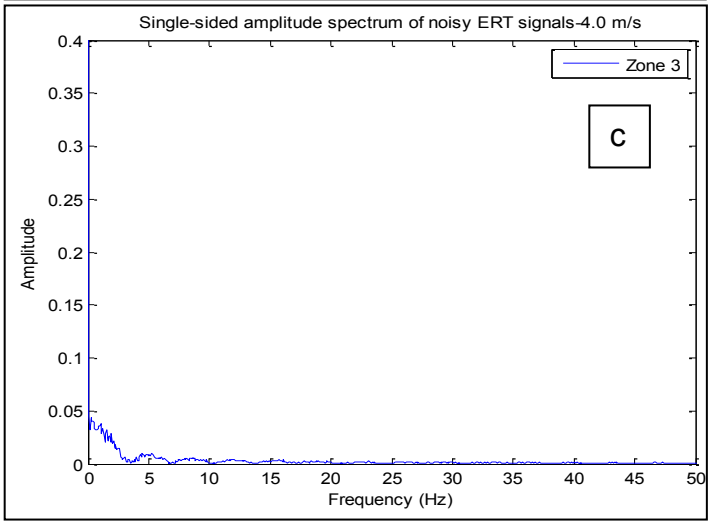
Single-sided amplitude spectrum of noisy ERT signals-4.0 m/s
Zone 3
c
Amplitude
Frequency (Hz)
0.4
0.35
0.3
0.25
0.2
0.15
0.1
0.05
0
0 5 10 15 20 25 30 35 40 45 50

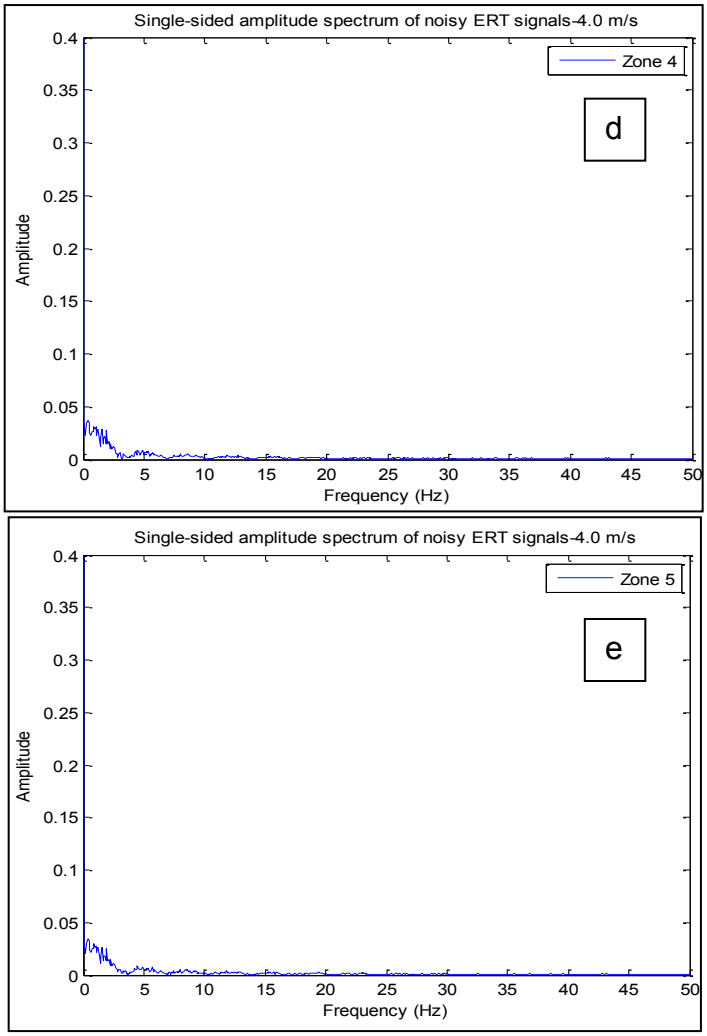

Figure 7.3 Showing the frequency component of the signal in each zone for flowing coarse sand at 4 m/s. (a) Zone 1, (b) Zone 2, (c) Zone 3, (d) Zone 4 and (e) Zone 5

By observing the signal in the frequency domain the main frequency components can well be identified along with amplitude of the signal. A zoomed plot example of the FFT is shown in Figure 7.4, which reveals the signature of flow in each zone.

In order to make the basis of the recognition scheme, distinctive features are required to be identified. A journey through literature revealed that there is a number of methods available for extracting flow features from flow process measurements, such as Signal-to-Noise ratio (SNR), Power Spectral Density Functions (PSDF), Probability Density Functions (PDF), Auto Correlation Functions (ACF) etc. (Lowe and Rezkallah,1999).

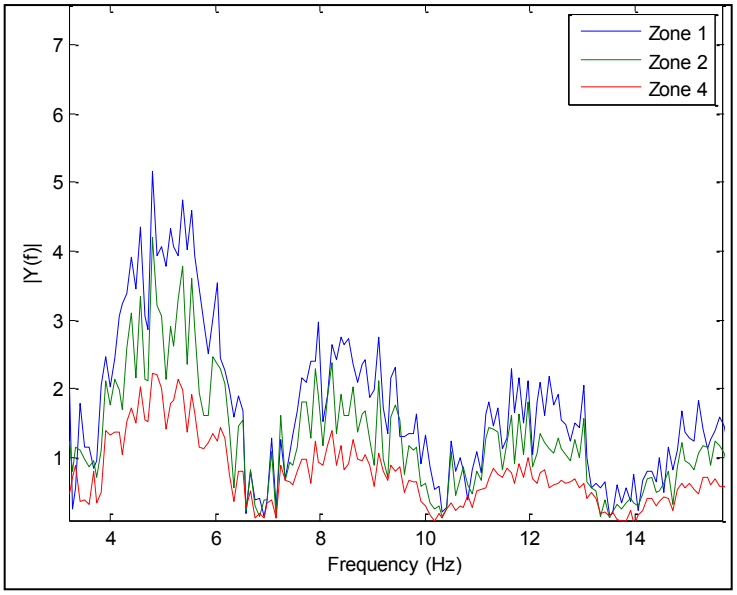

Figure 7.4 Showing a zoomed frequency components of zones 1, 2 and 4 wave form, obtained from FFT, for flowing coarse sand at 4.0 m/s

However, in this study the statistical analysis and power spectral analysis are employed to extract the flow information from the time series and frequency domain respectively. Therefore, it was decided to carry out a spectrum analysis of the signal, in which an attempt is made to measure the signal power. The spectrum of a signal shows how much power is contained in each of its components or frequency (Stoica and Moses, 2005). In order to estimate the power of any component of a signal a plot is required, in which the x-axis is the frequency components and on y-axis presents the power spectrum of the signal. Some of the most important methods of the spectrum objects are Power Spectral Density (PSD), Mean Square Spectrum (MSS) and Pseudo-spectrum. The power spectrum is also referred to as the Power Spectral Density (PSD). PSD is one of the most important method of spectrum analysis, as it highlights the strong and weak variations (energy) of a signal and also can be used for oscillatory and non-oscillatory signals in the time series data (Chatfield, 1989).

In statistical signal processing, the power spectrum of a signal is estimated from a sequence of time samples of the signal. In other words, the frequency content of the signal is characterised through spectral density. Generally the techniques to estimate the spectrum of a signal can fall into the scopes of two class methods, parametric and non-parametric methods. The theory and mathematical definition of these techniques are avoided in this study, however, the detailed description and theory of each technique can be found

in Stoica and Moses (2005). Spectral Analysis and Time Series. Academic Press). The spectrum of a signal is defined by the plot, in which the magnitude and phases of different frequency components are clearly indicated. In order to find spectrums of a signal the FFT has to be employed (Cerna and Harvey, 2000). In the analysis used in this study, the periodgram technique is adopted, which is considered as a non-parametric method and a common spectral estimator. The selection of periodogram is based on the fact that it is robust, simple, it can provide reasonably high resolution for a very long data length and computationally cheap for estimating the power spectrum of a signal. It is worth pointing out that the power spectrum does not readily determine the average power of the signal, but only power of a frequency component. Therefore, the area under the curve of PSD of a signal has to be integrated to obtain the average power of the signal under analysis. In other words, the area under the PSD curve renders the average power of the signal. The PSD of the signal is estimated by the periodogram, which uses directly sampled FFT. The PSD is a measure of power per unit of frequency, hence it has units of power/frequency. The MSS, on the other hand, is a measure of power at a specific frequency and has units of power. As previously mentioned the spectrum view is clearly have more information than the time domain. In order to determine the statistics of each signal in each zone, the plot of MSS were produced so as to estimate the relationship of the signal power and transport velocity at a specific frequency, as shown in Figures 7.5 and 7.6. Due to the vast amount of plots the analysis of only two conditions (1.5 m/s & 2.0 m/s) are shown here.

By observing the MSS plots, we can see that there is a relation between the velocity and the power of the signal. The power of the signal increases with increase of velocity. Since any reduction in slurry velocity can influence the amplitude, and the difference can be clearly seen from one zone to another or one flow condition to another, thus a distinctive feature can be extracted to make the basis of the recognition scheme.

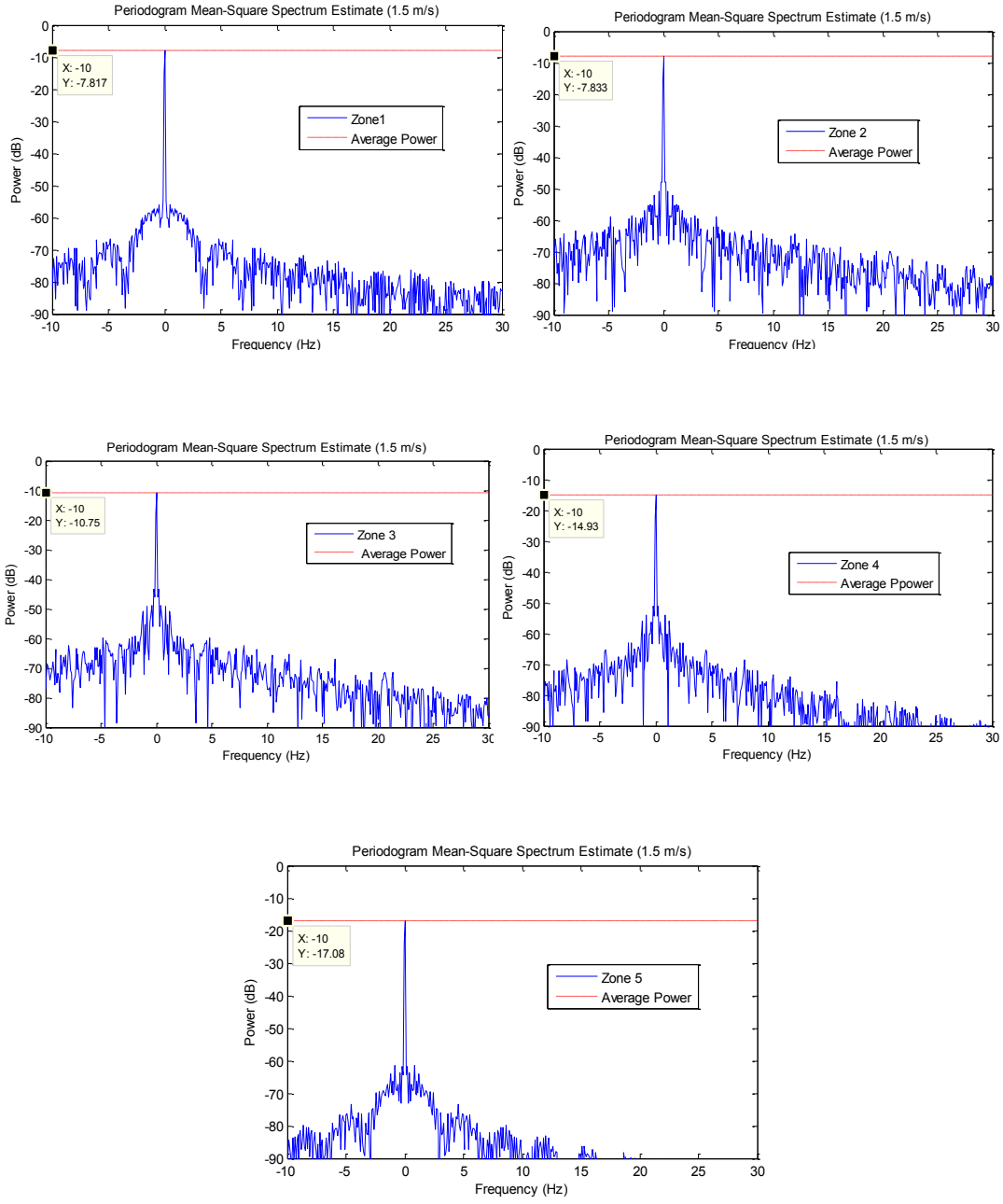

Figure 7.5 Showing the periodogram Mean-Square Spectrum for each zone at 1.5 m/s

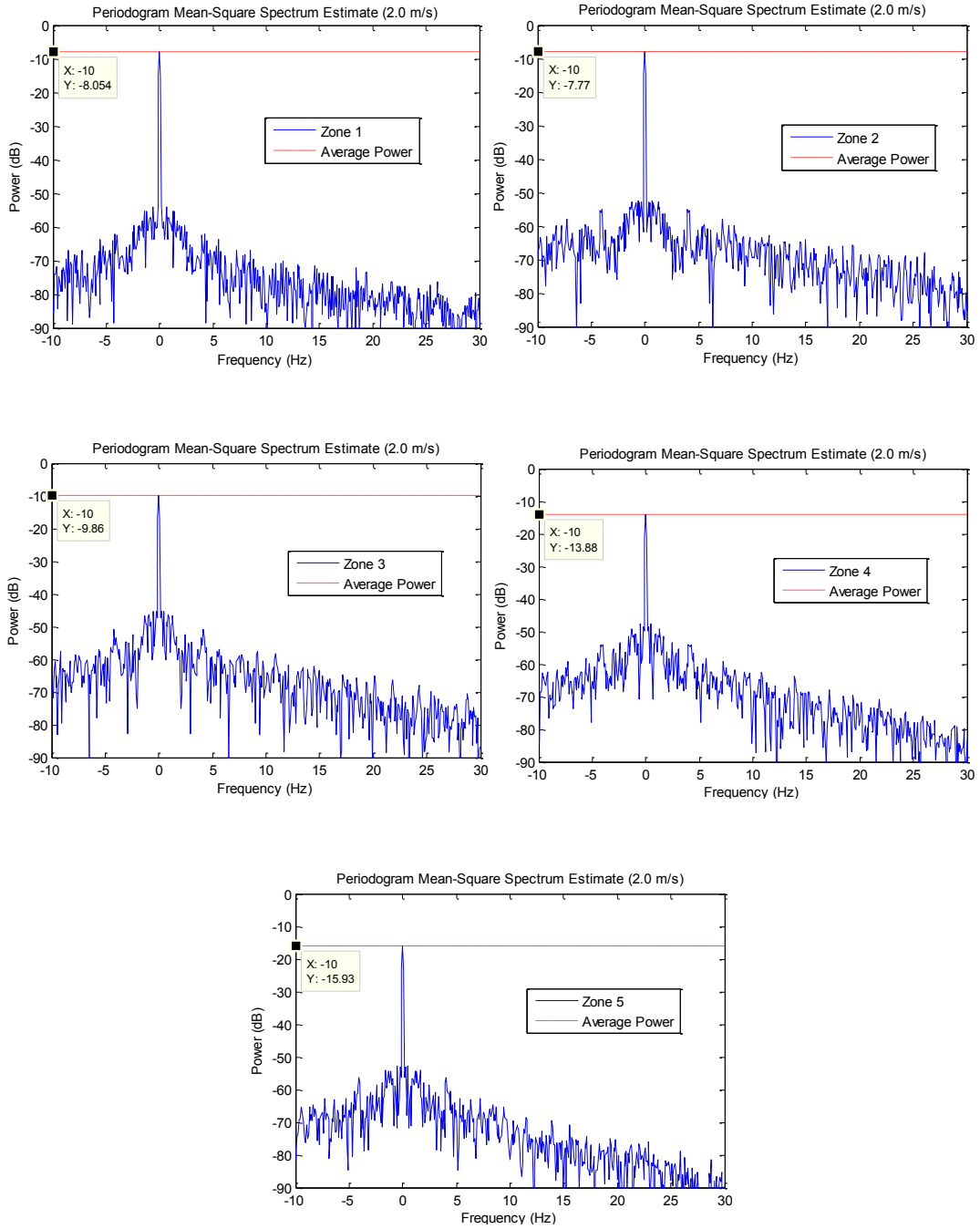

Figure 7.6 Showing the periodogram Mean-Square Spectrum for each zone at 2 m/s

This feature can be used to relate the signal power at the top half of the pipe to the signal power at the bottom half of the pipe. In other words, The average signal power decreases with increase of solid particles in each zone. Therefore, a threshold can be assigned, based on the relative difference between the signal power at the top half of the pipe and the bottom half of the pipe for each flow regime.

However, in order to determine the threshold for each signal, the average power of each signal is required. Since the methods of the PSD include a plot and average power. Then the PSD is considered to return the average power of each signal. The average power method uses a rectangle approximation to the integral to calculate the signal's average power using the PSD data. Therefore, the following steps were followed to calculate the average power of each signal:

1. Creating a periodogram spectrum with a Hamming window.
2. Create a power spectral density object.
3. Set the options for the periodogram.
4. Calculate the PSD.
5. Calculate the average power.

Once the average power of each zone is calculated, then the comparison is made between the signal power at the top half of the pipe and the power at the bottom half of the pipe. This can be done by calculating the ratio of the average power at the top of the pipe $(\mathrm{P}_1, \mathrm{P}_2 \ \& \ \mathrm{P}_3/2)$ to the average power across the five zones (or pipe cross-section); as shown below:

$$E = \frac{P_1 + P_2 + \left(\frac{P_3}{2}\right)}{3} \tag{7.4}$$

$$F = \frac{\left(\frac{P_3}{2}\right) + P_4 + P_5}{3} \tag{7.5}$$

$$D = \frac{E}{(E + F)} \tag{7.6}$$

Where:

E= Average signal power at the top half of the pipe.

F= Average signal power at the bottom half of the pipe.

D= Ratio of average signal power of the top half of the pipe to the average signal power across the pipe cross-section.

P_1= Average signal power in zone 1.

P_2= Average signal power in zone 2.

P_4= Average signal power in zone 4.

P_5= Average signal power in zone 5.

Again as the significant feature and relevant information regarding every flow regime is also contained in zone 3. Therefore, this zone, which splits the pipe cross-section in the middle, has also been taken into account in the signal analysis. One half of zone 3 is included into the top half of the pipe, as previously mentioned in the time domain signal analysis, whereas the other half is incorporate into the bottom half of the pipe. Therefore, based on the value of *D*, a threshold can be assigned for the flow regimes considered in this investigation. However, in order to assign the value of D to every flow regime some initial information regarding the boundaries between the investigated flow regimes is required. In order to define these boundaries it is paramount to know the transitional velocities for the condition used in this investigation. Therefore, the same information used in the analysis of the signal in the time domain, is also considered here to assign the boundaries between the flow regimes. Obviously this information has been obtained through visual observation of slurry flow and photographic evidence of the active flow regime for each condition. It is worth mentioning that the identification of these boundaries, at which one flow regime changes to another, can be extremely difficult by conventional visual observation of flow through a transparent pipe section. This is obviously due to the opacity of slurry and complex nature of slurry flow. Therefore, the transitional regime boundaries were arbitrary widened (±0.3 m/s) to include the velocity at which one flow regime changes to another.

The significant feature and relevant information regarding every flow regime can clearly be extracted by comparing the top half with the bottom half of the pipe. This can clearly be seen in the plot of power against the 5 zones, as shown in Figure 7.7.

Figure 7.7 showing the average signal power, for 10% coarse sand, against each zone as a function of velocity. It is evident that the velocity influences the signal power. By observing the plot, it can be seen that at the bottom of the pipe the average power of the signal decreases with decrease of velocity. At the top of the pipe, on the other hand, the average power of the signal increases with increase of velocity. This is clearly due to the difference in solids concentration between the top and bottom of the pipe.

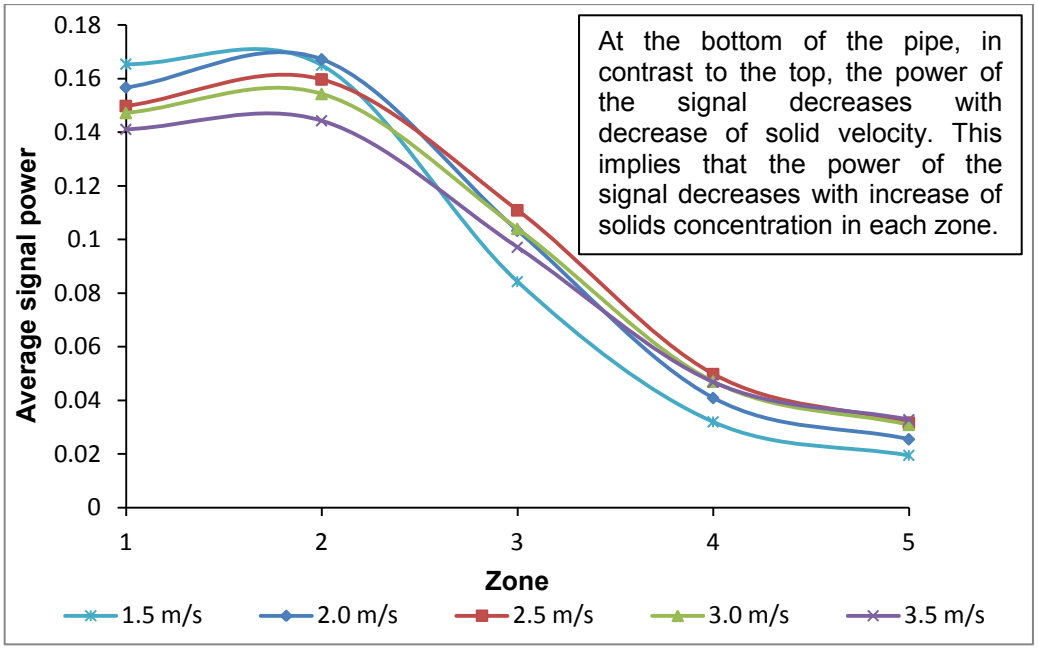

Figure 7.7 The average signal power against the 5 zones as a function of transport velocity

7.3.3 Threshold indication of the signal

7.3.3.1 Threshold indication of the signal (Relative Conductivity)

The information obtained from visual observation of flow regarding the transitional velocities has been used to determine the boundaries between flow regimes and the range of C for each flow regime. The threshold of C was determined by plotting the transport velocity against the relative difference between the top and the bottom of the pipe (C) for every condition as shown in Figure 7.8

Figure 7.8 is showing the value of C in each flow regime and every condition. The shaded areas represent the transitional regime boundary, which are also taken into account in the recognition scheme. Therefore, the threshold can be assigned for each flow regime/transitional region, as shown in Table 7.2.

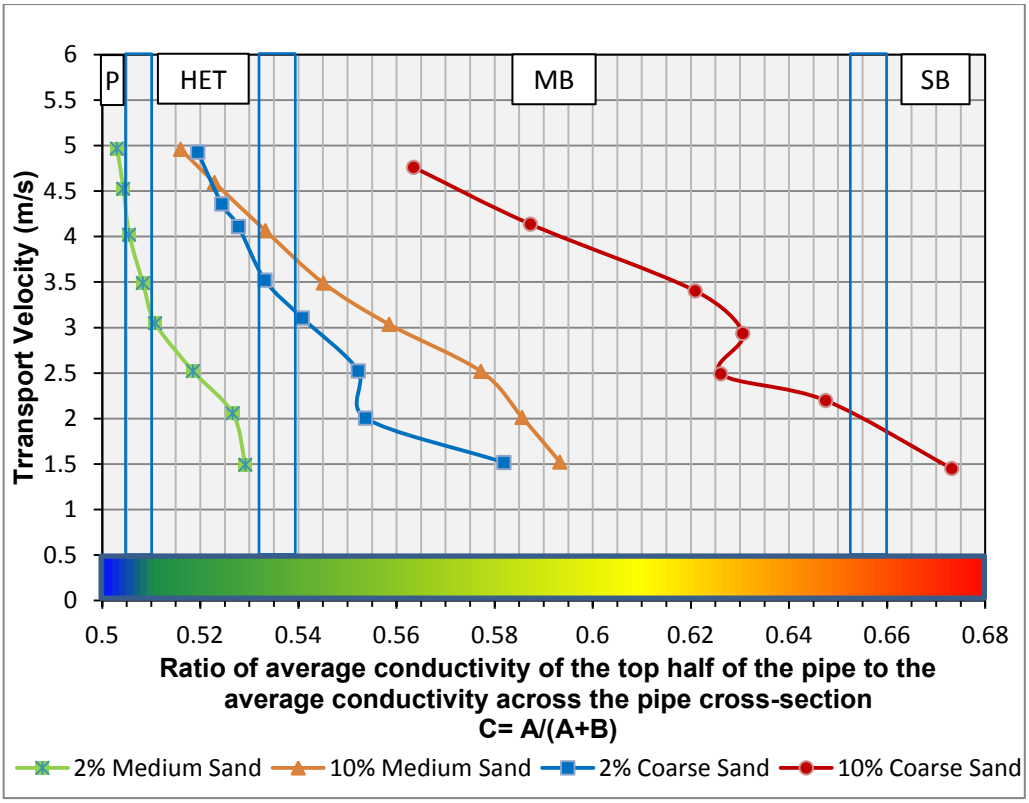

Figure 7.8 Showing the threshold of the signal based on the relative difference in the conductivity of the top and bottom of the pip. (P) Pseudo-homogeneous, (HET) Heterogeneous, (MB) Moving Bed, (SB) Stationary Bed

Table 7.2 Showing the range of C value for every flow regime or transitional region

Flow Regime	C range value
Homogeneous	0.499≤C<0.501
Pseudo-homogeneous	0.501≤C<0.505
Transitional Boundary (Pseudo-homogeneous Heterogeneous)	0.505≤C<0.510
Heterogeneous	0.510≤C<0.532
Transitional Region (Heterogeneous-Moving Bed)	0.532≤C<0.540
Moving Bed	0.540≤C<0.652
Transitional Region (Moving Bed-Stationary Bed)	0.652≤C<0.657
Stationary Bed	0.657≤C

7.3.3.2 Threshold indication of the signal (Average Power)

The information obtained from visual observation along with the photographs of the flow in terms of the transitional velocities has been used to determine the boundaries between the flow regimes and specify the range of D values for each flow regime. The threshold of D value was determined by plotting the transport velocity against the ratio of average power at the top of the pipe to the average power at the bottom of the pipe for every condition, as shown in Figure 7.9.

Figure 7.9 is showing the value of D within each flow regime and every condition. The shaded areas represent the transitional regime boundary, which are also included into the recognition scheme. Therefore, the threshold can be assigned for each flow regime/transitional region, as shown in Table 7.3.

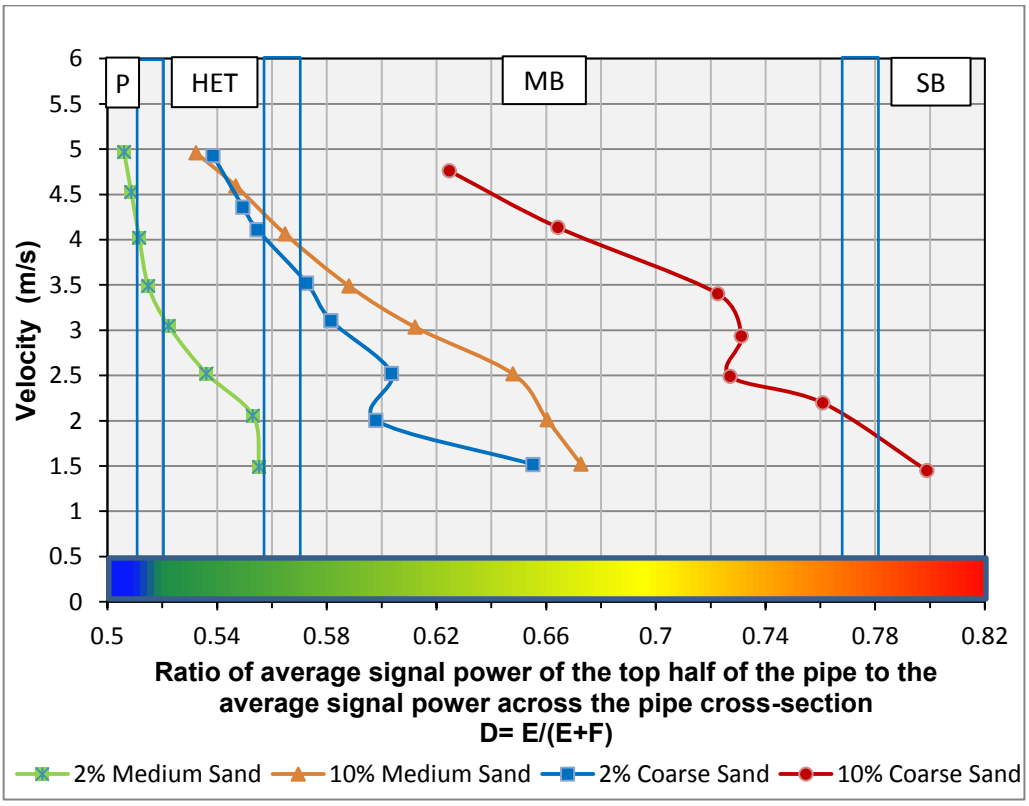

Figure 7.9 Showing the threshold of the signal based on the difference in the average power of the signal at the top and bottom of the pipe. (P) Pseudo-homogeneous, (HET) Heterogeneous, (MB) Moving Bed, (SB) Stationary Bed

Table 7.3 Showing the range of D value for every flow regime or transitional region

Flow Regime	D range value
Homogeneous	0.496≤D<0.504
Pseudo-homogeneous	0.504≤D<0.510
Transitional Boundary (Pseudo-homogeneous Heterogeneous)	0.510≤D<0.520
Heterogeneous	0.520≤D<0.555
Transitional Region (Heterogeneous-Moving Bed)	0.555≤D<0.570
Moving Bed	0.570≤D<0.770
Transitional Region (Moving Bed-Stationary Bed)	0.770≤D<0.780
Stationary Bed	0.780≤D

7.3.4 Decision making

The decision on the type of the active flow regime, including transitional regions, will be based on the assigned threshold values of C and D, as demonstrated by the flow chart shown in Figure 7.10. The flow chart representing the automated flow regime recognition process along with the visualisation of solids volume fraction across the pipe cross-section via 2D and 3D plots. In order to remove or reduce the subjectivity in recognizing the prevailing flow regime, or to make the best decision, the two threshold values were considered together at the same time, i.e. based on the assigned threshold values for each flow regime, the value of C AND D must apply to the output recognized flow regime. This implies that if one of the values is incorrect then it will not return any result, instead the returning message would be “Could not determine the flow regime”.

Also, since A is the product of the ratio of the mean conductivity of the top half of the pipe to the mean conductivity of the pipe cross section (A+B), ideally one would think that at homogeneous flow regime, A should be equal to 0.5. However, as this is highly unlikely to happen in real world, therefore, a range of threshold values of C and D has been assigned, within which homogeneous flow regime would be returned. The threshold values of C has been extended by ±0.001 and D by 0.004. Thus, in order for the recognition scheme to return homogeneous flow regime, the value of C has to be

between 0.499 and 0.501 and the value of D has to be between 0.496 and 0.504.

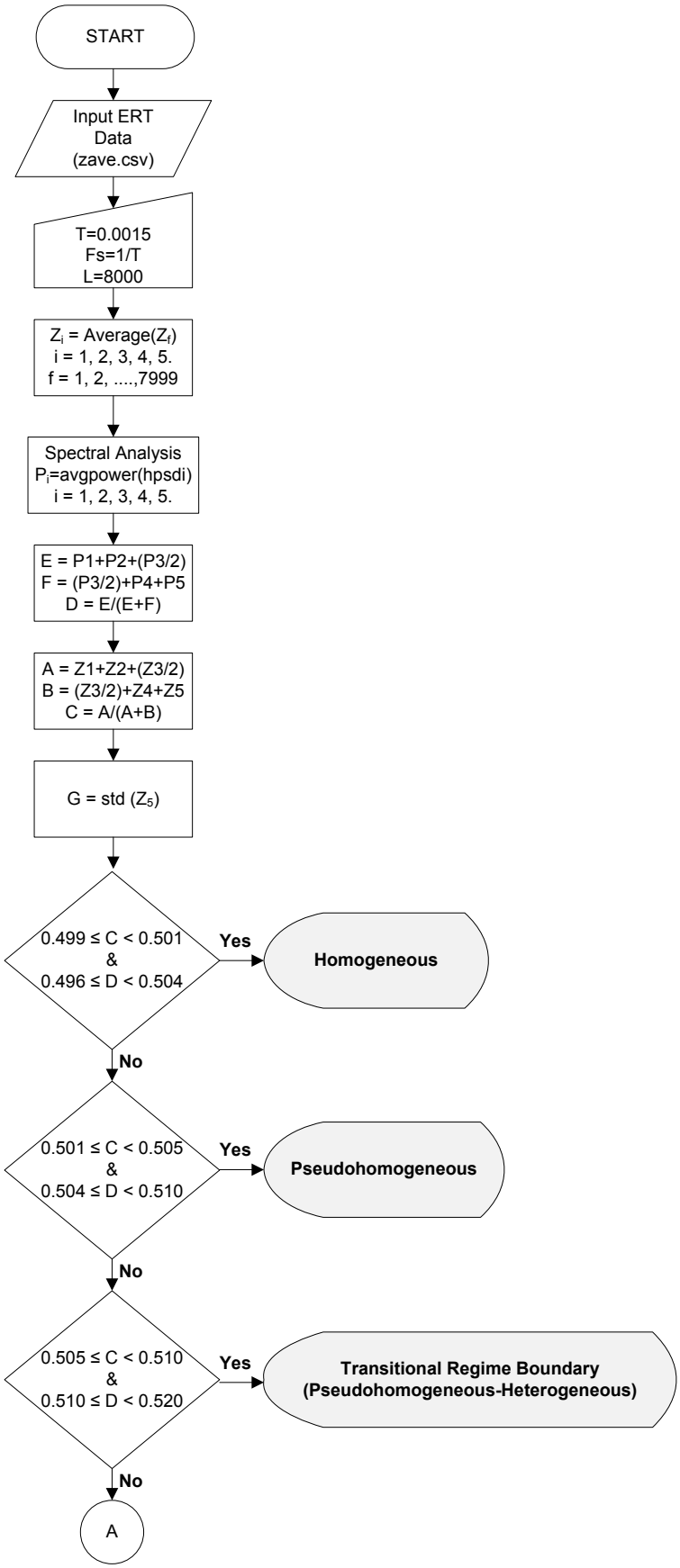

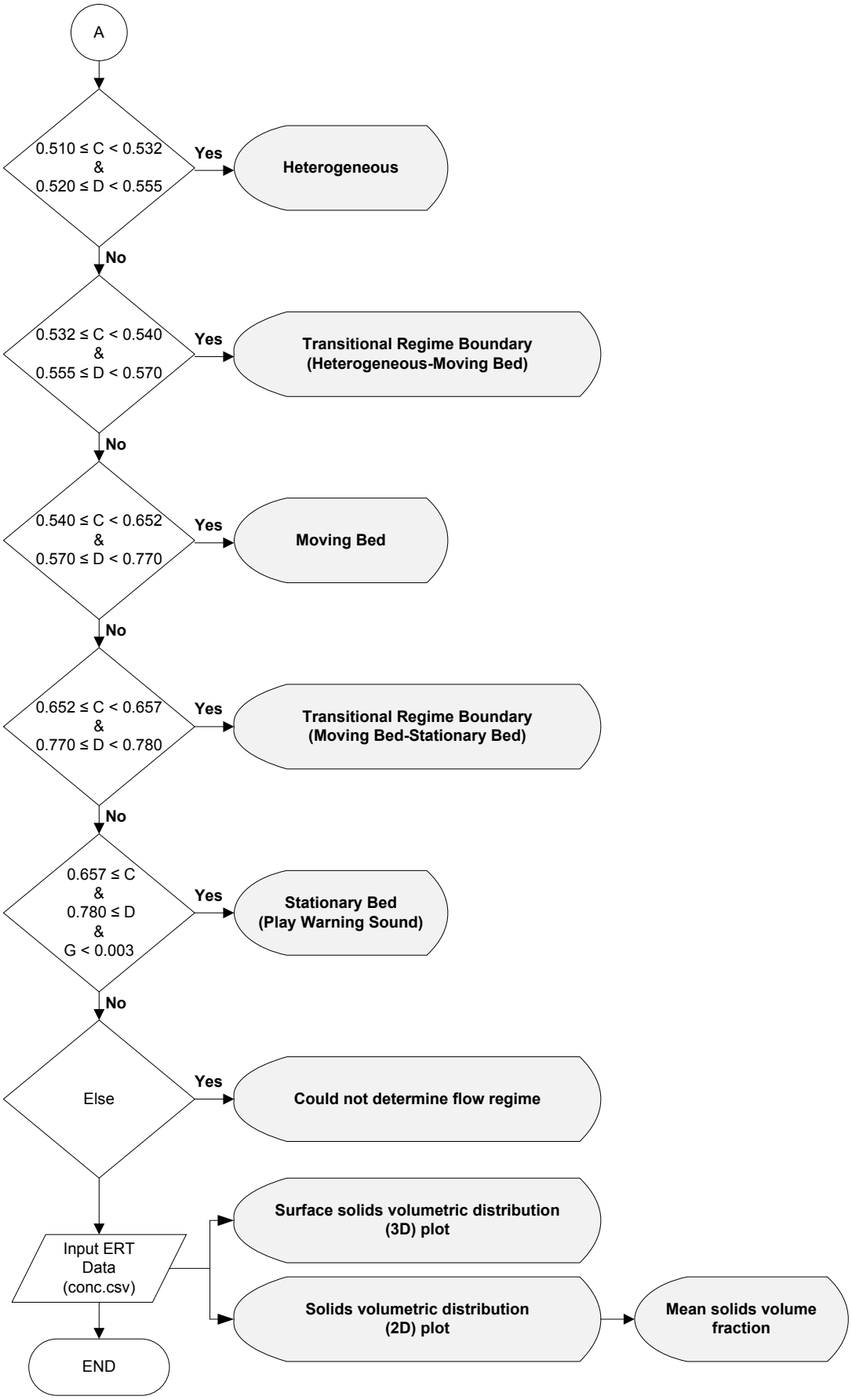

Figure 7.10 Sequential flow chart of the recognition process

As the transitional flow regime boundaries are very difficult to define, therefore, the transitional velocity, at which one flow regime changes to the next, has been corrected by ±0.3 m/s.

Since the stationary bed is the most sensitive flow regime and undesirable by many industries, then another condition has been assigned along with both conditions (C & D). The third condition is the standard deviation (STDEV) of the signal. As previously discussed, once a packed stationary bed is formed at the bottom of the pipe (zone5), then the signal in zone 5, unlike any other zones or conditions, does not show a turbulent fluctuation. Therefore, in order to determine that the flow regime is stationary bed, three conditions have to be met (C, D and G). G returns the standard deviation of the signal in zone5. Based on the experimental data and visual observation, the threshold for the standard deviation of the signal in zone 5 has been assigned as an arbitrary value (G<0.003), which determines stationary flow regime. Due to the sensitivity of this type of flow regime a warning sound (alarm) is included so as to warn the operator.

7.3.5 Program coding

MATLAB was used to code the program for automated flow regime recognition. The script of which is shown in Appendix D.

In order to determine the active flow regime, all that is required is to import the ERT measurement data (conductivity) in the form of zave. csv file, which is exported from the P2000 . It has been noted that, once the program is run, the elapsed time for determining the active flow regime is 30-35 s. This is due to the large amount of conductivity data in the zave file for 8000 frames. However, if on-line recognition of the flow regime is adopted, then it may not be necessary to input such a large data. The author believes that in order to continuously determine the flow regime, every 1000 frames would be sufficient. Since FICA system measures 8000 frames per second, then 1000 frames can be acquired in 0.125 s.

The code has been developed in such a way not only render the recognition of the active flow regime, but also to visualise the distribution of the solid particles across the pipe cross-section and measure the mean concentration. Therefore, along with the conductivity data (zave.csv), the concentration data (conc.csv) has also to be imported. In other words, by importing the conductivity data in the form of zave.csv file and concentration data in the form of conc.csv file, active flow regime is determined, 2D and 3D concentration profile is generated automatically, mean solids local

concentration is automatically calculated and displayed on the screen along with many other data statistics such as minimum solids local concentration, maximum solids concentration etc.

It is worth mentioning that the script, mentioned in Appendix D, is applicable for an electrode configuration, where the electrode number 1 positioned on the top of the pipe and the numbering continues clockwise viewing the direction of flow, as shown in Figure 7.11.

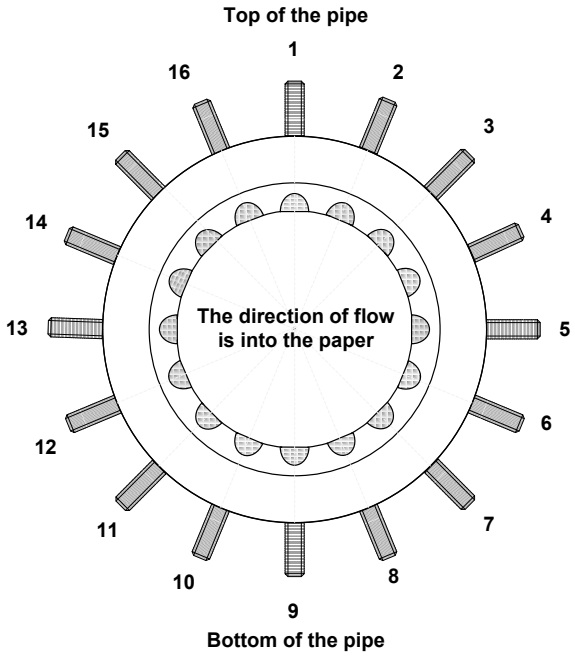

Figure 7.11 Electrode configuration for flow regime recognition

This configuration would obviously facilitate the importing concentration and conductivity data. In other words, this type of electrode configuration facilitate reading a range of consecutive columns in the conc.csv file rather than taking random columns, which is highly likely to increase the elapsed time of the computing. Since only the vertical centreline of the tomogram is considered for the purpose of flow regime recognition and plotting and measuring concentration, then it is not necessary to acquire all the data.

7.3.6 Running the program

Once the two files (zave.csv & conc.csv) are imported, the program can be run, immediately after which a wait-bar pops up delivering the message “Please wait...computation in progress”, as shown in Figure 7.12. First computation for flow regime recognition is carried out and the message is displayed within a massage box, then the computation continues to display solids volumetric distribution in the form of graph.

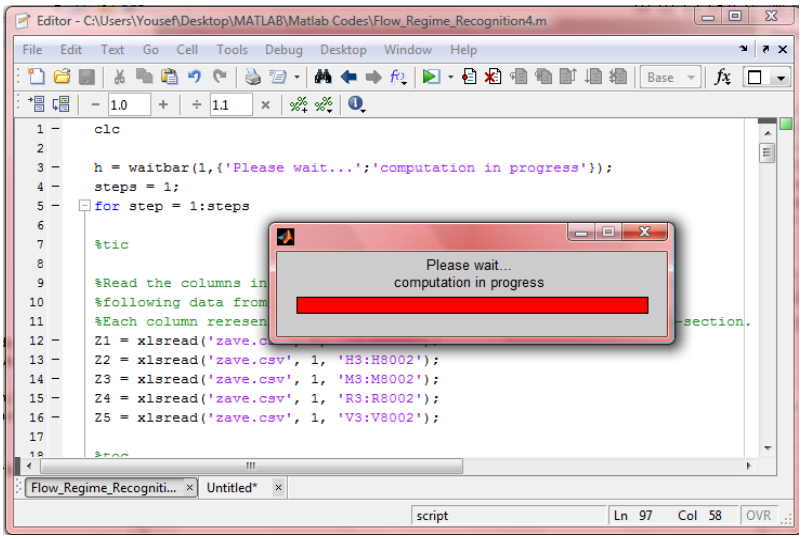

Figure 7.12 Initial running the program

After 30-35 seconds elapsed a message box pops up mentioning the type of prevailing flow regime, as shown in Figure 7.13. Each time the flow regime is determined a beep sounds, except for stationary bed flow regime, for which a warning sign and a suitable warning alarm sounds for 5 seconds to warn and draw the attention of the slurry line operator.

Immediately after displaying the active flow regime, another wait bar is displayed carrying the message “Please wait...Solids concentration distribution is displayed shortly”. Then two interactive graphs are displayed (2D and 3D), which represent the distribution of the volumetric solid fraction. This can be seen in Figures 7.14 & 7.15.

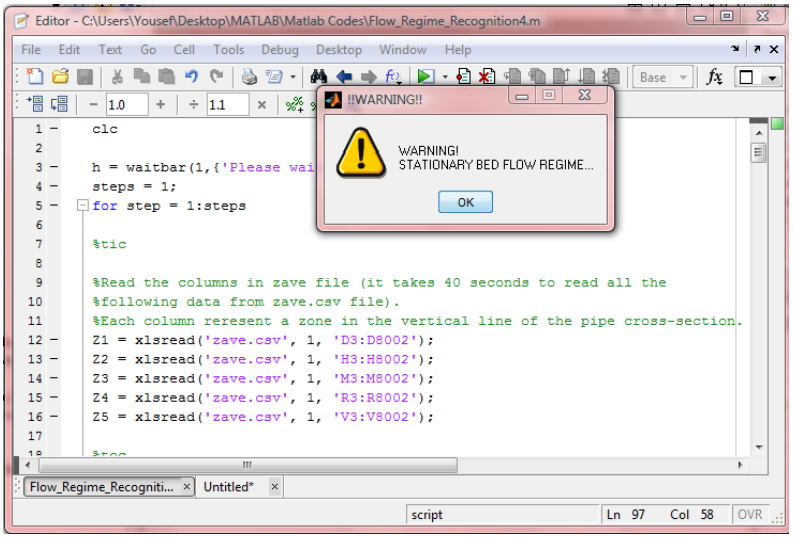

Figure 7.13 Message box conveying the result of flow recognition computation

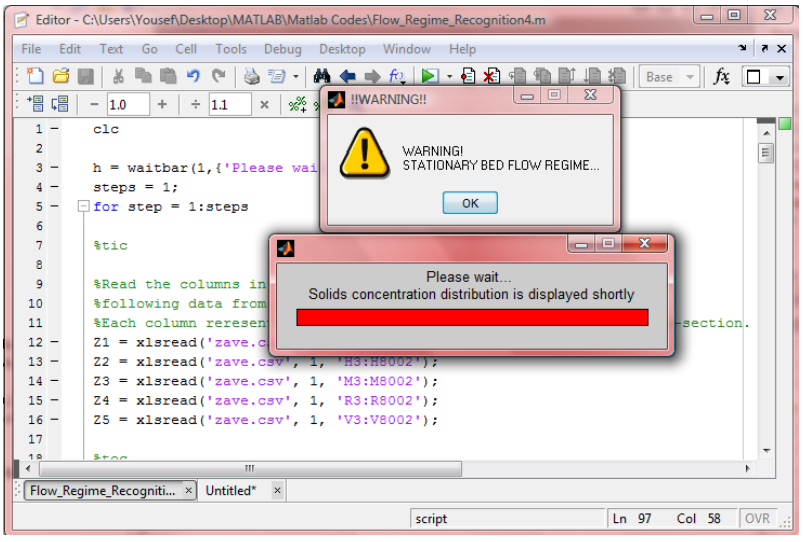

Figure 7.14 Wait-bar showing computation in progress

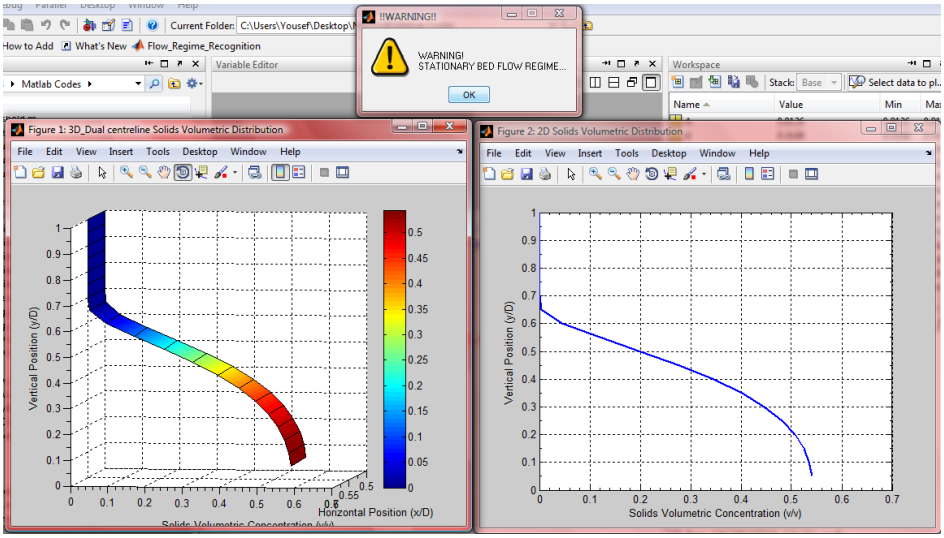

Figure 7.15 2D & 3D display of solids volumetric concentration distribution plot

The local solids concentration is automatically calculated and displayed on the graph. Also by going to Tools >Data statistics a table box is opened, which displays all the statistics regarding the concentration data (x-axis), such as minimum concentration, maximum concentration, mean solids local concentration etc. Each of statistical data regarding local solids concentration can be displayed on the graph by ticking the box against the required statistics. These are shown in Figures 7.16.

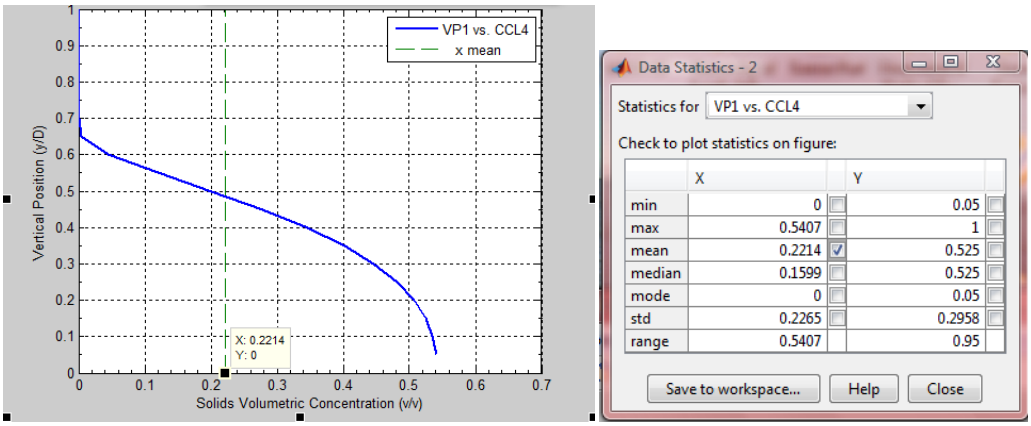

Figure 7.16 Display of solids local volume fraction distribution and data statistics

7.4 Evaluation of the method

In order to evaluate the recognition method, 31 test conditions were carried out within the range of velocity 1.5-5 m/s, which would undoubtedly cover all flow regimes considered in this recognition scheme. Different solid particle size (coarse & medium) at two different throughput concentrations (2% & 10%) were also used to evaluate the effect of particle size and solids concentration upon the recognition scheme. A summary of the evaluation results is demonstrated in Table 7.4, while the recognition results for different conditions are highlighted in Table 7.5.

Since the recognition decision is based on the analysis of the zones across the vertical centreline of the pipe cross-section, therefore it is believed that it can be applied on any pipe size conveying slurry. The results of the recognition method have been compared to the photographs of the flow and visual observation.

By observing the results in Table 7.5, it can be seen that out of 31 tests, the flow regime could not be determined or correctly determined only for three conditions. This error could be due to some systematic error in the original conductivity data input to the test or the result of visual observation may have been wrongly determined. The latter reason is more plausible due to opaque and murky nature of slurry, especially sand/water flow. However, a future investigation is recommended to determine the source of this error.

Table 7.4 Summary of recognition results

Total number of tests	31
Correct	28
Incorrect or unrecognised	3
Success rate	90.32%
Rate of error	9.68%

Table 7.5 Recognition results for different flow conditions

Sand	Test No.	Transport Velocity (m/s)	Actual Flow Regime	C	D	Recognised Flow Regime
2% Medium Sand	1	4.97	Transit.(P-HET)	0.503	0.506	P
	2	4.53	Transit.(P-HET)	0.504	0.508	P
	3	4.02	Transit.(P-HET)	0.505	0.511	Transit.(P-HET)
	4	3.49	Transit.(P-HET)	0.508	0.514	Trans.(P-HET)
	5	3.05	HET	0.510	0.522	HET
	6	2.52	HET	0.518	0.536	HET
	7	2.06	Transit.(HET-MB)	0.526	0.553	HET
	8	1.49	MB	0.529	0.555	Undetermined
10% Medium Sand	9	4.96	Trans.(P-HET)	0.516	0.532	HET
	10	4.59	HET	0.522	0.546	HET
	11	4.06	HET	0.533	0.564	Transit.(HET-MB)
	12	3.49	Transit.(HET-MB)	0.545	0.588	MB
	13	3.04	Transit.(HET-MB)	0.558	0.612	MB
	14	2.52	MB	0.577	0.647	MB
	15	2.01	MB	0.585	0.6604	MB
	16	1.52	MB	0.593	0.672	MB
2% Coarse Sand	17	4.93	HET	0.519	0.538	HET
	18	4.36	HET	0.524	0.549	HET
	19	4.11	HET	0.527	0.5546	HET
	20	3.52	Transit.(HET-MB)	0.533	0.572	Undetermined
	21	3.11	MB	0.540	0.581	MB
	22	2.52	MB	0.552	0.603	MB
	23	2.00	MB	0.553	0.597	MB
	24	1.52	MB	0.581	0.655	MB
10% Coarse Sand	25	4.76	HET	0.563	0.624	MB
	26	4.14	Transit.(HET-MB)	0.587	0.664	MB
	27	3.40	MB	0.620	0.722	MB
	28	2.94	MB	0.630	0.731	MB
	29	2.49	MB	0.626	0.727	MB
	30	2.20	MB	0.647	0.760	MB
	31	1.45	SB	0.673	0.798	SB

P: Pseudo-homogeneous **MB:** Moving Bed **HET:** Heterogeneous

SB: Stationary Bed **Trans:** Transitional Regime Boundary

7.5 Conclusions

A flow recognition method has been developed, which is based on the statistical signal analysis of the ERT data in both time and frequency domain. All common slurry flow regimes have been considered in the recognition scheme, including the transitional regime boundaries. The results of the evaluation suggest that the method is applicable to any particle size, solids concentration. It is also believed that the pipe size should not have any effect on the recognition scheme. However, application of the recognition method is paramount on different pipe sizes. The rate of recognition was determined to be 90.32% based on a sufficient number of tests carried out on different particle size and different concentration. Since the recognition decisions are based on the statistical ERT signal analysis, it is believed that it removes the subjectivity associated with recognition of the prevailing flow regime. This recognition method can be applied on any two phase solid/liquid flow, as long as one of the phases is non- or less conductive than the other one. It is believed that it can be useful for flow metering, especially for flow regime dependent flow meters. It can also be used in a non-invasive and on-line fashion for distinguishing the boundaries between different typical settling slurry flow regimes so as to enable the operator to take an appropriate control actions for other downstream operations such as separation, mixing etc. In addition, the recognition code has been developed in a way not only for recognition of the active flow regime, but also to visualise the distribution of the solid particles across the pipe cross-section and measure the mean concentration.

Chapter 8
Contributions, conclusions and future work recommendations

This final chapter highlights the contribution of present work, which includes the proposed ERT based measurement, flow visualisation and flow regime recognition technique along with the design of a multiphase flow system. A summary of the most important findings is presented. It also recommends the future scope in different areas of slurry flow in pipelines and exploration of further capabilities of the ERT system.

8.1 Author's contributions to slurry flow measurement, visualisation and the design of particulate flow system

Slurry transport has been a progressive technology for transporting a huge amount of solid materials across the world in both long distance pipelines and short commodity pipelines. Many slurry pipelines already exist and there will be more to build including all pipeline orientations. In order to ensure safe transport, optimised operation and reduction of financial costs by avoiding blockage, the operational engineer requires a reliable technique that suits all the conditions in industry. Clearly the complex nature of settling slurry flow forces the operator to continuously measure the local parameters governing the flow (solids concentration and solids velocity) and visualise the internal structure of the flow within the pipeline. Undoubtedly the measurement of these parameters and monitoring the flow within the pipe, in fast evolving processes requires a fast responding instrument (i.e. high frame rates of milliseconds). This study was performed in order to develop a new automated online measurement technique, which is based on the combination of a high performance ERT as the main sensor and the EMF as an auxiliary sensor. This will prove advantageous, as it will allow the operator to perform the measurement of each phase and to be able to see the changes in solids concentration and solids movement within the pipe. This work has also developed a new facility, which will act as a spring-board for better understanding of slurry flow behaviour and the interaction of solid-liquid inside pipeline, particularly inclined flow, which is complex and a very limited information has been reported about it. This thesis can be considered as a direct response to today's slurry engineering requirements and a step

forward for better controlling the processes and reducing unnecessary financial costs. The author's findings and observations provide a novel insight over the mechanisms of solid-liquid flow, along with a new ERT based technique for local flow measurement, flow visualisation and automated flow regime recognition. The results reveal the capabilities of the ERT and pave the way to a reliable and robust technique, which helps to further optimise the operation of settling slurry pipelines in industry. The main contribution is described as below:

8.1.1 Slurry flow measurement (Chapter 5)

8.1.1.1 Local solids volume fraction

A high performance dual-plane Electrical Resistance Tomography system has been employed to interrogate the internal structure of horizontal and vertical counter-gravity slurry flow. The exceptional capability of this system enabled acquiring high frame rates (1000 dfps) in a non-intrusive fashion. The reconstructed tomograms obtained from the ERT were collected and analysed to determine the in-situ solids concentration and solids concentration profile across the vertical plane of the pipe cross-section. The comparison of the results with that of flow diversion technique revealed that the ERT measurements give a reasonable estimation of the in-situ solids concentration in both orientations, horizontal and vertical. The description of these results can be found in sections 5.4.10.1 for horizontal flow and 5.5.3.1 for vertical flow. The tracking of solids concentration changes as a function of transport velocity was also generated, each of which represents the typical concentration profile of settling slurry flow. For further detail regarding the measured solids volumetric distribution, the reader is referred to sections 5.4.2 for horizontal flow and 5.5.1 for vertical counter-gravity flow. It seems that using a high performance ERT system for measurement of in-situ solids concentration is completely novel.

8.1.1.2 Local solids axial velocity

The high performance ERT system in conjunction with the cross-correlation technique can be used for local axial solids velocity and solids velocity distribution across the vertical plane of the pipe cross-section. The detailed description of solids velocity measurements can be found in sections 5.4.3 for horizontal flow and 5.5.1. To the author's knowledge the measurement of in-situ solids velocity and solids axial velocity distribution is rather novel for the flow conditions used in this study.

8.1.1.3 Slurry volumetric flow rate

The present work proposes a novel ERT based technique, which combines the Electrical Resistance Tomography and the Electromagnetic Flow Meter for performance of volumetric flow rate measurement of each constituent phase individually and measurement of mixture volumetric flow rate in vertical pipeline. Sections 5.5.2 and 5.5.3.3 highlights the detailed description of the measurement technique and final evaluation respectively.

8.1.1.4 Phase slip velocity

This project presents a new method of slip velocity estimation in vertical flow using the combination of the ERT and the EMF. The slip velocity can be determined through the track of volumetric flow rate of both phases (solid and liquid). The reader is directed to section 5.5.2 for detailed explanation.

8.1.1.5 Parameters relevant to stratified flow

This present research reports a new method for estimation of several parameters of stratified flow through an analysis of both profiles, solids concentration and solids axial velocity. These parameters are mean granular bed concentration, mean granular bed velocity, the height of granular bed, the height of shear layer and the height of turbulent zone at the upper part of horizontal pipeline. This technique can be used to measure the height of granular bed only if the height of bed is greater than 2.5 mm in 50 mm inner diameter pipe. In other words, this technique can only be used if the height of granular bed is greater than the ratio of pipe diameter to the number of pixels in the vertical plane of the tomogram. It is worth pointing out that the estimation of these parameters is paramount for the design of slurry pipeline and optimisation. The detailed discussion of this method is covered in sections 5.4.6 and 5.4.6.1.

8.1.1.6 Measurement of blocked horizontal line

In some highly concentrated-solids transport systems the solid particles travelling in horizontal flow in the form of contact load with transmitting the submerged weight to the internal pipe surface, such as that of Alberta oil-sand deposits (Schaan *et al.*, 2007). This implies that the solids are transported in sliding mass or sliding thick granular bed. This thick layer of sliding granular bed may generate a potential error in slurry measurement. This study reports an evaluation regarding the performance of the ERT while a thick coating of granular bed (up to 80% of the inner pipe diameter) covers the electrodes on the dual-plane ERT sensor. In other words, the ERT was successfully performed for measurement of a horizontal pipeline. To the

author's knowledge, the use of ERT for measurement of such high concentrated slurry has never been reported in the literature. Therefore, this can be considered as a novelty within the body of this thesis. The discussion of this finding is presented in section 5.4.5.5. The observation of the results revealed that the ERT can undoubtedly detect the pipeline blockage and measure the mean solids concentration and thickness of the stagnant granular bed. This finding can be useful for detection of blocked lines and for measurement of highly concentrated slurries.

8.1.2 Slurry flow visualisation (Chapter 5)

8.1.2.1 Slurry flow regime visualisation and characterisation using ERT

Usually the common flow regimes in horizontal slurry flow is visualised through solids concentration distribution across the vertical plane of the pipe cross-section. This thesis presents a novel method, by which several flow regimes, encountered in horizontal flow, can be visualised and characterised using solids axial velocity distribution. It appears that the method of flow regime visualisation via solids velocity distribution using the ERT technique is completely new. The flow regimes that can be visualised using this method are pseudo-homogeneous flow regime, heterogeneous flow regime, granular bed flow regime and pipe blockage. The visualisation results were compared qualitatively against the actual photograph of the flow and a good agreement was noticed. The only limitation of this method is that, in stratified flow, indicates only a packed granular bed. It is rather difficult to distinguish between moving bed and stationary bed based on the velocity profile. Besides, no feature can be observed to identify whether the bed is moving in the form of *en-bloc* sliding (mass) or stream layers. Therefore, the term "granular bed flow regime" is used for both flow regimes, moving bed and stationary bed. The discussion and evaluation of this visualisation method and characterisation is detailed in sections 5.4.5.1, 5.4.5.2, 5.4.5.3, 5.4.5.4 and 5.4.5.5.

8.1.3 Design of slurry system (Chapter 6)

8.1.3.1 Design and construction of pilot scale inclinable slurry flow

A review of the literature reveals that the behaviour of slurry flow has been systematically investigated since 1950s, while the focus has mainly been based on experimental investigations dealing with horizontal and vertical flow. Very limited work on inclined flow can be noticed. As a response to this issue, this study reports a novel design of a robust, versatile, durable and functional inclinable flow loop, which paves the way to further understanding

the behaviour of solid-liquid particles within an inclined pipe. The flow system can be used not only for two-phase flow such as slurry, but also for a multiphase flow such as gas-water-solid flow. The flow system includes various important and carefully selected instrumentations, which can be used as tools for further understanding and characterisation of slurry flow and identifying the potential effects on flow measurement scheme. The versatility of the system allows investigations on any desired pipe orientations (horizontal, vertical and inclined). The mechanical and hydraulic testing of the flow loop confirmed total functionality and safety of the system. The whole design and erection strategies are described in Chapter 6, where the reader is taken through the whole journey from project management to the final stage of testing.

8.1.4 Slurry flow regime recognition (Chapter 7)

8.1.4.1 Automated on-line flow regime recognition

This project has developed a novel automated technique for recognition of horizontal slurry flow regimes based on the statistical analysis of the high performance ERT signal in both, time and frequency domain. All common slurry flow regimes are considered including the transitional regime boundaries. The flow regimes that are recognised using this technique are: Homogeneous, pseudo-homogeneous, heterogeneous, moving bed and stationary bed. Since the stationary bed is the most undesirable flow regime, as the risk of pipe blockage is dominant, a warning sound (alarm) is included into the code, so as to warn the operator. The method has been evaluated and a recognition success rate is confirmed as 90.32%. The recognition decision is made based on the distribution of solid particles across five zones along the vertical plane of the pipe cross-section. This implies that the present technique is applicable to any settling slurry as long as one of the phases is non- or less conductive than the other. Besides, it removes the subjectivity associated with the recognition of the prevailing flow regime. One of the main aim in developing of this method is that it can be used for flow metering, especially for correction of flow regime dependent flow meters, such as ERT. It can also be used to distinguish the boundaries between common settling slurry flow regimes so as to enable the operator to take appropriate control actions for other downstream operations, such as separation, mixing etc. It also provides a visual distribution of the solid particles across the pipe cross-section with displaying the average solids volume fraction in the pipeline. Chapter 7 describes the whole technique.

8.2 General conclusions

1. A high performance dual-plane ERT system was used to interrogate the internal structure of horizontal and vertical upward slurry flows. It was found that the high temporal resolution of this system enabled a fast measurement and online monitoring of slurry flow in both orientations.
2. The local solids volumetric concentration and solids volumetric distribution across the pipe cross-section were determined for both flow orientations. While the dual-plane ERT system was combined with the cross-correlation technique and successfully measured the local solids axial velocity and solids velocity distribution across the pipe cross-section. The comparison of solids volumetric distribution and the solids velocity distribution, with the actual photographs of the flow, revealed that there is a good agreement between both methods.
3. The estimated local solids concentration was compared to that obtained from flow diversion technique. The error analysis of the ERT local solids concentration in horizontal flow, revealed that the error is random and a maximum of 19% was observed throughout the conditions used in this study. It was remarked that the ERT tends to overestimate the local solids concentration. This overestimation was noticed for both sands, medium and coarse.
4. The comparison of local solids axial velocity obtained from the ERT with that of flow diversion technique revealed that a randomly distributed error has been noticed with a maximum of 3.23% through horizontal test section, whereas a maximum error of 9.25% was remarked through vertical flow. It was also concluded that the ERT velocities are mostly underestimated at low velocities (3 m/s and below), which is considered as stratified velocity region. The reasons for this underestimation was associated to the instability of the conditions over the formed granular bed.
5. The observation of solids concentration profiles of both sands in vertical counter-gravity flow concluded that the coarse sand particles move in core peak flow pattern, while medium sand particles move in wall peak flow pattern. This is clearly due to the phenomenon of radial particle migration.
6. The solids velocity profiles obtained in vertical upward flow exhibits a uniform distribution throughout the centre region of the pipe cross-section. The flattened shape of velocity profiles were noticed for all conditions used in this study.

7. The evaluation of the proposed technique for measurement of slurry volumetric flow rate suggests a reasonably accurate estimation of the volumetric flow rate obtained from the ERT and the EMF.
8. Despite occurrence of some deviations in solids concentration and solids axial velocity and slurry volumetric flow rate, it can be concluded that for the range of conditions used in this study, overall, the high performance ERT system provides a reasonably accurate estimation of all parameters measured in both flow orientations and enables visualisation of solids and their motion within the pipelines.

8.3 Future scope

1. This research study has made contributions into the area of two/multiphase flow measurement, visualisation and characterisation, specifically slurry flows, which are clearly highlighted in Chapter 8 (Section 8.1) and can be found within the body of this thesis. Some of them have already been exposed to a form of peer review and can now be found in the public domain as published materials. Some others are contained in the framework of this thesis and have a great potential for future publications. The following papers are due to be published in the nearest future:

    i. An analysis of slurry flow within and around the boundary of stationary bed and blockage in horizontal pipeline, the details of which can be tracked in Chapter 5 (Sections 5.4.5.4 & 5.4.5.5). The contribution is planned to be published under the title ***"Measurement and characterisation of solid-liquid flow within the boundary of stationary bed and blockage"*** in *Chemical Engineering Journal* (Impact Factor = 3.461).

    ii. Measurement, visualisation and characterisation of stratified slurry flow in horizontal pipeline, which is detailed in Chapter 5 (Sections 5.4.6 & 4.5.6.1). The expected paper will be published under the title ***"Measurement and analysis of stratified slurry flow in pipeline using high performance Electrical Resistance Tomography system"*** in *Sensors and actuators B-Chemical* Journal (Impact Factor = 3.898).

    iii. A novel automated recognition technique for common slurry flow regimes in horizontal pipeline, which is described in Chapter 7. The paper containing the proposed technique will be published under

the title ***"Flow regime recognition of horizontal slurry flow using statistical analysis of the ERT signal"*** in *Sensors and actuators B-Chemical* Journal (Impact Factor = 3.898).

iv. A proposed inclinable flow rig, which is discussed in detail in Chapter 6. The paper will be published under the title ***"Design and construction of a pilot scale inclinable particulate flow system"*** in The *International Journal of Multiphase Flow* (Impact Factor = 2.230).

v. Measurement of the two phases in two phase flows, which is covered in Chapter 5 (Sections 5.5.2 & 5.5.3.3). The novel technique will be reported in a paper with the title ***"A new generation of dual-phase measurement and visualisation system"*** in *Sensors and actuators B-Chemical* Journal (Impact Factor= 3.898).

2. Further tests are required to investigate the overestimation of solids concentration and solids axial velocity at higher velocities (above 3 m/s).
3. Development of a better reconstruction algorithm is paramount, so as to take the ERT technique a couple of steps forward.
4. Since the ERT technique suffers from the effect of temperature and recipe change, then its combination with a cheap secondary sensor, such as differential pressure flow meter, can overcome this limitation. The role of the secondary sensor is to compensate the temperature change and to be used as a correction tool. This, undoubtedly, improvement will make the ERT technique far more attractive in the view point of industry.
5. Further tests are required for investigation of off-wall particle lift phenomenon. The use of additional technology for generating solids concentration profile may be important for the purpose of comparison.
6. It is recommended that the proposed flow regime recognition technique to be used on inclined flow. However, the threshold of the data may be subject to a minor alteration.
7. A graphical user-friendly interface is recommended for automatic flow regime recognition and reading the ERT data in a direct method.
8. In order to boost our knowledge and gain insight of complex inclined slurry flow intense experiments are required, mainly over critical slope, solids concentration, solids axial velocity, deposition velocity, flow regimes, pressure drop etc.

THE END

List of References and selected bibliography

1. Abdul Rahim, R., Fazalul Rahiman, M.H., Chan, K.S., Nawawi, S.W. (2007). Non-invasive imaging of liquid/gas flow using ultrasonic transmission-mode tomography. *Sensors and Actuators A: Physical*, **135**(2), pp. 337-345.
2. Abdul Rahim, R., Nayan, N.M., Rahiman, M.H. (2006). Ultrasonic tomography system for liquid/gas flow: frame rate comparison between visual basic and visual c++ programming. *Journal Teknologi*, **44**(D), pp. 131-150.
3. Abulnaga, B. (2002). *Slurry Systems Handbook*. New York: McGraw-Hill.
4. Albion, K., Briens. L., Briens, C. Berruti, F. (2007). Flow Regime determination in horizontal pneumatic transport of fine powders using non-intrusive acoustic probes. *Powder Technology*, **172**(3), pp. 157-166.
5. Bagnold, R.A. (1954). Gravity-free dispersion of large spheres in a Newtonian fluid under shear. *Proc. Royal Soc. A*, **225**, pp. 49-63.
6. Bagnold, R.A. (1956). The flow of Cohesionless Grains in Fluids. *Philosophy Transaction of the Royal Society*, London, Series A, **249**, pp. 99235-297.
7. Bain, A.G. and Bonnington, S.T. (1970). *The Hydraulic Transport of Solids by Pipelines*, 1st edition. Pergamon Press.
8. Baker, R.C. (2000). *Flow Measurement Handbook*. Cambridge: Cambridge University Press.
9. Barigoua, M., Fairhurst, P.G., Fryer, P.J., Painc, J.P. (2003). Concentric fow regime of solid–liquid food suspensions: theory and experiment. *Chemical Engineering Science*, **58**, pp. 1671-1686.
10. Bartosik, A.S. (1996). Modelling the Bagnold stress effects in vertical slurry flow. *J. Hydrol. Hydromech*, **44**(1), pp. 49-58.
11. Bernier, R.N., Brennen, C.E. (1983). Use of the electromagnetic flow meter in a two-phase flow. *International Journal of Multiphase Flow*, **9**(3), pp. 251-257.
12. Bevir, M.K. (1970). The theory of induced voltage electromagnetic flow meters. *Journal of Fluid Mechanics*, **43**(3), pp. 577-590.
13. Blake, A. (Ed.).(1985).*Handbook of Mechanics, Materials, and Structures.* New York: J. Wiley & Sons.

14. Blatch, N.S. (1906). Discussion: Water Filtration at Washington D.C. *Transaction of the American Society of Civil Engineers*, **57**, pp. 400-408.

15. Boden, S., Bieberle, M., Hampel, U. (2008). Quantitative measurement of gas hold-up distribution in a stirred chemical reactor using X-ray cone-beam computed tomography. *Chemical Engineering Journal*, **139**(2), pp. 531-362.

16. Brook, N. (1962). Flow measurement of solid-liquid mixtures using Venturi and other meters. *Proc. Instit. Mech. Engrg*., **176**, pp. 127-140.

17. Brown, N.P. (1991). Flow regimes of settling slurries in pipes. *In* Brown, N.P. Heywood, N.L. (eds). *Slurry Handling Design of Solid–Liquid Systems*. London. pp. 41–52.

18. Brown, P.B. & Heywood, N.I. (1991). *Slurry Handling: Design of solid-liquid Systems*. London: Elsevier Applied Science.

19. Bruggeman, D.A.G. (1935). Calculation of Various Physical Constants of Heterogeneous Substances, Part 1, Constant and Conductivity of Mixtures of Isotropic Substances, *Annual Physics*, Leipzig, **24**, pp. 636.

20. Cairns, R.C., Lawther, K.R. Turner, K.S. (1960). Flow Characteristics of Dilute Small Particle Suspensions, *British Chemical Engineering*, **5**, pp. 849-856.

21. Camarasa, E., Vial, C., Poncin, S., Wild, G., Midoux, N., Bouillard, J. (1999). Influence of coalescence behaviour of the liquid and of gas sparging on hydrodynamics and bubble characteristics in a bubble column. *Chem. Eng. Process*., **38**, pp. 329-344.

22. Carstens, M.R. (1969). A Theory for Heterogeneous Flow of Solids in Pipes, Proceedings of the Institution of Civil Engineers, *Journal of the Hydraulics Division*, **95**, pp. 275-286.

23. Cerna, M., Harvey, A. F. (2000). *National Instruments Application*, Note 041.

24. Cha, J.E., Ahn, Y.C., Kim, M.H. (2002). Flow measurement with an electromagnetic flow meter in two-phase bubbly and slug flow regimes. *Flow Measurement and Instrumentation*, **12**(5-6), pp. 329-339.

25. Charles, M. E., and G. S. Stevens. (1972). The pipeline flow of slurries—transitional velocities. Paper presented at the Second International Conference on Hydraulic Transport of Solids and Pipes. *Second conference of the British Hydromechanic Research Association*. Cranfield, England.

26. Chatfield, C. (1989). *The Analysis of Time Series-An Introduction* (4^{th} ed.). Chapman and Hall: London.

27. Cheney, M., Isaacson, D., Newell, J.C. (1999). Electrical impedance tomography. *Siam Rev*, **41,** pp. 85-101.

28. Cho, K.H., Kim, S. Lee, Y.J. (1999). A fast EIT image reconstruction method for the two-phase flow visualization. *International Communications in Heat and Mass Transfer,* **26,** pp. 637-646.

29. Clift, R. and Clift. D.H.M. (1981). Continuous measurement of the density of flowing slurries. *Int. J. Multiphase Flow*, **75**, pp. 555-561.

30. Condolios, E. and Chapus, E.E. (1963). Designing Solids Handling Pipelines, *Chemical Engineering*, **70**, pp. 131-138.

31. Dai.Y., Wang, M., Panayotopoulos, N., Lucas,G., Williams, A.R. (2004). 3-D Visualisation of a Swirling Flow Using Electrical Resistance Tomography, *4th World Congress on Industrial Process Tomography, Aizu, Japan,* pp 362-369.

32. Davies, J.T. (1987). Calculation of Critical Velocities to Maintain Solids in Suspension in Horizontal Pipes. *Chemical Engineering Science*, **42**(7), pp. 1667-1670.

33. Deng, X., Dong, F. Xu, L.J., Liu, X.P., Xu, L.A. (2001). The design of a dual-plane ERT system for cross correlation measurement of bubbly gas/liquid pipe flow. *Measurement Science and Technology,* **12**, pp. 1024-1031.

34. Dhodapkar, S. and Jacob, K. (2006). *Multiphase flow handbook*, edited by Clayton T. Crowe. NW: Taylor & Francis Group.

35. Divoux, J., Géminard C. (2007). Friction and dilatancy in immersed granular matter. Physical Review Letters, **99**, pp. 258-301.

36. Doron, P. and Barnea, D. (1993). A three-layer model for solid–liquid flow in horizontal pipes. *Int. J. Multiphase Flow*,**19**, pp. 1029-1043.

37. Doron, P. and Barnea, D. (1995). Pressure drop and limit deposit velocity for solid–liquid flow in pipes. *Chem. Eng. Sci.*, **50**, pp. 1595-1604.

38. Doron, P. and Barnea, D. (1996). Flow Pattern Maps for Solid-Liquid Flow in Pipes. *International Journal of Multiphase Flow*, **22**(2), pp. 273-283.

39. Doron, P., Granica, D. and Barnea, D. (1987). Slurry Flow in Horizontal Pipes-Experimental and Modeling, *International Journal of Multiphase Flow*, **13**(4), pp. 535-547.

40. Doron, P., Simkhis, M., Barnea, D. (1997). Flow of solid–liquid mixtures in inclined pipes. *International Journal of Multiphase Flow*, **23**, pp. 313-323.

41. Durand R., Condolios, E. (1952). Compterendu des Deuxiemes journees de L'Hydraulique, Paris, *societe Hydrotechnique de France*, pp. 29-55.

42. Durand, R. (1952). Basic Relationship of the Transportation of Solids in Pipes-Experimental Research, *Proceedings of the Minnesota International Hydraulics Convention*, American Society of Civil Engineers, Minneapolis, University of Minnesota, pp. 89-103.

43. Durand, R. and Condolios, E. (1953). The Hydraulic Transport of Coal and Solid Materials in Pipes. *Proceedings of Colloquium on the Hydraulic Transport of Coal*, National Coal Board, London, pp. 39-52.

44. Dyakowski, T. and Williams, R.A. (1996). Prediction of High Solids Concentration Regions Within a Hydrocyclone. *Powder Technology*, **87**, pp. 43-47.

45. Dyakowski, T., Jeanmeure, L.F.C., Jaworski, A.J. (2000). Applications of Electrical Resistance Tomography for Gas-Liquid and Liquid-Solids Flows- A Review. Powder Technology, **112**, pp. 174-192.

46. Ellis, H.S., and Round, G.F. (1963). Laboratory studies on the flow of nickel–water suspensions. *Canadian Mining and Metallurgical Bulletin*, **56**, pp. 773-781.

47. El-Reedy, A.M. (2011). *Construction management and design of industrial concrete and steel structures*. N.Y: Taylor & Francis Group.

48. Ercolani, E., Ferrini, F., Arrigoni, V. (1979). Electric and Thermal Probe for Measuring the Limit Deposit Velocity, *Proceedings of the Sixth International Conference on the Hydraulic Transport of Solids in Pipes*, BHRA, Canterbury, England, Paper A3, pp. 27-42.

49. Etuke, EO, Bonnecaze, RT. (1998). Measurement of angular velocities using electrical impedance tomography. *Flow Measurement and Instrumentation*, **9**, pp. 159-169.

50. Fazalul Rahiman, M.H., Abdul Rahim, R., Zakaria, Z. (2008). Design and modeling of ultrasonic tomography for two-component high-acoustic impedance mixture. *Sensors and Actuators A:Physical*, **147**, pp. 409-414.

51. Fowles, G. R., Cassiday, G. L. (1999). *Analytical Mechanics*, (6th ed.). Saunders College Publishing.

52. Fukushima, E. (1999). Nuclear magnetic resonance as a tool to study flow. Annu Rev. *Fluid Mech*, **31**, pp. 95-123.

53. GE Sensing. (2007). Panametrics Ultrasonic Flow Transducers for Liquids. Installation Guide, Installation Guide 916-055B.

54. Geisler, T. (2001). *Ultrasonic velocity profile measurements in experimental hydraulics*. Doctoral Thesis. Graz University of Technology , Faculty of Civil Engineering , Austria.

55. Giguere, R., Fradette, L., Mignon, D. Tanguy, P. A. (2008b). ERT algorithms for quantitative concentration measurement of multiphase flows. *Chemical Engineering Journal,* **141,** pp. 305-317.

56. Giguere, R., Fradette, L., Mignon, D. Tanguy, P. A. (2009). Analysis of slurry flow regimes downstream of a pipe bend. *Chemical Engineering Research & Design,* **87,** pp. 943-950.

57. Giguere, R., Fradette, L., Mignon, D., Tanguy, P.A. (2008a). Characterization of slurry flow regime transitions by ERT. *Chemical Engineering Research & Design*, **86**, pp. 989-996.

58. Gillies, R.G. (1991). Flow Loop Studies. *In* Brown, N. P. and Heywood, N.I. (eds.). *Slurry Handling: Design of Solid-liquid Systems*. Elsevier Applied Science.

59. Gillies, R.G. (1993). *Pipeline Flow of Coarse Particle Slurries*. Doctorial Thesis. University of Saskatchewan, Department of Chemical Engineering, Canada.

60. Gillies, R.G. and Shook, C.A. (1994). Concentration Distribution of Sand Slurries in Horizontal Pipe Flow. *Particulate Science and Technology*, **12**, pp. 45-69.

61. Gillies, R.G., Hill, K.B., McKibben, Shook, C.A. (1999). Solids Transport by Laminar Newtonian Flows. *Powder Technology*, **104**, pp. 269-277.

62. Gillies, R.G., Shook, C.A. (2000). Modeling high concentration settling slurry flows. *The Canadian Journal of Chemical Engineering*, **78**, pp. 709-716

63. Gillies, R.G., Shook, C.A., Wilson, K.C. (1991). An improved two layer model for horizontal slurry pipeline flow. The Canadian Journal of Chemical Engineering, **69,** pp. 173-178.

64. Govier, G.W. and Aziz, K. (1972). *The Flow of Complex Mixtures in Pipes*. New York: van Nostrand Reinhold Company.

65. Graf, W.H., Robinson, M., Yucel, O. (1970). The Critical Deposit Velocity for Solid-Liquid Mixtures. *Proceedings of the First International Conference on the Hydraulic Transport of Solids in Pipes*, BHRA, Coventry, England, Paper H5, pp. H5-77 to H5-88.

66. Hagler, T.W. Sr. (1956). Means for determining specific gravity of fluids and slurries in motion. *U. S. Pat.* 2678529.

67. Hazen, A. and Hardy, H.D. (1906). Discussion of Work for the Purification of the Water Supply of Washington, D.C., *Transaction of the American Society of Civil Engineers*, **57**, pp. 408-409.

68. Heindel, T.J, Grayb, J.N, Jensenb, T.C. (2008). An X-ray system for visualizing fluid flows. *Flow Measurement and Instrumentation*, **19**, pp. 67-78.

69. Henningsson, M, Ostergren, K, Dejmek, P. (2006). Plug flow of yoghurt in piping as determined by cross-correlated dual-plane electrical resistance tomography. *Journal of Food Engineering*, **76**, pp. 163-168.

70. Holden, P.J., Wang, M., Mann, R., Dickin, F.J. Edwards, R.B. (1999). On Detecting Mixing Pathologies Inside a Stirred Vessel Using Electrical Resistance Tomography. *Transactions of the Institution of Chemical Engineers*, **77**, Part A, pp. 709-712.

71. Holdich, R.G. and Sinclair, I. (1992). Measurement of Slurry Solids Content By Electrical Conductivity. *Powder Technology*, **72**, pp. 77-87.

72. Hong , S., Choi, J., Yan, C.K. (2002). Experimental study on solid–water slurry flow in vertical pipe by using ptv method. *Proceedings of the 12th International Offshore and Polar Engineering Conference*, pp. 462–466.

73. Hosseini, S., Patel, D., Ein-Mozaffari, F., Mehrvar, M. (2010). Study of solid-liquid mixing in agitated tanks through electrical resistance tomography. *Chemical Engineering Science*, **65**, pp. 1374-1384.

74. Hoult, D.I., Chen, C.N., Sank, V.J. (1986). The field-dependence of NMR imaging: Arguments concerning an optimal field-strength. *Magn Reson Med*, **3**(2), pp. 730-46.

75. Howard, G.W. (1939). Transportation of Sand and Gravel in a Four-Inch Pipe. *Transaction of the American Society of Civil Engineers*, **104**, pp. 1334-1348.

76. Ismail, I., Gamio, J.C., Bukhari, S.F.A., Yang, W.Q. (2005). Tomography for multi-phase flow measurement in the oil industry. *Flow Measurement and Instrumentation*, **16**, pp. 145-155.

77. ITS-Industrial Tomography Systems Ltd. (2005). *P2000 Electrical Resistance Tomography System, Operating Manual*. Manchester: UK.

78. Jaafar, W., Fischer, S., Bekkour, K. (2009). Velocity and turbulence measurements by ultrasound pulse Doppler velocimetry. *Measurement*, **42**(2), pp. 175-182.

79. Jin, H., Yang, S., Guo, Z., He, G., Tong, Z. (2005). The axial distribution of holdups in an industrial-scale bubble column with evaluated pressure

using γ-ray attenuation approach. *Chemical Engineering Journal*, **115**(1-2), pp. 45-50.

80. Kalaga, D.V., Kulkarni, A.V., Acharya, R., Kumar, U., Singh, G., Joshi, J.B. (2009). Some industrial applications of gamma-ray tomography. *Journal of the Taiwan Institute of Chemical Engineers*, **40**, pp. 602-612.

81. Kao, D.T.Y., Hwang, L.Y.(1979). Critical slope for slurry pipelines. P *Hydrotransport 6 Conference of the British Hydromechanical Research Association*, Cranfield, England.

82. Karnis, A, Goldsmith, H.L., Mason, S.G. (1966). The flow of suspensions through tubes: V. Inertial effects. *Canadian Journal of Chemical Engineering*, **44**, pp. 181-193.

83. Kaushal, D.R. and Tomita, Y. (2002). Solids Concentration Profiles and Pressure Drop in Pipeline Flow of Multisized Particulate Slurries. *International Journal of Multiphase Flow*, **28**, pp.1697-1717.

84. Kaushal, D.R., Sato, K., Toyota, T., Funatsu, K., Tomita. Y. (2005). Effect of particle size distribution on pressure drop and concentration profile in pipeline flow of highly concentrated slurry. *International Journal of Multiphase Flow*, **31**(7), pp. 809-823.

85. Kazanskij, I.B. (1979). Critical Velocity of Depositions for Fine Slurries-New Results. *Proceedings of the Sixth International Conference on the Hydraulic Transport of Solids in Pipes*, BHRA, Canterbury, England, Paper A4, pp. 43-56.

86. Kim, S., Nkaya, A.N., Dyakowski, T. (2006). Measurement of mixing of two miscible liquids in a stirred vessel with electrical resistance tomography. *International Communications in Heat and Mass Tranasfer*, **33**(9), pp. 1088-1095.

87. Koh, C.J., Hookham, P., Leal, L.G. (1994). An Experimental Investigation Of Concentrated Suspension Flows In A Rectangular Channel. *J. Fluid Mech*, **266**, pp. 1-32

88. Lahiri, S.K. (2009). *Study of slurry flow modelling in pipeline*. Doctoral Thesis. National Institute of Technology, India.

89. Lazarus, J.H., Neilson, I.D. (1978). A generalized correlation for friction head losses of settling mixtures in horizontal smooth pipelines. *Proceedings of the Fifth International Conference on the Hydraulic Transport of Solids in Pipes*, Hanover, Germany, Paper B1, pp. 1-32.

90. Li, H., Wang, M., Wu, Y., Ma, Y., Williams, R. (2005). Measurement of oil volume fraction and velocity distributions in vertical oil-in-water flows using Electrical Resistance Tomography and a local probe. *J Zhejiang Univ. Sci.*, **6A**(12), pp. 1412-1415.

91. Li, L. (2007). *Advanced flow visualization*. Doctoral thesis. Graduate School of The Ohio State University, The Ohio State University.

92. Liu, M., Wang, T., Yu, W., Wang, J. (2007). An electrical conductivity probe method for measuring the local solid holdup in a slurry system. *Chemical Engineering Journal*, **132**(1-3), pp. 37-46.

93. Lowe, D.C., Rezkallah, K.S. (1999). Flow regime identification in microgravity two-phase, flows using void fraction signals. *International Journal of Multiphase***, 25**(3), pp. 433-457.

94. Lucas, G.P., Cory, J., Waterfall, R.C., Loh, W.W., Dickin, F.J. (1999). Measurement of the solids volume fraction and velocity distribution in solids-liquid flows using dual-plane electrical resistance tomography. *Flow Meas. and Ins*, **10**(4), pp. 249-258.

95. MacTaggart, R.S., Nasr-El-Din, H. A., Masliyah, J.H. (1993). A conductivity probe for measuring local solids concentration in a slurry mixing tank. *Separations Technology*, **3**(3), pp. 151-160.

96. Mann, R. and Wang, M. (1997). Electrical Process Tomography: Simple and Inexpensive Techniques for Process Imaging. *Measurement and Control*, **30**, pp. 206-211.

97. Marashdeh, Q., Fan, L.S., Du, B., Warsito, W. (2008). Electrical capacitance tomography - a perspective. Ind. Eng. Chem. Res., **47**, pp. 3708-3719.

98. Matousek, V. (1996). Internal structure of slurry flow in inclined pipe. Experiments and mechanistic modelling. *13th International Conference on Slurry Handling and Pipeline Transport – Hydrotransport,* **13**, pp. 187-210.

99. Matousek, V. (1997). *Flow Mechanism of Sand-Water Mixtures in Pipelines*. Doctoral Thesis. University of Delft, Holland.

100. Matousek, V. (2002). Pressure drops and flow patterns in sand–mixture pipes, Experimental. Thermal and Fluid Science, **26**, pp. 693-702.

101. Matousek, V. (2009). Predictive model for frictional pressure drop in settling-slurry pipe with stationary deposit. Powder Technology, **192**, pp. 367-374.

102. Matousek,V. (2005). Research developments in pipeline transport of settling slurries. *Poweder Technology*, **156**(1), pp. 43-51.

103. Maxwell, J.C. (1881). *A Treatise on Electricity and Magnetism*. Oxford: Calendar Press.

104. McKee, S.L., Williams, R.A., Boxman, A. (1995). Development of Solid-Liquid Mixing Models Using Tomographic Techniques. *Chemical Engineering Journal*, **56**, pp. 101-107.

105. Meredith, R.E. and Tobias, C.W. (1962). *Advances in Electrochemistry and Electrochemical Engineering*, 2nd edition. New York: Interscience.

106. Mohinder, L. & Nayyar, P.E. (2000). *Piping handbook*. New York: Mcgrow-Hill.

107. Mosorov, V., Sankowski, D., Mazurkiewicz, L., Dyakowski, T. (2002). The ‘‘best-correlated pixels’’ method for solid mass flow measurements using electrical capacitance tomography. Measurement Science and Technology, **13**, pp. 1810-1814.

108. Muller, C.R., Holland, D.J., Sederman, A.J., Mantle, M.D., Gladden, L.F., Davidson, J.F. (2008). Magnetic Resonance Imaging of fluidised beds. *Powder Technology*, **183**(1), pp. 53-62.

109. Munir, B. (2011). *Visualisation & Quantitative Measurement of Vertical Two-phase Mass Flows in Pipeline*. Doctoral Thesis, University of Leeds, UK.

110. Nasr-El-Din, H., Shook, C.A., Colwell, J. (1987). A conductivity probe for measuring local concentrations in slurry systems. *International Journal of Multiphase Flow*, **13**(3), pp. 365-378.

111. Newitt, D.M., Richardson, J.F., Gliddon, B.J. (1961). Hydraulic conveying of solids in vertical pipes. *Transactions of the Institution of Chemical Engineers*, **3**9, pp. 93-100.

112. Newitt, D.M., Richardson, J.F., Abbott, M., Turtle, R.B. (1955). Hydraulic conveying of solids in horizontal pipes. *Transactions of the Institution of Chemical Engineers*, **33**, pp. 93-110.

113. Oroskar, A.R. and Turian, R.M. (1980). The Critical Velocity in Pipeline Flow of Slurries. *American Institute of Chemical Engineers Journal*, **26**(4), pp. 550-558.

114. Pachowko, A.D. (2004). *Design and modelling of a coarse particulate slurry handling system*. Doctoral thesis, University of Leeds, UK.

115. Pachowko, A.D., Poole, C., Wang, M. and Rhodes, D. (2004). Measurement of slurry density profiles in horizontal pipes by using electrical resistance tomography. *Proceedings of the Hydrotransport 16th International Conference*, Santiago, Chile.

116. Parvareh, A., Rahimi, M., Alizadehdakhel, A., Alsairafi, A.A. (2010). CFD and ERT investigations on two-phase flow regimes in vertical and horizontal tubes. *International Communications in Heat and Mass Transfer*, 37, pp. 304-311.

117. Parzonka, W., Kenchington, J.M., Charles, M.E. (1981). Hydrotransport of Solids in Horizontal Pipes: Effects of Solid Concentration and Particle

Size on Deposit Velocity. *Canadian Journal of Chemical Engineering*, **59**, pp. 291-296.

118. Peker, S. M., Helvacı, Ş. Ş., Yener, H. B., İkizler, B., Alparslan, A. (2008). *Solid-Liquid Two Phase Flow*. Oxford : Elsevier.

119. Perry, R.H., Green, D.W., Maloney, J.O. (1997). *Perry's Chemical Engineers' Handbook*, 7th Edition. New York: McGraw Hill.

120. Plaskowski, A., Beck, M.S., Byars, M., Dyakowski, T., He, R., Wang, S.J., Waterfall, R.C., Yang, W.Q. (1996). Industrial application of electrical capacitance tomography. Pomiary Automatyka Kontrola, **42**, pp. 113-115.

121. Pohlman, N.A., Severson, B.L., Ottino, J.M., Lueptow, R.M. (2006). Surface roughness effects in granular matter: influence on angle of repose and the absence of segregation. *Physical Review E*, **73**, pp. 031304.

122. Portillo, P.M., Vanarase, A.U., Ingram, A., Seville, J.K., Ierapetritou, M.G., Muzzio, F.J. (2010). Investigation of the effect of impeller rotation rate, powder flow rate and cohesion on powder flow behaviour in a continuous blender using PEPT. *Chemical Engineering Science*, **65**, pp. 5658.

123. Pougatch, K., Salcudean, M. (2008). Numerical modeling of deep sea air-lift, *Ocean Engineering*, **35**, pp. 1173.

124. Prager, S. (1963). Diffusion and Viscous Flow in Concentrated Suspensions, *Physica*, **29**, pp. 129-139.

125. Pugh, F.J. (1995). *Bed Load Velocity and Concentration Profiles in High Shear Stress Flows*. Doctorial Thesis, Queen's University, Canada.

126. Raguin, L.G., Ciobanu L. (2007). Multiple echo NMR velocimetry: fast and localized measurements of steady and pulsatile flows in small channels. *J. Magn. Reson*.,**184**, pp. 337-43.

127. Razzak, S.A., Barghi, S., Zhu, J.X. (2009). Application of electrical resistance tomography on liquid–solid two-phase flow characterization in an LSCFB riser. *Chem. Eng. Sci*, **64**, pp. 2851-2858.

128. Reinecke, N., Petritsch, G., Boddem, M., Mewes, D. (1998). Tomographic imaging of the phase distribution in two-phase slug flow. *Int. J. Multiphase Flow*, **24**, pp. 617-34.

129. Roco, M.C., Shook, C.A. (1984). Computational methods for coal slurry pipeline with heterogeneous size distribution. *Powder Technology*, **39**, pp. 159-176.

130. Roy, S., Kemoun, A., Al-Dahhan, M., Dudukovic, M.P., Skourlis, T.B., Dautzenberg, F.M. (2005). Countercurrent flow distribution in structured

packing via computed tomography. *Chemical Engineering and Processing*, **44**(1), pp. 59-69.

131. Schaan, J., Cook, N., Sanders, R.S. (2007). On-line wear measurements for commercial-scale, coarse-particle slurry pipelines. *The 17th International Conference on the Hydraulic Transport of Solids,* The South African Institute of Mining and Metallurgy and the BHR Group.

132. Schlaberg, H.I., Jia, J., Qiu, C., Wang, M., Hua, L. (2008). Development and application of the Fast Impedance Camera - a high performance dual-plane electrical impedance tomography system. *5th International Symposium on Process Tomography*.

133. Schmit, C.E., Perkins, J., Eldridge, R.B. (2004). Investigation of X-ray imaging of vapor-liquid contactors. 2. Experiments and simulations of flows in an air-water contactors. *Chemical Engineering Science*, **59**(6), pp. 1267-1283.

134. Schubert, M., Hessel, G., Zippe, C., Lange, R., Hampel, U. (2008). Liquid flow texture analysis in trickle bed reactors using high resolution gamma ray tomography. *Chemical Engineering Journal*, **140**(1-3), pp. 332-340.

135. Seager, A.D., Baber, D.C., Brown, B.H. (1987). Theoretical limits to sensitivity and resolution in impedance imaging, *Clinical Physiological Measurements,* **8** (Supplement A), pp. 13-31.

136. Seville, J.P.K., Ingram, A., Fan, X., Parker, D.J. (2009). Characterization of Flow, Particles and Interfaces. *Advances in Chemical Engineering*, **37**, pp. iii.

137. Shen, H.W. and Wang J.S. (1970). Incipient Motion and Limiting Deposit conditions of Solid Liquid Pipe Flow. *Proceedings of the First International Conference on the Hydraulic Transport of Solids in Pipes*, BHRA, Coventry, England, Paper H3, pp. H3-37 to H3-51.

138. Shercliff, J.A. (1962). *The theory of electromagnetic flow-measurement*. Cambridge: Cambridge University Press.

139. Shook , C.A., Bartosik, A.S. (1994). Particle-wall stresses in vertical slurry flows. *J. Powder Tech.*, **81**, pp. 119-134.

140. Shook, C. A. and Daniel, S. M. (1969). A Variable Density Model of the Pipeline Flow of Suspensions. *Canadian Journal of Chemical Engineering*, **47**, pp. 196-200.

141. Shook, C.A. (1982). Flow of stratified slurries through horizontal venturi meters. *The Canadian Journal of Chemical engineering*, **60**(3), pp. 342-345.

142. Shook, C.A. and Roco, M.C. (1991). *Slurry Flow: Principles and Practice*. London: Butterworth-Heinemann.

143. Shook, C.A., Masliyah, J.H. (1974). Flow of slurry through a venturi meter. *The Canadian Journal of Chemical Engineering*, **52**(2), pp. 228-233.

144. Shukla, A., Prakash, A. (2006). Ultrasonic technique to determine particle size and concentration in slurry systems. *Chemical Engineering Science*, **61**, pp. 2468-2475.

145. Smith, R.A. (1955). Experiments on the Flow of Sand-Water Slurries in Horizontal Pipes. *Transactions of the Institution of Chemical Engineers*, **33**, pp. 85-92.

146. Spells, K.E. (1955). Correlations for Use in Transport of Aqueous Suspensions of Fine Solids in Pipes. *Transactions of the Institution of Chemical Engineers*, **33**, pp. 79-84.

147. Stein, M., Martin, T.W., Seville, J.P.K., McNeil, P.A., parker, D.J. (1997). Positron emission particle tracking: Particle velocities in gas fluidised beds, mixers and other applications. *Non-Invasive Monitoring of Multiphase Flows*, pp. 309-333, Editors: Chaouki, J., Larachi, F., Dudukovic, M.P, Elsevier Science.

148. Stoica, P., Moses, R. (2005). *Spectra Analysis of Signal*. New Jersey: Prentice Hall.

149. Sundqvist, A. (1996). *Hydraulic Transport of Mineral and Ore Products-Friction Losses of Stratified Flows at High Solids Concentrations*. Doctoral Thesis, Lelea University of Technology.

150. Syrjänen, J., Haavisto, S., Koponen, A., Manninen, M. (2009). Particle velocity and concentration profiles of sand-water slurry in stirred tank-measurements and modelling. *Seventh International Conference on CFD in the minerals and process industries CSIRO*, Milbourne, Australia.

151. Tapp, H.S., Peyton, A.J., Kemsley, E.K., Wilson, R.H. (2003). Chemical engineering applications of electrical process tomography. *Sensors and Actuators B: Chemical,* **92,** pp. 17-24.

152. Thomas, D.G. (1964). Transport Characteristics of Suspensions: Part IX, Representation of Periodic Phenomena on a Flow Regime Diagram for Dilute Suspension Transport. *American Institute of Chemical Engineers Journal*, **10**(3), pp. 303-308.

153. Thorn, R., Johansen, G.A., Hammer, E.A. (1997). Recent developments in three- phase flow measurement. *Meas. Sci. Technology*,**8**, pp. 691-701.

154. Tortora, P.R., Ceccio, S.L., Mychkovsky, A.G., O'Hern, T.J., Torczynski, J.R. (2008). Radial profiles of solids loading and flux in a gas-solid circulating fluidized bed. *Powder Technology*, **180**(3), pp. 312-320.

155. Turian, R.M. and Yuan, T.Y. (1977). Flow of Slurries in Pipelines, *American Institute of Chemical Engineers Journal*, **23**(3), pp. 232-243.

156. Turian, R.M., Hsu, F.L., Ma, T.W. (1987). Estimation of the Critical Velocity in Pipeline Flow of Slurries. *Powder Technology*, **51**, pp. 35-47.

157. Turner, J.C.R. (1976). Electrical Conductivity of Liquid-Fluidized Bed of Spheres. *Chemical Engineering Science*, **31**, pp. 487-492.

158. US Army Corps Engineers. (1999). *Engineering and Design: Liquid Process Piping. Engineering Manual*. Department of the Army, Washington, DC 20314-1000.

159. Van Dinther, A.M.C., Schroën, C.G.P.H., Vergeldt, F.J., van der Sman, R.G.M., Boom, R.M. (2012). Suspension flow in microfluidic devices — A review of experimental techniques focusing on concentration and velocity gradients. *Advances in Colloid and Interface Science*, **173**, pp. 23-34.

160. Vocadlo, J.J. and Charles, M.E. (1972). Prediction of Pressure Gradient for the Horizontal Turbulent Flow of Slurries. *Proceedings of the Second International Conference on the Hydraulic Transport of Solids in Pipes*, BHRA, Coventry, England, Paper C1, pp. C1-1 to C1-12.

161. Vuarnoz, D., Sari, O., Egolf, P.W., Liardon, H. (2002). Ultrasonic velocity profiler uvp-xw for iceslurry flow characterisation. *Third International Symposium on Ultrasonic Doppler Methods for Fluid Mechanics and Fluid Engineering*, EPFL, Lausanne, Switzerland, 91.

162. Wang, J.Z., Tian, G.Y., Lucas, G.P. (2007). Relationship between velocity profile and distribution of induced potential for an electromagnetic flow meter. *Flow Measurement and Instrumentation*, **18**(2), pp. 99-105.

163. Wang, L., McCarthy, K.L., McCarthy, M.J. (2004). Effect of temperature gradient on ultrasonic Doppler velocimetry measurement during pipe flow. *Food Research International*, **37**(6), pp. 633-642.

164. Wang, M. and Yin, W. (2001). Measurement of the Concentration and Velocity Distribution in Miscible Liquid Mixing using Electrical Resistance Tomography. *Transactions of the Institution of Chemical Engineers*, **79**, part A, pp.883-886.

165. Wang, M., Dorward, A., Vlaev, D., Mann, R. (2000). Measurements of Gas-Liquid Mixing in a Stirred Vessel Using Electrical Resistance Tomography (ERT). *Chemical Engineering Journal*, **77**, pp. 93-98.

166. Wang, M., Jones, T.F., Williams, R.A. (2003). Visualization of asymmetric solids distribution in horizontal swirling flows using electrical resistance tomography. *Trans. IChemE*, **81**, Part A.

167. Wang, M., Jones, T.F., Yin, W., Ganeshalingam, J., Williams, R.A., Miles, N., Li, D., Lai, Y., Wu, Y. (2002). Measurement of Swirling Flow in a Hydraulic Conveying Loop using Electrical Resistance Tomography. *4th World Congress on Particle Technology*, Sydney, Australia, pp. 21-25.

168. Wang, M., Mann, R., Dickin, F.J. (1999). Electrical Resistance Tomographic Sensing System for Industrial Applications. *Chemical Engineering Communications*, **175**, pp.49-70

169. Wang, T., Wang, J., Ren, F., Jin, Y. (2003). Application of Doppler ultrasound velocimetry in multiphase flow. *Chemical Engineering Journal*, **92**, pp. 111-122.

170. *Warman Slurry Pumping Handbook*. (2000). Warman International Ltd. (Australasian Version).

171. Warman Centrifugal Slurry Pumps. (2009).*Slurry Pump Handbook*, (5th edition). Weir Slurry Group.

172. Wasp, E.J., Aude, T.C., Kenny, J.P., Seiter, R.H., Jacques, R.B. (1970). Deposition velocities transition velocities and spatial distribution of solids in slurry pipelines. *Proc. Hydro transport 1*, BHRA Fluid Engineering, Coventry, UK, paper H42, pp. 53-76.

173. Wasp, E.J., Kenny, J.P., Gandhi, R.L. (1977). *Solid-Liquid Flow Slurry Pipeline Transportation*, 1st ed. **1**, Series on Bulk Materials Handling, Trans. Technical Publ., Clausthal-Zellerfield, F.R.G.

174. Weissberg, H.L. (1963). Effective Diffusion Coefficient in Porous Media. *Journal of Applied Physics*, **34**, pp. 2636-2639.

175. Wicks,M. (1971). *Transportation of solids of low concentrations in horizontal pipes*. *In* Advances in Solid–Liquid Flow in Pipes and Its application, edited by I. Zandi. New York: Pergamon Press.

176. Williams, R.A. (1995). A Journey Inside Mineral Separation Processes. *Minerals Engineering*, **8**(7), pp. 721-737.

177. Williams, R.A. and Beck, M.S. (1995). *Process Tomography: Principles, Techniques and Applications*. Oxford: Butterworth-Heinemann.

178. Williams, R.A., Jia, X. and McKee, S.L. (1996). Development of Slurry Mixing Models Using Resistance Tomography. *Powder Technology*, **87**, pp. 21-27.

179. Williams, R.A., Jia, X., West, R.M., Wang, M., Cullivan, J.C., Bond, J., Faulks, I., Dyakowski, T., Wang, S.J., Climpson, N., Kostuch, J.A.,

Payton, D. (1999). Industrial Monitoring of Hydrocyclones Operation Using Electrical Resistance Tomography. *Minerals Engineering,* **12**(10), pp. 1245-1252.

180. Wilson, K.C. (1970). Slip Point of Beds in Solid-Liquid Pipeline Flow. Proceedings of the Institution of Civil Engineers, *Journal of the Hydraulics Division*, **96**, pp. 1-12.

181. Wilson, K.C. and Tse, J.K.P. (1984). Deposition limit for coarse-particle transport in inclined pipes. *Proc. Hydrotransport 9*, BHR Fluid Engineering Cranfield, UK, pp. 149-169.

182. Wilson, K.C., Addie, G.R, Clift, R. (1992). *Slurry transportation using centrifugal pumps*. New York: Elsevier Applied Sciences.

183. Wilson, K.C., Addie, G.R., Sellgren, A., Clift, R. (2006). *Slurry Transport Using Centrifugal Pumps*, (3rd ed.). NY: Springer.

184. Wilson, K.C., Clift, R., Sellgren, A. (2002). Operating Points of Pipelines Carrying Concentrated Heterogeneous Slurries. *Powder Technology*, **123**, pp. 19-24.

185. Wilson, K.C., Pugh, F.J. (1988). Dispersive-force modeling of turbulent suspension in heterogeneous slurry flow. *Can. J. Chem. Engg.*, **66**, pp. 721-727.

186. Wilson, K.C., Streat, M., Bantin, R.A. (1972). Slip-Model Correlation of Dense Two Phase Flow. *Proceedings of the Second International Conference on the Hydraulic Transport of Solids in Pipes*, BHRA, Coventry, England, Paper B1, pp. B1-1 to B1-10.

187. Wilson, W.E. (1942). Mechanics of Flow, with Non Colloidal Inert Solids. *Transactions of the American Society of Civil Engineers*, **104**, pp. 1576-1586.

188. Wilson, W.E. (1945). Transportation of Suspended Solids in Pipe Lines. *Transactions of the American Society of Mining Engineers*, **104**, pp. 675-684.

189. Windt, C.W. (2007). *Nuclear magnetic response imaging of sap flow in plants*. Doctoral Thesis, Wageningen University.

190. Wood, D.J. (1979). Pressure gradient requirements for re-establishment of slurry flow. *In Sixth International Conference on Hydraulic Transport of Solids in Pipes*. Cranfield, UK: BHRA Group, pp. 217.

191. Wood, R.J.K., Jones, T.F. (2003). Investigations of sand–water induced erosive wear of AISI 304L stainless steel pipes by pilot-scale and laboratory-scale testing. *Wear*; **255**, pp. 206-218

192. Worster, R.C., Denny, D.E. (1955). Hydraulic transport of solid materials in pipes. *Proceedings of the Institute of Mechanical Engineers*, UK, **38**, pp. 230-234.

193. Wu, Y., Li, H., Wang, M., Williams, A.R. (2005). Characterization of Air-water Two-phase Vertical Flow by Using Electrical Resistance Imaging. *The Canadian Journal of Chemical* Engineering, **83**, pp.37-41.

194. www.abb.co.uk. Accessed on 5th of April 2012.

195. www.coleparmer.co.uk. Accessed on 24th of October 2012.

196. www.cse-distributors.co.uk. Accessed on 12th of May 2010.

197. www.ect-instruments.com. Accessed on 18th of December 2012.

198. www.electricwinchshop.co.uk/winches. Accessed on 1st of June 2011.

199. www.endress.com. Accessed on 20th of June 2011.

200. www.flexible-tubing.com. Accessed on 27th of February 2011.

201. www.hydromatic.com. Accessed on 24th of October 2010.

202. www.hypertextbook.com/fact. Accessed on 20th of March 2011.

203. www.icenta.co.uk. Accessed on 5th of April 2012.

204. www.kayelaby.npl.co.uk. Accessed on 20th of March 2011.

205. www.krohne.com. Accessed on 27th of July 2011.

206. www.met-flow.com. Accessed on 15th of March 2012.

207. www.omega.co.uk/literature. Accessed on 25th of September 2011.

208. www.pipestock.com. Accessed on 17th of February 2011.

209. www.signal-processing.com. Accessed on 7th of August 2010.

210. www.territorioscuola.com. Accessed on 23rd of October 2010.

211. www.wyattflow.com/venturi-tube/bvt. Accessed on 2nd of August 2012.

212. Wyatt, D.G. (1986). Electromagnetic flow meter sensitivity with two phase flow. *International Journal of Multiphase Flow*, **12**(6), pp. 1009-1017.

213. Xia, J.X., Ni, J.R., Mendoza, C. (2004). Hydraulic lifting of manganese nodules through a riser. *Journal of Offshore Mechanics and Arctic Engineering*, **126**(1), pp. 72-77.

214. Yamaguchi, H., Niu, X.D., Nagaoka, S., de Vuyst, F. (2011). Solid–liquid two-phase flow measurement using an electromagnetically induced signal measurement method. *Journal of Fluids Engineering*, **133**, pp. 041302.

215. Yang, W. (2010). Design of electrical capacitance tomography sensors. *Meas. Sci. Technol.*, **21**, pp. 042001.

216. Yin, F., Afacan, A., Nandakumar, K., Chuang, K.T. (2002). Liquid holdup distribution in packed columns gamma ray tomography and CFD simulation. *Chemical Engineering and Processing*, **41**(5), pp. 473-483.

217. Yoder, J. (2008). The Changing Face of Coriolis, Technology Evolves to Meet More Measurement Needs [online]. Available from: www.flowreserach.com. [Accessed 22nd July 2012].

218. Zafar, U., Munir, B., Wang, B. (2009). Measurement and Visualisation of slurry horizontal flow using electrical resistance tomography. *8th International Conference On Measurement And Control Of Granular Materials (MCGM 2009)*, Shenyang, CHINA .

219. Zandi, I. and Govatos, G. (1967). Heterogeneous Flow of Solids in Pipelines, Proceedings of the Institution of Civil Engineers. *Journal of the Hydraulics Division*, **93**, pp. 145-159.

Appendix A
Publications during the course of this study

During the course of the timeline of this research study, the following papers and presentations have been produced.

1. Faraj, Y. and Wang, M. (2011). Slurry flow regime and velocity profile visualisation in horizontal pipeline using Electrical Resistance Tomography (ERT). *PSFVIP-8, the 8th Pacific Symposium Flow Visualisation and Image Processing*, Moscow, Russia.
2. Faraj, Y. and Wang, M. (2011). Slurry flow measurement in pipeline via Electrical Resistance Tomography (ERT). *BAAF, Beihang Autumn Academic Forum*. Beijing, China.
3. Faraj, Y. and Wang, M. (2012). ERT investigation on horizontal and counter-gravity slurry flow in pipelines. *Journal of Procedia Engineering*. **42**, pp. 588-606
4. Faraj, Y., Wang, M. (2013). ERT based volumetric flow rate measurement in vertical upward flow. *ChemEngDayUk, Proceedings of Chemical Engineering Day Uk*, Imperial College London, London, UK.
5. Faraj, Y. and Wang, M. and Jia, J. (2013). Application of the ERT for slurry flow regime characterisation. *WCIPT7, 7th World Congress on Industrial Process Tomography*, Krakow, Poland. (Accepted in Journal of Procedia Engineering)
6. Jia, J., Wang, M., Faraj, Y., Zhang, J. and Yu, X. (2013). Characterisation of Air-in-water Upward Flows with Electrical Impedance Tomography and Wire Mesh Sensor. *WCIPT7, 7th World Congress on Industrial Process Tomography*, Krakow, Poland. (Accepted in Journal of Procedia Engineering)
7. Wang, M., Jia, J., Faraj, Y., Wang, Q., Xie, C., Oddie, G., Primrose, K. and Qiu, C. (2013). A new visualisation and measurement technology for multiphase flows. *ISMTMF8, 8th International Symposium on Measurement Techniques for Multiphase Flows*, Guangzhou, China.
8. Jia, J., Faraj, Y. and Wang, M. (2013). Calibration methods of ERT sensor for handling wide flow dynamic ranges. *ISMTMF8, 8th International Symposium on Measurement Techniques for Multiphase Flows*, Guangzhou, China.

9. Faraj, Y. and Wang, M. (2013). Flow regime recognition of horizontal slurry flow using statistical analysis of the ERT signal. To be published in *Sensors and actuators B-Chemical*.

10. Faraj, Y. and Wang, M. (2013). Measurement and analysis of stratified slurry flow in pipeline using high performance Electrical Resistance Tomography system. To be published in *Chemical Engineering Journal*.

Appendix B
Calibration Results

The quantitative data obtained from the calibration process for the thermocouple, conductivity meter, pressure transducers, measuring tank, load cells and the ERT are shown below.

Table B.1 Thermocouple calibration results.

	Thermocouple (°C)	Thermometer (°C)
	15.6	15.2
	17	16.4
	17.9	17.1
	18.8	18.6
	20.3	19.5
	21.1	20.7
	22.1	21.5
	23.3	22.8
	24	23.5
	25.2	24.6
	26	25.4
	27.5	26.8
	28.4	27.6
	29	28
	29.9	29.4
	30.8	30.6
Average	**23.55625**	**22.98125**
Percent Error	**2.50%**	

Table B.2 Conductivity meter calibration results.

	Desktop (mS/cm)	Handheld (mS/cm)
	0.27	0.27
	1.2	1.26
	1.6	1.65
	2.3	2.12
	2.55	2.72
	3.09	3.27
	3.7	3.62
	3.5	3.45
	3.95	3.90
Average	**2.462**	**2.473**
Percent Error	**0.45%**	

Table B.3 Calibration results of two pressure transducers on horizontal line and two pressure transducers on vertical line against actual values.

Pressure Sensor	Height-h (m)	Actual P=998.2xgxh (kPa)	Current (mA)	Sensor reading before correction (kPa)	Sensor reading after correction (kPa)
P1-Horzontal line	0	0.000	4.053	3.341	0.971
	0.84	8.226	4.179	11.183	8.813
	1.6	15.668	4.292	18.279	15.909
	2.58	25.264	4.441	27.549	25.179
	3.45	33.784	4.582	36.349	33.979
P2-Horzontal line	0	0.000	4.030	1.905	0.305
	0.5	4.896	4.106	6.606	5.006
	1	9.792	4.191	11.936	10.336
	1.52	14.884	4.267	16.698	15.098
	2	19.585	4.344	21.481	19.881
	2.5	24.481	4.422	26.345	24.745
	3	29.377	4.499	31.208	29.608
P1-Vertical line	0	0.000	4.119	7.433	0.793
	0.64	6.267	4.204	12.757	6.117
	0.74	7.246	4.220	13.780	7.140
	1	9.792	4.266	16.617	9.977
	1.52	14.884	4.348	21.744	15.104
	2	19.585	4.423	26.456	19.816
	2.56	25.068	4.514	32.120	25.480
	3.07	30.062	4.594	37.125	30.485
P2-Vertical line	0	0.000	4.135	8.415	0.515
	0.5	4.896	4.215	13.426	5.526
	0.75	7.344	4.253	15.817	7.917
	1	9.792	4.293	18.320	10.420
	1.6	15.668	4.385	24.075	16.175
	1.98	19.389	4.443	27.712	19.812
	2.52	24.677	4.535	33.437	25.537
	3	29.377	4.606	37.865	29.965

Table B.4 Measuring tank & load cells calibration results.

	Weight added (kg)	Level (m)	Volume of conical contents (m^3)	Volume of cylindrical contents (m^3)	Total volume (m^3)	Actual weight W=ρv (kg)	Load cells reading (kg)
	15.0	0.10	0.007	0.009	0.016	15.96	15.00
	25.0	0.20	0.007	0.019	0.026	25.84	25.00
	35.0	0.30	0.007	0.029	0.036	35.72	35.00
	45.0	0.40	0.007	0.039	0.046	45.59	45.00
	55.0	0.50	0.007	0.049	0.056	55.47	55.00
	60.0	0.55	0.007	0.054	0.061	60.40	60.00
	65.0	0.60	0.007	0.059	0.065	65.34	65.00
	70.0	0.65	0.007	0.064	0.070	70.28	70.30
	75.0	0.70	0.007	0.069	0.075	75.22	75.30
	80.0	0.75	0.007	0.074	0.080	80.15	80.30
	85.0	0.80	0.007	0.079	0.085	85.09	85.40
	87.5	0.82	0.007	0.081	0.088	87.56	87.90
	90.0	0.85	0.007	0.084	0.090	90.03	90.90
Average	**60.58**					**60.97**	**60.78**
Percent Error	**0.45%**						

Table B.5 ERT calibration results.

	Probe conductivity (µS/cm)	ERT conductivity (µS/cm)
	279	278
	282	281
	282	281
	284	284
	299	299
	325	324.5
	352	351
	372	371
	402	401
Average	**319.7**	**318.9**
Percent Error	**0.20%**	

Appendix C
Piping related charts

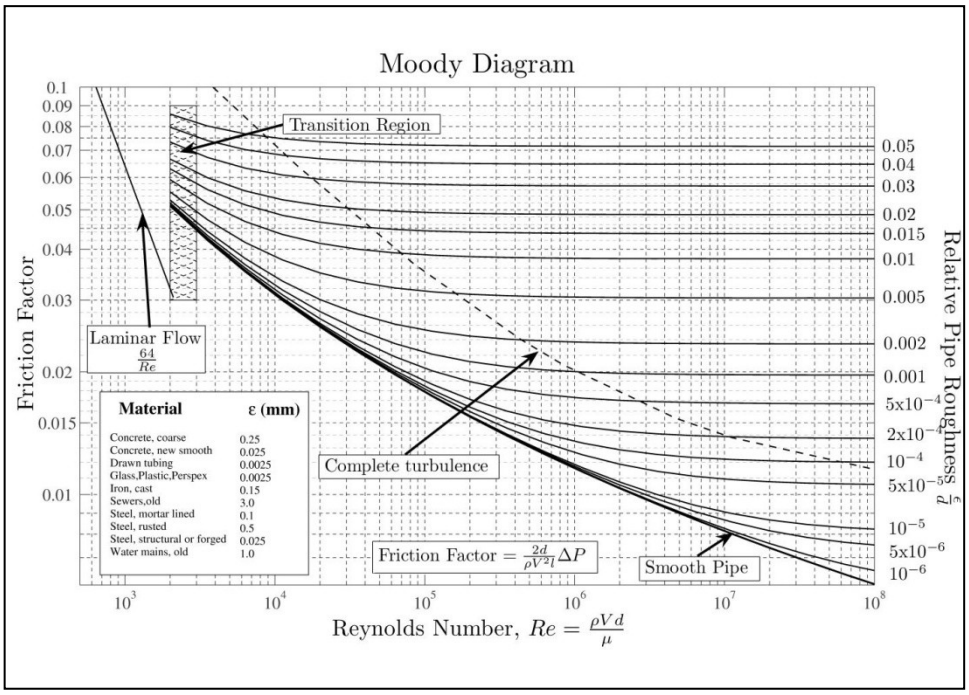

Figure C.1 Moody diagram (from www.territorioscuola.com)

Fitting	Loss Coefficient, K
Globe valve, fully open	10.0
Angle valve, fully open	5.0
Swing check valve, fully open	2.5
Gate valve, fully open	0.2
Short-radius elbow	0.9
Medium-radius elbow	0.8
Long-radius elbow	0.6
45 degree elbow	0.4
Close return bend	2.2
Standard tee, flow through run	0.6
Standard tee, flow through branch	1.8
Square entrance	0.5
Exit	1.0

Figure C.2 Minor loss coefficients for pipe fittings(www.hydromatic.com & Warman Centrifugal Slurry Pumps).

Appendix D
MATLAB script for automated flow regime recognition

The full MATLAB script, which has been developed for automated flow regime recognition, measurement of solids volume fraction and visualisation of solids volumetric distribution across the horizontal pipe cross-section is shown below:

```
clc

h = waitbar(1,{'Please wait...';'computation in progress'});
steps = 1;
for step = 1:steps

%tic

%Read the columns in zave file (it takes 40 seconds to read all the
%following data from zave.csv file).
%Each column reresent a zone in the vertical line of the pipe cross-
section.
Z1 = xlsread('zave.csv', 1, 'D3:D8002');
Z2 = xlsread('zave.csv', 1, 'H3:H8002');
Z3 = xlsread('zave.csv', 1, 'M3:M8002');
Z4 = xlsread('zave.csv', 1, 'R3:R8002');
Z5 = xlsread('zave.csv', 1, 'V3:V8002');

%toc

importfile('Warning.mat');
T = 0.0015; % Sample Time
Fs = 1/T; % Sampling Frequency
L = 8000; % Length of Signal
% Sum of a 50 Hz sinusoid and a 120 Hz sinusoid

NFFT = 2^nextpow2(L); % Next power of 2 from length of y

V = fft (Z1,NFFT)/L; % Zone 1
W = fft (Z2,NFFT)/L; % Zone 2
X = fft (Z3,NFFT)/L; % Zone 3
Y = fft (Z4,NFFT)/L; % Zone 4
Z = fft (Z5,NFFT)/L; % Zone 5

f = Fs/2*linspace(0,1,NFFT/2+1);

Plot single sided amplitude spectrum
plot(f,2*abs(V(1:NFFT/2+1)),f,2*abs(W(1:NFFT/2+1)),f,2*abs(X(1:NFFT/
2+1)),f,2*abs(Y(1:NFFT/2+1)),f,2*abs(Z(1:NFFT/2+1)))

plot(f,2*abs(V(1:NFFT/2+1)))
plot(f,2*abs(W(1:NFFT/2+1)))
plot(f,2*abs(X(1:NFFT/2+1)))
plot(f,2*abs(Y(1:NFFT/2+1)))
```

```
plot(f,2*abs(Z(1:NFFT/2+1)))
title('Single-sided amplitude spectrum of noisy ERT signals-2.0
m/s')
xlabel('Frequency (Hz)')
ylabel('Amplitude')
ylabel('|Y(f)|')
axis([0 50 0 0.06])

legend('Zone 1','Zone 2','Zone 3','Zone 4','Zone 5');

legend('Zone 1')
legend('Zone 2')
legend('Zone 3')
legend('Zone 4')
legend('Zone 5')
fprintf('%8.3f, %8.3f\n',f, 2*abs(V(1:NFFT/2+1)));

%Create periodogram
h1 = spectrum.periodogram('hamming');

% Create options object and set properties
hopts1 = psdopts(h1,Z1);
set(hopts1,'Fs',Fs,'SpectrumType','onesided','centerdc',true);
%msspectrum(h1,v,hopts1);

h2 = spectrum.periodogram('hamming');
hopts2 = psdopts(h2,Z2);  % Default options
set(hopts2,'Fs',Fs,'SpectrumType','onesided','centerdc',true);
%msspectrum(h2,w,hopts2);

h3 = spectrum.periodogram('hamming');
hopts3 = psdopts(h3,Z3);  % Default options
set(hopts3,'Fs',Fs,'SpectrumType','onesided','centerdc',true);
%msspectrum(h3,x,hopts3);

h4 = spectrum.periodogram('hamming');
hopts4 = psdopts(h4,Z4);  % Default options
set(hopts4,'Fs',Fs,'SpectrumType','onesided','centerdc',true);
%msspectrum(h4,y,hopts4);

h5 = spectrum.periodogram('hamming');
hopts5 = psdopts(h5,Z5);  % Default options
set(hopts5,'Fs',Fs,'SpectrumType','onesided','centerdc',true);
%msspectrum(h5,z,hopts5);

b = axis; axis([b(1) b(2) -120 20]); % Zoom in X.
set(gca,'XLim',[-10 30],'YLim',[-90 0])
set(gcf,'Color',[1 1 1])

% The average power is calculated by integrating under the power
spectral
% density (PSD), then, the PSD method is used on the spectrum object
(h),
% and then the power average method is used. The area under PSD
curve is
% the measure of average power
hpsd1 = psd(h1,Z1,hopts1);
       P1= avgpower(hpsd1);
hpsd2 = psd(h2,Z2,hopts2);
       P2= avgpower(hpsd2);
```

```
hpsd3 = psd(h3,Z3,hopts3);
       P3= avgpower(hpsd3);
hpsd4 = psd(h4,Z4,hopts4);
       P4= avgpower(hpsd4);
hpsd5 = psd(h5,Z5,hopts5);
       P5= avgpower(hpsd5);

meanZ1=mean(Z1);
meanZ2=mean(Z2);
meanZ3=mean(Z3);
meanZ4=mean(Z4);
meanZ5=mean(Z5);

 E=P1+P2+(P3/2);
 F=(P3/2)+P4+P5;

 D = E/(E+F);

 A=meanZ1+meanZ2+(meanZ3/2);
 B=(meanZ3/2)+meanZ4+meanZ5;
 C=A/(A+B);

 G=std(Z5);

 if(C>=0.499 && C<0.501 && D>=0.496 && D<504)
 fprintf('HOMOGENEOUS FLOW REGIME\n');
 msgbox('HOMOGENEOUS FLOW REGIME...','FLOW REGIME', 'replace')
 beep

 elseif  (C>=0.501 && C<0.505 && D>=0.504 && D<0.510)

 fprintf('PSEUDO-HOMOGENEOUS FLOW REGIME\n');
 msgbox('PSEUDO-HOMOGENEOUS FLOW REGIME...','FLOW REGIME',
'replace')
 beep

 elseif  (C>=0.505 && C<0.510 && D>=0.510 && D<0.520)

 fprintf('TRANSITIONAL REGIME BOUNDARY(PSUDOHOMOGENEOUS-
HETEROGENEOUS)\n');
 msgbox({'TRANSITIONAL REGIME BOUNDARY';'(PSUDOHOMOGENEOUS-
HETEROGENEOUS)...'},'FLOW REGIME', 'replace')
 beep

 elseif  (C>=0.510 && C<0.532 && D>=0.520 && D<0.555)

 fprintf('HETEROGENEOUS FLOW REGIME\n');
 msgbox('HETEROGENEOUS FLOW REGIME...','FLOW REGIME', 'replace')
 beep

 elseif  (C>=0.532 && C<0.540 && D>=0.555 && D<0.570)

 fprintf('TRANSITIONAL REGIME BOUNDARY(HETEROGENEOUS-MOVING
BED)\n');
 msgbox({'TRANSITIONAL REGIME BOUNDARY';'(HETEROGENEOUS-MOVING
BED)...'},'FLOW REGIME', 'replace')
 beep

 elseif  (C>=0.540 && C<0.652 && D>=0.570 && D<0.770)
```

```
 fprintf('MOVING BED FLOW REGIME\n');
 msgbox('MOVING BED FLOW REGIME...','FLOW REGIME', 'replace')
 beep

 elseif  (C>=0.652 && C<0.657 && D>=0.770 && D<0.780)

 fprintf('TRANSITIONAL REGIME BOUNDARY(MOVING BED-STATIONARY
BED)\n');
 msgbox({'TRANSITIONAL REGIME BOUNDARY';'(MOVING BED-STATIONARY
BED...)'},'FLOW REGIME', 'replace')

 % Play warning sound (Alarm).
play(WARNING);
disp('WARNING!');

 elseif(C>=0.657 && D>=0.780 && G<0.003)

 fprintf('STATIONARY BED FLOW REGIME\n\a');
 msgbox({'WARNING!';'STATIONARY BED FLOW
REGIME...'},'!!WARNING!!','warn', 'replace')

% Play warning sound (Alarm).
play(WARNING);
disp('WARNING!');

 else

 fprintf('COULD NOT DETERMINE FLOW REGIME\n');
 msgbox({'SORRY...';' COULD NOT DETERMINE FLOW
REGIME...!'},'HELP','error', 'replace')

 end

waitbar(step / steps)
 close(h)
end

%The following is to display 2D & 3D plot of solids volumetric
distribution
%and through which the mean concentration can be determined (Data
Analysis
%Tool)

h = waitbar(1,{'Please wait...';' Solids concentration distribution
is displayed shortly'});
steps = 1;
for step = 1:steps
    %tic

%It takes approximately 112 seconds for reading and calculation of
the following concentrations

Conc1 = xlsread('conc.csv',1, 'EK3:FD8000');
Conc2 = xlsread('conc.csv',1, 'FE3:FX8000');
CCL1 = mean (Conc1);
CCL2= mean (Conc2);
CCL3 = [CCL1;CCL2]; % Concentration matrix (two column vector), used
in 3D plot.
```

```
CCL4 = mean(CCL3); % Mean concentration of the dual centreline, Used
for the x-axis of the 2D Plot.

%toc

VP1 = (1:-0.05:0.05);
VP2 = (1:-0.05:0.05);
VP = [VP1;VP2]; % Vertical Position of the pipe cross-section, used
in 2D &3D plot.

HP1(1:20)=0.5;
HP2(1:20)=0.55;
HP = [HP1;HP2]; % It is an array of 2 raws, indicating the
horizontal position of the pipe cross-section and used in 3D plot.

%Creating surface (3D)plot of the vertical dual centerline of the
concentration tomogram.
 Surface_Solids_Volumetric_Distribution(HP, CCL3, VP)

 %Creating (2D)plot of the vertical centerline of the concentration
tomogram.
 Two_Dimenssional_Concentration_Distribution_Plot(CCL4, VP1)

    waitbar(step / steps)
end
close(h)
```

Appendix E
Horizontal & vertical flow loop sensor data

The following tables showing the flow loop sensor data obtained from the EMF, the pressure transducers, the thermocouple and the measuring tank (flow diversion technique), for each sand and different transport velocities.

Table E.1 Flow loop sensor data for flowing medium sand at 2% throughput concentration.

Solid Particle	EMF (m/s)	T (°C)	P1 Horizontal (kPa)	P2 Horizontal (kPa)	P1 Vertical (kPa)	P2 Vertical (kPa)	dp Horizontal (kPa)	Discharge Velocity (m/s)	Delivered Conc. (v/v)	µm/µl	Slurry Viscosity (pa.s)	Slurry Reynolds Number (Re_m)
2% Medium Sand	4.97	16.61	98.40	87.00	64.40	25.12	11.40	4.97	0.0242	1.06	0.00106	233595
	4.53	18.48	86.17	76.91	57.32	20.48	9.27	4.49	0.0224	1.06	0.00106	211908
	4.02	19.87	76.13	69.22	51.30	16.94	6.91	4.08	0.0243	1.06	0.00106	191872
	3.49	20.91	66.30	60.93	45.10	13.06	5.38	3.49	0.0268	1.06	0.00106	164167
	3.05	21.65	59.31	55.05	40.89	10.40	4.27	3.05	0.0245	1.06	0.00106	143458
	2.52	22.25	51.90	48.97	36.90	7.60	2.93	2.55	0.0251	1.06	0.00106	119708
	2.06	22.25	46.82	44.79	33.95	5.66	2.03	2.12	0.025	1.06	0.00106	99490
	1.49	22.25	41.51	40.52	30.86	3.69	0.98	1.54	0.0239	1.05	0.00105	73096

Table E.2 Flow loop sensor data for flowing medium sand at 10% throughput concentration.

Solid Particle	EMF (m/s)	T (°C)	P1 Horizontal (kPa)	P2 Horizontal (kPa)	P1 Vertical (kPa)	P2 Vertical (kPa)	dp Horizontal (kPa)	Discharge Velocity (m/s)	Delivered Conc. (v/v)	µm/µl	Slurry Viscosity (pa.s)	Slurry Reynolds Number (Re_m)
10% Medium Sand	4.96	26.00	106.9	95.43	70.32	29.18	11.42	5.59	0.0838	1.37	0.00137	204271
	4.59	27.25	93.30	84.39	62.25	23.82	8.91	4.47	0.0926	1.37	0.00137	163334
	4.06	27.84	83.47	76.20	56.68	19.51	7.26	4.00	0.0913	1.37	0.00137	146078
	3.49	28.15	73.09	67.68	50.22	15.38	5.41	3.47	0.0962	1.37	0.00137	126714
	3.04	28.36	65.79	61.42	45.74	12.30	4.37	3.19	0.0927	1.37	0.00137	116452
	2.52	28.46	57.75	54.87	40.72	8.87	2.87	2.54	0.0955	1.37	0.00137	92683
	2.01	28.48	52.29	50.18	37.35	6.63	2.10	2.02	0.0979	1.37	0.00137	73928
	1.52	28.42	48.77	46.81	35.12	5.21	1.96	1.58	0.0968	1.37	0.00137	57626

Table E.3 Flow loop sensor data for flowing coarse sand at 2% throughput concentration.

Solid Particle	EMF (m/s)	T (°C)	P1 Horizontal (kPa)	P2 Horizontal (kPa)	P1 Vertical (kPa)	P2 Vertical (kPa)	dp Horizontal (kPa)	Discharge Velocity (m/s)	Delivered Conc. (v/v)	µm/µl	Slurry Viscosity (pa.s)	Slurry Reynolds Number (Re_m)
2% Coarse Sand	4.93	17.17	105.6	94.37	68.49	29.45	11.27	4.82	0.0302	1.09	0.00109	220517
	4.36	18.76	90.13	82.55	59.16	23.55	7.58	4.53	0.0325	1.09	0.00109	207337
	4.11	19.67	79.39	73.40	52.29	19.50	6.00	4.29	0.0295	1.09	0.00109	196205
	3.52	20.32	69.17	65.00	46.22	15.34	4.17	3.66	0.0315	1.09	0.00109	167651
	3.11	20.73	61.45	58.52	41.98	12.27	2.93	3.18	0.032	1.09	0.00109	145717
	2.52	21.02	53.17	51.60	37.09	8.81	1.57	2.45	0.0344	1.09	0.00109	112076
	2.00	21.27	47.79	47.25	33.38	6.56	0.54	2.03	0.0302	1.09	0.00109	93116
	1.52	21.47	43.97	43.88	31.10	5.17	0.10	1.50	0.0283	1.09	0.00109	68446

Table E.4 Flow loop sensor data for flowing coarse sand at 10% throughput concentration.

Solid Particle	EMF (m/s)	T (°C)	P1 Horizontal (kPa)	P2 Horizontal (kPa)	P1 Vertical (kPa)	P2 Vertical (kPa)	dp Horizontal (kPa)	Discharge Velocity (m/s)	Delivered Conc. (v/v)	µm/µl	Slurry Viscosity (pa.s)	Slurry Reynolds Number (Re_m)
10% Coarse Sand	4.76	16.87	117.9	106.5	76.10	34.01	11.38	5.24	0.1141	1.46	0.00146	179204
	4.14	18.77	99.74	91.45	64.71	27.38	8.29	4.61	0.1209	1.50	0.00150	153441
	3.40	20.15	80.59	75.61	52.64	18.77	4.98	3.62	0.1279	1.50	0.00150	120614
	2.94	20.64	71.86	67.79	46.47	14.55	4.07	3.36	0.1235	1.50	0.00150	111956
	2.49	21.19	66.07	63.20	43.05	12.08	2.88	2.58	0.1274	1.50	0.00150	85844
	2.20	21.68	60.99	58.70	39.66	9.87	2.29	2.09	0.1349	1.60	0.00160	65281
	1.45	22.10	58.04	55.32	37.12	8.74	2.72	1.40	0.1283	1.50	0.00150	46678

Appendix F
Local solids volumetric concentration data

The following tables showing the solids volumetric concentration for medium and coarse sand in both, horizontal flow and vertical upward flow, obtained from the ERT at twenty locations across the vertical plane of the pipe cross-section at different transport velocities. The quantitative results of blocked line is also presented.

F.1 Local solids volumetric concentration in horizontal flow

Table F.1.1 Local solids volumetric concentration for horizontal flow of medium sand at 2% throughput concentration.

		Top of Pipe																	Bottom of Pipe		
Mixture Velocity m/s	**y (mm)**	50	47.5	45	42.5	40	37.5	35	32.5	30	27.5	25	22.5	20	17.5	15	12.5	10	7.5	5	2.5
	y/D	1	0.95	0.9	0.85	0.8	0.75	0.7	0.65	0.6	0.55	0.5	0.45	0.4	0.35	0.3	0.25	0.2	0.15	0.1	0.05
5	**solids volumetric concentration (v/v)**	0.033	0.033	0.034	0.034	0.035	0.037	0.038	0.039	0.040	0.040	0.041	0.041	0.042	0.042	0.043	0.044	0.046	0.047	0.048	0.049
4.5		0.028	0.028	0.028	0.029	0.031	0.033	0.035	0.037	0.038	0.040	0.041	0.042	0.042	0.043	0.044	0.044	0.045	0.047	0.048	0.049
4		0.022	0.023	0.024	0.025	0.027	0.029	0.032	0.034	0.036	0.038	0.040	0.041	0.042	0.042	0.043	0.044	0.045	0.046	0.048	0.049
3.5		0.020	0.020	0.021	0.022	0.024	0.027	0.030	0.033	0.037	0.040	0.043	0.045	0.046	0.047	0.049	0.050	0.052	0.054	0.055	0.057
3		0.015	0.014	0.015	0.016	0.017	0.020	0.023	0.026	0.030	0.034	0.037	0.040	0.042	0.045	0.048	0.051	0.055	0.059	0.062	0.065
2.5		0.017	0.017	0.017	0.018	0.020	0.022	0.025	0.028	0.032	0.036	0.040	0.045	0.051	0.058	0.066	0.076	0.086	0.096	0.105	0.111
2		0.016	0.016	0.016	0.016	0.017	0.018	0.019	0.021	0.023	0.026	0.030	0.037	0.046	0.059	0.075	0.094	0.114	0.134	0.151	0.165
1.5		0.017	0.016	0.016	0.015	0.015	0.014	0.013	0.011	0.010	0.009	0.010	0.015	0.025	0.042	0.065	0.094	0.125	0.155	0.181	0.202

Table F.1.2 Local solids volumetric concentration for horizontal flow of medium sand at 10% throughput concentration.

		Top of Pipe																	Bottom of Pipe		
Mixture Velocity m/s	**y (mm)**	50	47.5	45	42.5	40	37.5	35	32.5	30	27.5	25	22.5	20	17.5	15	12.5	10	7.5	5	2.5
	y/D	1	0.95	0.9	0.85	0.8	0.75	0.7	0.65	0.6	0.55	0.5	0.45	0.4	0.35	0.3	0.25	0.2	0.15	0.1	0.05
5	**solids volumetric concentration (v/v)**	0.094	0.094	0.096	0.098	0.102	0.106	0.111	0.116	0.122	0.127	0.132	0.137	0.141	0.144	0.148	0.151	0.154	0.156	0.159	0.161
4.5		0.070	0.071	0.073	0.076	0.080	0.085	0.092	0.099	0.106	0.113	0.121	0.127	0.134	0.140	0.145	0.151	0.156	0.160	0.164	0.167
4		0.052	0.053	0.055	0.058	0.063	0.069	0.076	0.085	0.094	0.105	0.115	0.126	0.136	0.146	0.156	0.166	0.175	0.183	0.189	0.194
3.5		0.038	0.038	0.039	0.042	0.047	0.053	0.061	0.071	0.083	0.097	0.111	0.126	0.142	0.157	0.173	0.188	0.201	0.213	0.222	0.229
3		0.025	0.025	0.025	0.027	0.030	0.035	0.042	0.053	0.066	0.082	0.100	0.121	0.144	0.168	0.192	0.214	0.235	0.252	0.266	0.276
2.5		0.013	0.012	0.010	0.010	0.010	0.012	0.017	0.027	0.042	0.062	0.089	0.119	0.154	0.189	0.224	0.256	0.285	0.308	0.325	0.337
2		0.007	0.005	0.002	0.001	0.001	0.001	0.004	0.012	0.028	0.051	0.081	0.117	0.156	0.197	0.236	0.273	0.304	0.330	0.349	0.362
1.5		0.005	0.002	0.000	0.000	0.000	0.000	0.002	0.009	0.028	0.056	0.090	0.129	0.170	0.212	0.252	0.290	0.322	0.350	0.371	0.386

Table F.1.3 Local solids volumetric concentration for horizontal flow of coarse sand at 2% throughput concentration.

		Top of Pipe																	Bottom of Pipe		
Mixture Velocity m/s	**y (mm)**	50	47.5	45	42.5	40	37.5	35	32.5	30	27.5	25	22.5	20	17.5	15	12.5	10	7.5	5	2.5
	y/D	1	0.95	0.9	0.85	0.8	0.75	0.7	0.65	0.6	0.55	0.5	0.45	0.4	0.35	0.3	0.25	0.2	0.15	0.1	0.05
5	**solids volumetric concentration (v/v)**	0.005	0.001	0.000	0.003	0.013	0.027	0.042	0.055	0.067	0.076	0.082	0.085	0.086	0.086	0.084	0.082	0.080	0.077	0.076	0.075
4.5		0.000	0.000	0.000	0.000	0.003	0.016	0.030	0.045	0.057	0.067	0.074	0.080	0.083	0.086	0.087	0.087	0.087	0.086	0.085	0.085
4		0.000	0.000	0.000	0.000	0.001	0.011	0.026	0.040	0.052	0.063	0.071	0.078	0.083	0.087	0.091	0.094	0.096	0.097	0.098	0.099
3.5		0.000	0.000	0.000	0.000	0.001	0.011	0.025	0.038	0.050	0.061	0.070	0.079	0.087	0.095	0.103	0.110	0.117	0.122	0.126	0.130
3		0.000	0.000	0.000	0.000	0.000	0.008	0.021	0.033	0.045	0.056	0.066	0.077	0.090	0.103	0.117	0.132	0.145	0.156	0.166	0.173
2.5		0.000	0.000	0.000	0.000	0.000	0.001	0.009	0.020	0.030	0.041	0.053	0.067	0.085	0.107	0.132	0.157	0.182	0.203	0.221	0.234
2		0.000	0.000	0.000	0.000	0.000	0.001	0.009	0.018	0.027	0.036	0.047	0.061	0.080	0.103	0.130	0.160	0.189	0.215	0.236	0.252
1.5		0.000	0.000	0.000	0.000	0.000	0.000	0.000	0.001	0.003	0.011	0.029	0.058	0.096	0.142	0.191	0.240	0.284	0.322	0.351	0.371

Table F.1.4 Local solids volumetric concentration for horizontal flow of coarse sand at 10% throughput concentration.

		Top of Pipe																	Bottom of Pipe		
Mixture Velocity m/s	**y (mm)**	50	47.5	45	42.5	40	37.5	35	32.5	30	27.5	25	22.5	20	17.5	15	12.5	10	7.5	5	2.5
	y/D	1	0.95	0.9	0.85	0.8	0.75	0.7	0.65	0.6	0.55	0.5	0.45	0.4	0.35	0.3	0.25	0.2	0.15	0.1	0.05
4.5	**solids volumetric concentration (v/v)**	0.088	0.087	0.087	0.088	0.09	0.095	0.104	0.1181	0.1383	0.1632	0.191	0.2191	0.2451	0.2669	0.284	0.295	0.301	0.302	0.301	0.3
4		0.036	0.034	0.032	0.03	0.03	0.034	0.044	0.0631	0.0912	0.127	0.1671	0.2075	0.2447	0.2761	0.3	0.317	0.327	0.332	0.333	0.332
3.5		0.002	4E-04	1E-05	2E-08	0	0	5E-05	0.0046	0.0342	0.082	0.1399	0.2012	0.2596	0.3103	0.351	0.381	0.401	0.413	0.419	0.421
3		4E-07	0	0	0	0	0	3E-06	0.0005	0.015	0.065	0.1288	0.1965	0.2608	0.3167	0.362	0.396	0.419	0.433	0.441	0.444
2.5		0	0	0	0	0	0	0	6E-05	0.0035	0.0382	0.0993	0.1667	0.2326	0.2913	0.34	0.377	0.403	0.421	0.431	0.436
2		0	0	0	0	0	6E-06	2E-04	0.0021	0.0122	0.0568	0.1305	0.2079	0.28	0.3415	0.39	0.427	0.452	0.468	0.477	0.481
1.5		0	0	0	0	0	0	1E-04	0.0044	0.044	0.1194	0.2004	0.2774	0.3453	0.4017	0.447	0.481	0.507	0.524	0.535	0.541

Table F.1.5 Local solids volumetric concentration for blocked horizontal line with coarse sand at 10% throughput concentration.

		Top of Pipe																	Bottom of Pipe		
Mixture Velocity m/s	**y (mm)**	50	47.5	45	42.5	40	37.5	35	32.5	30	27.5	25	22.5	20	17.5	15	12.5	10	7.5	5	2.5
	y/D	1	0.95	0.9	0.85	0.8	0.75	0.7	0.65	0.6	0.55	0.5	0.45	0.4	0.35	0.3	0.25	0.2	0.15	0.1	0.05
0.0	**solids volumetric concentration (v/v)**	0.0	0.0	0.0	0.0	0.0	0.0	0.2	0.3	0.5	0.5	0.6	0.6	0.6	0.6	0.6	0.6	0.6	0.6	0.6	0.6

F.2 Local solids volumetric concentration in vertical flow

Table F.2.1 Local solids volumetric concentration for vertical flow of medium sand at 2% throughput concentration.

		Top of Pipe																	Bottom of Pipe		
Mixture Velocity m/s	**r (mm)**	25	22.5	20	17.5	15	12.5	10	7.5	5	2.5	0	-2.5	-5	-7.5	-10	-12.5	-15	-17.5	-20	-22.5
	r/D	0.5	0.45	0.4	0.35	0.3	0.25	0.2	0.15	0.1	0.05	0	-0.05	-0.1	-0.15	-0.2	-0.25	-0.3	-0.35	-0.4	-0.45
4.5	**solids volumetric concentration (v/v)**	0.051	0.043	0.033	0.023	0.015	0.009	0.007	0.008	0.011	0.014	0.018	0.023	0.027	0.031	0.035	0.038	0.041	0.044	0.044	0.045
3.5		0.047	0.039	0.029	0.019	0.011	0.006	0.004	0.005	0.008	0.012	0.016	0.021	0.025	0.029	0.033	0.036	0.039	0.041	0.041	0.044
2.5		0.047	0.039	0.029	0.019	0.011	0.007	0.005	0.006	0.009	0.013	0.017	0.021	0.025	0.029	0.032	0.035	0.038	0.040	0.039	0.043
1.5		0.045	0.038	0.028	0.018	0.011	0.006	0.005	0.007	0.010	0.014	0.018	0.022	0.025	0.029	0.032	0.035	0.037	0.038	0.038	0.043

Table F.2.2 Local solids volumetric concentration for vertical flow of medium sand at 10% throughput concentration.

		Top of Pipe																	Bottom of Pipe		
Mixture Velocity m/s	**r (mm)**	25	22.5	20	17.5	15	12.5	10	7.5	5	2.5	0	-2.5	-5	-7.5	-10	-12.5	-15	-17.5	-20	-22.5
	r/D	0.5	0.45	0.4	0.35	0.3	0.25	0.2	0.15	0.1	0.05	0	-0.05	-0.1	-0.15	-0.2	-0.25	-0.3	-0.35	-0.4	-0.45
4.5	**solids volumetric concentration (v/v)**	0.155	0.147	0.136	0.124	0.114	0.105	0.098	0.095	0.093	0.094	0.097	0.102	0.108	0.114	0.121	0.126	0.131	0.134	0.134	0.128
3.5		0.156	0.148	0.137	0.125	0.115	0.106	0.100	0.096	0.094	0.095	0.097	0.102	0.107	0.113	0.119	0.124	0.129	0.131	0.131	0.126
2.5		0.154	0.146	0.136	0.125	0.115	0.106	0.100	0.097	0.096	0.096	0.099	0.103	0.108	0.113	0.119	0.124	0.127	0.130	0.130	0.123
1.5		0.154	0.146	0.136	0.126	0.116	0.109	0.104	0.101	0.101	0.103	0.106	0.111	0.116	0.122	0.128	0.133	0.137	0.139	0.139	0.133

Table F.2.3 Local solids volumetric concentration for vertical flow of coarse sand at 2% throughput concentration.

		Top of Pipe																	Bottom of Pipe		
Mixture Velocity m/s	**r (mm)**	25	22.5	20	17.5	15	12.5	10	7.5	5	2.5	0	-2.5	-5	-7.5	-10	-12.5	-15	-17.5	-20	-22.5
	r/D	0.5	0.45	0.4	0.35	0.3	0.25	0.2	0.15	0.1	0.05	0	-0.05	-0.1	-0.15	-0.2	-0.25	-0.3	-0.35	-0.4	-0.45
4.5	**solids volumetric concentration (v/v)**	0.034	0.027	0.019	0.012	0.010	0.011	0.016	0.023	0.031	0.037	0.041	0.042	0.041	0.038	0.035	0.031	0.029	0.027	0.026	0.032
3.5		0.036	0.029	0.021	0.015	0.012	0.013	0.018	0.025	0.033	0.039	0.043	0.044	0.043	0.040	0.037	0.034	0.032	0.030	0.028	0.034
2.5		0.041	0.034	0.026	0.020	0.017	0.019	0.024	0.031	0.038	0.044	0.048	0.049	0.048	0.045	0.042	0.039	0.036	0.034	0.032	0.036
1.5		0.044	0.037	0.028	0.021	0.017	0.018	0.021	0.027	0.033	0.038	0.041	0.042	0.040	0.037	0.035	0.032	0.031	0.030	0.030	0.036

Table F.2.4 Local solids volumetric concentration for vertical flow of coarse sand at 10% throughput concentration.

		Top of Pipe																	Bottom of Pipe		
Mixture Velocity m/s	**r (mm)**	25	22.5	20	17.5	15	12.5	10	7.5	5	2.5	0	-2.5	-5	-7.5	-10	-12.5	-15	-17.5	-20	-22.5
	r/D	0.5	0.45	0.4	0.35	0.3	0.25	0.2	0.15	0.1	0.05	0	-0.05	-0.1	-0.15	-0.2	-0.25	-0.3	-0.35	-0.4	-0.45
4.5	**solids volumetric concentration (v/v)**	0.112	0.108	0.103	0.102	0.105	0.112	0.123	0.136	0.148	0.157	0.163	0.164	0.160	0.153	0.144	0.134	0.124	0.116	0.108	0.097
2.5		0.116	0.114	0.111	0.113	0.118	0.128	0.142	0.156	0.170	0.180	0.186	0.186	0.182	0.174	0.163	0.151	0.139	0.127	0.116	0.104

Appendix G
Local solids axial velocity data

The following tables showing the solids axial velocity for medium and coarse sand in both, horizontal flow and vertical upward flow, obtained from the ERT at twenty locations across the vertical plane of the pipe cross-section at different transport velocities. The quantitative results of blocked line is also presented.

G.1 Local solids axial velocity in horizontal flow

Table G.1.1 Local solids axial velocity for horizontal flow of medium sand at 2% throughput concentration.

		Top of Pipe																	Bottom of Pipe		
Mixture Velocity m/s	**y (mm)**	50	47.5	45	42.5	40	37.5	35	32.5	30	27.5	25	22.5	20	17.5	15	12.5	10	7.5	5	2.5
	y/D	1	0.95	0.9	0.85	0.8	0.75	0.7	0.65	0.6	0.55	0.5	0.45	0.4	0.35	0.3	0.25	0.2	0.15	0.1	0.05
5	**Solids axial Velocity (m/s)**	7.779	7.779	7.779	7.779	7.779	7.779	7.779	7.779	7.779	7.779	7.779	7.779	7.779	7.779	7.779	7.779	3.889	3.889	3.889	3.889
4.5		3.889	3.889	3.889	3.889	3.889	3.889	3.889	3.889	3.889	3.889	3.889	3.889	3.889	3.889	3.889	3.889	3.889	3.889	3.889	3.889
4		3.889	3.889	4.019	4.105	4.105	3.749	3.889	3.889	3.889	3.889	3.889	3.889	3.889	3.889	3.889	3.889	3.889	3.889	3.889	3.889
3.5		4.149	4.149	4.149	4.149	4.149	4.149	4.149	4.149	4.149	4.149	4.149	4.149	4.149	4.149	4.149	4.149	2.829	2.829	2.829	2.829
3		2.146	1.695	2.146	2.146	2.146	2.146	4.445	3.637	2.829	2.829	2.829	2.829	2.963	2.963	2.963	2.963	2.963	2.963	2.963	2.963
2.5		1.830	1.830	1.830	1.830	1.830	1.830	2.068	2.305	2.305	2.305	2.305	2.305	2.305	2.305	2.305	2.305	2.305	2.305	2.264	2.264
2		1.830	1.830	1.830	1.830	1.830	1.830	1.830	1.830	1.830	1.830	1.830	1.988	1.988	1.830	1.830	1.830	1.830	1.830	1.785	1.687
1.5		1.027	1.027	0.965	0.912	0.912	0.940	0.851	0.877	0.964	1.224	1.305	1.482	1.482	1.451	1.358	1.292	1.237	1.201	1.158	1.129

Table G.1.2 Local solids axial velocity for horizontal flow of medium sand at 10% throughput concentration.

		Top of Pipe																Bottom of Pipe		
Mixture Velocity m/s	**y (mm)**	50	47.5	45	42.5	40	37.5	35	32.5	30	27.5	25	22.5	20	17.5	15	12.5	10	7.5	5	2.5
	y/D	1	0.95	0.9	0.85	0.8	0.75	0.7	0.65	0.6	0.55	0.5	0.45	0.4	0.35	0.3	0.25	0.2	0.15	0.1	0.05
4.5	**Solids axial Velocity (m/s)**	4.733	5.186	5.186	5.186	5.186	5.186	5.186	5.186	5.186	5.186	5.186	5.186	5.186	5.186	5.186	4.787	4.787	4.787	4.559	4.075
3.5		3.661	3.661	3.661	3.661	3.661	3.661	3.661	3.661	3.661	3.661	3.661	3.661	3.661	3.627	3.457	3.457	3.457	3.457	3.397	3.232
3		3.457	3.457	3.457	3.457	3.457	3.457	3.457	3.457	3.457	3.457	3.457	3.457	3.457	3.427	3.231	2.829	2.808	2.767	2.706	2.706
2.5		2.706	2.706	2.706	2.706	2.706	2.706	2.706	2.706	2.706	2.706	2.706	2.706	2.593	2.593	2.489	2.349	2.264	2.210	2.197	2.148
2		2.146	2.146	2.146	2.146	2.146	2.146	2.146	2.146	2.146	2.146	2.146	2.146	2.134	2.032	1.926	1.858	1.813	1.747	1.670	1.611
1.5		1.322	1.627	1.830	1.830	1.830	1.830	1.830	1.830	1.830	1.822	1.696	1.589	1.556	1.543	1.478	1.378	1.317	1.281	1.224	1.287

Table G.1.3 Local solids axial velocity for horizontal flow of coarse sand at 2% throughput concentration.

		Top of Pipe																Bottom of Pipe		
Mixture Velocity m/s	**y (mm)**	50	47.5	45	42.5	40	37.5	35	32.5	30	27.5	25	22.5	20	17.5	15	12.5	10	7.5	5	2.5
	y/D	1	0.95	0.9	0.85	0.8	0.75	0.7	0.65	0.6	0.55	0.5	0.45	0.4	0.35	0.3	0.25	0.2	0.15	0.1	0.05
5	**Solids axial Velocity (m/s)**	5.119	5.119	5.186	5.186	5.186	5.186	5.119	4.616	4.445	4.396	4.149	4.149	4.149	4.149	4.149	4.149	4.149	4.149	4.149	3.976
4.5		4.149	4.149	4.346	4.445	4.445	4.445	4.445	4.445	4.445	4.445	4.445	4.445	4.445	4.445	4.445	4.445	4.445	4.445	4.297	4.149
4		4.198	4.346	4.445	4.445	4.445	4.445	4.445	4.445	4.445	4.445	4.445	4.445	4.445	4.445	4.346	4.149	4.149	4.019	3.889	3.699
3.5		3.423	3.423	3.423	3.423	3.423	3.423	3.423	3.423	3.423	3.423	3.423	3.423	3.423	3.423	3.260	3.260	3.260	3.112	2.976	2.976
3		3.112	3.112	3.112	3.112	3.112	3.112	3.112	3.112	3.112	3.112	3.112	3.112	3.112	3.062	3.013	2.941	2.817	2.740	2.678	2.624
2.5		2.393	2.393	2.393	2.393	2.393	2.393	2.334	2.320	2.305	2.320	2.334	2.393	2.379	2.320	2.305	2.065	2.001	1.977	1.977	1.977
2		1.596	1.596	1.596	1.596	1.596	1.596	1.596	1.596	1.596	1.596	1.596	1.596	1.596	1.596	1.596	1.596	1.383	1.383	1.383	1.383
1.5		1.489	1.383	1.383	1.383	1.383	1.489	1.489	1.596	1.596	1.638	1.638	1.638	1.638	1.383	1.066	1.194	0.750	0.750	0.750	0.750

Table G.1.4 Local solids axial velocity for horizontal flow of coarse sand at 10% throughput concentration.

		Top of Pipe																Bottom of Pipe		
Mixture Velocity m/s	**y (mm)**	50	47.5	45	42.5	40	37.5	35	32.5	30	27.5	25	22.5	20	17.5	15	12.5	10	7.5	5	2.5
	y/D	1	0.95	0.9	0.85	0.8	0.75	0.7	0.65	0.6	0.55	0.5	0.45	0.4	0.35	0.3	0.25	0.2	0.15	0.1	0.05
4.5	**Solids axial Velocity (m/s)**	5.657	5.657	5.657	5.657	5.657	5.657	5.657	5.657	5.657	5.657	5.657	5.657	5.657	5.657	5.657	5.186	5.186	5.186	5.186	4.787
4		5.189	5.189	5.189	5.189	5.186	5.186	5.186	5.186	5.186	4.986	4.787	4.787	4.787	4.787	4.445	4.445	4.297	4.149	4.149	4.019
3.5		3.889	3.661	3.661	3.661	3.661	3.661	3.661	3.661	3.661	3.661	3.661	3.457	3.457	3.275	3.275	3.112	3.112	2.963	2.829	2.706
3		2.489	2.489	2.489	2.489	2.489	2.489	2.593	2.706	2.829	2.829	2.706	2.706	2.593	2.593	2.489	2.489	2.393	2.393	2.393	2.305
2.5		2.489	2.489	2.441	2.393	2.393	2.393	2.393	2.393	2.393	2.393	2.393	2.305	2.305	2.223	2.184	2.146	2.074	2.007	2.007	2.007
2		1.830	1.830	1.830	1.830	1.830	1.830	1.830	1.830	1.830	1.830	1.804	1.729	1.682	1.638	1.638	1.596	1.556	1.556	1.537	1.537
1.5		1.945	1.945	1.886	1.915	1.915	1.915	1.886	1.886	1.779	1.556	1.482	1.296	1.245	1.092	0.950	0.892	0.841	0.770	0.776	0.776

Table G.1.5 Local solids axial velocity for blocked horizontal line with coarse sand at 10% throughput concentration.

		Top of Pipe																Bottom of Pipe		
Mixture Velocity m/s	**y (mm)**	50	47.5	45	42.5	40	37.5	35	32.5	30	27.5	25	22.5	20	17.5	15	12.5	10	7.5	5	2.5
	y/D	1	0.95	0.9	0.85	0.8	0.75	0.7	0.65	0.6	0.55	0.5	0.45	0.4	0.35	0.3	0.25	0.2	0.15	0.1	0.05
0.0	**Solids axial Velocity (m/s)**	0.221	0.221	0.222	0.222	0.222	0.222	0.222	0.222	0.222	0.222	0.222	0.222	0.222	0.222	0.222	0.222	0.222	0.222	0.221	0.221

G.2 Local solids axial velocity in vertical flow

Table G.2.1 Local solids axial velocity for vertical flow of medium sand at 2% throughput concentration.

		Top of Pipe																	Bottom of Pipe		
Mixture Velocity m/s	**r (mm)**	25	22.5	20	17.5	15	12.5	10	7.5	5	2.5	0	-2.5	-5	-7.5	-10	-12.5	-15	-17.5	-20	-22.5
	r/D	0.5	0.45	0.4	0.35	0.3	0.25	0.2	0.15	0.1	0.05	0	-0.05	-0.1	-0.15	-0.2	-0.25	-0.3	-0.35	-0.4	-0.45
4.5	**Solids axial Velocity (m/s)**	3.457	3.457	3.457	5.186	5.186	5.186	5.186	5.186	5.186	5.186	5.186	5.186	5.186	5.186	5.186	5.186	5.186	4.787	4.787	2.007
3.5		2.007	3.275	3.275	3.275	3.275	3.275	3.275	3.275	3.275	3.275	3.275	3.275	3.275	3.275	3.275	3.275	3.275	3.275	2.007	2.007
2.5		2.747	3.043	2.909	2.750	2.782	2.778	2.766	2.679	2.593	2.593	2.593	2.593	2.679	2.766	2.778	2.782	2.750	2.909	3.043	2.747
1.5		1.350	1.316	1.326	1.394	1.395	1.336	1.316	1.258	1.343	1.518	1.518	1.343	1.258	1.316	1.336	1.395	1.394	1.326	1.316	1.350

Table G.2.2 Local solids axial velocity for vertical flow of medium sand at 10% throughput concentration.

		Top of Pipe																	Bottom of Pipe		
Mixture Velocity m/s	**r (mm)**	25	22.5	20	17.5	15	12.5	10	7.5	5	2.5	0	-2.5	-5	-7.5	-10	-12.5	-15	-17.5	-20	-22.5
	r/D	0.5	0.45	0.4	0.35	0.3	0.25	0.2	0.15	0.1	0.05	0	-0.05	-0.1	-0.15	-0.2	-0.25	-0.3	-0.35	-0.4	-0.45
4.5	**Solids axial Velocity (m/s)**	4.324	4.542	5.020	5.186	5.186	5.186	5.186	5.186	5.186	5.186	5.186	5.186	5.186	5.186	5.186	5.186	5.186	5.020	4.542	4.324
3.5		3.335	3.463	3.504	3.568	3.591	3.646	3.661	3.661	3.661	3.661	3.661	3.661	3.661	3.661	3.646	3.591	3.568	3.504	3.463	3.335
2.5		2.663	2.616	2.684	2.706	2.706	2.706	2.706	2.706	2.706	2.706	2.706	2.706	2.706	2.706	2.706	2.706	2.706	2.684	2.616	2.663
1.5		1.416	1.484	1.517	1.556	1.563	1.595	1.634	1.656	1.750	1.778	1.778	1.750	1.656	1.634	1.595	1.563	1.556	1.517	1.484	1.416

Table G.2.3 Local solids axial velocity for vertical flow of coarse sand at 2% throughput concentration.

		Top of Pipe																	Bottom of Pipe		
Mixture Velocity m/s	**r (mm)**	25	22.5	20	17.5	15	12.5	10	7.5	5	2.5	0	-2.5	-5	-7.5	-10	-12.5	-15	-17.5	-20	-22.5
	r/D	0.5	0.45	0.4	0.35	0.3	0.25	0.2	0.15	0.1	0.05	0	-0.05	-0.1	-0.15	-0.2	-0.25	-0.3	-0.35	-0.4	-0.45
4.5	**Solids axial Velocity (m/s)**	4.546	4.783	4.963	5.131	5.186	5.186	5.186	5.186	5.186	5.186	5.186	5.186	5.186	5.186	5.186	5.186	5.131	4.963	4.783	4.546
3.5		3.540	3.589	3.653	3.661	3.661	3.661	3.661	3.661	3.661	3.661	3.661	3.661	3.661	3.661	3.661	3.661	3.661	3.653	3.589	3.540
2.5		2.420	2.451	2.478	2.489	2.514	2.630	2.607	2.489	2.489	2.489	2.489	2.489	2.489	2.607	2.630	2.514	2.489	2.478	2.451	2.420
1.5		1.391	1.413	1.431	1.450	1.476	1.514	1.556	1.556	1.556	1.556	1.556	1.556	1.556	1.556	1.514	1.476	1.450	1.431	1.413	1.391

Table G.2.4 Local solids axial velocity for vertical flow of coarse sand at 10% throughput concentration.

		Top of Pipe																	Bottom of Pipe		
Mixture Velocity m/s	**r (mm)**	25	22.5	20	17.5	15	12.5	10	7.5	5	2.5	0	-2.5	-5	-7.5	-10	-12.5	-15	-17.5	-20	-22.5
	r/D	0.5	0.45	0.4	0.35	0.3	0.25	0.2	0.15	0.1	0.05	0	-0.05	-0.1	-0.15	-0.2	-0.25	-0.3	-0.35	-0.4	-0.45
4.5	**Solids axial Velocity (m/s)**	5.249	5.304	5.403	5.539	5.628	5.657	5.657	5.657	5.657	5.657	5.657	5.657	5.657	5.657	5.657	5.628	5.539	5.403	5.304	5.249
2.5		2.815	2.780	2.781	2.781	2.790	2.811	2.829	2.829	2.829	2.829	2.829	2.829	2.829	2.829	2.811	2.790	2.781	2.781	2.780	2.815

This page has been intentionally left blank